

# Simulation of the Suppression of Fires Using Water Mists

HM Iqbal Mahmud

Centre for Environmental Safety and Risk Engineering (CESARE)  
College of Engineering and Science  
Victoria University

A thesis submitted to Victoria University in fulfilment of the  
requirements of the degree of Doctor of Philosophy

March 2016



*This thesis has been submitted to the College of Engineering and Science of Victoria University, Melbourne, in fulfilment of the requirements for the degree of Doctor of Philosophy.*

This thesis is dedicated  
To  
My Beloved Parents

## Abstract

As warships can carry weapons on board, the unlikely occurrence of fire is one of the most feared events on board. Until recently, halon 1301 (bromo-tri-fluoro methane,  $\text{CF}_3\text{Br}$ ) has been the primary fire-fighting agent for protecting the machinery spaces of ships. Halon 1301 is not only harmful to humans, but it also depletes the ozone layer. Water-mist fire suppression systems (WMFSS) have been considered as a potential candidate for the replacement of halon-based fire suppression systems by fire protection industries. WMFSS is already being used in commercial buildings, passenger and naval ships, etc. However, it is essential to examine the efficacy of water-mist droplets in suppressing fires. The efficacy of a water-mist system can be investigated in two ways: (i) experimental investigation; and (ii) numerical analysis. This study is a combination of an experimental study (water mist spray without fire) and two types of numerical studies using (a) semi-empirical equations based model developed in this study; and (b) a state of the art computational fluids dynamics (CFD) based fire model.

Prior to determine the efficacy of water mists in suppressing fire using a CFD-based fire model, the model needs to be validated for the type of simulation events. In this study, fire dynamic simulator (FDS), has been chosen which is being developed for compartment fires and it is widely used among fire research groups. The uniqueness of this model is its pyrolysis model, which allows fire growth and suppression modelling. The capability of FDS has been examined in three areas: namely, predicting (i) behaviour of evaporation of water droplets at high temperatures induced by fire; (ii) distribution of flux densities of water-mist nozzle sprays; (iii) burning rates of polymethyl methacrylate (PMMA) fires with and without water-mist sprays.

A semi-empirical model has been developed with the primary aim of developing a detailed understanding of the science of droplet evaporation using equations of the conservation of mass, momentum and energy. The variable thermo-physical properties of water and air, and the change of the Reynolds number of droplets due to the change of their diameters and velocities, have been considered. The effect of the high evaporation rate on the mass and heat transfer coefficients has also been included. A particular feature of this model is that it accounts for the effects of thermal radiation on the rate of evaporation of droplets. Results from the model indicate that the predicted terminal velocity is within 4% of the experimental data and the saturation temperature is within 5% of the adiabatic saturation temperature. A key finding of this work is that droplets with a smaller diameter suspend in the air for a longer time and have a higher rate of evaporation compared to larger droplets. In contrast, droplets with a larger diameter have a higher capability of penetrating the smoke layer. The secondary aim is to validate FDS in terms of single droplet evaporation against this semi-empirical model. It has been found that predictions of FDS show good agreement with results of the semi-empirical model.

The effectiveness of a spray in suppressing a fire is greatly influenced by its distribution pattern on a horizontal surface. Hence, it is essential that any CFD based model can predict the distribution of the flux densities of a spray. Full-scale experiments have been conducted on water sprays emanating from a single and multi-orifice nozzle, and the distributions of flux densities have been measured. Numerical simulations have been performed using FDS. The predicted results show good agreement with the experimental data.

The ultimate value of FDS is its ability to predict the growth and extinguishment of fires. In this work the success of FDS in predicting the rate of burning of PMMA before and after activation of water-mist sprays has been examined. Results from

FDS are compared with published experimental data. It has been found that FDS prediction of burning rate is within 23% of the experimental data.

Having gained confidence in the ability of FDS in accurately predicting the evaporation of droplets, distribution of sprays, and burning and suppression of fires, more realistic scenarios have been examined by conducting a comparative parametric study. The effect of different factors, such as obstructions, location of fires, number of nozzles and size of droplets, has been investigated. The results indicate that the spray is the most effective for unobstructed fires and the least effective for horizontally obstructed fires provided that both of them are located directly underneath the nozzle. The spray produced by a single nozzle shows a marginally better performance in suppressing fires when it is unobstructed and directly underneath the nozzle.

In the analysis, it appears that the cooling of hot gases and burning surfaces play a major role in suppressing unobstructed fires. Whereas the blocking of air entrainment and attenuation of radiation feedback to the fuel surface play a major role in suppressing horizontally obstructed fires while the fire is directly underneath the nozzle. In case of size of droplets, due to higher momentum and greater volume, larger droplets have better capacity to penetrate the fire plume and reach the depth of the fire before their evaporation, respectively. These result in exhibiting better performance in fire suppression.

## **Declaration**

‘I, HM Iqbal Mahmud, declare that the PhD thesis entitled “Simulation of the suppression of fires using water mists” is no more than 100,000 words in length including quotes and exclusive of tables, figures, appendices, bibliography, references and footnotes. This thesis contains no material that has been submitted previously, in whole or in part, for the award of any other academic degree or diploma. Except where otherwise indicated, this thesis is my own work.’

Signature: \_\_\_\_\_

Date: \_\_\_\_\_

## **Acknowledgements**

It has been a long journey on the way to completing my PhD. During the past few years I have enjoyed the guidance, support and company of the many people who have contributed to my research.

Firstly, I would like to express my gratitude to Almighty Allah to give me the opportunity to climb the crest of academic education.

Then, I would like to thank my supervisors, Associate Professor Khalid Moinuddin and Professor Graham Thorpe, for their offer to embark on this fantastic voyage several years ago. Their inspiration, guidance, support, constructive comments, suggestions, clues, and of course patience, have helped me complete this voyage. I greatly appreciate their consistent and continuous support in solving the research problems that I have encountered during my PhD. Words cannot describe how grateful I am to them for their inestimable support.

I would also like to express my gratitude to Ian Burch, Zenka Mathys, Brigitta Suendermann and Grant Gamble from Defence Science and Technology Organisation (DSTO), who have helped me find the clues to solve the technical problems in the experimental and numerical work. I also appreciate their advice and continuous support throughout the duration of the work and their technical help in the experimental set-up for the water-mist spray test. I also acknowledge the technical and financial assistance provided by DSTO, Australia.

I wish to acknowledge the technical support in my experiments provided by postgraduate students, Sk Md Kamal Uddin, Md Mahfuz Sarwar and Mohammad Mahmudur Rahman, and a research fellow in CESARE, Maurice Guerrieri.

I would also like to express my gratitude to the members of the FDS Google discussion group and the FDS support group who have helped me enormously in my numerical study. Especially I would like to give thanks to Kevin McGrattan (NIST, USA), Topi Sikanen (VTT, Finland), Jason Floyd (Hughes Associates, USA), Simo Hostikka (VTT, Finland), Randall McDermott (NIST, USA), Elizabeth Blanchard (CSTB, France) and others for their valuable information in preparing my FDS input scripts and explaining the FDS results in terms of the relevant physics.

I also gratefully acknowledge the financial assistance through the Victoria University funded scholarship schemes (VUIPRS) and Victoria University Fee waiver scholarship.

I would also like to express my gratitude to my parents, brothers, friends and other family members who have missed me over the last few years. I want to thank all of them for their understanding and the support that they gave me while I was dedicating my time to this project.

Finally, I would like to give special thanks to my wife and daughter for their earnest cooperation and understanding, as well as their love and affection.

HM Iqbal Mahmud

March 2016

# Table of Contents

Abstract .....	i
Declaration .....	iv
Acknowledgements .....	v
Table of Contents .....	vii
List of Figures .....	xii
List of Tables.....	xix
Nomenclature .....	xxi
Chapter 1 Background study and scope .....	1
1.1 Background to the project.....	1
1.2 Mechanisms of suppression of fires by water mist sprays .....	3
1.3 Numerical modelling of the suppression of fires.....	9
1.4 Aims of the research .....	19
1.5 Methodology.....	19
Chapter 2 CFD model description .....	21
2.1 Introduction .....	21
2.2 Features and program version of FDS .....	21
2.3 Governing equations.....	22
2.3.1 Modelling of mass, species and enthalpy transport .....	22
2.3.2 Modelling of pyrolysis.....	26
2.3.3 Modelling of radiation transport.....	26

2.3.4	Modelling of combustion.....	27
2.3.5	Modelling of water-mist .....	28
2.4	Geometry and numerical grid .....	30
Chapter 3	Development of a semi-empirical model for the evaporation of water droplets .....	32
3.1	Introduction .....	32
3.2	Mathematical formulation .....	35
3.2.1	Mass transfer model.....	36
3.2.2	Heat transfer model.....	37
3.2.3	Momentum model.....	39
3.2.4	Calculation of rate constants.....	41
3.2.5	Correction to the rate constants for high mass transfer rate .....	43
3.2.6	Thermophysical properties of air and water .....	45
3.3	Computational procedure .....	46
3.4	Model verification and validation.....	49
3.4.1	Comparison with experimental data .....	49
3.4.2	Comparison with theoretical adiabatic saturation temperature.....	50
3.5	Use of the model as a validation tool .....	50
3.5.1	Comparison with FDS .....	51
3.5.2	Comparison with the study by Li and Chow [2008].....	54
3.5.3	Comparison with the study by Barrow and Pope [2007].....	55
3.6	Parametric study .....	58
3.7	Scattering, absorption and extinction characteristics of water mist in a radiated medium .....	67
3.8	Conclusions .....	67
Chapter 4	Spray distribution – a benchmark experiment and validation of FDS .....	72
4.1	Introduction .....	72

4.2	Experiment details .....	73
4.2.1	Nozzle specification.....	73
4.2.2	Experimental set-up and procedure .....	74
4.3	Numerical model .....	79
4.3.1	Domain set-up.....	79
4.3.2	Modelling of sprays .....	81
4.3.3	Input variables for determining the median diameter of droplets.....	82
4.3.4	Input variables for determining the distribution of flux densities ....	82
4.4	Results and discussion .....	84
4.4.1	Median diameter of droplets.....	84
4.4.2	Distribution of flux densities of sprays.....	85
4.5	Conclusions .....	94
Chapter 5 Validation of FDS for the burning of PMMA and the suppression of fires by water mists.....		95
5.1	Introduction .....	95
5.2	The experiments of Magee and Reitz [1974] .....	96
5.3	Numerical simulation .....	98
5.3.1	Computational domain.....	98
5.3.2	Operating and boundary conditions.....	100
5.3.3	Sensitivity analysis .....	100
5.3.4	External radiation flux .....	104
5.3.5	Flammability parameters and chemical kinetics.....	105
5.4	Results and discussion.....	107
5.5	Conclusions .....	117
Chapter 6 Parametric study using FDS to assess the efficacy of water mist sprays .....		119
6.1	Introduction .....	119

6.2	Numerical simulation .....	122
6.2.1	Computational domain.....	122
6.2.2	Type and location of fuel load .....	123
6.2.3	Location of the nozzles .....	124
6.2.4	Types of obstructions.....	125
6.2.5	Orientation of nozzle, obstruction and fire load in the simulation .	126
6.2.6	Specification of the spray .....	132
6.2.7	Material properties of pinewood, ignition of the wood crib, and activation of the water-mist nozzle.....	132
6.3	Results and discussion .....	134
6.3.1	Effect of obstructions.....	135
6.3.2	Effect of location of fires .....	142
6.3.3	Effect of number of nozzles.....	149
6.3.4	Effect of size of droplets.....	155
6.4	Conclusions .....	159
Chapter 7 Summary and conclusions.....		163
7.1	Development of a semi-empirical model for evaporation of water droplets .....	164
7.1.1	Model development and validation.....	164
7.1.2	Evaluation of the characteristics of the different sizes of droplets .	165
7.2	Spray distribution – a benchmark experiment and validation of FDS .....	165
7.3	Validation of FDS for the burning of PMMA and the suppression of fires by water-mist spray .....	166
7.3.1	Simulation of PMMA fire without the presence of a water-mist system .....	166
7.3.2	Simulation of PMMA fire with the presence of a water-mist system .....	167
7.4	Parametric study using FDS to assess the efficacy of water-mist sprays...	167
7.5	Recommendations for future study.....	168

7.5.1	Expanding the droplet evaporation model .....	169
7.5.2	Experimental measurement of the median size of droplets .....	169
7.5.3	Further investigation on factors that affect the efficacy of water- mist sprays in suppressing fires .....	169
References .....		170
Appendix A Calculation of the theoretical adiabatic saturation temperature .....		182
Appendix B Scattering, absorption and extinction of radiation by water mists .....		185
B.1	Introduction .....	185
B.2	Theory of scattering.....	186
B.3	Characteristics of water mist in scattering.....	190
B.4	Conclusions .....	195
Appendix C Journal papers .....		196

## List of Figures

Figure 1.1: Illustration of consumption of oxygen by a fire and displacement of oxygen by water vapour.....	7
Figure 3.1: Time step dependency test (a) temperature ( $T$ ); and (b) velocity ( $v$ ). ....	48
Figure 3.2: Terminal velocity of droplets. ....	49
Figure 3.3: Saturation temperature of droplets. ....	50
Figure 3.4: Computational domain set-up of the FDS model.....	52
Figure 3.5: Terminal velocity of the droplets. ....	53
Figure 3.6: Saturation temperature of the droplets. ....	53
Figure 3.7: The history of the diameter of a droplet in the air.....	54
Figure 3.8: Time of evaporation of the droplets. ....	55
Figure 3.9: The history of the Nusselt number of droplets diameter 200 $\mu\text{m}$ .....	56
Figure 3.10: The drag force on the droplets with diameter 200 $\mu\text{m}$ . ....	57
Figure 3.11: Distance travelled by the droplets. ....	57
Figure 3.12: Temperature profile of droplets (a) close view (0–2 seconds); (b) detailed view (0–8 seconds).....	59
Figure 3.13: Diameter and position history of droplets with different initial drop size (a) 100 $\mu\text{m}$ ; (b) 200 $\mu\text{m}$ ; (c) 300 $\mu\text{m}$ ; (d) 400 $\mu\text{m}$ ; (e) 500 $\mu\text{m}$ ; (f) 750 $\mu\text{m}$ ; and (g) 1000 $\mu\text{m}$ . ....	62
Figure 3.14: Per cents of mass loss of droplets with different initial drop size.....	63
Figure 3.15: Heat absorbed by droplets of different droplet sizes.....	64
Figure 3.16: Velocity and position of droplets with different initial drop sizes (a) 100 $\mu\text{m}$ ; (b) 200 $\mu\text{m}$ ; (c) 300 $\mu\text{m}$ ; (d) 400 $\mu\text{m}$ ; (e) 500 $\mu\text{m}$ ; (f) 750 $\mu\text{m}$ ; and (g) 1000 $\mu\text{m}$ . ....	66

Figure 4.1: Schematic of the single-orifice nozzle (after Tanner and Knasiak [2003]). .....	73
Figure 4.2: Schematic view of the multi-orifice nozzle (a) side elevation; (b) plan view (after Tanner and Knasiak [2003])......	74
Figure 4.3: Schematic view of the experimental set-up.....	75
Figure 4.4: Location of nozzle (a) <i>Case A</i> ; (b) <i>Case B</i> .....	76
Figure 4.5: Schematic view of the measurements of the angle of sprays (a) spray produced by the single-orifice nozzle; (b) spray produced by the multi-orifice nozzle. .....	76
Figure 4.6: Computational domain for simulating the spray produced by the single- orifice nozzle.....	80
Figure 4.7: The grid system on the floor in the computational domain.....	80
Figure 4.8: Computational domain set-up used to simulate the spray produced by the multi-orifice nozzle.....	81
Figure 4.9: Comparison of the numerical results on the distribution of flux densities for different size of droplets with the experimental measurement in the first case... 84	
Figure 4.10: Comparison of the numerical results on the distribution of flux densities for the hypothetical size of droplets with the experimental measurement in the second case. ....	85
Figure 4.11: Distribution of flux densities ( $L/m^2/min$ ) of the spray produced by the single-orifice nozzle (a) experimental; (b) numerical.....	86
Figure 4.12: The distribution of the flux density of sprays for the single-orifice nozzle along the centreline axes as indicated in Figure 5.12: $\oplus$ Experimental values along the major axis; $\ominus$ Experimental values along the minor axis; $\triangle$ Numerical values along the radii of X direction; $\bullet$ $\times$ Numerical values along the radii of the Y direction. ....	88
Figure 4.13: Distribution of flux densities ( $L/m^2/min$ ) of sprays for the multi-orifice nozzle for <i>Case A</i> (a) experimental; (b) numerical.....	89

Figure 4.14: The distribution of flux densities of spray for the multi-orifice nozzle along the major and minor axes of ellipses for case A -○- Experimental values along the major axis; -⊖- Experimental values along the minor axis; -△- Numerical values along the radii of X direction; -✖- Numerical values along the radii of Y direction.	90
Figure 4.15: Distribution of flux densities ( $L/m^2/min$ ) of spray for multi-orifice nozzle for <i>Case B</i> (a) experimental; (b) numerical.	92
Figure 4.16: The distribution of the flux density of spray for the multi-orifice nozzle along the orifice axis for case B -○- Experimental values along the major axis; -⊖- Experimental values along the minor axis; -△- Numerical values along the radii of X direction; -✖- Numerical values along the radii of Y direction.	93
Figure 5.1: Experimental set-up for the burning of vertical specimens after the studies by Magee and Reitz [1974].	97
Figure 5.2: Three-dimensional view of the computational domain for the simulation of fires produced by the horizontally placed PMMA slabs.	99
Figure 5.3: Three-dimensional view of the computational domain for the simulation of fires produced by the vertically placed PMMA slabs.	100
Figure 5.4: Grid convergence test for PMMA fire [Abu-Bakar and Moinuddin 2015].	102
Figure 5.5: The effect of insulation on the rear surface of the PMMA slab.	103
Figure 5.6: The effect of the use of the absorption coefficient of PMMA in the simulation.	104
Figure 5.7: Three-dimensional view of the burning of the vertically oriented PMMA slab.	108
Figure 5.8: Burning rates of the vertically oriented PMMA slabs for the different flux of radiation ( $kW/m^2$ ) before and after activation of the spray.	109
Figure 5.9: Burning and suppression of fire produced by the vertically oriented PMMA slab for the radiation flux rate of $15.89 kW/m^2$ .	110

Figure 5.10: Comparison between the experimental and numerical steady state burning rates for the vertically oriented PMMA slab before activation of the spray. .....	112
Figure 5.11: Comparison between the experimental and numerical steady state burning rates for the horizontally oriented PMMA slab before activation of the spray. .....	112
Figure 5.12: Comparison between the experimental and numerical values of difference in steady state burning rates before and after activation of spray for horizontally oriented PMMA slab. ....	112
Figure 5.13: Burning rates of the horizontally oriented PMMA slabs at different levels of radiation fluxes (kW/m <sup>2</sup> ). ....	113
Figure 5.14: Burning of fire produced by the horizontally oriented PMMA slab for the radiation flux of 15.89 kW/m <sup>2</sup> . ....	114
Figure 5.15: Comparison between the experimental and numerical steady state burning rates of the horizontally oriented PMMA slab. ....	115
Figure 5.16: Convective and radiative heat transfer from the flame to the PMMA slab (a) vertical specimen; (b) horizontal specimen. ....	117
Figure 6.1: ISO room (a) plan view; (b) elevation [Moinuddin et al. 2011]. ....	122
Figure 6.2: Location of timber crib in the ISO room (a) adjacent to the open door (Case <i>a</i> ); (b) centre of the room (Case <i>b</i> ); (c) distant from the open door (Case <i>c</i> ). ....	124
Figure 6.3: Plan view of the locations of the nozzles in the ISO room (a) a single nozzle (Case <i>A</i> ); (b) a double nozzle (Case <i>B</i> ). ....	124
Figure 6.4: Side elevation of the location of the nozzles in the ISO room (a) a single nozzle (Case <i>A</i> ); (b) a double nozzle (Case <i>B</i> ). ....	125
Figure 6.5: Condition of obstructions (a) no obstruction (Case <i>1</i> ); (b) horizontal obstruction (Case <i>2</i> ); (c) vertical obstruction (Case <i>3</i> ). ....	125
Figure 6.6: Location of the estimation of gas temperature and concentration of oxygen. ....	134

Figure 6.7: Comparison of the effect of the condition of the obstruction on the suppression of fires (HRR) by water spray (a) single nozzle –adjacent to the open door; (b) single nozzle – centre of the room; (c) single nozzle – distant from open door; (d) double nozzle – adjacent to the open door; (e) double nozzle – centre of the room; and (f) double nozzle – distant from the open door. .... 136

Figure 6.8: Comparison of the effect of obstructions on the reduction of temperatures of the burning surface and hot gases by water spray; the fire is related to Figure 6.7 (b) which is located at the centre of the room and the spray is from a single nozzle (a) temperature; (b) concentration of oxygen; (c) radiation; (d) % reduction of temperature; (e) % reduction of concentration of oxygen; and (f) % reduction of radiation. .... 140

Figure 6.9: Comparison of the effect of obstructions on the reduction of temperature of the burning surface and hot gases by water spray; the fire is related to Figure 6.7 (c) which is located at a distance from open door and the spray is from a single nozzle (a) temperature; (b) concentration of oxygen; (c) radiation, (d) % reduction of temperature; (e) % reduction of concentration of oxygen; and (f) % reduction of radiation. .... 141

Figure 6.10: Comparison of the effect of location of fires on suppression of fires (HRR) by water spray (a) single nozzle – adjacent to the open door,; (b) single nozzle – centre of the room; (c) single nozzle – distant from the open door; (d) double nozzle – adjacent to the open door; (e) double nozzle – centre of the room; and (f) double nozzle – distant from the open door. .... 144

Figure 6.11: Comparison of the effect of the location of fire on the reduction of temperature of the burning surface and hot gases by water spray; the fire is related to Figure 6.10 (a) which is unobstructed and the spray is from a single nozzle (a) temperature; (b) concentration of oxygen; (c) radiation; (d) % reduction of temperature; (e) % reduction of concentration of oxygen; and (f) % reduction of radiation. .... 147

Figure 6.12: Comparison of the effect of the location of fire on the reduction of temperature of the burning surface and hot gases by water spray; the fire is related to Figure 6.10 (c) which is vertically obstructed and the spray is from a single nozzle

(a) temperature; (b) concentration of oxygen; (c) radiation; (d) % reduction of temperature; (e) % reduction of concentration of oxygen; and (f) % reduction of radiation. ....	148
Figure 6.13: Comparison of reduction of HRR by the spray produced by the single and double nozzles. ....	150
Figure 6.14: Comparison of the effect of the number of nozzles on the reduction of temperature of the burning surface and hot gases by water spray; the fire is related to Figure 6.13 (b) which is unobstructed and located at the centre of the room (a) temperature; (b) concentration of oxygen; (c) radiation; (d) % reduction of temperature; (e) % reduction of concentration of oxygen; and (f) % reduction of radiation. ....	153
Figure 6.15: Comparison of the effect of the number of nozzles on the reduction of temperature of the burning surface and hot gases by water spray; the fire is related to Figure 6.13 (g) which is vertically obstructed and located adjacent to the open door (a) temperature; (b) concentration of oxygen; (c) radiation; (d) % reduction of temperature; (e) % reduction of concentration of oxygen; and (f) % reduction of radiation. ....	154
Figure 6.16: The effect of the size of droplets on HRR of fires (a) no obstruction; and (b) horizontal obstruction. ....	157
Figure 6.17: Comparison of the effect of the size of the droplets on the reduction of temperatures of the burning surface and hot gases by the spray at the time of suppression of fire; the fire is related to Figure 6.16 (a), which is unobstructed and located centre of the room (a) temperature; (b) oxygen concentration; (c) radiation; (d) % reduction of temperature; (e) % reduction of concentration of oxygen; and (f) % reduction of radiation. ....	158
Figure A.1: A schematic diagram of the adiabatic saturation process (after Çengel and Turner [2005]). ....	183
Figure B.1. Conceptual diagram of the attenuation of thermal radiation by a water spray. ....	186

Figure B.2: The scattering of incident radiation of wavelength, $\lambda$ , by a water droplet. .....	187
Figure B.3: Complex refractive index of water. ....	190
Figure B.4: Efficiency factors for water-mist droplets (a) extinction efficiency factor, $q_{ext}$ ; (b) absorption efficiency factor, $q_{abs}$ ; and (c) scattering efficiency factor, $q_{ext}$ .....	191
Figure B.5: Monochromatic radiation intensity for a spectrum of wavelength at 1500K.....	192
Figure B.6: Transmissivity of water droplets for different sizes at a wavelength of 3 $\mu\text{m}$ . ....	193
Figure B.7: The minimum concentration of water loading for different size of droplets.....	194
Figure B.8: A spectrum of radiation passing through a medium filled with droplets. .....	194
Figure B.9: The attenuation of thermal radiation by water-mist droplets. ....	195

## List of Tables

Table 1.1: Surface area to volume ratio of the different size of water droplets.....	4
Table 3.1: The dependence of the calculated saturation temperature ( $T$ ) and terminal velocity ( $v$ ) of the droplet on the time step .....	48
Table 3.2: The input parameters in the FDS model .....	52
Table 4.1: Input parameters for the simulation of determining the median diameter of droplets of a spray .....	82
Table 4.2: Spray parameters for the simulation of determining the distribution of flux densities of sprays .....	83
Table 5.1: Arrhenius parameters .....	105
Table 5.2: Materials properties for the FDS input file .....	106
Table 5.3: The experimental and numerical values of the steady state burning rates for the vertically oriented PMMA slab .....	111
Table 5.4: The experimental and numerical values of steady state burning rates for the horizontally oriented PMMA slab .....	115
Table 6.1: Combination of the location of the fire, condition of obstruction and number of nozzles for different cases in the ISO room .....	126
Table 6.2: Graphical presentation of the combination of the location of the fire, type of obstruction and number of nozzles for different cases .....	128
Table 6.3: Location of nozzle, obstruction and fuel load for Case 1(A) .....	129
Table 6.4: Location of nozzle, obstruction and fuel load for Case 1(B).....	129
Table 6.5: Location of nozzle, obstruction and fuel load for Case 2(A) .....	130
Table 6.6: Location of nozzle, obstruction and fuel load for Case 2(B).....	130
Table 6.7: Location of nozzle, obstruction and fuel load for Case 3(A) .....	131
Table 6.8: Location of nozzle, obstruction and fuel load for Case 3(B).....	131

Table 6.9: Specification of the spray .....	132
Table 6.10: Material properties for the FDS input file .....	133
Table 6.11: Combination of parameters for the comparison of HRR with respect to the type of obstruction and time of suppression of fires with respect to 65% of HRR .....	137
Table 6.12: Combination of parameters for the comparison of HRR with respect to the location of fires .....	145
Table 6.13: Combination of parameters for the comparison of HRR with respect to location of fires .....	151
Table 6.14: The surface area to volume ratio for different sizes of droplets .....	155
Table 6.15: Combination of parameters for the analysis of the effect of the size of droplets.....	156

# Nomenclature

$A$	surface area in Chapter 3, $m^2$
$A$	pre-exponential factor in Chapter 6, 1/sec
$Bi$	biot number
$C_d$	drag coefficient
$c_{pa}$	specific heat capacity of air, $J/kg^\circ C$
$c_{pw}$	specific heat capacity of water, $J/kg^\circ C$
$D$	diameter, m
$E$	activation Energy, $kJ/mol$
$F$	force, $kg.m/s^2$
$G$	gravitational acceleration, $m/s^2$
$H$	total pressure, Pa
$HoR$	heat of reaction, $kJ/kg$
$HoC$	heat of combustion, $kJ/kg$
$h_c$	convective heat transfer coefficient, $W/m^2^\circ C$
$h_m$	mass transfer coefficient, m/s
$k$	thermal conductivity, $W/(m \cdot K)$
$K$	K-factor for water mist nozzle spray, $L/(\text{min} \cdot \text{psi}^{1/2})$
$L$	latent heat of vaporisation of water, $J/kg$
$M$	molecular weight, $kg/mol$
$m$	mass in Chapter 3, kg
$m$	refractive index in Appendix B
$\dot{m}$	mass flow rate of water particle from droplet surface, $kg/s$
$m_w''$	water mass flux from spray, $kg/m^2$
$N$	molar flux, $\text{moles}/m^2s$
$Nu$	Nusselt number

$P$	vapour pressure, Pa
$\bar{p}$	background pressure, Pa
$Pr$	Prandtl number
$Q$	discharge rate of water, L/min
$R$	universal gas constant, 8314 J/(kg.mol.K)
$\tilde{R}$	dimensionless flux ratio
$r_{\alpha\beta}$	rate of reaction, 1/s
$Re$	Reynolds number
$RH$	relative humidity, %
$S$	mass stoichiometric coefficient for air
$Sc$	Schmidt number
$Sh$	Sherwood number
$T$	temperature, °C
$t$	time, sec
$V$	volume, m <sup>3</sup>
$v$	air droplet relative velocity, m/s
$x$	mole fraction
$x = (x; y; z)$	position vector, m
$U$	velocity vector for instantaneous velocity component u, v and w in x, y and z directions, respectively, m/s
$\bar{U}$	filtered velocity vector, m/s
$Y$	vapour mass fraction
$y_i$	fraction of ith gaseous products yield
$dY/dT$	pyrolysis rate
$Z$	lumped mass fractions

### ***Greek symbols***

$\theta$	dimensionless correction factor
$\Phi$	generalised form of variables
$\mu$	viscosity, Pa.s
$\rho$	density, kg/m <sup>3</sup>
$\kappa$	absorption coefficient, 1/m
$\phi$	dimensionless rate factor
$\mathcal{D}$	mass diffusivity coefficient
$\sigma$	Stefan-Boltzmann constant in Chapter 3, W/m <sup>2</sup> /K <sup>4</sup>
$\gamma, \sigma$	empirical constants for curve fitting of spray distribution
$\varepsilon$	emissivity factor
$\tau_{ij}$	viscous stress tensor
$\tau_{turb}$	filtered turbulence
$\Delta$	filter width
$\delta x, \delta y, \delta z$	characteristic length or cell size, m

### ***Subscripts***

$A$	gas/liquid A
$a$	air
$atm$	<i>atmosphere</i>
$AB$	binary system of A and B
$B$	gas/liquid B
$b$	buoyancy
$bw$	boundary wall
$c$	convective heat
$cr$	critical value

<i>d</i>	drag
<i>e</i>	evaporation
<i>f</i>	flame
<i>g</i>	gravitation
<i>ijk</i>	gas phase cell indices
<i>m</i>	mass transfer
<i>p</i>	water particle/droplet
<i>s</i>	droplet surface
<i>sat</i>	saturation
<i>turb</i>	turbulence
<i>w</i>	water
$\infty$	refers to the far field value

### ***Superscripts***

- transfer coefficient for high mass transfer rate

# Chapter 1

## Background study and scope

# Chapter 1

## Background study and scope

---

### 1.1 Background to the project

Fire is one of the most feared events on board ship. The danger is particularly acute on warships that might carry weapons. Until recently, halon 1301 (bromo-tri-fluoro methane,  $\text{CF}_3\text{Br}$ ) has been the primary fire-fighting agent for protecting the machinery spaces of ships [Darwin and Williams 2000]. It has been used as a fire extinguishing agent because of its efficacy in the suppression of fires; however, such chemicals are not only harmful to humans, but they also deplete the ozone layer. As a result, their manufacture and use has been banned under the Montreal Protocol [Burch 2006].

The environmental and health issues of current extinguishing agents have resulted in a move to explore alternatives that are non-hazardous and non-harmful to the environment. Water is one such alternative as it does not have a deleterious effect on the ozone layer, the release of water vapour does not contribute to global warming, water vapour is non-toxic (it is not a cardiac sensitiser) and it does not produce toxic products as a result of thermal breakdown.

Water in the form of a mist has been shown to be an effective extinguishing agent. The National Fire Protection Association (NFPA) has defined water mist as a water spray in which 99% of the water is in droplets whose diameter ( $D_{v99}$ ) is less than 1000  $\mu\text{m}$  [NFPA 2010]. During the past several years, water mist technology has

been developed and regarded as a promising substitute, since it can extinguish fires quickly with little water and, at the same time, without damaging the environment [Liu 2003].

The effectiveness of water-mist systems can be investigated in two ways: (i) experimental investigation; and (ii) numerical analysis. These two techniques have their own advantages and shortcomings. In the case of full-scale experiments, the focus is on the production of a real fire scenario and the investigation of the growth and suppression of fires, which is very cost-intensive, as they require large experimental set-ups, expensive data collection systems and a large space for performing the experiments. These types of fire tests are destructive; as a result more than one test is not possible with a single experimental set-up. Moreover, repeatability of a specific test might not be possible due to the unstable nature of fires and uncertainties in the experiment [Chen et al. 2010].

On the other hand, a computational-based model can be a tool to investigate the suppression of fires using water mists. Nowadays, as computer-processing power becomes more available at lower costs, computational fluid dynamics (CFD) based models are increasingly being used in all aspects of fire safety engineering. An important feature of numerical simulation is that it can be used to explore complicated fire scenarios multiple times, with minor changes in the scenario, as required. However it is important to examine the accuracy of a particular numerical model before using it for the design and analysis of fire suppression systems. The results of a numerical model need to be verified by using analytical solutions and/or be validated against the test results of full-scale fire experiments.

## 1.2 Mechanisms of suppression of fires by water mist sprays

The suppression of fires by water mists is basically a physical mechanism and no significant chemical or gaseous reaction is involved [Kim 2002], unless chemical agents are added to enhance the efficiency of suppression. However, the mechanisms of suppression are complex and continue to be the subject of research. Some fundamental research on the mechanisms of the suppression of fires by water mist sprays was conducted in the 1950s and 1960s [Liu and Kim 2000]. The studies by Braidech et al. [1955] and Rasbash et al. [1960] identified two primary mechanisms in suppressing fires: the cooling of flame and hot gases by the extraction of heat, and the displacement of oxygen from the flame area.

Research in the middle of the 1990s, however, identified some additional mechanisms that also contribute to the suppression of fires by water-mist sprays. Investigations by Wighus [1995] and Mawhinney et al. [1994] suggest that the attenuation of thermal radiation by water mists also plays a significant role in reducing radiation feedback to the fuel surface and prevents fires from spreading to unignited fuel sources. The experimental study by Dembele et al. [2001] and the numerical study by Hostikka and McGrattan [2006] have also supported this observation. Some other mechanisms that participate in the suppression of fires, such as kinetic effects of water droplets on the flame and wetting of the fuel surface, are reported in a review by Liu and Kim [2000]. Therefore, the extinguishing mechanisms of the suppression of fire through water-mist sprays can be classified as follows:

- (i) the extraction of heat from flames and burning surfaces
- (ii) the displacement of oxygen
- (iii) the attenuation of thermal radiation.

**i) Extraction of heat from flames and burning surfaces**

Flame and hot gas cooling refers to the extraction of heat from the flame and surrounding hot gases by water droplets. As water has a high heat capacity and latent heat of vaporisation, it is highly effective in absorbing heat from the flame and hot gases produced by a fire. Furthermore, due to the atomisation of droplets in a water-mist spray, the size of the droplets is very fine. This increases the surface area to volume ratio of water droplets, and as a result, it enhances the rate of evaporation of the droplets by extracting heat from the flame, hot gases, smoke layer and hot boundaries. The finer the droplets the greater the surface area to volume ratio of water. In Table 1.1 a comparison is presented on the surface area to volume ratio for the different size of droplets.

Table 1.1: Surface area to volume ratio of the different size of water droplets

Droplet size ( $\mu\text{m}$ )	Surface area of each droplet ( $\text{mm}^2$ )	Volume of one droplet ( $\text{mm}^3$ )	Surface area to volume ratio ( $\text{mm}^{-1}$ )	Total surface area for 1 $\text{m}^3$ of water spray ( $\text{m}^2$ )
1000	3.142	0.5237	6	6000
500	0.7855	0.0655	12	12000
250	0.19638	0.00818	24	24000
100	0.03142	0.000524	60	60000

As the finer droplets have a higher capacity for extracting heat from a flame due to higher surface to area ratio, they reduce the temperature of the flame and hot gases. If the flame temperature is reduced below the critical value necessary to sustain combustion, known as the limiting adiabatic flame temperature, the flame will be extinguished. For most hydrocarbons and organic vapours, this critical temperature limit is approximately 1600 K (1326°C) [Drysdale 2011]. The cooling of the adiabatic flame temperature also reduces the radiation of heat from the flame and hot

gases, thus reducing the pyrolysis rate of the fuel that drives the fire to the extinguishing limit.

Yu-chuan et al. [2004-2005] studied the effect of the size of the water droplets of a spray on the suppression of a liquid pool fire. To evaluate the optimal size of water droplets in extinguishing the liquid pool fire, they studied three liquids: methanol, diesel and heptane. According to their study, droplets less than 700  $\mu\text{m}$  in diameter provided better extinguishment of fires produced by one litre of liquid under a constant water flow rate, whereas the water droplet size of  $D_{90}$  greater than 1000  $\mu\text{m}$  did not show satisfactory results in extinguishing fires. They also found that the fire extinguishing time did not exhibit a significant variation when the water droplet sizes ranged from 700  $\mu\text{m}$  to 300  $\mu\text{m}$ . Chow [1989] showed theoretically that there was insignificant evaporation of droplets with diameters greater than 500  $\mu\text{m}$ . Bill and Ural [1999] suggest that water mists can be used in fire suppression as total flooding agents with much better success in comparison with gaseous flooding systems since mists are much less affected by fire shielding or location as well as ventilation.

Experiments have been reported that establish a correlation between the size of a fire and the quantity of water required from a spray to cool the fire enough for suppression. Wighus [1995], in a study of the extinguishment of unconfined propane fires by water mist, proposed a relationship to establish this connection. In his study, it was found that if about one-third of the heat produced by the fire in a ventilated space was removed by the water spray, the fire might be extinguished.

Kanury [1994] identified the factors that affect the rate of evaporation of water droplets; they are: (i) adiabatic gas or air temperature; (ii) surface area of the droplets; (iii) the heat transfer coefficient between the water droplet and the hot air; and (iv) the relative velocity of the droplets in the surrounding air. Fuss et al. [2002] studied the effect of submicron water drops on the burning velocity of methane/air

mixtures and compared it with the suppression effect of gaseous thermal agents  $N_2$  and  $CF_4$  and the chemical agent  $CF_3Br$ . The diameter of water mists used in the study was less than  $1\ \mu m$ . The results indicated that water mists were about 3.5 times more efficient by mass than the inert agents  $N_2$  and  $CF_4$ , and twice as efficient as water vapour at reducing the methane/air burning velocity.

### **ii) Displacement of oxygen**

Due to high air temperatures, hot surfaces and very fine size of droplets, some of the water mists evaporate. As a result, the volume occupied by the water increases to approximately 1500 times its initial volume and results in the dilution of the oxygen concentration around the flame by displacing the air [Burch 2006]. A study conducted by Rosander and Giselsson [1984] showed that the concentration of oxygen in a room with a volume of  $100\ m^3$  could decrease to approximately 10% when 5.5 litres of water are completely converted into steam. The reduction of the oxygen concentration in a compartment by water mist is a function of the fire size, the length of the pre-burn period, the compartment volume and the ventilation conditions in the compartment. As the fire size or the length of the pre-burn period of the fire increases, the average temperature in the compartment increases.

Furthermore the volumetric expansion of water droplets can disrupt the entrainment of air into the flame. If the collective effect of the depletion of oxygen due to consumption by fire and dilution of oxygen by water vapour can reduce the oxygen concentration below the critical value, the limiting oxygen concentration (LOC) necessary to sustain combustion will result in the fire being extinguished [Back Iii et al. 2000]. The LOC for most hydrocarbon fires is around 12–14% [Beyler 2002]. For solid fuels the critical oxygen concentration required for combustion is even lower. According to Drysdale [2011], the LOC for fires produced by burning of solid fuel is around 7%. Wighus [1991] and Kung [1977] conducted experiments separately on

the effectiveness of the suppression of fires by water sprays. They found that the combined effect of the depletion of oxygen by water vapour, and together with the cooling of flame and hot gases by the evaporation of water droplets, resulted in the extinguishment of fires provided that the droplets were supplied either in the flame zone or in the layer of smoke and hot gases. This reduction of oxygen concentration may be the dominant mechanism of extinguishment when the direct cooling of the flame is not possible due to the obstruction of the fire from a spray. The depletion and dilution of oxygen in the fire environment are illustrated in Figure 1.1.

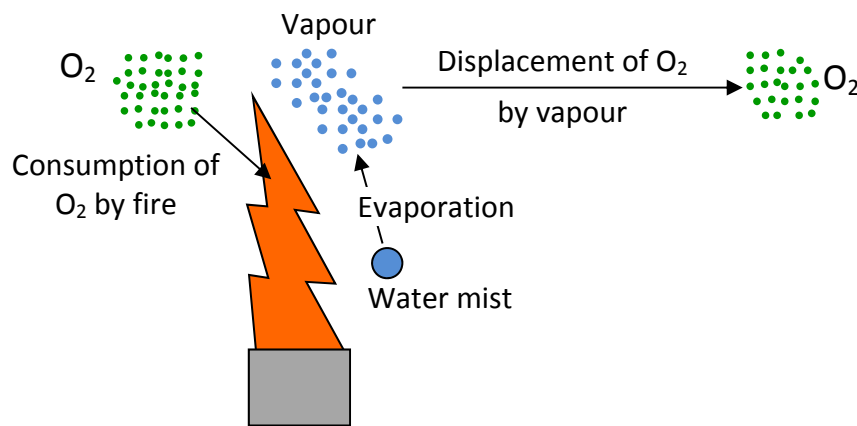


Figure 1.1: Illustration of consumption of oxygen by a fire and displacement of oxygen by water vapour.

### (iii) Attenuation of thermal radiation

Fine mists suspend in air and envelop the fire, resulting in the isolation of the fire from the surroundings. As a result, it forms a thermal barrier and prevents radiation feedback to the fire source, as well as to the unburned fuel source. Also, water vapour in the air, resulting from the evaporation of droplets, absorbs radiant heat from the fire. An experimental study showed that the radiation heat flux to the walls in a test compartment was reduced by more than 70% by the activation of the water-mist system [Mawhinney 1995]. The attenuation of thermal radiation by fine mist is

also evident from a numerical study by [Hostikka and McGrattan \[2006\]](#) and the predicted results are further supported by the experimental data of [Dembele et al. \[2001\]](#). The study by [Hostikka and McGrattan \[2006\]](#) found that sprays from three nozzles with a flow rate of 0.33 L/min from each, attenuated the thermal radiation by about 65%. [Ravigururajan and Beltran \[1989\]](#) also theoretically estimated the attenuation of thermal radiation by a very fine water mist with a range of incident wavelength of 0.6 to 25  $\mu\text{m}$ . They found that finer droplets could significantly attenuate the thermal radiation at a lower concentration of water loading compared to that of the larger droplets. Their study indicated that to achieve a level of attenuation at a target temperature of 650 K, the droplets with a diameter of 100  $\mu\text{m}$  required 10 times larger concentration of water loading compared to that for the droplets with 10  $\mu\text{m}$ , and it was 36 times higher for the droplets of 1000  $\mu\text{m}$ . Wavelength is also an important factor in attenuating the radiation by water mist. In the same study, the authors found that the maximum attenuation factor was achieved when the droplet radii are on the order of the incident wavelengths. The attenuation of thermal radiation is illustrated in Figure 1.2.

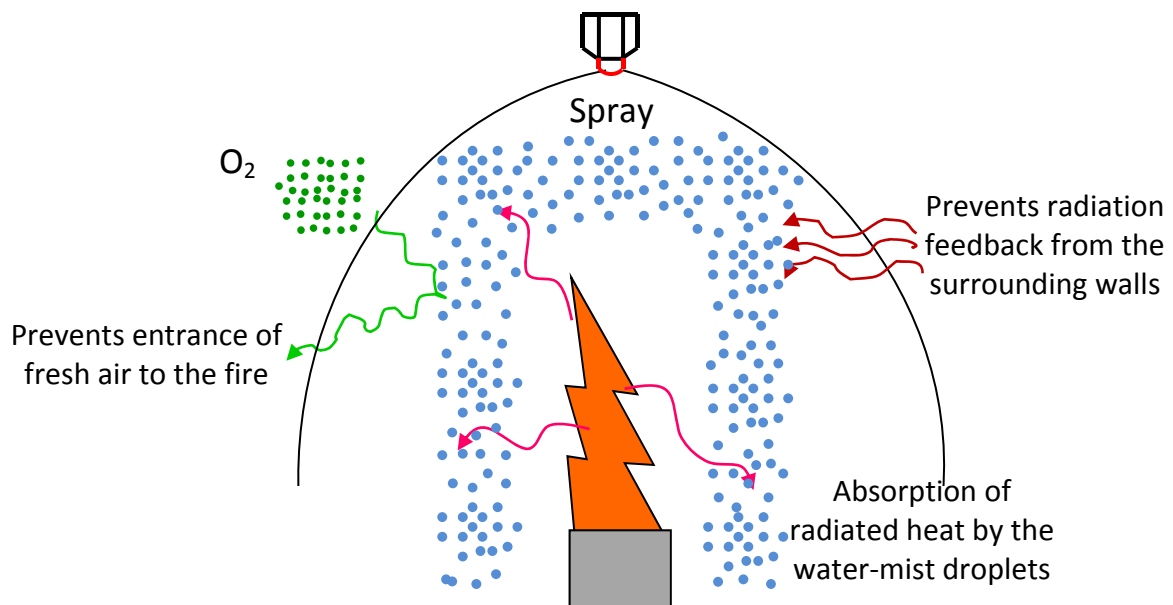


Figure 1.2: Illustration of attenuation of thermal radiation by a water-mist spray.

The relationship between the evaporation of water droplets and the absorption of radiation by small droplets in the range of 50–100  $\mu\text{m}$  was studied by [Lage and Rangel \[1993\]](#). They identified that the absorption of radiation played a potentially important role in the evaporation of droplets. Another advantage of isolating fires is that it prevents fresh air (oxygen) being entrained by the fire plume which results in the depletion of oxygen in the vicinity of the flames.

### **1.3 Numerical modelling of the suppression of fires**

Thus far we have considered the mechanisms by which water mists suppress fires. It is clear that water-mist systems are highly efficacious at suppressing fires but there remains a pressing need to develop design tools that can simulate those mechanisms. Numerous experimental studies are available in the literature on the suppression of fires using water-mist sprays. The experimental data generated by those studies are used to identify the capability of different CFD based tools in simulating the behaviour of the suppression of fires.

[Prasad et al. \[2002\]](#) conducted a numerical study on the suppression of fires using water mists in large enclosures. They computed the effect of the diameter of droplets, injection velocity of droplets, location of the nozzle and orientation of the nozzle in suppressing fires. Results indicate that for the orientation of the top injection of water mists, the time of suppression decreased with the increase of the density and velocity of the droplets and increased with the increase of the diameter of the droplets. Results also show that for similar values of injection parameters, the time for suppression was smallest for the orientation of top injection. However water-mist injection through the side walls, the front and rear walls, and through the floor were found to be less efficient than the orientation of top injection. In this study the authors did not compare their results with any experimental data for the purpose of validation of the model.

[Kim and Ryou \[2003\]](#) conducted experiments on the suppression of fires using water-mist sprays and compared the results with those predicted by FDS (ver. 3.0). Extinction times, temperature fields and oxygen concentrations were measured in an enclosed compartment. The temperature predictions made by the model showed good agreement with the measured data within 10°C for both methanol and hexane fires without the application of water-mist sprays. However the numerical model failed to predict the extinguishment of fires. [Hart \[2005\]](#) carried out a numerical study on the suppression of fires in a tunnel using water-mist spray. For numerical simulation the author used FLUENT, a commercial CFD package, and for validation of the model he used the experimental data from the study by [Kim and Ryou \[2003\]](#) on pool fires. [Hart \[2005\]](#) found that the experimental data showed a significant difference of ceiling temperatures in the enclosure with the prediction of the model.

The suppression of obstructed fires is not similar to that of unobstructed fires. The mechanisms that play a major role in the extinguishment of an obstructed fire by water mists are the dilution of oxygen by water vapour, the cooling of hot gases by water droplets and the attenuation of thermal radiation feedback to the fire sources. [Li and Chow \[2006\]](#) developed a zone model to study the suppression of obstructed fires by a total flooding water mist system in a chamber with different ventilation conditions. The model was verified by comparing it with two sets of experimental data reported in the literature. The extinguishment of fires was predicted based on the limiting oxygen volume fraction and was used to analyse the critical size of the fires, the influence of ventilation, size of the droplet, pre-burn time, etc. It was found that the initial vertical velocity had little effect on the extinguishment by water mists with small droplets. For larger droplets, a lower initial velocity would be better in extinguishing the fire provided that the discharged water mists acted on the fire directly. Longer extinguishing time was predicted when the droplet size was increased. In their study it was observed that the extinguishing time of the fire was

inversely proportional to the pre-burn time. This was because the longer pre-burn period led to a high room air temperature and both oxygen depletion due to the fire, and oxygen displacement due to the formation of more water vapour caused by high temperatures, would increase. However this finding of their study contradicted the study by [Jenft et al. \[2014\]](#) where it was observed that extinction was achieved in a shorter time for the smaller pre-burned period of the fire.

The effectiveness of water mists in suppressing fires is enhanced if the droplets are able to penetrate the base of the fires. Hence it is essential to quantify the transport of the low momentum water mists into the firebases. [Adiga et al. \[2007\]](#) investigated the effect of air entrainment due to water-mist injection and the interactions between the fire source and the water mists. To perform this they conducted both numerical and experimental studies on the effect of ultra-fine water mists for the extinguishment of fire in a methane and heptane pool fire. In the numerical simulation, FLUENT was used to simulate the transport and entrainment of mist into the firebase and its interaction with the fire, and finally, the time of extinguishment. The results showed that at the base of the compartment, the fire directed the air in the direction of the base. If mists were positioned at these locations, with a suitable flow condition, they were entrained into the firebase; otherwise the droplets fell out or were swept across the firesides downstream. If the mist was transported near the firebase, with a matching flow condition, the entrainment was efficient and the extinction was quicker; otherwise the extinction was delayed. In the case of the extinguishment of the fire, it was found that the model failed to predict the time of extinguishment as compared to their experimental data. [Kim and Ryou \[2003\]](#) also mentioned the effect of mist entrainment into the firebase. They described the burning rate as highly affected by the water mists in a real situation because of additional factors such as air entrainment due to water-mist injection and strong interactions between the fire source and water mists. They also suggested further

theoretical and experimental study for better simulation with the variation of burning rates.

Many fires involve the combustion of solids. [Cong et al. \[2008\]](#) investigated the extinguishment of a burning horizontal sheet of polymethyl methacrylate (PMMA) using water mists. For the numerical study, FDS (ver. 3.0) was adopted to simulate the interaction between water mists and the burning of PMMA. In the study, numerical data of the heat release rate (HRR), production rate of smoke, carbon dioxide and carbon monoxide emitted from the fire in the process of the suppression by water mists was compared with the experimental measurements. The results showed that the predicted HRR was about 35% higher than the measured value during the steady state combustion, but when the water mist was activated, the predicted HRR reduced much more quickly compared to that of the measured value.

[Alexander and Li \[2009\]](#) performed a comparative study on some available CFD codes for modelling the suppression of fires using water mist. They considered several CFD software packages, mainly FDS and CFX, to determine whether they were appropriate for modelling water-mist fire suppression. A number of test cases were used to examine the functionality of these software packages. Comparison of an FDS simulation was performed using the [Vaari \[2002\]](#) test scenario. [Alexander and Li \[2009\]](#) found that the fire in the FDS simulation was suppressed inside the room but not at the opening or outside the opening of a room, which reveals that the fire was suppressed locally, not globally. CFX 11 was used to determine whether a water-mist fire suppression scenario could be simulated using this code. However, as addressed by the authors, the simulation was not successful as no discernible water mist could be detected in the flow domain.

[Yang et al. \[2010\]](#) investigated the characteristics of room fire suppression with a water-mist system through a full-scale fire experiment and numerical simulations

using FDS (ver. 4.0) with a heat release rate of 6 MW. In their study it was found that in the temperature field of the fire without suppression, the numerical results were in qualitatively good agreement with the experimental data, but not when water mist was employed. They performed a fire test without water mist to validate the predictions of FDS. In the numerical simulation the grid size was 100 mm after a grid sensitivity analysis and HRR of the fire was prescribed in the simulation. It was found that the numerical model predicted temperature successfully without the suppression of fire. However it is established that if the HRR is prescribed as the experimental measurements, FDS can accurately predict temperatures and radiation flux time histories at various points [Moinuddin and Li 2010].

Trelles and Mawhinney [2010] carried out a study in which they performed tests on a water-mist system against large fires in tunnels and integrated the test data with CFD simulations. FDS (ver. 4.0) was used to simulate a series of full-scale fire tests of water-mist systems conducted in 2006 in a highway test tunnel. From a comparison of experimental data with numerical results, it was found that agreement was deemed to be good enough in an unsuppressed fire and in the fire growth regime of suppressed fire, but not in the suppression regime.

Byström et al. [2012] conducted an experiment of a full-scale compartment fire produced by a wood crib under low ambient temperature ( $-10^{\circ}\text{C}$ ). They explored the growth of the fire and the distribution of temperature in the experiment and compared the results with the predictions of FDS (ver. 5.0). An important consideration in their study was not specifying the heat release rate (HRR) curve in the numerical simulation, rather allowing the model to calculate the HRR based on the fuel mass, properties, arrangement, compartment dimensions and ambient temperature. A grid size of 100 mm was used for the computational domain far from the fire source and a grid size of 50 mm was used for the domain near the fire source. However they did not report any grid independency with these grid sizes. The

measured and calculated HRR curves agreed well and the calculated temperatures of hot smoke at different positions also agreed well with the measured values before the application of water spray. However they did not present any of the FDS results after activation of the water spray.

Experimental evidence and numerical analysis showed that the variation of size and location of fires and the diameter of droplets affect the performance of the suppression by water-mist sprays. [Liang et al. \[2013\]](#) conducted a study on the effect of those factors in suppressing fires. They used ultra-fine mists (UFM) of diameter equal to or less than 10  $\mu\text{m}$  in their experiments, and varied the locations of fires in a closed space. The results indicate that larger fires were easier to suppress in a compartment space and the fire located closer to the spray was extinguished more quickly. They also modelled the experiment using FLUENT. They used two types of model in FLUENT for simulating the UFM: one was the discrete phase model (DPM) and the other was the density gas model (DGM). The numerical results showed that DGM was more suitable for predicting UFM transportation and flow behaviour compared to the DPM model.

[Zhao et al. \[2010\]](#) also carried out a study using FLUENT to explore the effect of those factors, including the angle of the spray and pressure of water flow, in suppressing fires in the engine room of a ship. The numerical results indicated that large-scale fires were more easily suppressed by water-mist spray compared to small-scale fires and the droplets with diameters in a range of 200  $\mu\text{m}$  to 400  $\mu\text{m}$  showed better performance in suppressing fires. The smaller cone angle of a spray displayed a high flame cooling effect and the increase of spray pressure also enhanced the flame cooling effect. However the authors did not present any validation of the numerical data.

## Chapter 1: Background study and scope

The effect of time on the application of water-mist spray on the suppression of fires was studied experimentally by [Jenft et al. \[2014\]](#). The authors also performed a numerical study to address the capability of FDS in simulating the experimental observations. In the experiment, two different cases were considered where water-mist spray was applied at two different times: early application on a developing fire (and still cool environment) and late application on a developed fire (and high temperature environment). The experimental results showed that the flame was suppressed at an earlier time in the latter case. In the case of FDS, validation of the model was obtained before the application of water-mist spray with the condition that the HRR was prescribed in the simulation. However the model failed to follow the experimental observations on the suppression of fires.

From this literature review it is clear that the current CFD based models are good at predicting the temperature field of a fire, production of gases and movement of smoke, etc., with a prescribed design fire. However, as mentioned earlier, if the HRR is prescribed in any CFD model, it can predict those parameters at various points correctly. Moreover the model was good at predicting those parameters without the application of water-mist sprays, but not in the case of the suppression of fires with the application of water-mist sprays. Actually, the performance of a spray in suppressing fires is influenced by the distribution pattern of a spray, size distribution of droplets, size of the fire, location of the fire and droplet-fire interaction, etc. One of the important features is that the model should be capable of predicting the behaviour of the evaporation of water-mist droplets in high temperatures induced by room fires. Many studies [[Back et al. 2000](#); [Novozhilov 2001](#); [Wighus and Brandt 2001](#); [Vaari 2002](#)] have been conducted over the past few decades on the interaction of sprinklers with hot air or smoke layers. These studies basically focused on the convective heat transfer phenomena between large water droplets and the hot air

layer, without considering or paying much attention to the evaporation of droplets, as the evaporation for large droplets was insignificant in those cases.

[Radford \[1996\]](#) developed a zone model for studying the characteristics of sprinklers discharging comparatively bigger water droplets where only the direct convective cooling effect of water droplets was considered. Therefore the work by these authors is applicable for large water droplets where convective cooling is predominating, but not valid for sprays with fine droplets, as fine water droplets would evaporate while travelling through a layer of hot air. Moreover the droplets of water mist have a higher surface area/volume ratio that results in the rapid evaporation of droplets by extracting heat from the flame and hot gases. However a few works can be found in the literature on the behaviour of water droplets in the hot air layer, considering the simultaneous changes of heat and the mass of droplets with the change of the momentum of moving water droplets. Moreover there is a significant amount of radiation emitted from a fire that also affects the rate of evaporation of droplets. Therefore it is essential to identify the capability of any CFD based model in predicting the evaporation of water mist sprayed from a nozzle in a fire-induced hot environment.

Performance of a spray depends on its distribution pattern produced on a horizontal plane. Hence predicting the distribution of a spray injected from a nozzle is important for a CFD based model. Various experimental and numerical studies [[Putorti et al. 1995](#); [Chow and Yin 1999](#); [McGrattan 2001](#); [Widmann 2001](#); [Ren et al. 2011](#)] have been conducted on the characterisation of spray patterns; however, most are related to sprays from conventional sprinklers. Spray kinematics and the dispersion of water-mist sprays are governed by the initial size of the droplets and the velocity characteristics of the spray [[Ren et al. 2011](#)]. The initial size of the water mist produced by a nozzle is smaller in size compared to the droplets of spray produced by a conventional sprinkler and the mists are injected with a high velocity

from the nozzle. As a result, the spray dynamics of water mists, such as momentum, drag force, buoyancy force, etc., produced by a nozzle are unlike that of a conventional sprinkler. A benchmark experiment would be useful to quantify the distribution of a water mist spray on a horizontal surface produced by a nozzle and to validate any CFD based model in predicting the distribution of the spray. This is because no experimental study has been found in the archived literature on the distribution of a spray produced by a water mist nozzle.

Another important feature of any CFD based model in simulating the burning of a solid or liquid fuel is that the model is capable of predicting the pyrolysis of the material [Abu-Bakar and Moinuddin 2015]. The burning of any material is instigated by the release of volatiles from the material due to the decomposition of it caused by high temperatures. Pyrolysis has the main role in controlling the rate of mass loss and the history of temperatures at surface and in-depth [Lee 2006]. Moreover the suppression of a fire by water droplets is also affected by the reduction of pyrolysis of the material. When the droplets of a spray reach a fire, they wet the burning surface and cool it by extracting heat from the hot surface. As the result the pyrolysis of the material is reduced and the fire is extinguished. Therefore a CFD based model should be capable of predicting the rate of pyrolysis to simulate both the growth and suppression of a fire by water spray.

Pope and Bailey [2006] measured gas temperatures in an experiment of a post-flashover compartment fire and compared the results with the prediction by FDS (ver. 4.0) using a prescribed HRR in the simulation. They found that FDS was able to predict the temperatures accurately. Recently, Byström et al. [2012] and Yang et al. [2010] conducted a similar study, as mentioned earlier, using FDS (ver. 5.0) and found that FDS was able to predict the gas temperature accurately with a prescribed HRR. However, in their study, FDS failed to predict the time of suppression of the fire. Although the HRRs of the fires were prescribed in those studies, the capability

of a CFD model cannot be assessed until it can predict the growth and spread of a fire without prescribing a design fire. As mentioned above, pyrolysis of the material governs the prediction of the growth, spread and suppression of a fire and the model should be capable of predicting the burning rates of a material resulting from its pyrolysis.

Therefore three fields are identified from the above literature review for investigating the capability of a state-of-the-art CFD model before using it for simulating the growth of a fire and its suppression by water-mist spray. These three fields that the model should be capable of simulating are (i) the behaviour of the evaporation of water droplets at high temperature; (ii) the distribution of spray on a horizontal surface; and (iii) the growth of fire in terms of its burning rate and suppression by water-mist sprays in which they are governed by the pyrolysis of fuel.

In this study a state-of-the-art CFD based model, FDS (ver. 6.0), is used as this offers several advantages over other CFD based tools. One is that FDS can simulate the pyrolysis of fuels that are considered very important in modelling the growth of fires and their suppression by water mist. Another main advantage is that it has been developed and tested for modelling compartment fires, which is the result of the work of an international team and researchers. Moreover, in recent years, it has been used for a large number of studies and applications for the interaction of water sprays with fire plumes and smoke layers [Kim and Ryou 2003; Yang et al. 2010; Zhang and Chow 2013]. It has also been used to evaluate the performance of sprinklers or water-mist nozzles and the extinction times of fire [Kim and Ryou 2003; Yang et al. 2010; Jenft et al. 2014], reconstruction of arson fires [Pope and Bailey 2006; Shen et al. 2008] and for the modelling of firefighting [Kim and Ryou 2003; Byström et al. 2012]. Moreover, another version of FDS, wildland fire dynamic simulator (WFDS) is being used for simulating wildland fires [Mell et al. 2010; Moinuddin et al. 2010; Mell et al. 2011].

After validating and verifying the FDS model in those fields, this study can be further extended by conducting a qualitative parametric exploration using it on the effect of different factors in suppressing fires by water-mist sprays. The factors may include the location of the fire, obstruction on the fire, number of nozzles and size of the droplets.

### **1.4 Aims of the research**

The literature review presented above has identified several areas worthy of further research. We have selected four main areas for detailed study. They are:

1. To develop a detailed understanding of the science of the evaporation of water droplets by constructing a semi-empirical model, and validating and verifying it against experimental and analytical data. The proposed model is compared with a state-of-the-art CFD based model (FDS).
2. To design and conduct a benchmark experiment to measure the distribution of flux densities produced by spray nozzles. The results can be used to validate any CFD based model in simulating the distribution of a spray.
3. To investigate the capability of FDS in predicting the growth of fires and their suppression by water mists.
4. To conduct a parametric study using FDS in predicting the effect of factors, such as the location of fires, obstructions, the number of nozzles and the size of droplets on the suppression of fire using water-mist spray.

### **1.5 Methodology**

To achieve the first aim of this project, a semi-empirical model of water droplet evaporation is developed based on the conservation of mass, momentum and energy,

and the proposed model is validated against the experimental and analytical data. The proposed model has also been used to validate a state-of-the-art CFD based model, FDS (ver. 6.0). Then the semi-empirical model is used to examine the behaviour of different sizes of water mist in a smoke layer induced by a room fire.

To achieve the second aim, a benchmark experiment is designed and conducted to characterise the distribution of water flux densities of sprays produced by the water-mist nozzle on a horizontal surface. As no experimental study has been found in the archived literature on the distribution of sprays produced by water mist nozzle, the result of this experiment can be useful to validate the capability of any CFD based model in this scenario. In this study, simulations are carried out to examine the capability of FDS in predicting the distribution of the water flux densities of the spray.

To achieve the third aim, the capability of FDS is examined in predicting the burning rates of PMMA in the presence and absence of water mist. The predicted burning rates of PMMA are compared with the experimental data. In this case the published data by [Magee and Reitz \[1974\]](#) has been used to validate the numerical results of FDS.

To achieve the fourth aim of this project, a parametric study has been conducted using FDS to evaluate the performance of water-mist spray under a range of fire conditions. The parameters involve the effect of obstructions, the locations of fires, the number of nozzles and the size of the droplets.

# Chapter 2

## CFD model description

# Chapter 2

## CFD model description

---

### 2.1 Introduction

In the last decade, the Fire Dynamics Simulator (FDS) and the coupled three-dimensional visualisation program, Smokeview, have been widely used as a CFD based tool for the prediction of fire generation, growth and the spread and suppression of fires, and for the prediction of smoke and gas movement in building fires. FDS has been developed by the National Institute of Standards and Technology (NIST), USA. The FDS model is appropriate for low-speed, thermally driven flow, with an emphasis on smoke and heat transport from fires [McGrattan et al. 2014]. The details of the model are presented in the following sections.

### 2.2 Features and program version of FDS

The first version of the program was publicly released in February 2000. Since then the program has seen several major improvements and new features implemented. This study is carried out using FDS (ver. 6.0) by compiling the FORTRAN source codes before release of the official version. Once the official version was released in November 2013, it has been used for the study. FDS was developed primarily as a tool for solving practical problems in fire protection engineering and also as a tool to study fundamental fire dynamics and combustion.

FDS can be used to model the following phenomena:

- low speed transport of heat and combustion products (mainly smoke) from fire
- convective heat transfer between the gas and solid surfaces
- radiative heat transfer
- pyrolysis
- fire growth
- flame spread
- activation of sprinklers and heat detectors
- fire suppression by sprinklers/nozzle.

FDS is a CFD based software package that is widely used by fire safety professionals. There are many studies where FDS has been used for simulations. Selected studies are reviewed and listed in the references.

### **2.3 Governing equations**

The computational domain is discretised into cells or control volumes and the value of the unknown variable  $\Phi$  is calculated at the cell centre. Since these cells are not infinitely small or small enough to capture small turbulent eddies, turbulence models are solved along with the flow equations in order to approximately factor in the effects of these turbulent eddies on the flow field. Once the boundary conditions and initial conditions are applied, the differential form of the governing mass, momentum and energy equations are discretised at each node to generate a large system of algebraic equations that are numerically solved to obtain the values of all the required variables  $\Phi$  at all the cell centres. The governing equations that have been used in FDS are presented below.

#### **2.3.1 Modelling of mass, species and enthalpy transport**

The hydrodynamic model Fire Dynamics Simulator numerically solves a form of Navier-Stokes equation appropriate for low thermally driven flow (Mach number <

0.3) with an emphasis on smoke and heat transport from fires. The core algorithm is an explicit predictor-corrector scheme that is second order accurate in space and time. The basic conservation equations for the mass and momentum for a Newtonian fluid are presented as a set of partial differential equations and solved by the Fire Dynamics Simulator program. The airflow, including the thermal distribution, is simulated by solving one set of the coupled state conservation equations of mass, momentum and energy.

(i) *Continuity equation*

The mass transport equations are solved using the basic predictor-corrector scheme [McGrattan et al. 2014, p. 14]:

$$\frac{\partial \rho}{\partial t} + \nabla \cdot \rho U = 0 \quad (2.1)$$

where the first term describes the density changes with time and the second term defines the mass convection.  $U$  is the vector describing the instantaneous velocity in the u, v and w directions.

(ii) *Momentum equation*

$$\frac{\partial \rho \bar{U}}{\partial t} + \nabla \cdot (\rho \bar{U} \bar{U}) = -\nabla p + \nabla \cdot \tau_{ij} + \rho g + \nabla \cdot \tau_{turb} \quad (2.2)$$

Here, the left hand side represents the increase in momentum and inertia forces, while the right hand side comprises forces acting on it. In this equation,  $\bar{U}$  represents filtered velocity (approximately instantaneous). The forces on the right hand side include pressure  $p$ , gravity  $g$  and a measure of the viscous stress tensor  $\tau_{ij}$  acting on the fluid within the control volume.  $\tau_{ij}$  is defined as:

$$\tau_{ij} = \mu \left( 2 S_{ij} - \frac{2}{3} (\nabla \cdot \bar{U}) \delta_{ij} \right) \quad (2.3)$$

where  $\mu$  is the molecular viscosity and  $S_{ij}$  is

$$S_{ij} = \frac{1}{2} \left( \frac{\partial u_i}{\partial x_j} + \frac{\partial u_j}{\partial x_i} \right) \quad (2.4)$$

It further includes a term  $\tau_{turb}$  representing filtered turbulence known as sub-grid scale Reynolds stress that is further described below.

FDS uses large eddy simulation (LES) methodology to model turbulence [McGrattan et al. 2014, p. 21]. LES is a technique used to model the dissipative processes (viscosity, thermal conductivity, material diffusivity) that occur at length scales smaller than those that are explicitly resolved on the numerical grid. FDS has four turbulence models: the constant coefficient Smagorinsky model, the dynamic Smagorinsky model, Deardorff's model and Vreman's model. The Deardorff model is the default in FDS. The LES turbulence model equation is shown below:

$$\tau_{turb} = \mu_{turb} \left( 2 S_{ij} - \frac{2}{3} (\nabla \cdot \bar{U}) \delta_{ij} \right) \quad (2.5)$$

$$\text{where } \mu_{turb} = \rho (C_s \Delta)^2 |S| \quad (2.6)$$

$$|S| = \left( 2 S_{ij} S_{ij} - \frac{2}{3} (\nabla \cdot U)^2 \right)^{\frac{1}{2}} \quad (2.7)$$

In the above,  $C_s = 0.2$  is a constant model coefficient,  $\Delta = (\delta x \delta y \delta z)^{\frac{1}{3}}$  is the filter width,  $S$  is the strain rate.

### (iii) Equation of state

FDS does not solve the energy balance equation [McGrattan et al. 2014, p. 9]. FDS uses the ideal gas equation for temperature and the Poisson equation for pressure (though the energy balance equation is ideal) to realise a quicker solution. The ideal gas equation:

$$\bar{p} = \frac{\rho R T}{M} \quad (2.8)$$

where  $\bar{p}$  is the background pressure,  $R$  is the molar gas constant = 8.3145 kJ/(kmol K) and  $M$  is the molecular weight.

(iv) *Poisson equation for pressure*

$$\nabla^2 H = - \frac{\partial (\nabla \cdot U)}{\partial t} - \nabla \cdot F \quad (2.9)$$

$$F = -U \times \omega - \tilde{p} \nabla \left( \frac{1}{\rho} \right) - \left( \frac{1}{\rho} \right) [(\rho - \rho_0) g + f_b + \nabla \cdot \tau_{ij}] \quad (2.10)$$

Here,  $H$  is the total pressure ( $\bar{p} + \tilde{p} - \rho g h$ ), where  $h$  is the height from ground level.  $U$  is the velocity vector describing the instantaneous velocity component of  $u$ ,  $v$  and  $w$  in  $x$ ,  $y$  and  $z$  directions, respectively.  $F$  is referred to collectively as momentum flux.  $\tilde{p}$  is the perturbation pressure, while  $\omega$  represents vorticity.  $\rho$  is the instantaneous density and  $\rho_0$  represents density at initial temperature.  $g$  is the acceleration of gravity and  $f_b$  is the external force vector (excluding gravity).  $\tau_{ij}$  is the viscous stress tensor and is described earlier.

(v) *Species equation*

To simulate smoke transport, FDS needs to track at least six gas species (Fuel, O<sub>2</sub>, CO<sub>2</sub>, H<sub>2</sub>O, CO, N<sub>2</sub>) plus soot particulate [McGrattan et al. 2014, p. 6]. The following species equation is solved for each species represented by  $Y_i$  (mass fraction of  $i$ th species) where  $i = 1, 2, 3 \dots$  etc.

$$\frac{\partial(\rho Y_i)}{\partial t} + \frac{\partial}{\partial x} (\rho u Y_i) + \frac{\partial}{\partial y} (\rho v Y_i) + \frac{\partial}{\partial z} (\rho w Y_i) = \nabla \cdot \rho D_i \nabla Y_i + \dot{w}''' \quad (2.11)$$

$\dot{w}'''$  is the production rate of the  $i$ th species during combustion,  $D_i$  is the diffusion coefficient of  $i$ th species.

### 2.3.2 Modelling of pyrolysis

In the case of solid fuel, FDS assumes that heat conduction occurs only in the direction normal to the surface [McGrattan et al. 2014, p. 67]. The one-dimensional heat transfer equation for the solid phase temperature  $T_s(x, t)$ , as mentioned below, is applied in the direction  $x$  pointing into the solid:

$$\rho_s c_s \frac{\partial T_s}{\partial t} = \frac{\partial}{\partial x} \left( k_s \frac{\partial T_s}{\partial x} \right) + \dot{q}_s''' \quad (2.12)$$

The source term,  $\dot{q}_s'''$ , consists of chemical reactions and radiative absorption:

$$\dot{q}_s''' = \dot{q}_{s,c}''' + \dot{q}_{s,r}''' \quad (2.13)$$

Here, the term  $\dot{q}_{s,c}'''$  is the heat production (loss) rate that is given by the pyrolysis mode for different types of fuel. The source term in the pyrolysis model is:

$$\dot{q}_{s,c}''' = -\rho_s(0) \sum r_{\alpha\beta}(x) H_{r,\alpha\beta} \quad (2.14)$$

where  $r_{\alpha\beta}$  is the rate of reaction which depends on Arrhenius function and  $H_{r,\alpha\beta}$  is the heat of reaction. It is assumed that fuel pyrolysis takes place on the surface, thus the heat required to vaporise the fuel is extracted from the incoming energy flux. The pyrolysis rate is given by an Arrhenius expression [McGrattan et al. 2014, p. 51]:

$$r_{\alpha\beta} = A \rho_s e^{-E/RT} \quad (2.15)$$

Values of the pre-exponential factor  $A$  and the activation energy  $E$  for the solid have to be selected carefully to describe the burning behaviour. The actual burning rate is determined by the overall energy balance for the solid fuel.

### 2.3.3 Modelling of radiation transport

The radiation equation is solved using a technique similar to a finite volume method for convective transport, thus the name given to it is the finite volume method (FVM)

[McGrattan et al. 2014, p. 10]. Using approximately 100 discrete angles, which are updated over multiple time steps, the finite volume solver requires about 20% of the total CPU time of a calculation, a modest cost given the complexity of radiation heat transfer.

The net contribution from thermal radiation in the energy equation is defined by [McGrattan et al. 2014, p. 9]:

$$\dot{q}_r''' \equiv -\nabla \cdot \dot{q}_r'' = \kappa(x) [U(x) - 4\pi I_b(x)] \quad (2.16)$$

$$U(x) = \int_{4\pi} I(x, s') ds' \quad (2.17)$$

where  $\kappa(x)$  is the absorption coefficient,  $I_b(x)$  is the source term, and  $I(x, s)$  is the solution of the radiation transport equation (RTE) for a non-scattering gray gas.

Water droplets can absorb and scatter thermal radiation. This is important in scenarios involving water-mist suppression systems, but also plays a role in all sprinkler cases. The absorption and scattering coefficients are based on Mie theory. The scattering from the gaseous species and soot is considered negligible and is not included in the model.

### 2.3.4 Modelling of combustion

#### (i) *Mixing-controlled model*

FDS uses the eddy dissipation concept (EDC) to model the reaction system for the combustion of fuel, with the approximation of ‘mixed is burnt’ [McGrattan et al. 2014, p. 41]. In the EDC model, all the reactants are initially unmixed and the rate of chemical kinetics is infinite. The mean chemical source term is:

$$\dot{m}_F''' = -\rho \frac{\min\left(\frac{Z_F, Z_A}{S}\right)}{\tau_{mix}} \quad (2.18)$$

where  $Z_F$  and  $Z_A$  are the lumped mass fractions of fuel and air, respectively, and  $s$  is the mass stoichiometric coefficient for air. The quantity  $\tau_{mix}$  is a time scale for mixing.

*(ii) Heat release rate*

The heat release rate per unit volume is calculated by summing the species mass production rates times the respective heat of formation:

$$\dot{q}_F''' = - \sum_{\alpha} \dot{m}_{\alpha}''' \Delta h_{f,\alpha} \quad (2.19)$$

### 2.3.5 Modelling of water-mist

*(i) Heat and mass transfer model*

In FDS, droplets are represented as discrete spheres travelling through air. Over the course of a time step, the droplets in a given grid cell evaporate as a function of the liquid equilibrium vapour mass fraction of particle,  $Y$ , the local air phase vapour mass fraction,  $Y_{\infty}$ , the droplet temperature,  $T$ , and the local air temperature,  $T_{\infty}$ . The mass and energy transfer between hot air and water droplet can be described by the following set of equations:

$$\frac{dm}{dt} = - A h_m \rho (Y - Y_{\infty}) \quad (2.20)$$

$$m c \frac{dT_p}{dt} = A h (T_{\infty} - T) + \frac{dm}{dt} L \quad (2.21)$$

The vapour mass fraction of the air,  $Y_{\infty}$ , is calculated from the gas phase mass conservation equations, and the liquid equilibrium vapour mass fraction,  $Y$ , is calculated from the Clausius-Clapeyron equation. The mass and heat transfer coefficient between water droplet and air are described by empirical correlations.

*(ii) Transport model*

In FDS, water droplet transport is modelled by the Lagrangian approach [McGrattan et al. 2014, p. 77]. The velocity and position of a droplet is obtained from the law of the conservation of momentum. The trajectory and position of each droplet satisfies the following equations:

$$\frac{d}{dt} (m v) = m g - \frac{1}{2} \rho C_d \pi r^2 v^2 \quad (2.22)$$

$$\frac{dx}{dt} = v \quad (2.23)$$

where the drag coefficient,  $C_d$ , depends primarily on the Reynolds number based on the droplet terminal velocity, which can be well represented by:

$$C_d = \begin{cases} 24 / Re & Re < 1 \\ 24 (0.85 + 0.15 Re^{0.687}) / Re & 1 < Re < 1000 \\ 0.44 & Re > 1000 \end{cases} \quad (2.24)$$

Reynolds number of droplets is represented by:

$$Re = \frac{\rho v D}{\mu} \quad (2.25)$$

where  $\mu$  is the dynamic viscosity of air.

*(iii) Droplet size distribution model*

FDS takes a sample of spherical droplets to calculate the distribution pattern. The droplet size distribution is expressed in terms of its cumulative volume fraction (CVF), which is represented by a combination of lognormal and Rosin-Rammler distributions [McGrattan et al. 2014, p. 79].

$$F(d) = \begin{cases} (2\pi)^{-\frac{1}{2}} \int_0^{D_{CVF}} (\sigma D)^{-1} e^{-\frac{[\ln(\frac{D}{D_m})]^2}{2\sigma^2}} dD & (D_{CVF} \leq D_m) \\ 1 - e^{-0.693(\frac{D_{CVF}}{D_m})^\gamma} & (D_{CVF} > D_m) \end{cases} \quad (2.26)$$

where  $D$  is the generic droplet diameter and  $D_m$  is the median droplet diameter. The median droplet diameter is a function of the sprinkler/nozzle orifice diameter, operating pressure and geometry.  $\gamma$  and  $\sigma$  are empirical constants used for the curve fitting of distribution patterns.

## 2.4 Geometry and numerical grid

FDS uses a rectilinear grid system to create a computational domain. It uses uniform meshing of the cells as default. However cells can be stretched in one or two directions of the three-dimensional coordinate system. FDS also allows creating the computational domain with regions of different grid resolutions that are known as multiple meshing. Both the grid stretching and the use of multiple meshes allow the user to apply better grid resolutions in critical areas (e.g. near the fire region) without unnecessarily increasing the demand for computational resources by applying fine mesh to the entire computational domain. The use of multiple meshes is also required when an FDS simulation is to be run in parallel processing on more than one computer.

FDS approximates the governing equations using a second-order accurate finite difference technique on a collection of either uniformly spaced or stretched three-dimensional grids. Multiple meshes of a single computational domain can be processed using message passing interface (MPI) libraries in a parallel computing system. Scalar quantities are assigned to the centre of each grid cell; vector

## Chapter 2: CFD model description

components are assigned at the appropriate cell faces. This is what is commonly referred to as a staggered grid.

Defining the obstruction in a computational domain using a rectangular grid system is a limitation of FDS, where certain geometric features of that obstruction do not conform to the rectangular grid. An example of such obstruction is the inclined part of an ISO hood. However this can be approximated by small rectangular obstructions in the parts. The more complex shape of any geometry (e.g. non-linear or curved geometry) is difficult to model in FDS.

## Chapter 3

Development of a semi-empirical model  
for the evaporation of water droplets

# Chapter 3

## Development of a semi-empirical model for the evaporation of water droplets

---

### 3.1 Introduction

The performance of WMFSS depends on many interacting factors such as the mass flow rate of water and the diameter, velocity and spatial distribution of the droplets. The droplets have the potential to cool the surrounding air, attenuate thermal radiation, and the water vapour produced by evaporation of droplets reduces the fuel vapour/air ratio by displacing oxygen [Braidech et al. 1955; Rasbash et al. 1960; Grant et al. 2000; Liu and Kim 2000; Liu and Kim 2001; Shu et al. 2005; Yao and Chow 2005; Yang et al. 2010; Mizukami et al. 2013]. Not all the droplets evaporate before striking burning surfaces and this provides a direct method of suppressing fires [Braidech et al. 1955; Rasbash et al. 1960; Mawhinney et al. 1994; Wighus 1995; Grant et al. 2000; Liu and Kim 2001].

A distinguishing feature of water-mist nozzles is that they produce fine mists consisting of droplets with diameters of less than 1000  $\mu\text{m}$ . The fine mists display fog-like behaviour that renders their fire suppression characteristics quite differently from conventional water sprays. Studies of the interaction of conventional sprinkler sprays with hot air or smoke layers [Morgan 1979; Morgan and Baines 1979; Chow and Cheung 1994; Chow and Tang 1994; Cooper 1995; Chow and Yao 2001; Zhang and Chow 2013] have focused primarily on the convective heat transfer phenomena between large water droplets and the hot air layer. It has been found that the

evaporation of larger droplets discharged by conventional sprinklers is not affected significantly by the fire plume [Morgan 1979; Yao and Chow 2005]. In contrast, the small droplets of water that comprise fine mists have a higher surface area/volume ratio and this results in their rapid evaporation. The mechanisms of extinction are complex and research is ongoing to understand the entire mechanism of the suppression of fire using water mist [Liu and Kim 2000]. However, to understand the mechanism of the extinguishment of fire, the knowledge of evaporative water droplet behaviour in a hot air environment is imperative.

A number of studies [Ranz and Marshall 1952; Yuen and Chen 1978; Renksizbulut and Yuen 1983; Novozhilov 2001; Thomas 2002; Vaari 2002; Li and Chow 2004; Barrow and Pope 2007; Liu et al. 2007; Li and Chow 2008; Fujita et al. 2010] reported in the published literature account for the rate of evaporation of droplets in the analysis. The rate of evaporation of falling droplets differs from that of stationary droplets due to different heat and mass transfer coefficients resulting from the change of momentum. *Ceteris paribus*, the drag coefficients of droplets depend on their diameters and velocities. In the case of water droplets emanating from a nozzle, these two variables change and this affects the drag coefficient. However this phenomenon was neglected by Novozhilov [2001] in his analysis of the transport of water droplets. When sprinkler systems are activated at a temperature of 60°C, say, the relative humidity (RH) of the surrounding air is very low, typically 5%. This is in sharp contrast with the data generated by Li and Chow [2008] who assumed that the RH of the air was 53%, yet the dry bulb temperature was 60°C. Varri [2002] assumed the droplet temperature to be identical to the surrounding air temperature in his transient one-zone model that described the total flooding water-mist fire suppression.

The Reynolds number ( $Re$ ) does have an effect on the heat and mass transfer coefficient in between water and air. However Barrow and Pope [2007] neglected

this effect by assuming the  $Re$  of droplets to be zero and this has limited the use of their model. The use of a one-zone model and its limitations in studying water-mist fire suppression systems is reported by [Li and Chow \[2004\]](#). However none of these reported studies considered the effects of thermal radiation on the behaviour of water droplets although radiative heat transfer is important in the case of fire. In addition, the effect of a high mass transfer rate and low humidity should be considered in the case of a room fire.

If we are able to accurately model the behaviour of water mists, we must be able to quantify the rate of evaporation of water considering all of the issues as discussed above. The principal objective of this work is to develop a detailed model of the evaporation of water droplets by considering:

- (i) the contribution of radiation emanating from the flame and the surrounding boundary walls to the rate of evaporation of water droplets
- (ii) the effect of high mass transfer rates on the mechanism of evaporation
- (iii) the change of the momentum of the droplets
- (iv) the variable thermo-physical properties of water and air.

In this study, the proposed model is validated and verified against experimental and theoretical data available in the published literature. The proposed semi-empirical model can be used as a validation tool for more comprehensive CFD based models. In this study we have validated Fire Dynamic Simulator (FDS) version 6.0, for example. In the second part, the proposed model will be used for a parametric study.

Subsequently the proposed model is used to assess the behaviour of water mists while travelling in a hot air layer. The profile of the temperature, diameter and position of the droplet is studied with different initial droplet sizes. The suspension time in the air and the evaporation rate of the droplet are also studied. The effect of the high mass transfer rate due to high air temperature is also observed.

## 3.2 Mathematical formulation

The rate of evaporation of a moving droplet is a manifestation of simultaneous heat, mass and the momentum transfer process as between the particle and the surrounding air. Momentum transfer affects the motion of the particle, mass transfer causes changes of the particle size, and heat transfer determines the temperature of the particle. In fact, these mechanisms are interdependent [Novozhilov 2001]. In the proposed model, the effect of the high mass transfer rate, due to high temperature and low humidity, are taken into account by modifying the heat and mass transfer coefficients.

The changes of diffusivity of water vapour through air, density and the latent heat of vaporisation of water with the change of temperature are also taken into account to improve the accuracy of the model. The droplet is considered a ‘lumped mass’ on account of the low Biot number [Holman 2002]. The shape of the droplet was assumed to be spherical, as this was not expected to give any significant error in the computation [Kakatsios and Krikkis 2001]. The assumption of uniform temperature distribution in the droplet considerably simplified the analysis of the overall computational process, since it avoided the need for a conjugate heat conduction analysis for the internal transient temperature distribution inside the droplet [Barrow and Pope 2007].

The hot air or smoke layer is assumed to be in a quasi-steady-state and this refers to a stable smoke layer which is finally formed when the ceiling jet reached the boundary wall and rebounded several times [Li and Chow 2008]. This assumption is more appropriate for the nozzles and smoke layers that are located away from the fire source or burning object. This is also supported by the experimental observations in [Bullen 1977; Veltre 1997]. Moreover this assumption is also used in a few analytical and numerical studies [Morgan 1979; Novozhilov 2001; Li et al. 2009;

[Tang et al. 2013](#); [Tang et al. 2014](#)]. The distance of the stable smoke layer from the spray nozzle can be quantified using Alpert's equation [[Alpert 1972](#)], taking into account the size of the fire and the height of the ceiling [[Alpert 1972](#); [Drysdale 2011](#)]. The mathematical models of mass and heat transfer and the momentum of a droplet are discussed in the following sections.

### 3.2.1 Mass transfer model

According to the theory of mass transfer, the mass flux per unit area from the interfacial surface of a water droplet is proportional to the mass concentration difference across the boundary layer of the droplet [[ASHRAE 1985](#)]. The mass flow rate through the surface area of the droplet can be balanced by a proportionality constant  $h_m$ ; which is mass transfer constant. Therefore the mass flow equation can be expressed as:

$$\dot{m} = h_m A (\rho_s - \rho_\infty) \quad (3.1)$$

where  $\rho_s$  and  $\rho_\infty$  are the mass concentration of water vapour on the droplet surface and in the air, respectively. The rate of change of droplet diameter can be determined from the following equation:

$$\frac{dD}{dt} = 2 h_m \frac{(\rho_s - \rho_\infty)}{\rho_w} \quad (3.2)$$

where,  $\rho_w$  is the density of water. The mass concentration of the water vapour at the surface of the droplet depends on the partial vapour pressure at the droplet surface. Under thermodynamic equilibrium conditions, the partial vapour pressure at the droplet surface depends on the surface temperature [[Li and Chow 2008](#)]. Under this condition, evaporation keeps the droplet surface in saturated condition until the droplet is totally vaporised due to heat transfer [[Hinds 1999](#)]. The vapour concentration at the surface is the saturated mass fraction of air at the temperature of

the droplet. As the mass concentration of the water particle depends on the vapour pressure of water, this can be found out from the ideal gas equation of state i.e.

$$P V = n R T \quad (3.3)$$

$$\rho = \frac{P m}{n R T} \quad (3.4)$$

where,  $P$  is the vapour pressure in Pascal,  $V$  is the volume in  $\text{m}^3$ ,  $\rho$  is the density in  $\text{kg}/\text{m}^3$ ,  $m$  is the mass in kg,  $R$  is the universal gas constant  $8314 \text{ J}/(\text{Kg}.\text{mol}.\text{K})$ , and  $T$  temperature in  $^{\circ}\text{C}$ . According to the definition of absolute humidity,  $\phi = P / P_{sat}$ ;

Therefore,

$$\rho = \frac{\phi P_{sat} m}{n R T} \quad (3.5)$$

when the relative humidity (RH) = 100 %, then  $\phi = 1$  and  $P = P_{sat}$ .

### 3.2.2 Heat transfer model

When a droplet is exposed to a higher temperature, it receives heat from its surroundings and its temperature rises to a threshold limit, at a given pressure. This temperature is known as steady state or saturation temperature. At this temperature the water droplet changes its phase from liquid to vapour [Çengel and Turner 2005]. In this situation the absorbed heat leads the droplet to evaporate and the evaporation keeps the droplet surface in its saturated condition until the droplet is completely vaporised due to heat and mass transfer. Under thermal steady state conditions, the heat of vaporisation is supplied to the droplet surface from the surrounding air, flame and hot objects. Therefore, the energy equation for droplets can be set up, as the heat transfer rate to the droplet is equal to the rate of heat absorbed by a droplet where the heat would vaporise some water and change its temperature.

The heat transfer rate from air to droplet due to convection can be expressed by using the transient energy equation:

$$\dot{Q}_c = h_c A (T_\infty - T) \quad (3.6)$$

The heat storage rate in the droplet is given by:

$$\dot{Q}_{st} = \frac{d}{dt} (m c_{pw} T) \quad (3.7)$$

The energy flux rate leaving the droplet surface due to evaporation can be expressed as:

$$\dot{Q}_e = \dot{m} L \quad (3.8)$$

The heat transfer rate from a boundary wall to the droplet due to radiation can be expressed by using the following transient energy equation:

$$\dot{Q}_{rad-bw} = \sigma \varepsilon A (1 - F) (T_{bw}^4 - T^4) \quad (3.9)$$

The heat transfer rate from a flame to the droplet due to radiation can be expressed by using the following transient energy equation:

$$\dot{Q}_{rad-f} = \sigma \varepsilon F A (T_f^4 - T^4) \quad (3.10)$$

In Eq. (3.6) to (3.10),  $h_c$  is the convective heat transfer coefficient,  $m$  is the mass of the droplet,  $C_{pw}$  is the specific heat capacity of the water,  $\sigma$  is the Stefan-Boltzmann constant,  $\varepsilon$  is the emissivity coefficient,  $F$  is the view factor and  $L$  is the latent heat of evaporation.

According to the conservation of energy, convective heat transfer to the droplet surface will be equal to heat stored in the droplet plus heat leaving the droplet due to the evaporation of the water particle from the droplet surface i.e.

$$\dot{Q}_c + \dot{Q}_{rad} = \dot{Q}_{st} + \dot{Q}_e \quad (3.11)$$

$$\begin{aligned} \underbrace{h_c A (T - T_\infty)}_{\text{convective heat}} + \underbrace{[\sigma \varepsilon F A (T_f^4 - T^4) + \sigma \varepsilon A (1 - F) (T_{bw}^4 - T^4)]}_{\text{radiative heat}} \\ = \underbrace{\frac{d}{dt} (m c_{pw} T)}_{\text{stored energy/heating}} + \underbrace{\dot{m} L}_{\text{evaporation}} \end{aligned} \quad (3.12)$$

In the above equation, temperature ( $T$ ) and mass of droplet ( $m$ ) are both changing with time. Therefore, considering the rate of change of temperature and mass, the transient equation of the conservation of heat can be expressed as:

$$\begin{aligned} c_{pw} m \frac{dT}{dt} = h_c A (T_\infty - T) + \{\sigma \varepsilon F A (T_f^4 - T^4) + \sigma \varepsilon A (1 - F) (T_{bw}^4 - T^4)\} \\ - \frac{dm}{dt} L \end{aligned} \quad (3.13)$$

In the calculation, temperature distribution throughout the droplet volume was assumed to be uniform and this assumption is equivalent to saying that internal conduction resistance is very small compared to surface convection resistance in the droplet. As the droplet diameter is very small, such an assumption yield estimates within about 5 per cent [Holman 2002]. However this assumption is valid when the following condition is met:

$$Bi = \frac{h_c (V / A)}{k_w} < 0.1 \quad (3.14)$$

For water-mist droplets of 1000  $\mu\text{m}$  or smaller, Biot number,  $Bi$ , is found to be less than 0.07 in our study and therefore ‘lumped mass’ assumption can be applied.

### 3.2.3 Momentum model

The velocity of the droplet can be obtained by solving the momentum equation for the droplet. When a body is falling from a height, body force (or weight) works in the downward direction and the resistance of air drag and buoyancy force work in the

upward direction. Therefore, according to the conservation of momentum, the resultant momentum of a droplet is:

$$F_r = F_g - F_d - F_b \quad (3.15)$$

where  $F_r$  denotes resultant force and  $F_g$ ,  $F_d$  and  $F_b$  denote force due to gravity, drag and buoyancy, respectively. The drag force on a body depends on the density of fluid through which the object is moving, velocity of the object and area of the object. When a droplet is moving through air, drag force can be calculated by:

$$F_d = \frac{1}{2} \rho_a v^2 C_d A_{proj} \quad (3.16)$$

The buoyancy force on the droplet can be expressed by:

$$F_b = \frac{1}{6} \rho_a \pi D^3 g \quad (3.17)$$

In Eq. (3.16) and (3.17),  $\rho_a$  is the air density,  $C_d$  is the coefficient of drag and  $v$  is the velocity (or relative velocity) of the droplet. In the case of a droplet travelling through a stationary hot layer,  $v$  becomes the absolute velocity. Therefore the momentum equation can be written as:

$$\frac{d(mv)}{dt} = mg - \frac{1}{2} \rho_a v^2 C_d A_{proj} - \frac{1}{6} \rho_a \pi D^3 g \quad (3.18)$$

Here,  $m$  and  $v$  are both changing with time. Expanding the above equation by partial differentiation, the equation for droplet velocity can be obtained as:

$$\frac{dv}{dt} = g \frac{(\rho_w - \rho_a)}{\rho_w} - \frac{3}{4} \frac{C_d \rho_a v^2}{\rho_w D} - \frac{3v}{D} \frac{dD}{dt} \quad (3.19)$$

In the above equation,  $\rho_a$  is the air density,  $C_d$  is the coefficient of drag and  $v$  is the velocity (or relative velocity) of the droplet. In the case of a droplet travelling

through a stationary hot layer,  $v$  becomes the absolute velocity. It is to be noted that  $C_d$  for a droplet depends on the  $Re$ , which is based on the air droplet relative velocity. [Brown and Lawler \[2003\]](#) proposed a correlation between the drag coefficient and  $Re$  and compared it with 178 experimental data points. The proposed correlation was found to be quite satisfactory in relation to the experimental data in the range of  $Re < 2 \times 10^5$ . Therefore the correlation by [Brown and Lawler \[2003\]](#) is used here which is:

$$C_d = \frac{24}{Re} (1 + 0.15 Re^{0.681}) + \frac{0.407}{1 + \frac{8710}{Re}} \quad (3.20)$$

The position of a droplet in the air can be found from the velocity equation:

$$\frac{dy}{dt} = v \quad (3.21)$$

where  $y$  is a position vector. It is along the downward direction of the movement of the droplet with upward positive.

### 3.2.4 Calculation of rate constants

The mass transfer coefficient,  $h_m$ , can be calculated by using the correlation for Sherwood number,  $Sh$ . [Smolík et al. \[2001\]](#) did an experimental study on the evaporation of a water droplet in ventilated conditions and connected the evaporation theory with heat and mass transfer. They measured the mass transfer of water droplets to air and compared it with predicted values using the correlation by [Woo and Hamielec \[1971\]](#), [Ranz and Marshall \[1952\]](#), [Wedding et al. \[1986\]](#) and [Beard and Pruppacher \[1971\]](#). In the comparison they found that the prediction by [Beard and Pruppacher \[1971\]](#) was in good agreement with the experimental results. The correlation for the mass transfer number by [Beard and Pruppacher \[1971\]](#) is:

$$Sh = 2.0 + 0.216 \left( Re^{\frac{1}{2}} Sc^{\frac{1}{3}} \right)^2, \quad For \left( Re^{\frac{1}{2}} Sc^{\frac{1}{3}} \right) < 1.4 \quad (3.22)$$

$$Sh = 1.56 + 0.616 \left( Re^{\frac{1}{2}} Sc^{\frac{1}{3}} \right), \text{ For } \left( Re^{\frac{1}{2}} Sc^{\frac{1}{3}} \right) \geq 1.4 \quad (3.23)$$

$$\text{where, } Sh = \left( \frac{h_m D}{\mathcal{D}_{AB}} \right) \text{ or, } h_m = \left( \frac{Sh \mathcal{D}_{AB}}{D} \right) \quad (3.24)$$

In the above equations, Schmidt number,  $Sc$ , is a dimensionless number defined as the ratio of momentum diffusivity (viscosity) and mass diffusivity, and the Reynolds number,  $Re$ , is the ratio of inertia force to viscous force. The equation of Schmidt and Reynolds number can be calculated using the following equations:

$$Sc = \frac{\nu_a}{\mathcal{D}_{AB}} = \frac{\mu_a}{\rho_a \mathcal{D}_{AB}} \quad (3.25)$$

$$Re = \frac{\rho_a v D}{\mu_a} \quad (3.26)$$

The convective heat transfer coefficient,  $h_c$ , can be calculated by using the correlation for Nusselt number,  $Nu$ . [Beard and Pruppacher \[1971\]](#) proposed an improved correlation for  $Nu$  from laboratory experiments. They did experiments on drop diameters in the range of 40 to 1200  $\mu\text{m}$ . The correlation for Nusselt number by them can be expressed as:

$$Nu = 2.0 + 0.216 \left( Re^{\frac{1}{2}} Pr^{\frac{1}{3}} \right)^2, \text{ For } \left( Re^{\frac{1}{2}} Pr^{\frac{1}{3}} \right) < 1.4 \quad (3.27)$$

$$Nu = 1.56 + 0.616 \left( Re^{\frac{1}{2}} Pr^{\frac{1}{3}} \right), \text{ For } \left( Re^{\frac{1}{2}} Pr^{\frac{1}{3}} \right) \geq 1.4 \quad (3.28)$$

$$\text{where } Nu = \frac{h_c D}{k_a} \text{ or, } h_c = \frac{k_a Nu}{D} \quad (3.29)$$

This relationship was found to be in good agreement with the numerical results of [Woo and Hamielec \[1971\]](#). [Smolík et al. \[2001\]](#) also confirmed this relationship to be in good agreement with their experimental results for evaporation of 1-hexanol droplets. In addition, [Pruppacher and Rasmussen \[1979\]](#) investigated the evaporation

rate of large water droplets falling at terminal velocity in air. Their results showed that the applicable range of Eq. (3.27) and (3.28) can be extended to drop diameters up to 5000  $\mu\text{m}$ .

In the above equations, Prandtl number,  $Pr$ , is the ratio of viscous diffusion rate ( $\nu$ ) to thermal diffusion rate ( $\alpha$ ) of air i.e.

$$Pr = \frac{\nu}{\alpha} = \frac{c_p \mu_a}{k} \quad (3.30)$$

[Slattery and Bird \[1958\]](#) proposed a correlation from a combination of kinetic theory and corresponding states arguments to calculate the mass diffusivity coefficient,  $\mathcal{D}_{AB}$ . According to their correlation for a binary gas mixture,  $\mathcal{D}_{AB}$  is inversely proportional to the pressure, increases with increasing temperature, and is almost independent of composition for a given gas pair. The advantage of this correlation is that it is convenient to use it, as the critical temperature and molar volume of different species are available. The correlation, given by [Slattery and Bird \[1958\]](#), is as given below:

$$\frac{P \mathcal{D}_{AB}}{(P_{cA} P_{cB})^{1/3} (T_{cA} T_{cB})^{5/12} \left( \frac{1}{M_A} + \frac{1}{M_B} \right)^{1/2}} = a \left( \frac{T}{\sqrt{T_{cA} T_{cB}}} \right)^b \quad (3.31)$$

where  $a$  and  $b$  are the constant of the empirical relationship. For an air-water system,  $a = 3.64 \times 10^{-4}$  and  $b = 2.334$ . The advantage of this correlation is that it is convenient to use it, as the critical temperature and molar volume of different species are available.

### 3.2.5 Correction to the rate constants for high mass transfer rate

The use of coefficients,  $h_m$  and  $h_c$ , are limited to the case of low mass transfer rate. In the case of high temperature and low humidity, the evaporation rate is high and this invokes the high mass transfer rate and affects the heat transfer rate as well.

Hence correction factors,  $\theta_m$  and  $\theta_c$ , are applied to get the coefficient of mass and heat transfer, respectively, for high mass transfer rates [Bird et al. 1960]. The correction factors,  $\theta_m$ , can be calculated using the following expressions [Bird et al. 1960]:

$$\theta_m = \frac{h_m^*}{h_m} \quad (3.32)$$

where  $h_m^*$  is the coefficient of mass transfer for high mass transfer rate. Therefore,  $h_m$  in Equations (3.1) and (3.2) is replaced by  $h_m^*$ .  $\theta_m$  and can be calculated from the following equations:

$$\theta_m = \frac{\ln(R_m + 1)}{R_m} \quad (3.33)$$

$$R_m = \frac{x_{w0} - x_{w\infty}}{1 - x_{w0}} \quad (3.34)$$

where  $x_{w0}$  is the mole fraction water at the surface of the droplet and  $x_{w\infty}$  is the mole fraction of water in air. The value of  $x_{w0}$  can be determined by using the relation [Bird et al. 1960]:

$$x_{w0} = \frac{P_{water}}{P_{air}} \quad (3.35)$$

where  $P_{water}$  and  $P_{air}$  are water vapour and air pressure, respectively, in an air-water system. The correction factors,  $\theta_c$ , can be calculated using the following expressions [Bird et al. 1960]:

$$\theta_c = \frac{h_c^*}{h_c} \quad (3.36)$$

where  $h_c^*$  is the coefficient of heat transfer for a high mass transfer rate. Therefore,  $h_c$  in Equation (3.6) is replaced by  $h_c^*$ .  $\theta_c$  and can be calculated from the following equations:

$$\theta_c = \frac{\ln(R_c + 1)}{R_c} \quad (3.37)$$

$$R_c = e^\phi - 1 \quad (3.38)$$

$$\phi = \frac{N_{w0} c_{pw}}{h_c} \quad (3.39)$$

$$N_{w0} = h_m \ln(1 + R_m) \quad (3.40)$$

where  $N_{w0}$  is the molar flux of a water particle at the droplet surface.

### 3.2.6 Thermophysical properties of air and water

The density of humid air can be calculated using the ideal gas law as the sum of the densities of the two gases, dry air and water vapour, in proportion with their partial pressures i.e.

$$\rho_{humid\ air} = \frac{P_{dry\ air} M_a}{R T} + \frac{P_{vapor} M_w}{R T} \quad (3.41)$$

Saturation vapour pressure can be obtained from the equation suggested by [Buck \[1981\]](#):

$$P_{sat} = [1.0007 + (3.46 \times 10^{-6} P_{air})] \times 6.1121 \times \exp\left[\frac{17.502 T}{240.97 + T}\right] \quad (3.42)$$

This is an empirical relationship, where  $P_{sat}$  and  $P_{air}$  are in mbar, and  $T$  is in °C.

It is to be noted that the latent heat of evaporation of water,  $L$ , is not constant, rather it varies with temperature; the higher the temperature of the liquid water the lesser will be the heat required to evaporate it. A fourth order temperature dependent equation derived from the steam chart [[Çengel and Turner 2005](#)] is used to determine  $L$  within the range of 0 to 100°C. The relationship between  $L$  and  $T$  is as follows:

$$L = 7 \times 10^{-8} T^4 - 2 \times 10^{-5} T^3 + 4 \times 10^{-4} T^2 - 2.3657 T + 2500.9 \quad (3.43)$$

The other temperature dependent on the physical properties of air, such as viscosity [Touloukian et al. 1975], thermal conductivity [Touloukian and Makita 1970] and specific heat capacity [Touloukian et al. 1970], were determined by using the following correlations:

$$\mu_a = (0.1005 + 0.07848 \times T - 0.6696E - 4 \times T^2 + 0.3376E - 7 \times T^3) \times 10^{-6} \quad (3.44)$$

$$k_a = (-6.4224 + 0.1571 \times T - 0.2101E - 3 \times T^2 + 0.16E - 6 \times T^3) \times 10^{-3} \quad (3.45)$$

$$c_{pa} = (1023.2 - 0.176021 + 4.02405E - 4 \times T^2 - 4.87272E - 8 \times T^3) \quad (3.46)$$

Here,  $T$  is in K. The density of water is calculated by using the following correlation [Sifner and Klomfar 1996]:

$$\rho_w = (0.322 + 0.64166 \times Z^{(1/3)} + 0.35409 \times Z^{(2/3)} - 0.16449 \times Z^{(5/3)} - 0.56509 \times Z^{(16/3)} - 14.65649 \times Z^{(43/3)} - 2.17251 \times Z^{(110/3)}) \times 10^3 \quad (3.47)$$

where  $Z = 1 - \frac{T}{T_c}$ ;  $T_c$  is the critical temperature of water in K.

### 3.3 Computational procedure

A computational model has been developed using the equations of conservation of mass, momentum and energy as defined in the previous section. The governing differential equations are discretised and solved explicitly using a finite difference approach. The initial droplet conditions of  $D$ ,  $T$ ,  $v$  and  $y$ , together with the relevant thermophysical properties of water and air, are specified. The sequence of calculation is:

- i) Initialise  $D$ ,  $T$ ,  $v$  and  $y$  of droplet, and  $T$  and  $RH$  of air.
- ii) The mass transfer and heat transfer coefficients are calculated using Equations (3.24) and (3.29), respectively, incorporating a correction factor for high mass and heat transfer rate, using Equations (3.32) and (3.36), respectively.
- iii) The discretised differential Equations (3.2), (3.13), (3.19) and (3.21) are solved sequentially using the Euler method, to obtain the time trajectories of  $D$ ,  $T$ ,  $v$  and  $y$  of the droplet.

A general form of the discretised equations can be expressed as:

$$\phi_{t+\Delta t} = \phi_t + \left. \frac{d\phi}{dt} \right|_t \Delta t \quad (3.48)$$

where the variable  $\phi$  can represent the diameter, temperature and velocity i.e.  $D$ ,  $T$  and  $v$ . The position vector of the droplets in air is discretised as follows:

$$y = \sum_{i=1}^N v \times \Delta t \quad (3.49)$$

where  $N = \text{time}/\Delta t$ .

It is essential that the histories of  $D$ ,  $T$ ,  $v$  and  $y$  are independent of the time step,  $\Delta t$ . In our analysis it has been found that if the ratio of the diameter of droplets to the time step is less than or equal to 0.01, the solution is independent of the time step. Here, as an example, a time step independency test has been conducted for droplets with diameter 200  $\mu\text{m}$ . Figure 3.1 represents the graphical presentation of the results of the analysis and Table 3.1 represents the numeric values of the analysis.

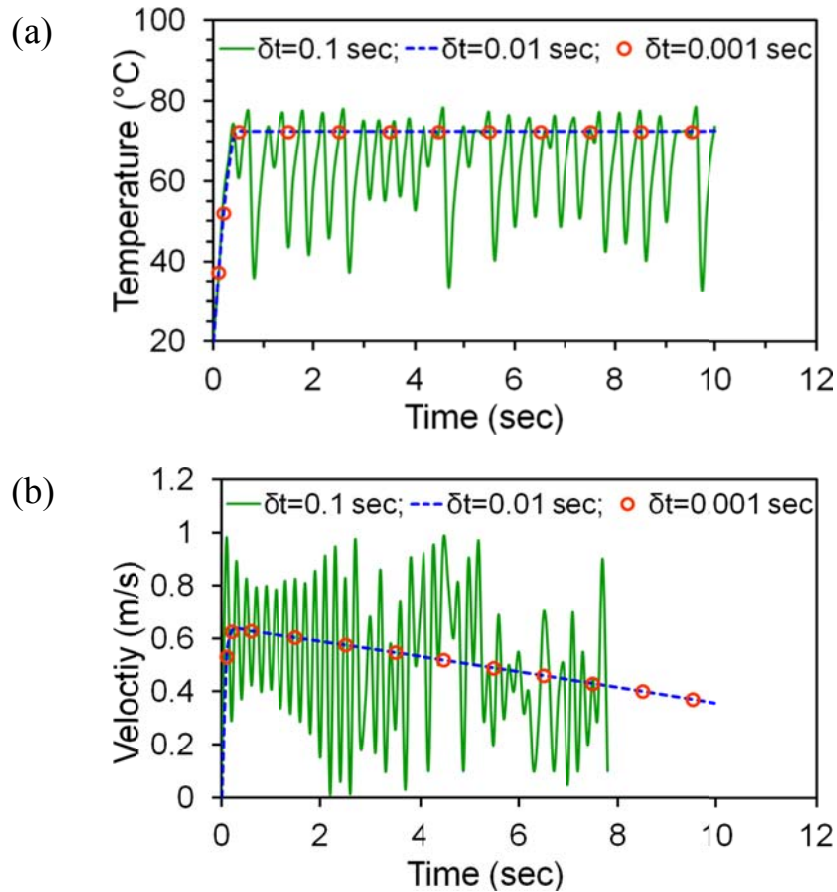


Figure 3.1: Time step dependency test (a) temperature ( $T$ ); and (b) velocity ( $v$ ).

Temperature ( $T$ ) and the terminal velocity ( $v$ ) of droplets are compared with three different time steps of 0.1, 0.01 and 0.001 seconds. In the analysis, numerical instabilities are observed when the time step is 0.1 seconds. However it has been found that the results of temperature and velocity, for the time steps of 0.01 and 0.001 seconds, are identical up to six and four significant digits, respectively. Hence a time step of 0.01 seconds can be used.

Table 3.1: The dependence of the calculated saturation temperature ( $T$ ) and terminal velocity ( $v$ ) of the droplet on the time step

Time step, $\Delta t$ (s)	0.1	0.01	0.001
Saturation temperature, $T$ (°C)	72.8018	72.4004	72.4004
Terminal velocity, $v$ (m/s)	0.6251	0.4308	0.4308

### 3.4 Model verification and validation

For the validation of the proposed model, computed results of this model are compared against the experimental data (terminal velocity) of [Gunn and Kinzer \[1949\]](#). For verification of this model, the predicted results of the saturation temperature are compared with adiabatic saturation temperature. A brief description of the theory of adiabatic saturation temperature used in this study is described in Appendix A and the details are described in reference [\[Thorpe 2001\]](#).

#### 3.4.1 Comparison with experimental data

[Gunn and Kinzer \[1949\]](#) carried out an experimental study to determine the terminal velocity of free falling water droplets in stagnant air. The experiment was conducted at 20°C air temperature, 1 atm pressure, 50% relative humidity and an initial temperature of the droplet of 20°C. The calculated value of the terminal velocity of the proposed model is compared with the experimental values and is presented in Figure 3.2. It can be observed that the predicted values from the proposed model almost collapsed on the experimental data. The deviation between predicted data and experimental values is not greater than 4%.

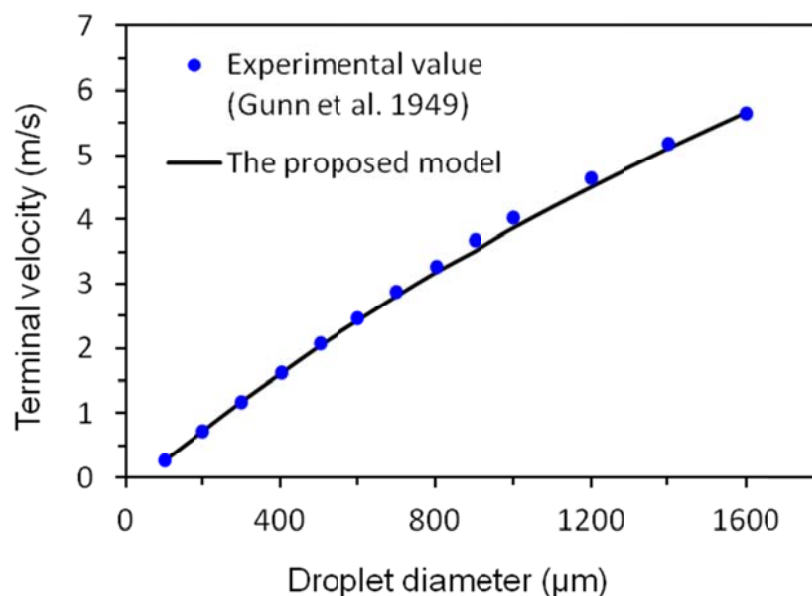


Figure 3.2: Terminal velocity of droplets.

### 3.4.2 Comparison with theoretical adiabatic saturation temperature

The predicted value of steady state temperature is compared with the theoretical adiabatic saturation temperature for different air temperature and presented in Figure 3.3. Air temperature is varied from 5 to 95°C with relative humidity 40%. Initial water temperature is taken as 20°C. It is found that the predicted values by the proposed model agree well with the values of adiabatic saturation temperature. A comparison of the predicted values of terminal velocity and the saturation temperature of droplets with the experimental data and adiabatic saturation temperature reveals that the proposed model is capable of predicting these two parameters reasonably well. This provides the confidence to use the model as a tool to study the behaviour of individual water droplets and to validate CFD based models.

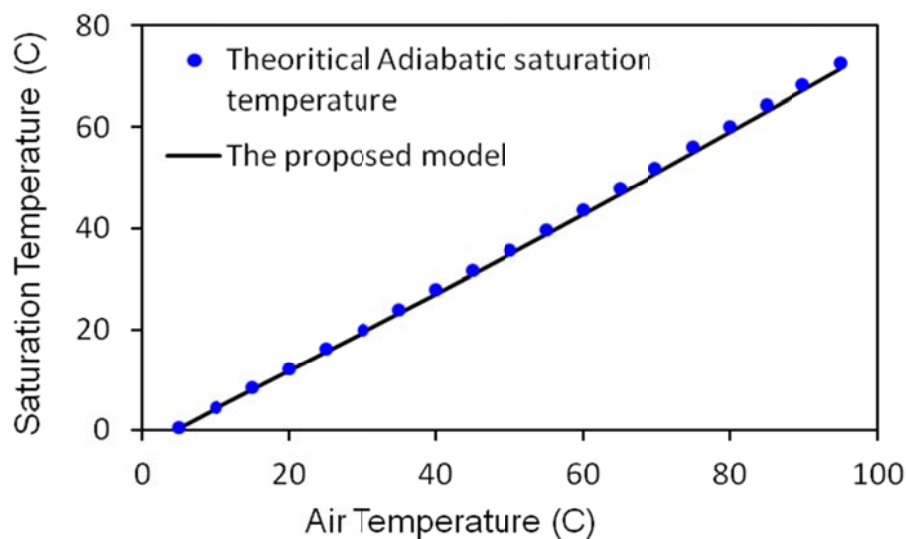


Figure 3.3: Saturation temperature of droplets.

### 3.5 Use of the model as a validation tool

In the previous section the proposed model has been validated and verified against experimental and analytical data. In this section this model is used to verify a more

comprehensive CFD based model. We have taken FDS as an example for validation. The theory of the droplet model used in FDS is described briefly in Appendix B. This model is also compared with two other models by [Li and Chow \[2008\]](#) and [Barrow and Pope \[2007\]](#). The details of the theory of the droplet model in FDS [[McGrattan et al. 2014](#)] and the details of the model by [Li and Chow \[2008\]](#) and [Barrow and Pope \[2007\]](#) are reported in the corresponding references.

### 3.5.1 Comparison with FDS

In FDS, droplets are represented as discrete spheres that have travelled through air and the transport of the droplet is modelled by the Lagrangian approach. A semi-empirical heat and mass transfer model is used to simulate the droplet evaporation. The velocity and position of the droplet is obtained from the theory of the conservation of momentum. Details of these models are given in the FDS Technical Reference Guide, Volume 1: Mathematical model [[McGrattan et al. 2014](#)].

A computational domain with dimensions of  $0.5 \text{ m} \times 0.5 \text{ m} \times 10 \text{ m}$  is created to calculate the terminal velocity and saturation temperature of the droplets. The set-up for the computational domain in the FDS model is presented in Figure 3.4. The nozzle is located at the top of the domain and a single droplet of a certain diameter is allowed to fall from the top of the domain. All sides of the domain are kept open to be consistent with the conditions associated with the proposed model. Once the computational domain is set up, the input parameters for computational measurements are incorporated in the model. The input variables are the diameter of the droplets, the initial temperature of the air and the droplets, and the relative humidity of the air. Then, the simulation is allowed to run to calculate the terminal velocity and saturation temperature of the droplets. The input parameters for the numerical model are tabulated in Table 3.2.

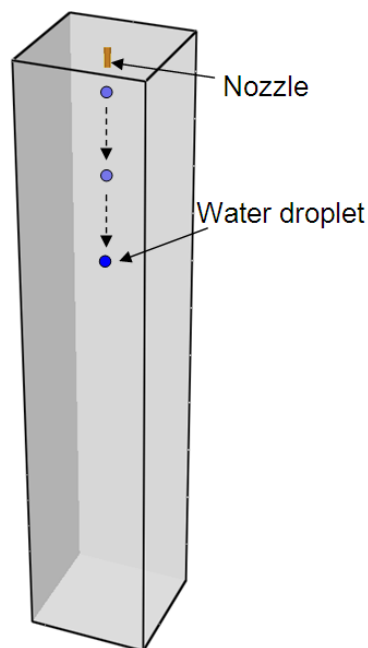


Figure 3.4: Computational domain set-up of the FDS model.

Table 3.2: The input parameters in the FDS model

Input parameters	Model for terminal vel.	Model for saturation temp.
Droplet diameters, $\mu\text{m}$	100 ~ 1600	1000
Initial droplet temperature, $^{\circ}\text{C}$	20	20
Surrounding air temperature, $^{\circ}\text{C}$	20	5 ~ 95
Relative humidity of air, %	50	40

The terminal velocities of droplets of different sizes are calculated using the proposed model and FDS. The simulation of the falling of the water droplets in air is modelled using FDS. The calculated values of the terminal velocity of the proposed model are compared with the prediction of FDS and presented in Figure 3.5. It is observed that FDS predicted values are very close to the calculated values of the proposed model. The differences in the prediction by the two models are less than 8%.

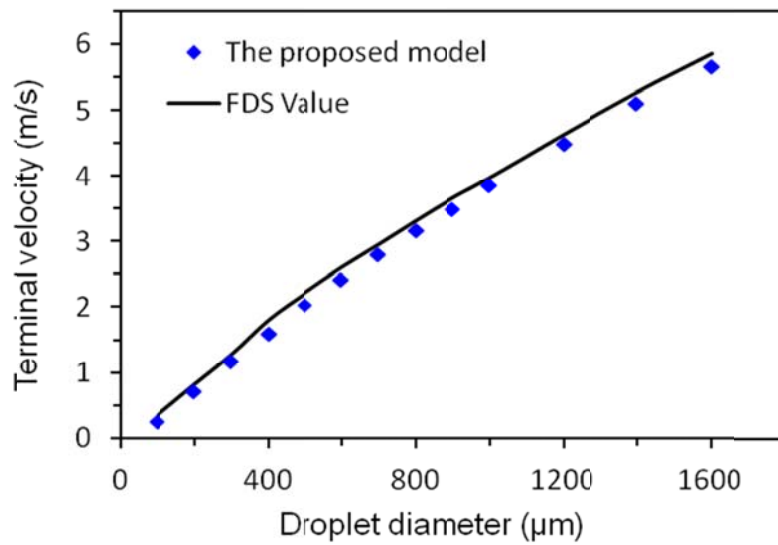


Figure 3.5: Terminal velocity of the droplets.

The proposed model and FDS are again used to calculate the saturation temperatures of the same size of droplet (1000 μm) at different temperatures of the surrounding air. The surrounding air temperature is varied between 5 and 95°C. The comparison of the results is presented graphically in Figure 3.6. Like Figure 3.5, a very close result is observed. FDS prediction does not differ by more than 10% of the calculated values by the proposed model. Hence it enforces our confidence in the FDS's capability in predicting the parameters (i.e. temperature, velocity, etc.) associated with the behaviour of an evaporative droplet in hot air.

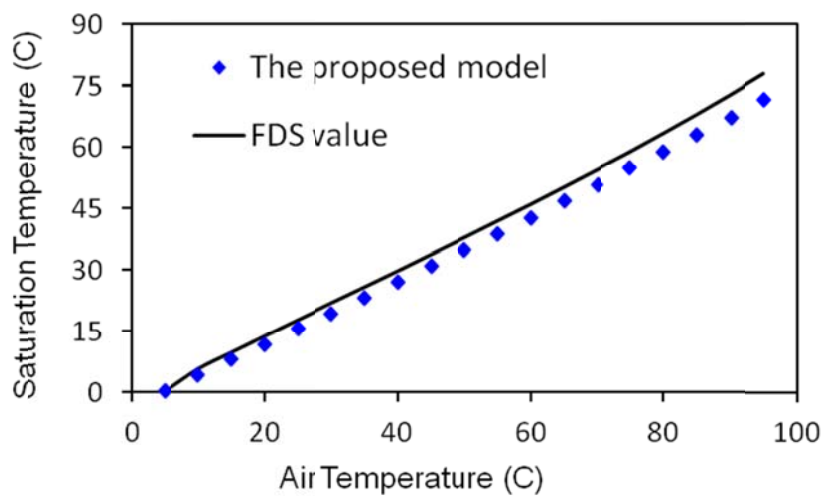


Figure 3.6: Saturation temperature of the droplets.

### 3.5.2 Comparison with the study by Li and Chow [2008]

Li and Chow [2008] conducted a study on the evaporation of water-mist droplets. They determined the diameter history of individual droplets travelling through the hot air. The same analysis was replicated, in two cases, using the proposed model with the same initial conditions as used in [Li and Chow 2008] (initial droplet diameter 100  $\mu\text{m}$ , air temperature 60°C, droplet temperature 10°C and relative humidity 76%). In the first case, the contribution of radiation is ignored, and in the second case, the contribution of radiation is considered in the model. The results of the analysis using the proposed model are compared with their results and presented in Figure 3.7. The results of the proposed model, in the first case, are almost identical with the results by Li and Chow [2008]. However the analysis by Li and Chow [2008] predicted a slower evaporation rate, in the second case, compared to the prediction of that by the proposed model. It may be primarily due to the fact that Li and Chow [2008] did not consider the contribution of radiation emanating from a flame and the surrounding boundary walls on the evaporation of the droplet. However the flame and the boundary walls emanate a substantial amount of energy through radiation. As a result, the subject droplets in the analysis by Li and Chow [2008] received a lesser amount of energy. Hence their analysis showed a slower rate of evaporation compared to the analysis of that of the proposed model.

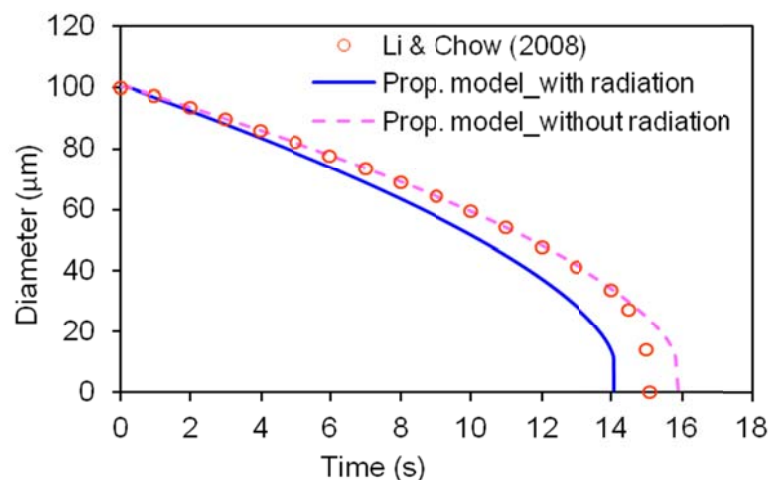


Figure 3.7: The history of the diameter of a droplet in the air.

### 3.5.3 Comparison with the study by Barrow and Pope [2007]

Barrow and Pope [2007] conducted a theoretical analysis of an evaporating water droplet moving in moist air. They determined the time of evaporation and distance travelled by a range of droplets of different sizes. The same study is replicated using the proposed model with the same initial condition as used in [Barrow and Pope 2007] (initial ambient temperature 28°C, droplet temperature 15.5°C and relative humidity 40%). A comparison of the results is presented in Figure 3.8. It is found that the model by Barrow and Pope [2007] predicts that droplets with a diameter exceeding 50  $\mu\text{m}$  evaporate more slowly than predicted by the proposed model. This is likely because Barrow and Pope [2007] assumed  $Re$  to be zero, which results in the rate of heat and mass transfer to be controlled by diffusive processes; these are slower than those that involve advection.

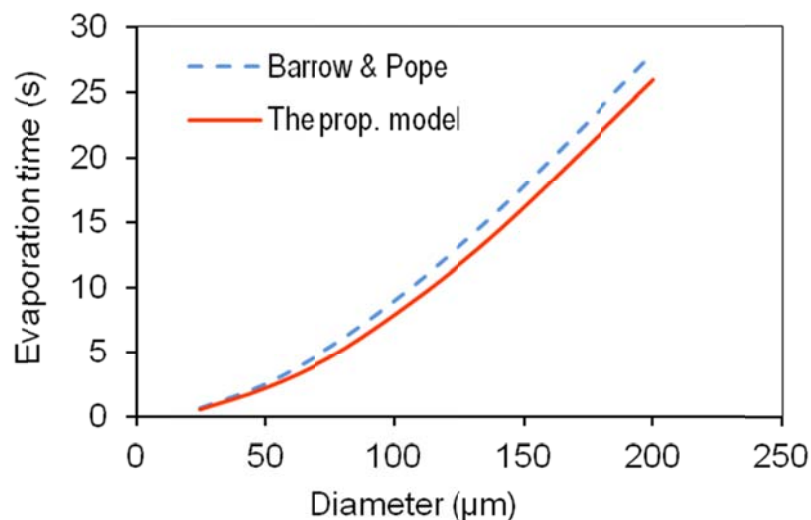


Figure 3.8: Time of evaporation of the droplets.

This assumption may be applicable when the droplet diameter is less than about 50  $\mu\text{m}$  or reduced to this size in the downstream due to evaporation. However this assumption breaks down for droplets larger than 50  $\mu\text{m}$  and this results in higher Nusselt numbers and, consequently, higher values of the heat transfer coefficient. The history of Nusselt numbers of droplets with a diameter of 200  $\mu\text{m}$  is presented in

Figure 3.9. It can be seen that at the start of the evaporation process, when the droplets are large, the Nusselt number predicted by Barrow and Pope [2007] is about 2/3 that predicted by the proposed model. Hence the rate of heat and mass transfer is predicted by Barrow and Pope [2007] to be lower than that predicted by the proposed model. Hence the proposed model may provide more accurate predictions of the rate at which oxygen is displaced from the fire surroundings. The cooling rate of the surrounding air might also be more accurately calculated by the proposed model.

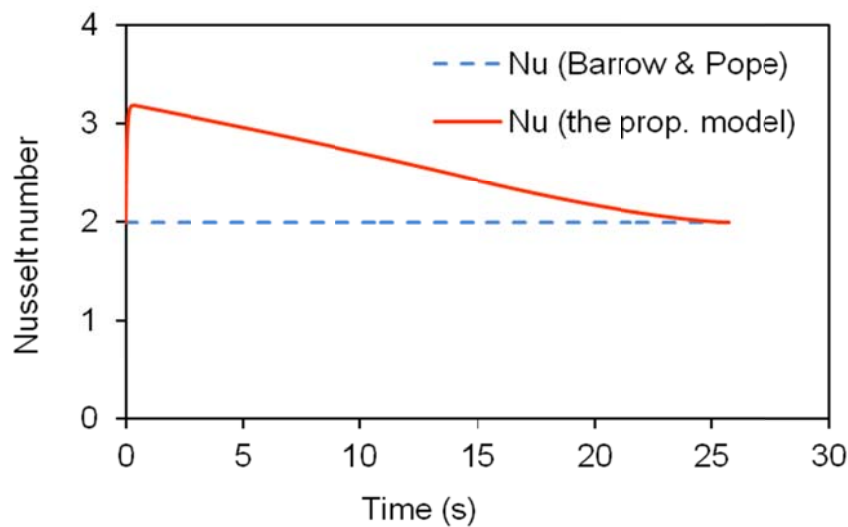


Figure 3.9: The history of the Nusselt number of droplets diameter 200  $\mu\text{m}$ .

In the conservation of the momentum equation of droplets, Barrow and Pope [2007] used Stokes' law to calculate the drag force,  $F_d$ . However, Stokes' law is restricted to  $Re$  of less than about 0.1 [Çengel and Turner 2005], hence this law underpredicts the drag force when  $Re$  exceeds this value. Barrow and Pope's [2007] model is therefore expected to underpredict the drag force for droplets larger than 50  $\mu\text{m}$  in diameter. The drag force history of droplets with diameters of 200  $\mu\text{m}$  is presented in Figure 3.10.

It can be seen that the drag force estimated by Barrow and Pope's [2007] model is lower by up to 40% compared to the value of the proposed model. As a result, it predicts that the distance travelled by the droplets is larger. A comparison of the

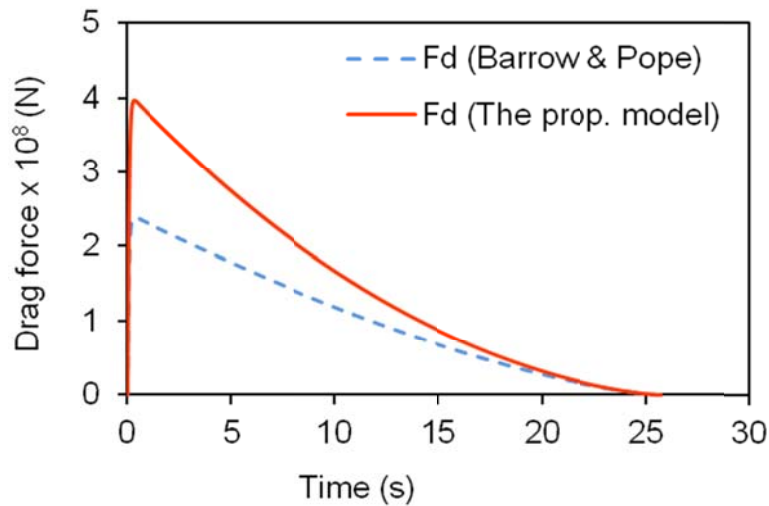


Figure 3.10: The drag force on the droplets with diameter 200  $\mu\text{m}$ .

results of the distance travelled by the droplets is presented in Figure 3.11. The droplets of diameter 200  $\mu\text{m}$  have travelled about 15 meters from the point of insertion in the air by the model of Barrow and Pope [2007], whereas the droplets have travelled only 10 meters as estimated by the proposed model. As a result, one might expect that the proposed model would predict that the droplets penetrate the hot air or smoke layer induced by a fire to a greater extent than predicted by Barrow and Pope [2007]. This may be a crucial consideration when one needs to know whether the droplets will contact any hot surface in a fire environment.

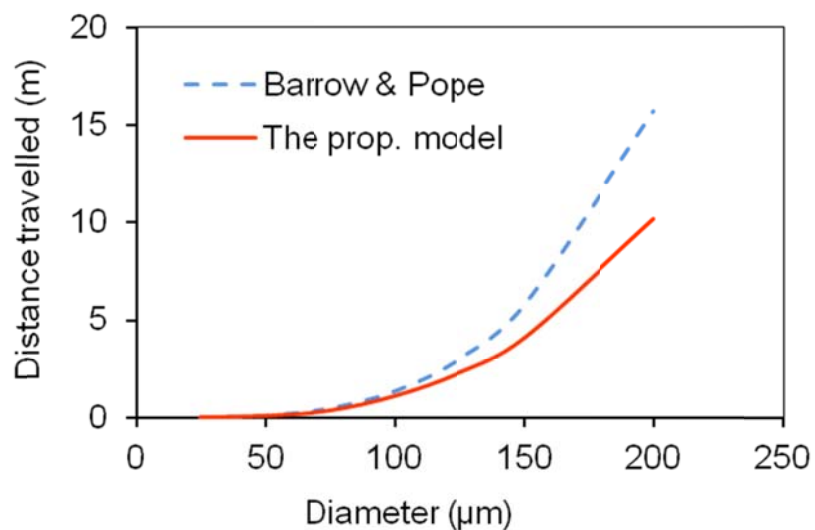


Figure 3.11: Distance travelled by the droplets.

### 3.6 Parametric study

In the parametric study, initial air conditions in a room i.e. temperature and relative humidity, are taken to be 20°C and 50%, respectively. The initial temperature of water droplets is taken to be 20°C. However, due to fire, the temperature of the room rises and when it reaches 75°C, the water-mist nozzle is deemed to be activated, as it is used as the activation temperature for most water-mist nozzles or sprinklers [Fleming 2008]. Due to increased air temperature, the relative humidity of the air also falls to 3%. The travel path of the droplets is taken as the room height of a residential or commercial building i.e. 3.0 m. The time is set to zero when the water droplets begin to fall from a ceiling mounted nozzle and the simulation is terminated when the droplets reach the floor. The airflow is assumed to be in a quiescent state, as the droplets are considered to be located far from the fire.

The temperature histories of the droplets, with initial diameters of 100, 200, 300, 400, 500, 750 and 1000  $\mu\text{m}$ , are illustrated in Figure 3.12. It can be seen that the droplet is initially heated up and increased in temperature with the progress of time. After a certain time it reaches a condition of thermal equilibrium, and at this temperature the heat absorbed by the water droplets contributes to evaporation until it has totally disappeared.

From Figure 3.12, it is found that the smaller the initial droplet size, the less time it takes to reach saturation temperature. As the size of the droplet increases, the time to reach equilibrium temperature increases. However, it is observed that the saturation temperature does not depend on the size or initial temperature of the droplets; it only depends on the initial temperature and relative humidity of the air. For 75°C air temperature, 20°C water temperature and 3% relative humidity, the equilibrium temperature of droplets is found to be 27°C.

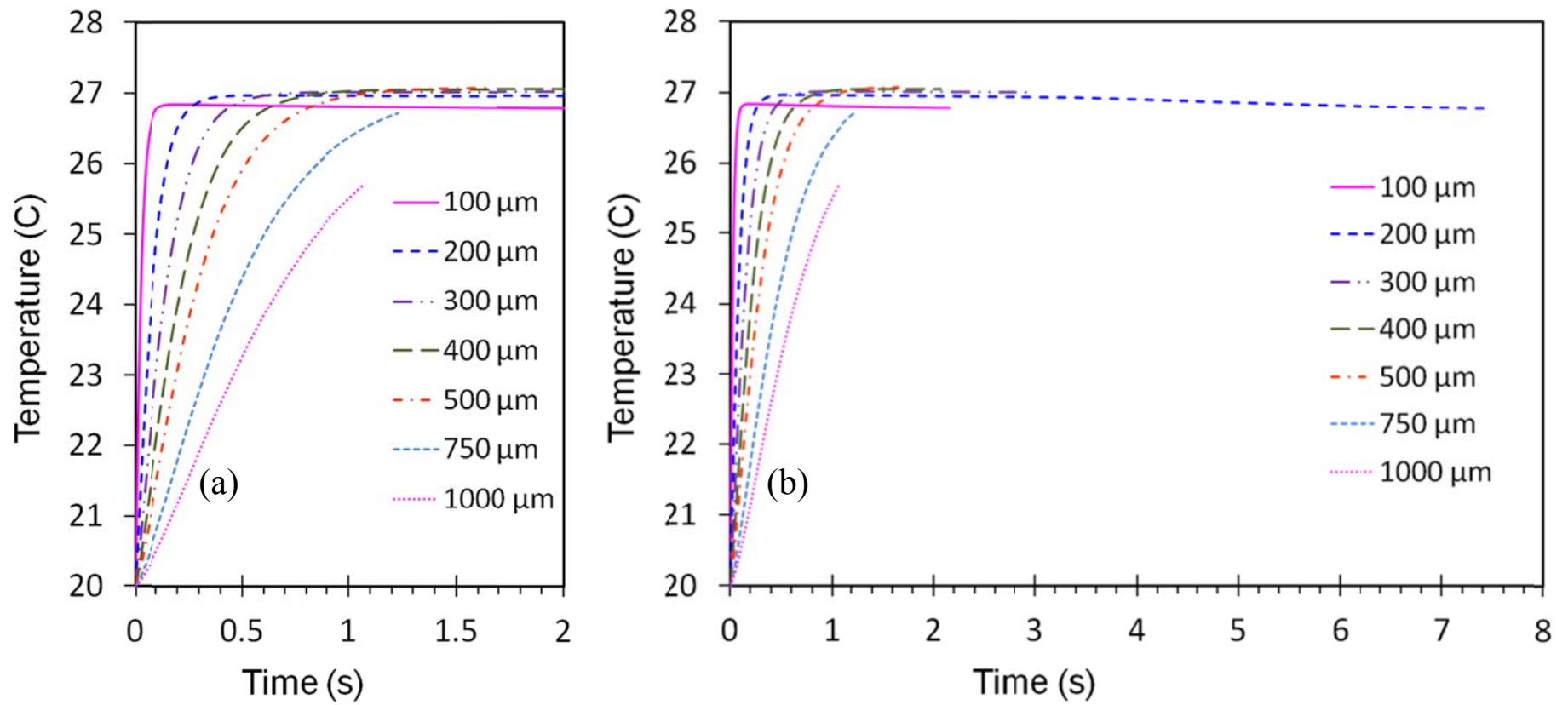
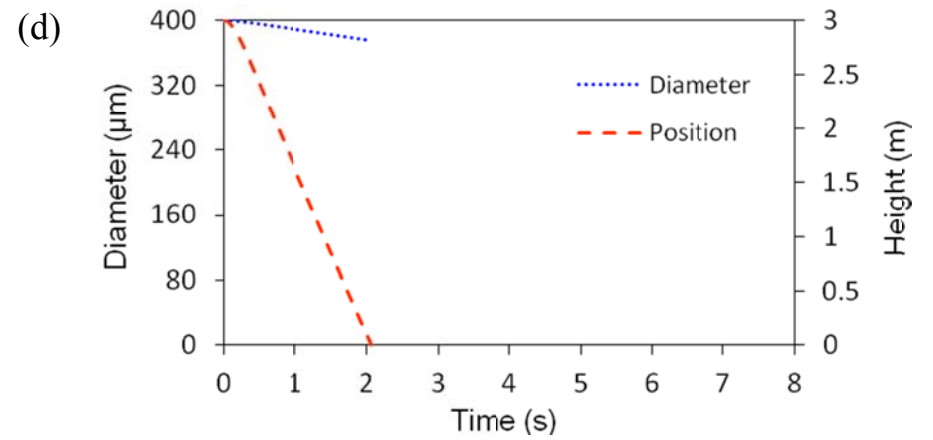
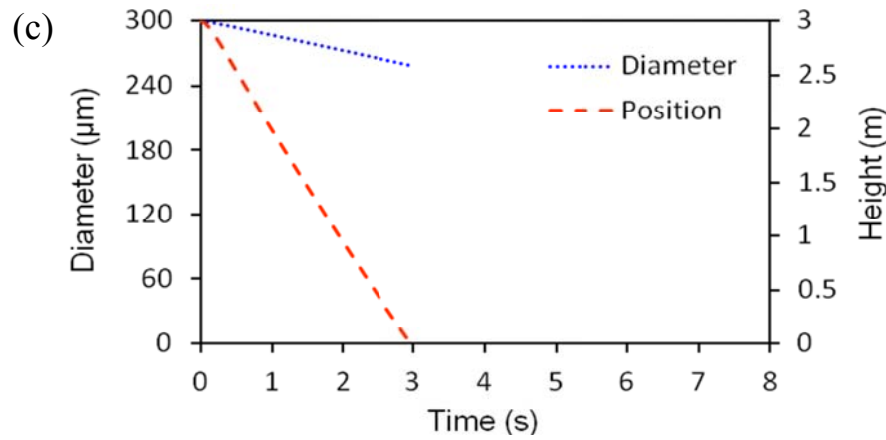
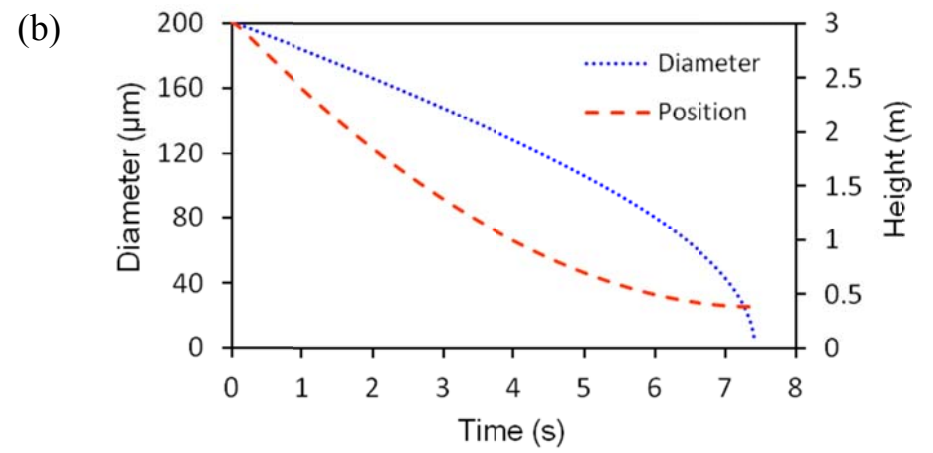
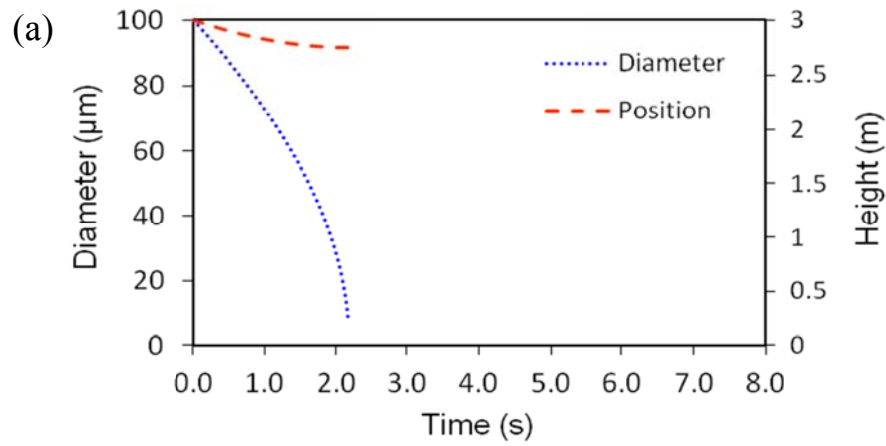


Figure 3.12: Temperature profile of droplets (a) close view (0–2 seconds); (b) detailed view (0–8 seconds).

The history of the diameter and spatial position of droplets for different initial sizes is shown in Figure 3.13. The analysis shows that the smaller droplet has a longer lifetime in the air. A droplet with an initial diameter of 200  $\mu\text{m}$  size has the highest lifetime. It is suspended for 7.42 seconds, whereas a droplet with an initial diameter of 1000  $\mu\text{m}$  is suspended for only 1.06 seconds. However, a droplet of 100  $\mu\text{m}$  completely evaporated before it reached the floor at a height of 2.75 m and after 2.16 s. The change of diameter of droplets larger than an initial diameter of 500  $\mu\text{m}$  is insignificant, because they reach the floor before they disappear due to evaporation. This means that droplets with a smaller diameter have a longer time in the air and, on the contrary, droplets with a bigger size have a better performance in penetrating a layer of hot air or smoke.



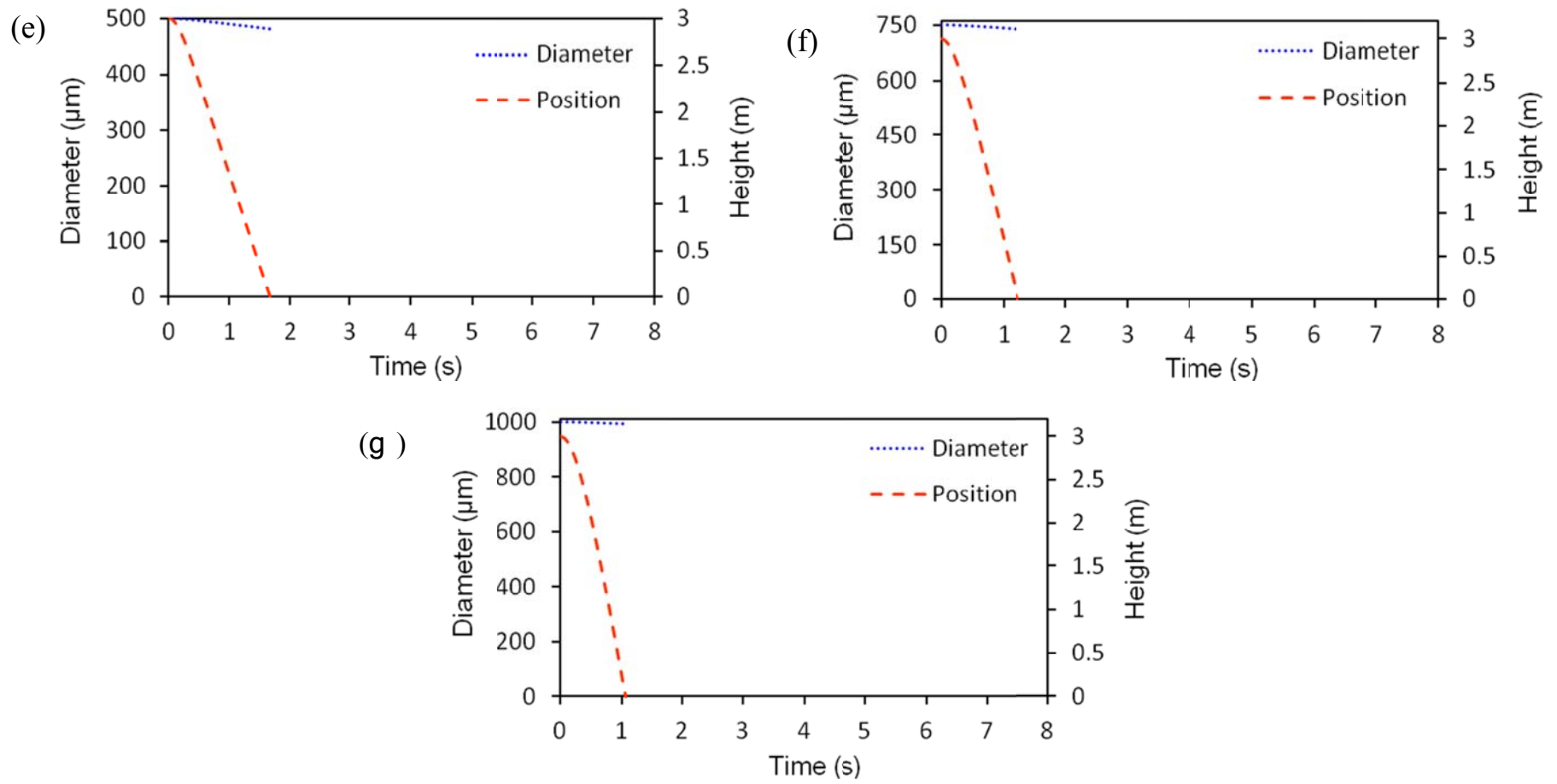


Figure 3.13: Diameter and position history of droplets with different initial drop size (a) 100  $\mu\text{m}$ ; (b) 200  $\mu\text{m}$ ; (c) 300  $\mu\text{m}$ ; (d) 400  $\mu\text{m}$ ; (e) 500  $\mu\text{m}$ ; (f) 750  $\mu\text{m}$ ; and (g) 1000 $\mu\text{m}$ .

In the analysis, it is observed that water droplets with a smaller size have a better performance in evaporative cooling and droplets with a bigger size have a better performance in convective cooling. The percentage of mass loss with time for the different sizes of droplet is shown in Figure 3.14. The results show that droplets with a diameter 100  $\mu\text{m}$  and 200  $\mu\text{m}$  have evaporated completely within 2.16 and 7.42 s, respectively. The per cent of mass loss of 300, 400, 500  $\mu\text{m}$  are 36, 18 and 11%, respectively. However, the evaporation of droplets with a size of 750 and 1000  $\mu\text{m}$  is insignificant.

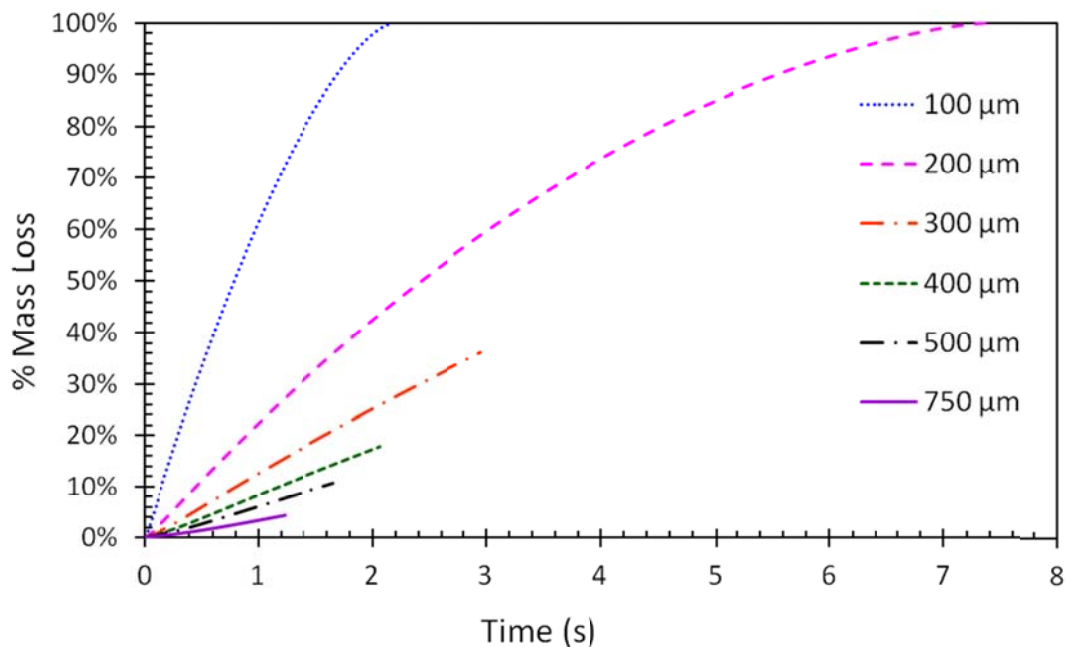


Figure 3.14: Per cents of mass loss of droplets with different initial drop size.

The heat absorbed by a single droplet, in terms of per droplet, as well as per unit mass with different droplet sizes, is determined and shown in Figure 3.15. The heat absorbed by water droplets includes both stored energy in the droplets and energy used in evaporation by water droplets. In the case of smaller droplets, the quantity of absorbed heat is smaller compared to the bigger drop size. However, for a fixed mass of water, the smaller the drop size, the greater the number of droplets and, consequently, the larger amount of surface area. As a result, the quantity of total

absorbed heat by a smaller droplet is greater for a fixed amount of water mass. From Figure 10, it is observed that in terms of per droplet, a droplet of 1000  $\mu\text{m}$  absorbed 40 J/droplet, whereas, a droplet of 100  $\mu\text{m}$  absorbed only 1.35 J/droplet. However, in terms of one kilogram of water, 100  $\mu\text{m}$  droplets absorbed 2580 MJ energy, whereas water droplets of 1000  $\mu\text{m}$  absorbed only 75.8 MJ.

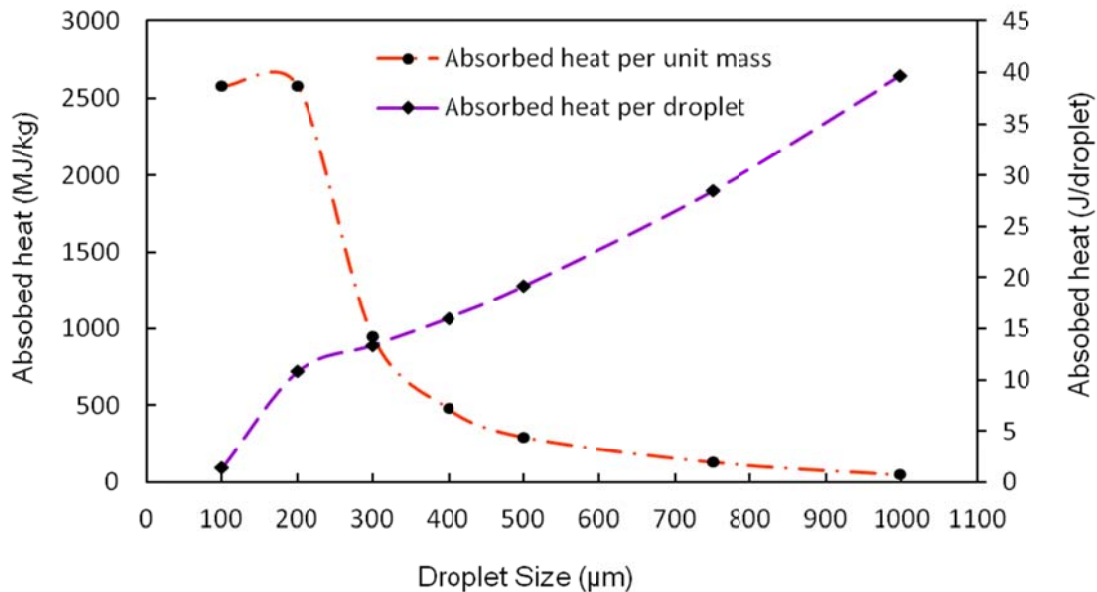
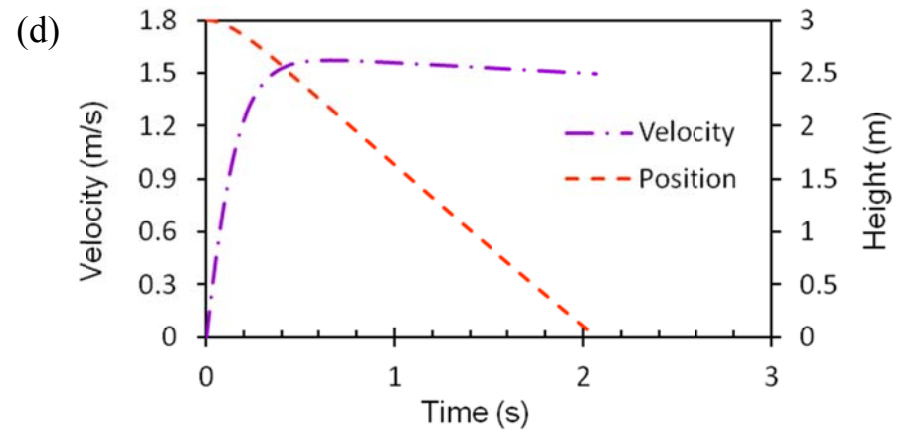
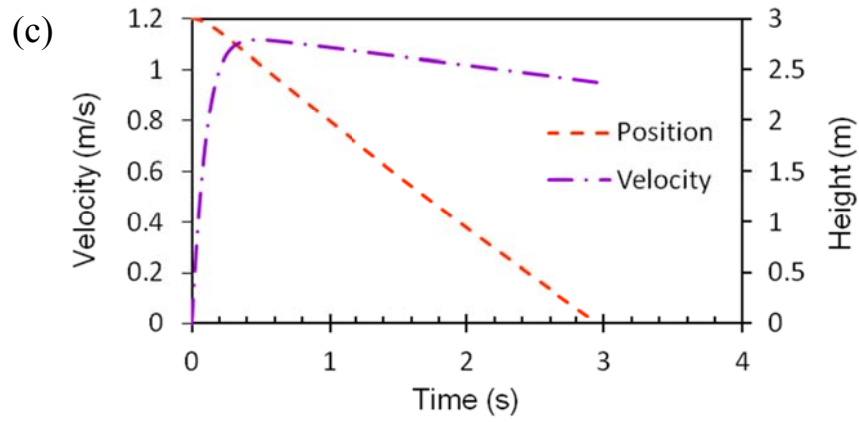
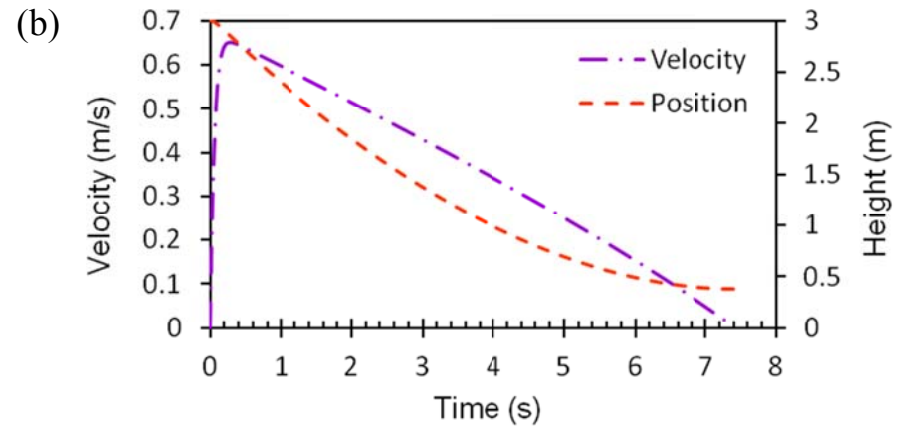
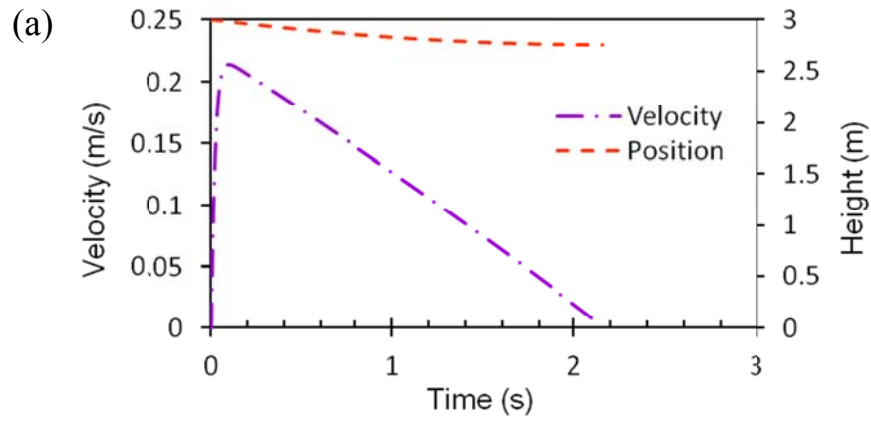


Figure 3.15: Heat absorbed by droplets of different droplet sizes.

The velocity and corresponding vertical position of the droplets with different droplet sizes are illustrated in Figure 3.16. From this figure, it is observed that droplets with initial diameters of 100 and 200  $\mu\text{m}$  attain a velocity due to gravity until they reached their terminal velocity and at the same time reached an equilibrium thermal state. Afterwards, they have begun to decrease their velocity due to vaporisation and, finally, reduced to zero when totally vaporised. In this case, they reached the terminal velocity and equilibrium thermal state at 0.081 and 0.284 s, respectively, and continued to evaporate until they disappeared at 2.16 and 7.42 s, respectively. However, the change in the velocity of droplets with a diameter greater than 400  $\mu\text{m}$  is insignificant, as the change in diameter is very small.



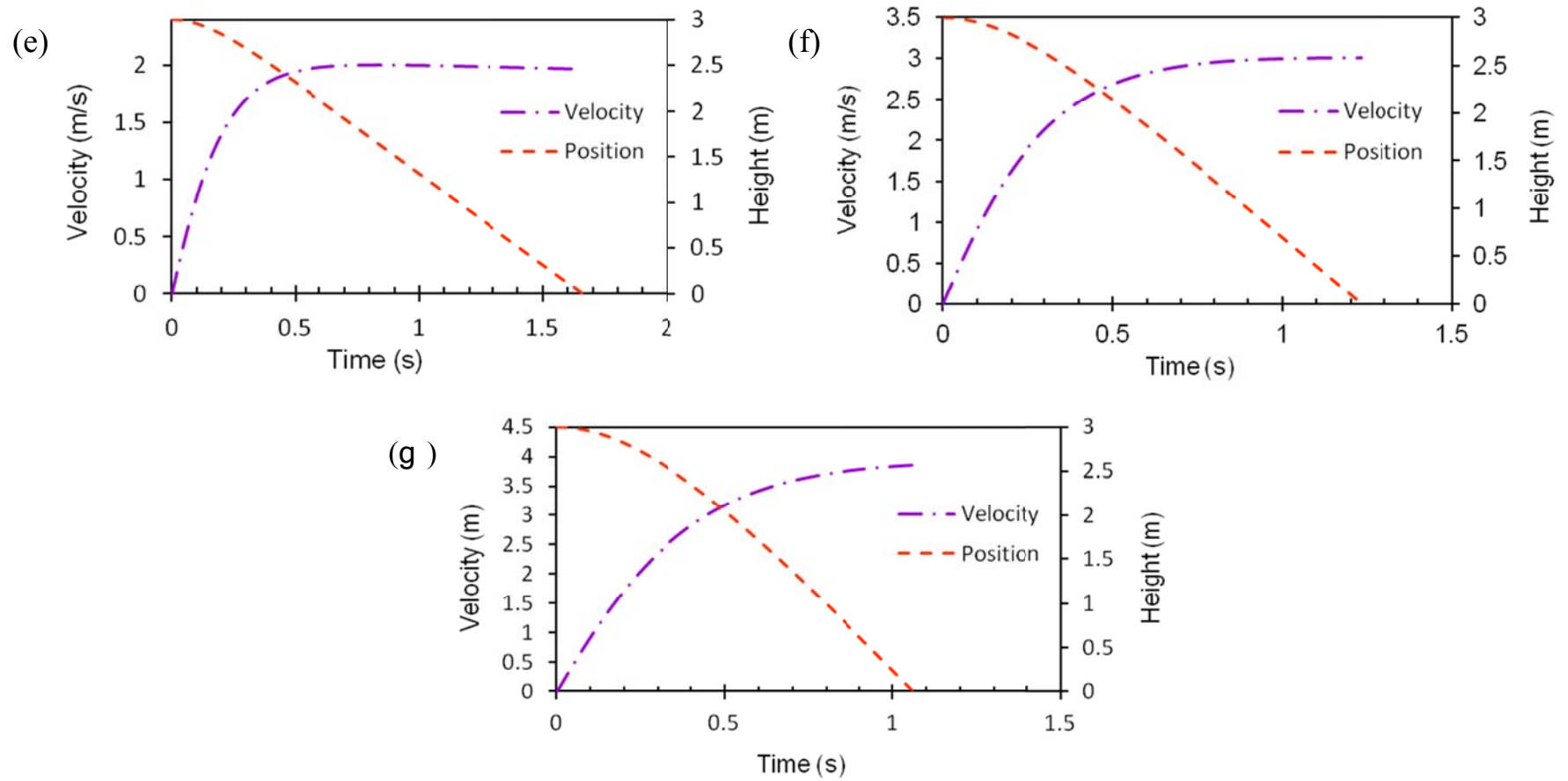


Figure 3.16: Velocity and position of droplets with different initial drop sizes (a) 100  $\mu\text{m}$ ; (b) 200  $\mu\text{m}$ ; (c) 300  $\mu\text{m}$ ; (d) 400  $\mu\text{m}$ ; (e) 500  $\mu\text{m}$ ; (f) 750  $\mu\text{m}$ ; and (g) 1000  $\mu\text{m}$ .

### **3.7 Scattering, absorption and extinction characteristics of water mist in a radiated medium**

Attenuating the radiation also plays an important role in reducing the transmission of heat developed by fires. Water mists can reduce the propagation of heat from fires to unburnt fuel by blocking the thermal radiation. Water droplets attenuate radiation by absorbing and scattering when it passes through the droplets. The properties of water mists in scattering, absorption and extinction of thermal radiation are evaluated based on the theory of [Mie \[1908\]](#). The attenuation of thermal radiation for different sizes of droplets is calculated and compared. The results of this analysis are presented in Appendix B.

A significant outcome of this analysis is that the smaller droplets are more effective in attenuating thermal radiation compared to the larger droplets due to their ability to scatter radiation. The analysis shows that a mist with a loading of 100 gm of water mist in 1 m<sup>3</sup> of air, droplets with a diameter of 100 μm can attenuate the thermal radiation up to 80%, whereas this attenuation is only 20% for droplets with a diameter of 500 μm. The effect of water loading is also evaluated. Results show that a higher water loading gives better attenuation with the limit of a minimum level of concentration. However, the amount of minimum concentration of loading is lower for the smaller size of droplets.

### **3.8 Conclusions**

A semi-empirical model of the interaction of water droplets with hot air has been developed based on the principles of the conservation of mass, momentum and energy, and some empirical correlations. The contribution of radiation emanating from a flame is considered on the evaporation of a droplet. The effect of a high evaporation rate and the change of  $Re$  to the mass and heat transfer coefficient is also

considered in the model. A forward finite difference technique is used to solve the resulting ordinary differential equations. A time step convergence analysis is conducted and an appropriate time step is selected leading to time step convergent results.

This proposed model has been validated and verified against experimental data and adiabatic saturation temperature. The validation indicates that the proposed model predicted the terminal velocity within 4% of the experimental data. The saturation temperature of droplets predicted by the proposed model agreed well with the calculated adiabatic saturation temperature. In the study, it is found that the proposed model is consistent with FDS and this has given us confidence in the use of this model. In comparison, [Li and Chow \[2008\]](#) and [Barrow and Pope's \[2007\]](#) models should be treated with caution as they predict the longevity of the droplets, and the distance through which they penetrate through a smoke layer or hot air environment induced by a fire. This work provides a further tool with which to predict the behaviour of water droplets evaporating in a hot environment.

The characteristics of the evaporating droplets were evaluated using the proposed model and are presented in this chapter. The temperature profile, travel time history, velocity profile, evaporation rate and absorbed heat of a freely falling droplet are predicted. The findings of this study can be summarised as follows:

- i) The saturation temperature of droplets is independent of the initial diameter and temperature of the droplets; it depends on the temperature and relative humidity of ambient air.
- ii) The suspension time in air is longer for the smaller size of droplets, whereas the penetration capability is greater for the larger size of droplets through a hot air environment.

- iii) The evaporation rate is higher for smaller droplets, whereas the quantity of heat absorbed is greater for the bigger size of droplets. However, the total amount of absorption of heat per unit mass of water is higher for the smaller size of droplets.
- iv) The terminal velocity is larger for the bigger size of droplets. However, it is found that the speed of the smaller size of droplets has begun to reduce due to reduction of the diameter by evaporation.
- v) The effect of the high mass transfer rate on evaporation of a droplet is insignificant within the range 0–100°C of air temperature.
- vi) In this study, a case study is conducted where the droplets are considered travelling through a hot smoke layer. The temperature of the smoke layer is 75°C and relative humidity of air is 3%. In the analysis, the droplets with a size of less than 200  $\mu\text{m}$  are found to be the most effective in evaporative cooling, as they have totally vaporised due to evaporation before reaching the floor. Moreover, the total absorbed heat per unit mass of water is highest for droplets sizes 100 and 200  $\mu\text{m}$ . However, suspension time is highest for the droplet size 200  $\mu\text{m}$ . The suspension time of this size is much higher than other sizes of droplets, which can lead this size to be the most effective where the suspension time is very important to block heat transfer from the source of fires.

This physical model has given us the confidence to analyse the behaviour of individual water droplets travelling through a hot environment induced by a room fire. This model can be used to evaluate the performance of different sizes of droplets in different actions of fire suppression mechanisms i.e. whether a particular size of droplet is suitable for the cooling of hot gas by heat extraction or the dilution of fuel vapours/air ratio by evaporation of water droplets, or whether it is suitable for the

wetting and cooling of a fuel surface by reaching there before complete evaporation. The model can also be used for the validation of comprehensive CFD based models to obtain confidence in the use of that particular model. In this study, an example of the verification of a complex CFD model, FDS6, is presented.

In this part of the study we have elucidated the physics of the evaporation of water-mist droplets in hot air or a smoke layer and validated FDS in predicting the evaporation of individual droplets. However, as the performance of a spray in suppressing a fire is greatly influenced by its distribution pattern, any CFD based tool should be able to predict this phenomenon in its simulation. Hence this study is further proceeded to investigate the capability of FDS in predicting the distribution of flux densities on a horizontal surface.

# Chapter 4

Spray distribution – a benchmark  
experiment and validation of FDS

# Chapter 4

## Spray distribution – a benchmark experiment and validation of FDS

---

### 4.1 Introduction

The performance of water-mist fire suppression systems (WMFSS) is crucially dependent on the characteristics of sprays produced by nozzles [Liu and Kim 2000]. One of the important parameters essential for specifying water-mist systems is the distribution of the flux density of the spray [Lefebvre 1989]. Therefore a good understanding of the spatial distribution of water-mist droplets and their distribution of flux density on surfaces is essential for fire researchers to design an effective WMFSS. Hence one of the objectives of this research is to verify the accuracy of FDS in predicting the distribution of the flux density of water-mist sprays.

In this work, two types of nozzles, a single and a multi-orifice nozzle, are used in the experiments. The distribution of the flux density of sprays produced by a single and a multi-orifice nozzle are quite different. The single-orifice nozzle results in spray in which the flux distribution is concentrated in a region beneath the nozzle. However in the case of multi-orifice nozzles, the flux distribution is concentrated in several regions that correspond to the individual orifices. Single-orifice nozzles are typically designed to produce somewhat coarser droplets that can reach and directly extinguish burning surfaces. Multi-orifice nozzles may incorporate this feature, but they also produce fine mists from their peripheral orifices. These fine mists have the desirable features of being able to reach the regions that are otherwise occluded and they cool

the surrounding gases and attenuate the thermal radiation by blocking and isolating the fires.

Therefore this work investigates, experimentally, the distribution of flux density of water sprays emanating from a single and a multi-orifice nozzle. The numerical simulations are carried out in FDS using the same input parameters of the experiments. FDS, version 6, is used for the simulation, and the accompanying smoke-view tool, version 5.6, is used for the visualisation of the sprays. The predicted data of FDS are compared with the measured data and validated against the experiment.

This chapter also described a simple technique for determining the median size of droplets of a spray produced by a nozzle that required only experimental data of the distribution of flux densities of water spray and a CFD model to mimic the experiment and calculate the distribution of flux density.

## 4.2 Experiment details

### 4.2.1 Nozzle specification

#### 4.2.1.1 Single-orifice nozzle

The schematic of the single-orifice nozzle used in the experiment is shown in Figure 4.1. The orifice has an opening of 1.524 mm and is located centrally in the body of the nozzle that discharges an axi-symmetric spray around the nozzle axis.

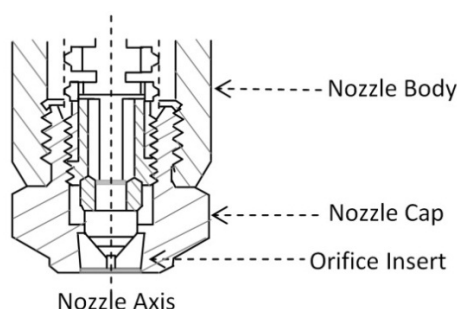


Figure 4.1: Schematic of the single-orifice nozzle (after [Tanner and Knasiak \[2003\]](#)).

#### 4.2.1.2 Multi-orifice nozzle

The schematic of the multi-orifice nozzle used in the experiment is shown in Figure 4.2. The nozzle comprises a central orifice of 1.524 mm in diameter, placed along the inlet nozzle axis, and six orifices of 0.508 mm in diameter, placed equi-angularly around the perimeter of the nozzle at an azimuthal angle of  $60^\circ$  with the inlet nozzle axis. The central orifice discharges axi-symmetrically around the inlet nozzle axis and the peripheral orifices discharge axi-symmetrically around the axis of that individual orifice.

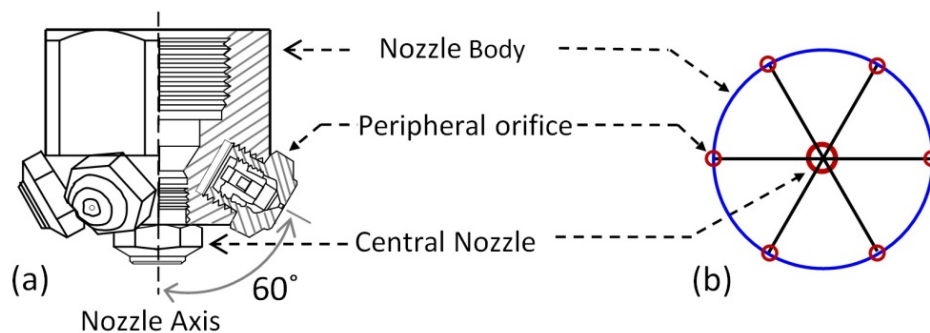


Figure 4.2: Schematic view of the multi-orifice nozzle (a) side elevation; (b) plan view (after [Tanner and Knasiak \[2003\]](#)).

### 4.2.2 Experimental set-up and procedure

#### 4.2.2.1 Determination of flux density distribution

An experimental rig is constructed to measure the distribution of the flux density produced by the sprays. This is achieved by placing a  $2\text{ m} \times 2\text{ m} \times 0.1\text{ m}$  water collection tray beneath the nozzles. To spatially resolve the distribution of flux densities, the tray is divided into 400 compartments, each with dimensions of  $10\text{ cm} \times 10\text{ cm} \times 10\text{ cm}$ . The single-orifice and the multi-orifice nozzle heads are clamped at heights of 2.3 m and 2.0 m, respectively, above the floor. Water is supplied to the nozzles by means of a pump that could operate up to a pressure of 400 bars. The experimental rig is illustrated in Figure 4.3.

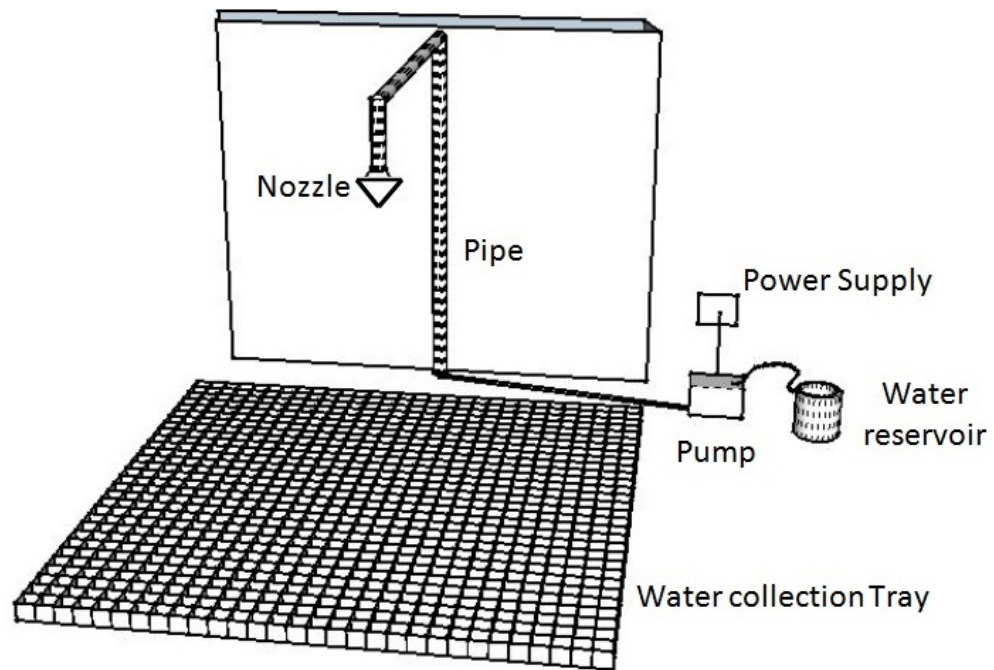


Figure 4.3: Schematic view of the experimental set-up.

The experiments are designed to measure the distribution of flux density produced by the single and the multi-orifice nozzles. It has been found that the key feature of the distribution of flux density produced by the single-orifice nozzle is best obtained by placing the nozzle head above the centre of the water collection tray. This set-up is designated as *Case A*. However, as might be expected, multi-orifice nozzles produce a maximum intensity of distribution directly beneath the centre of the nozzles and in regions that correspond to their azimuthal orifices. Hence, in this situation, experiments are carried out with the multi-orifice nozzle located above the centre and at one of the corners of the water collection tray. The former set-up is similar to that of the single-orifice nozzle and referred to as *Case A*, and the latter set-up is referred to as *Case B*. In both cases, the boundary wall was located at 2 m away from the nozzle head. The locations of the nozzles and boundary wall for these two cases are shown in Figure 4.4.

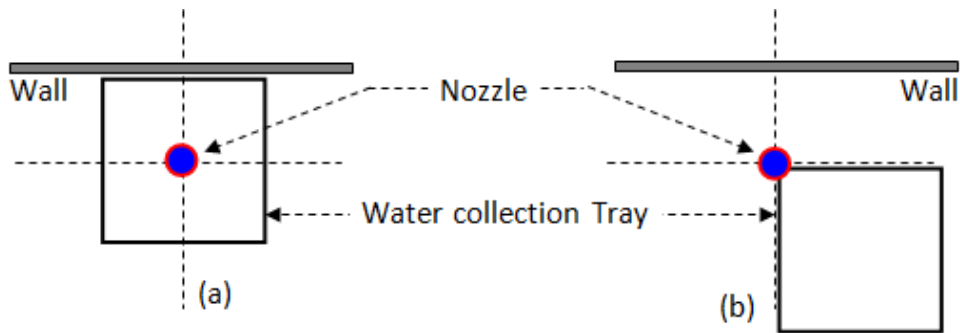


Figure 4.4: Location of nozzle (a) *Case A*; (b) *Case B*.

To supply the water from the reservoir to the nozzle head, the pump is operated at a pressure of 34.5 bars for the single-orifice nozzle spray and this has produced a volume flow rate of 1.7 L/min. In the case of the multi-orifice nozzle, the pump is operated at a pressure of 70 bars and this has produced a volume flow rate from the central orifice comparable to that produced by the single-orifice nozzle; the total volume flow rate is 8.8 L/min. The nozzles are allowed to operate until their flow regime is stabilised. The sprayed water is collected on the tray that enabled the flux densities ( $\text{L}/\text{m}^2/\text{min}$ ) to be measured to an accuracy exceeding 99%. The angles of the sprays for both of the nozzles are determined from the photographs of sprays. Schematic views of measuring the angle of sprays are illustrated in Figure 4.5. The parameters of the spray i.e. water flow rates, spray angles and spray heights of the experiment were used as input parameters in the FDS model.

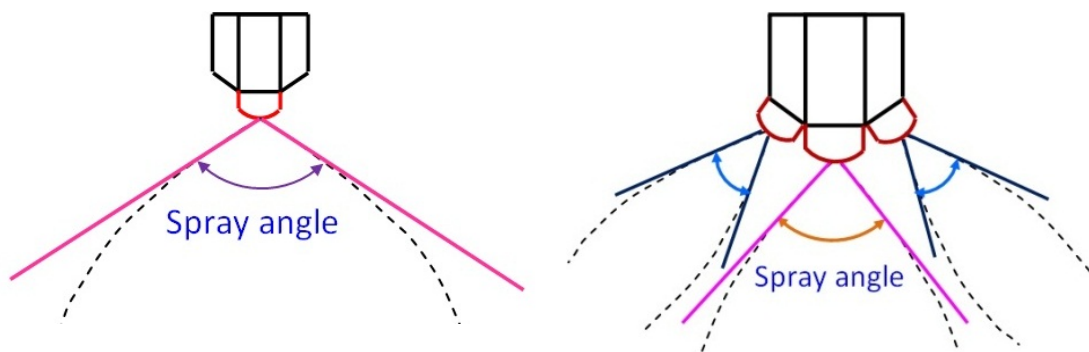


Figure 4.5: Schematic view of the measurements of the angle of sprays (a) spray produced by the single-orifice nozzle; (b) spray produced by the multi-orifice nozzle.

In the experiment: the volume flow rates of the sprays produced by the nozzles are measured. In the case of the multi-orifice nozzle spray, the flow rates for the central and the azimuthal orifices and for the whole nozzle are measured separately: they are 2.2, 1.1 and 8.79 L/min, respectively. The measured flow rates from the nozzle heads are also corroborated by means of the following correlation [Tanner and Knasiak 2003]:

$$Q = K \sqrt{P} \quad (4.1)$$

where  $Q$  is the discharge rate of water and  $P$  is the operating pressure of the water flow. According to the manufacturer's data, the  $K$ -factor of the multi-orifice nozzle is 0.073 L/min/psi<sup>1/2</sup>, which gives a flow rate of 8.74 L/min. This also validates the accuracy of the experimental measurement of the water flow rate.

#### 4.2.2.2 Determination of median diameter of droplets

The median diameter of the droplets of the spray produced by the multi-orifice nozzle is available from the manufacturer's data. The median diameter of the droplets of the spray produced by the single-orifice nozzle is determined using the same experimental set-up, and the procedure of determining the median diameter of droplets is described below.

Firstly, the flux density distribution of the nozzle is measured for a certain flow pressure ( $P_l$ ). The water flow rate and spray angle are also recorded. A numerical tool is required to simulate this experiment. This is followed by carrying out simulations with a range of the median diameters of droplets. The distribution of flux densities is calculated for the spray of each median size of the diameter of the droplets. These are compared with the corresponding experimental data of the distribution of flux densities for the flow pressure of  $P_l$ . When the numerical data of distribution matches the experimental measurement, the corresponding size of the droplet can be taken as the hypothetical size of the droplet ( $d_{ml}$ ) of the spray. Then, a

mathematical relationship is used to determine the second median size of the droplet ( $d_{m2}$ ) for a different flow pressure ( $P_2$ ). If the numerical tool can accurately simulate the second set of distribution of flux densities using  $d_{m2}$  and  $P_2$ , this will provide confidence that the numerical tool is well validated. Hence  $d_{m1}$  and  $d_{m2}$  can be considered the actual median diameters of droplets corresponding to the pressures of  $P_1$  and  $P_2$ , respectively.

According to Fleming [2008], the median diameter of droplets generated by a sprinkler has been empirically found to be inversely proportional to one-third of the power of water pressure and directly proportional to the two-third power of the orifice diameter i.e.

$$d_m \propto \frac{D^{2/3}}{P^{1/3}} \quad (4.2)$$

where  $d_m$  is the median size of droplets,  $D$  is the orifice diameter and  $P$  is the flow pressure. Therefore, for a specific nozzle, the relationship between two median diameters of droplets corresponding to two different pressures can be expressed as:

$$\frac{d_{m1}}{d_{m2}} = \left(\frac{P_2}{P_1}\right)^{1/3} \quad (4.3)$$

From the first experiment and numerical simulation,  $d_{m1}$  is determined for the corresponding  $P_1$ . Conducting a second experiment with a different flow pressure ( $P_2$ ), a second set of the distribution of flux densities is collected. Using Eq. 4.3,  $d_{m2}$  is calculated for the corresponding  $P_2$ . Finally, this median diameter of droplets and the corresponding pressure are used as input parameters for the spray in the numerical model. If it is found that the numerical distribution of flux densities matches the experimental measurements, then it can be concluded that the numerical model is capable of predicting the distribution of flux densities, and the corresponding hypothetical median size of droplets,  $d_{m1}$  and  $d_{m2}$ , can be considered

the true median diameter of droplets at pressures  $P_1$  and  $P_2$ , respectively. Therefore, using this method, the median diameter of droplets of a spray can be estimated corresponding to their flow pressure.

### **4.3 Numerical model**

CFD simulations are run using FDS (ver. 6.0) and the accompanying program, Smokeview (ver. 5.6), is used for visualisation of the model. A brief description of the spray model in FDS is described in Chapter 2.

#### **4.3.1 Domain set-up**

##### **4.3.1.1 Single-orifice nozzle spray**

A computational domain for the simulation of spray produced by a single-orifice nozzle is established that represents a region in space as shown in Figure 4.6. The dimensions of the floor are 2 m  $\times$  2 m and the vertical height of the domain is 2.4 m. In order to represent the laboratory set-up, one of the vertical boundaries is considered to be an impermeable solid wall. The three other vertical boundaries are considered to be open to flow, as is the upper horizontal boundary. The lower horizontal boundary is the floor on which the volume flux of water emanating from the nozzle impinges. The dots on this surface coincide with the centres of the 10 cm  $\times$  10 cm regions in which the fluxes are estimated. The grid system on the floor of the domain is illustrated in Figure 4.7. The nozzle head is located at a height of 2.3 m above the floor.

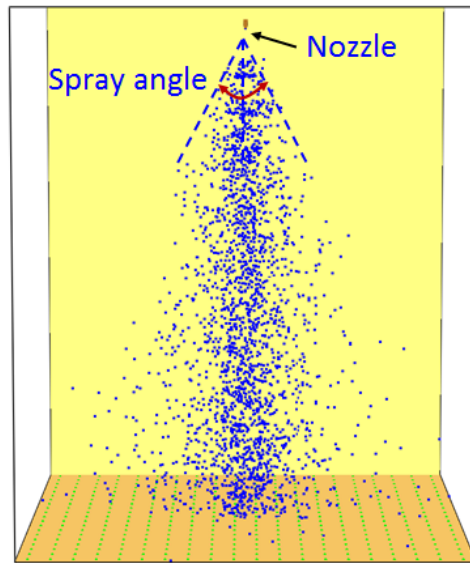


Figure 4.6: Computational domain for simulating the spray produced by the single-orifice nozzle.

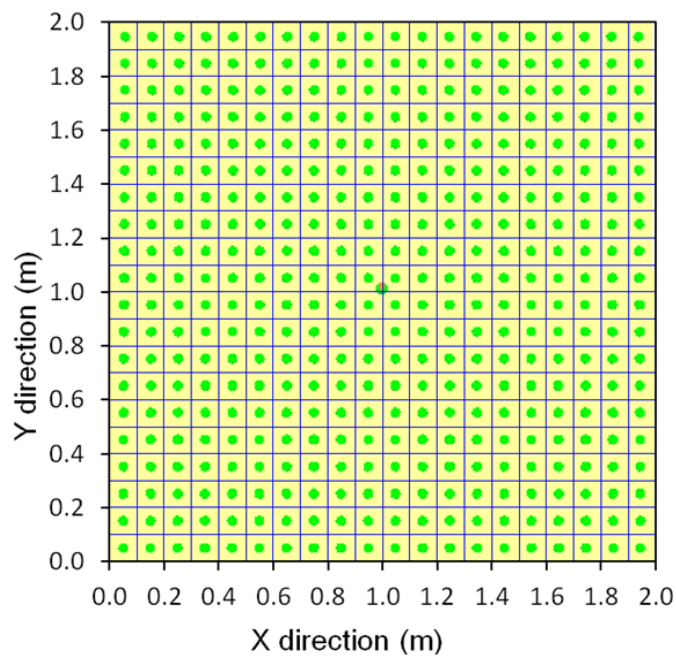


Figure 4.7: The grid system on the floor in the computational domain.

#### 4.3.1.2 Multi-orifice nozzle spray

A similar computational domain is also established to simulate the spray produced by the multi-orifice nozzle, as shown in Figure 4.8. In this case, the dimensions of the horizontal floor are  $6\text{ m} \times 6\text{ m}$  and the height of the domain is  $2.1\text{ m}$ . To be consistent with the conditions associated with the experiment, one of the vertical

boundaries that has a dimension of 6 m × 2.1 m is designated as being impermeable whereas the other three and the horizontal roof are kept open.

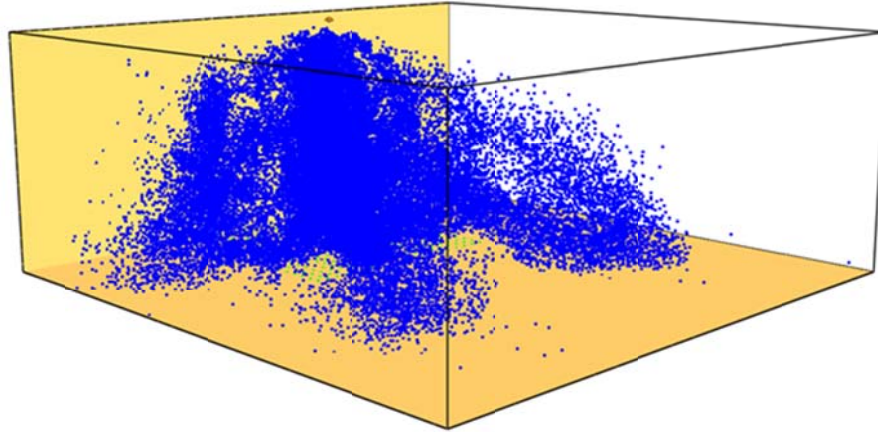


Figure 4.8: Computational domain set-up used to simulate the spray produced by the multi-orifice nozzle.

The multi-orifice nozzle is located at a height of 2.0 m from the floor. The lower horizontal boundary is the floor on which the volume flux of water emanating from the nozzle impinges. The dots on this surface coincide with the centres of the 10 cm × 10 cm regions in which the fluxes are estimated.

A computational grid sensitivity analysis is carried out to ensure that the numerical results converged. The study considered cell sizes 2.5, 5.0 and 10.0 cm. It was observed that the computed flux densities are almost identical when the grid sizes are 2.5 and 5.0 cm. Hence, in this work, a grid size of 5.0 cm is used to discretise the computational domain for both the single-orifice and the multi-orifice nozzle spray.

#### **4.3.2 Modelling of sprays**

The single-orifice nozzle is modelled as a spray entering the domain in a downward vertical direction i.e. 0° azimuthal angle with the nozzle axis. The multi-orifice nozzle is modelled as a collection of single nozzles by assigning each nozzle a different orientation and spray property. In the case of the multi-orifice nozzle, the

peripheral orifices are oriented so that they are separated by an azimuthal angle of  $60^\circ$ . The spray from the nozzle is described as a droplet inlet boundary condition.

### 4.3.3 Input variables for determining the median diameter of droplets

Once the computational domain is set up, the input parameters are incorporated for the simulation. The input variables are the median diameter of droplets, flow rate of water, angle of spray and height of spray. Those parameters (except the median diameter of droplets) are measured in the experiment and used as input variables in the numerical simulation. The median diameter of droplets in the spray is varied and the Rosin-Rammler lognormal distribution pattern is used for the distribution of size droplets. The details of the distribution function and its spread coefficient are available in the FDS Technical Reference Guide [McGrattan et al. 2014]. The volume accumulation rate on the floor is calculated in the simulation. The input parameters of simulation are tabulated in Table 4.1.

Table 4.1: Input parameters for the simulation of determining the median diameter of droplets of a spray

Parameter	Value
Flow pressure ( $P_1$ )	34.5 bar
Flow pressure ( $P_2$ )	75.8 bar
Spray pattern type	Solid cone
Spray angle	$65^\circ$
Spray height	2.3 m

### 4.3.4 Input variables for determining the distribution of flux densities

The input variables for determining the distribution of flux densities are the flow rate of water, angle of spray, height of spray, median diameter of droplets and velocity of droplets. The parameters of the sprays produced by the nozzles are specified with the aid of the experimental measurements and manufacturer's data. The details of the

spray parameters for both the single-orifice and multi-orifice nozzles are tabulated in Table 4.2.

Table 4.2: Spray parameters for the simulation of determining the distribution of flux densities of sprays

Nozzle type	Single-orifice	Multi-orifice	
Input variables		Central	Peripheral
Diameter, mm	1.524	1.524	0.508
Orientation (azimuthal angle)	0°	0°	60°
Flow rate, L/min	1.7	2.2	1.1
Spray angle	65°	45°	15°
Spray height, m	2.3	2.0	2.0
Droplet velocity, m/s	15.5	18.8	89.6
Spray pattern	Solid	Solid	Solid

The angles of spray for the single-orifice nozzle and for the central and peripheral orifices of the multi-orifice nozzle are measured from the photographs of sprays, as reported in the previous section. The flow rates of each individual orifice, and of the whole nozzle head, are measured in the experiment. The velocity of the droplets was calculated from the simple geometrically based relationship between the flow rate and discharge area. The median diameter of droplets for the spray produced by the single-orifice nozzle is determined using a technique described in this chapter. The median size of the droplets for the multi-orifice nozzle spray is taken from the experimental data provided by the manufacturer [Tanner and Knasiak 2003].

A Rosin-Rammler lognormal distribution pattern is used for the distribution of droplet sizes. The simulation is allowed to run for 65 seconds; the nozzle is activated at the beginning of the simulation and stopped at 60 seconds; the additional 5 seconds are to allow the water droplets to fall down from the nozzle, based on the primary calculation.

## 4.4 Results and discussion

### 4.4.1 Median diameter of droplets

In the first experiment, the distribution of flux densities of the spray is measured when the operating pressure,  $P_1$ , is 34.5 bars. Then, the numerical simulation is conducted with the droplet sizes of 300, 350, 400 and 500  $\mu\text{m}$  and the distribution of flux densities for each size of droplets is compared with the experimental data. When the numerical data of distribution is matched with the experimental measurements, the corresponding size of droplets is taken to be the hypothetical median size of droplets ( $d_{m1}$ ) of the spray. Comparison of the numerical results with the experimental data is presented in Figure 4.9. The hypothetical median diameter of droplets is 350  $\mu\text{m}$  at 34.5 bars.

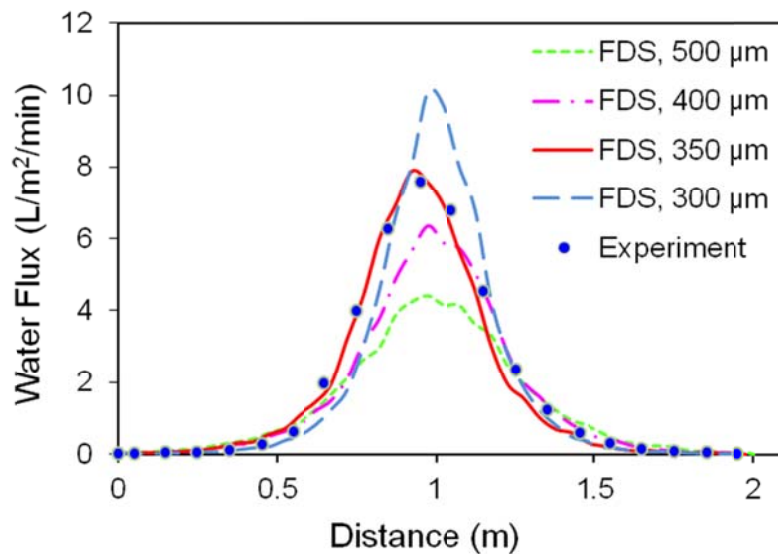


Figure 4.9: Comparison of the numerical results on the distribution of flux densities for different size of droplets with the experimental measurement in the first case.

A second experiment is carried out using a pressure  $P_2$  of 75.8 bars and the corresponding distribution data are collected. Using Equation 2, the expected  $d_{m2}$  of the spray is calculated for  $P_2$ . In this case the median diameter of droplets is 275  $\mu\text{m}$ . Finally, this size of droplets and the corresponding pressure are used to generate the

spray using FDS, and the distribution of flux densities is computed in the simulation. The numerical data of the distribution of flux densities are compared with the experimental measurements and the results are presented in Figure 4.10. It is found that the numerical data has closely matched the experimental measurements. As a result, it appears that the hypothetical median diameter of droplets of 350 and 275  $\mu\text{m}$  are the actual size of the droplets at the corresponding flow pressure of 34.5 and 75.8 bars, respectively.

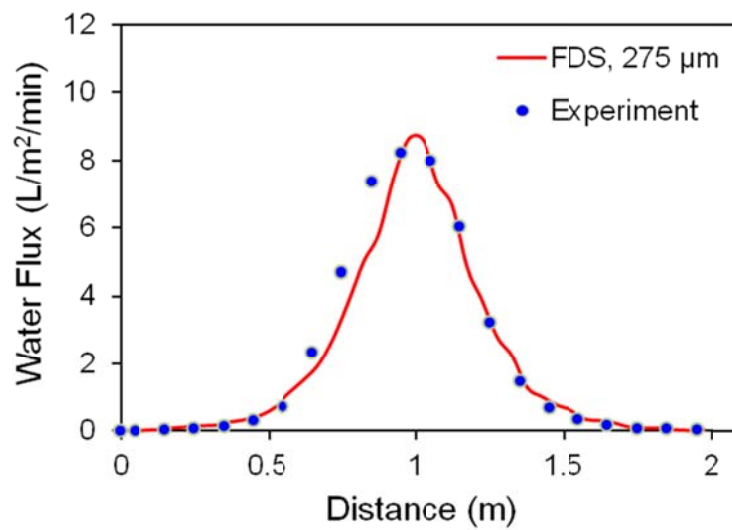


Figure 4.10: Comparison of the numerical results on the distribution of flux densities for the hypothetical size of droplets with the experimental measurement in the second case.

#### 4.4.2 Distribution of flux densities of sprays

##### 4.4.2.1 Single-orifice nozzle spray

In the experiment with sprays produced by the single-orifice nozzle, the distribution of flux densities is measured at a distance 2.3 m below the nozzle. The input parameters used in the FDS model correspond with the experimental environment. These include the flow rate of water, velocity of the droplet and angle and height of the spray. The numerical simulations are carried out and the distributions of flux densities of the sprays are calculated in the simulations. The distributions of flux

densities are measured in the experiment and calculated in the numerical simulations in  $L/m^2/min$  and the contour maps are illustrated in Figures 4.11 (a) and (b), respectively.

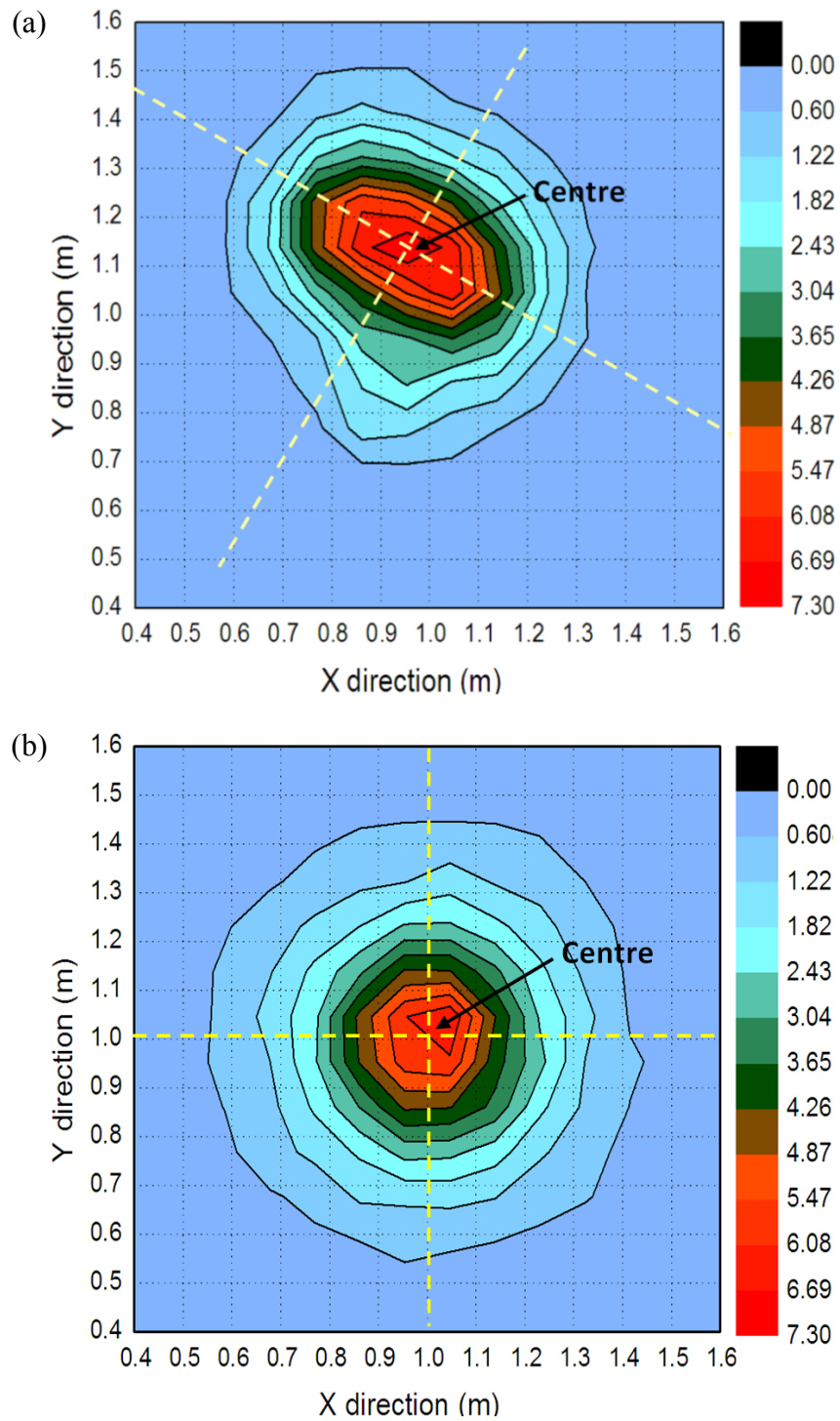


Figure 4.11: Distribution of flux densities ( $L/m^2/min$ ) of the spray produced by the single-orifice nozzle (a) experimental; (b) numerical.

The contour maps are drawn from ordinate 0.4 to 1.6 m on both the X- and Y-axes, as 90% of the water of the spray is found to be within this region. As expected, the flux density is highest at the centre of the floor, both in the experiment and in the numerical simulation, and it is decreased monotonically in a radial direction from the centre. The contour maps in Figure 4.11 indicate that there is discrepancy between the contour maps generated in the experiment and by the computer model. The contour map of the distribution produced by the experiment is elliptical in shape and it has translated 15 cm from the centre of the tray in the positive Y-direction.

The eccentricities of the ellipses produced by the distribution of the spray are calculated. The value of eccentricity of the ellipse for the distribution generated in the experiment is 0.70, whereas the eccentricity of that by the numerical model is 0.2. This indicates that the shape of the distribution of the spray generated by the numerical model is almost circular. Other than the elliptical in the shape of the maps, the predicted distribution pattern and intensity of flux densities of the numerical model are reasonably agreed with that of the experiment.

The distribution of water volume flux along the axes of the ellipse and radii of the circle are illustrated in Figure 4.12. In the experimental study, the pattern of distribution along the major and minor axes of the ellipse is not identical, whereas the simulation results along the centreline have shown an almost identical pattern of distribution. However both experimental and numerical data show a bell-shaped pattern of distribution.

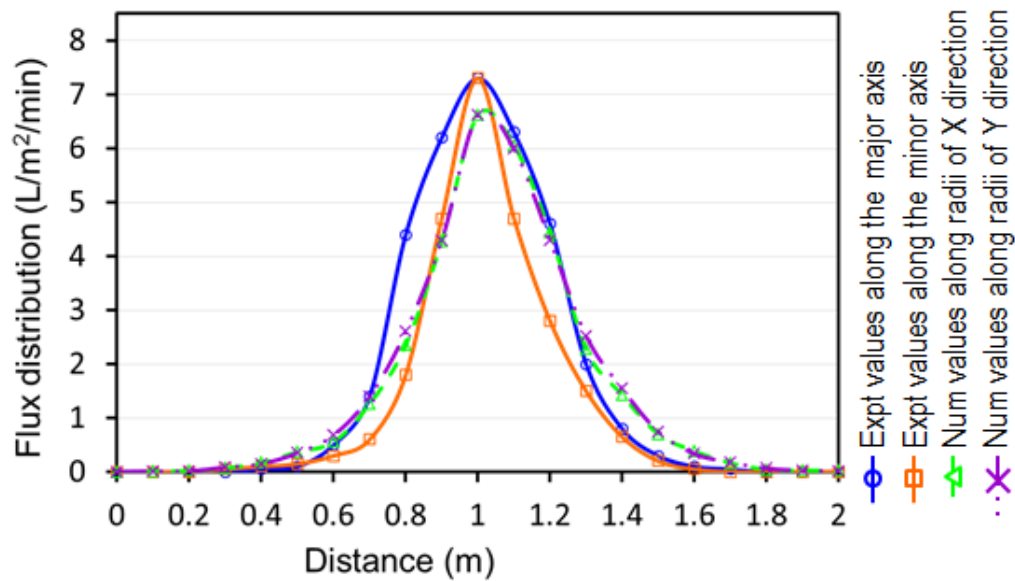


Figure 4.12: The distribution of the flux density of sprays for the single-orifice nozzle along the centreline axes as indicated in Figure 5.12:  $\circ$  Experimental values along the major axis;  $\square$  Experimental values along the minor axis;  $\triangle$  Numerical values along the radii of X direction;  $\times$  Numerical values along the radii of the Y direction.

#### 4.4.2.2 Multi-orifice nozzle spray

The distribution of flux density of the sprays produced by the multi-orifice nozzle is measured experimentally at a distance 2.0 m beneath the nozzle. The experiments are conducted for two cases: *Case A* and *Case B*. In *Case A*, the position of the nozzle is above the centre of the water collection tray, and in *Case B*, the position of the nozzle is above one of the corners of the water collection tray. The distributions of flux densities obtained in the experiments and numerical simulations are displayed by means of contour plots for *Case A* and the results are given in Figure 4.13 (a) and (b), respectively.

The experimental results indicate that the distributions are elliptical in shape and decreased with the distance from the centre of the tray. The position of the highest volume flux is displaced 20 cm from the centre of the tray in both the X and Y directions. A possible reason is that the spray is affected by the wall in the vicinity of

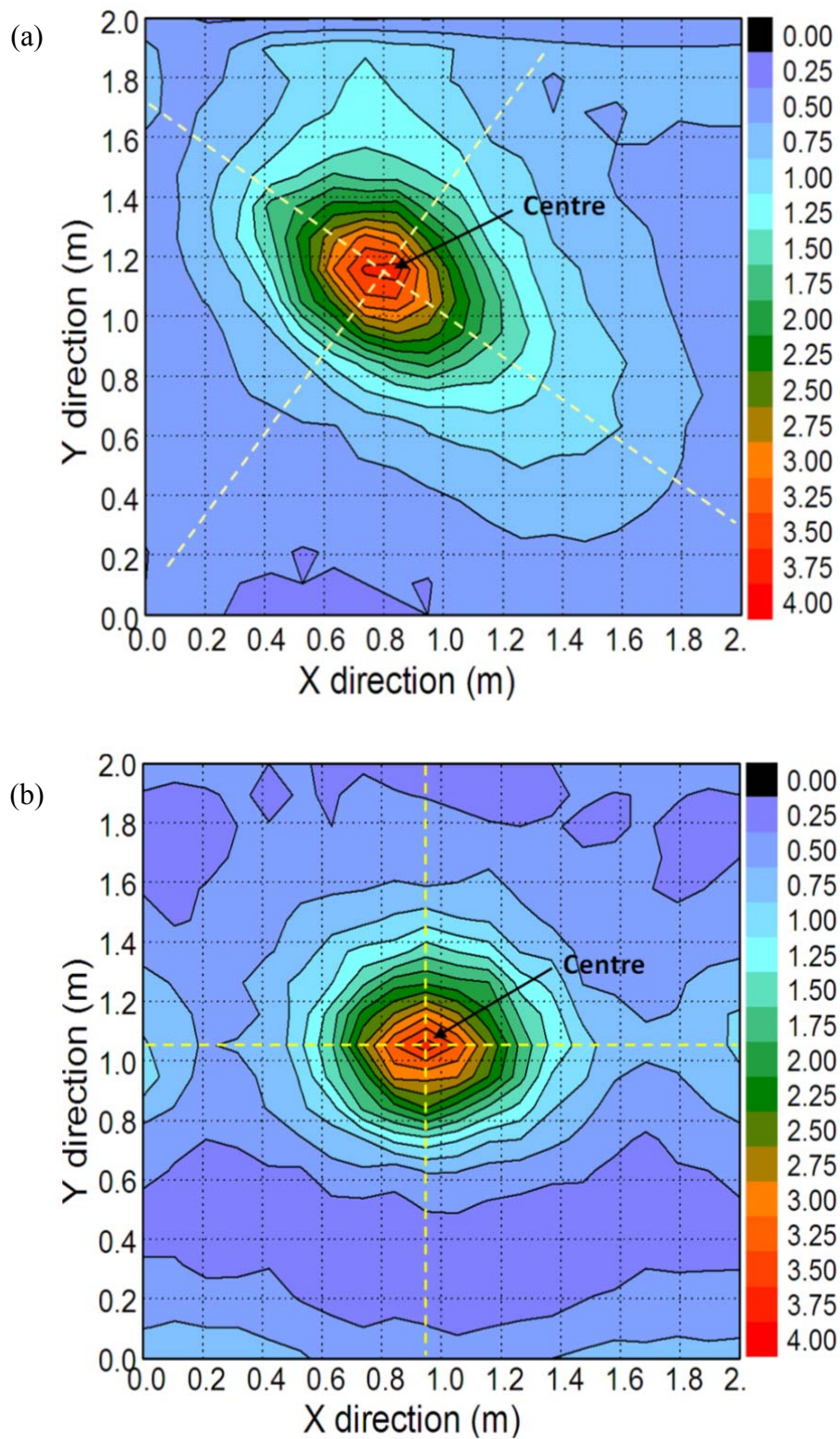


Figure 4.13: Distribution of flux densities (L/m<sup>2</sup>/min) of sprays for the multi-orifice nozzle for *Case A* (a) experimental; (b) numerical.

the spray. A hint of this artefact is provided in the numerical results that have also produced an elliptical shape of distribution, and the position of the height volume flux is displaced towards the wall. In the numerical case it is displaced by about 10 cm. The eccentricity of the ellipse for the experimentally obtained distribution is 0.74, whereas it is 0.58 for the numerically obtained distribution of the spray. This confirms that the distribution generated experimentally is more ellipsoidal than that generated by the numerical model.

The water fluxes along the major and minor axes of the numerically and experimentally obtained distributions are shown in Figure 4.14. The centre of the ellipse of Figure 4.13 (a) is superimposed on the centre of the ellipse of Figure 4.13 (b) and corresponding values of the distribution of flux densities are compared. The figure shows that the numerical model has under predicted the distribution of water flux around the periphery of the ellipse. However it has predicted the distribution near the centre of the ellipse of the spray with accuracy greater than 90%, which

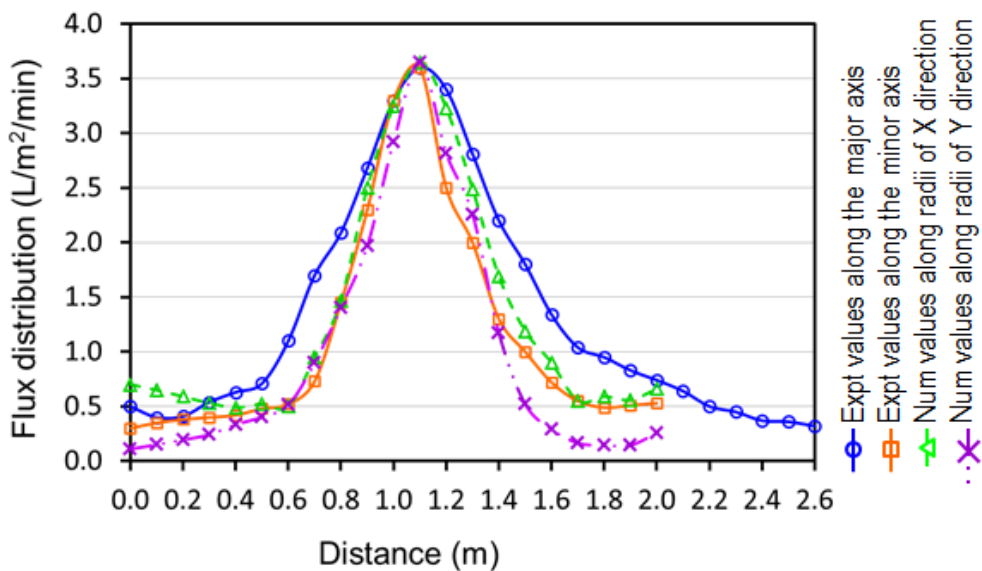


Figure 4.14: The distribution of flux densities of spray for the multi-orifice nozzle along the major and minor axes of ellipses for case A —●— Experimental values along the major axis; —■— Experimental values along the minor axis; —△— Numerical values along the radii of X direction; —×— Numerical values along the radii of Y direction.

provides some validation of the model. The distributions are approximately bell-shaped in both cases and the numerical predictions and the experimental measurements are generally in good agreement.

The distributions of flux densities in the experiment and numerical simulation for *Case B* are shown in Figure 4.15 (a) and (b), respectively. The maximum flux densities of the sprays for the peripheral orifices are at locations (0.9, 0.4) and (0.9, 0.2) for the experimental and numerical distributions, respectively. The distributions patterns of the sprays are elliptical in shape for both experimentally and numerically generated sprays.

The axis of the orifice is depicted by a line connecting the centres of the ellipses of the distributions of sprays produced by the central and peripheral orifices. The distances of the centres of ellipses from the corner of the water collection tray along the orifice axis for the experimentally and numerically obtained distribution on the floor are 186 and 200 cm, respectively. The eccentricities of the experimentally and numerically obtained distributions are 0.72 and 0.16, respectively. This signifies that the numerical model has predicted a more circular distribution of flux compared to that of the experiment. The peripheral orifices in the nozzle body are oriented at an angle of  $60^\circ$  to each other. Therefore it is expected that the angle separating the peripheral distribution should also be  $60^\circ$ . This expectation is met by the numerical model to within the experimental error.

In *Case B*, one of the orifice's axes is directed along an edge of the water collection tray and another one along a line at an angle of  $60^\circ$  to the edge as indicated in Figure 4.15. In the numerically obtained distribution, half of the ellipse of the distribution produced by a peripheral orifice along the direction of the X-axis is captured on the water collection tray; however no such pattern is observed in the experimentally produced distribution. A possible reason is that there is a wall 2.0 m away from the

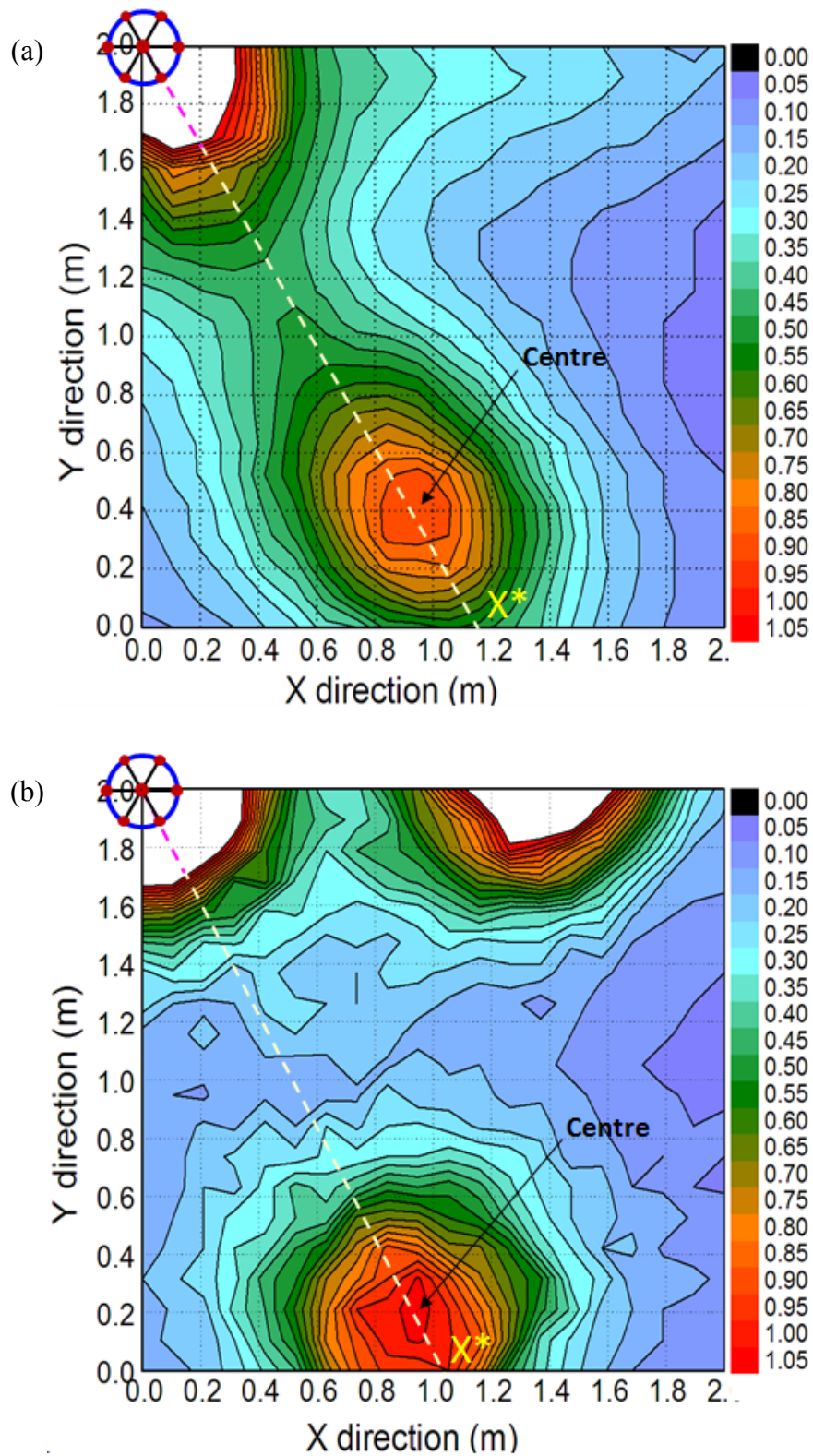


Figure 4.15: Distribution of flux densities ( $L/m^2/min$ ) of spray for multi-orifice nozzle for *Case B* (a) experimental; (b) numerical.

edge of the water collection tray and one of the orifices is directed to the wall. The spray from this orifice hit the boundary wall and part of the spray bounced back and mixed with the spray produced by the orifice directed along the edge of the water collection tray (along the X-axis). As a result, no elliptical shape is created for the spray produced by this peripheral orifice in the experiment.

The distribution of water flux along the orifice axis is illustrated in Figure 4.16. It can be seen that the numerical model has overpredicted the distribution near the centre of the ellipse of the spray for both the central and peripheral orifices and underpredicted it around the periphery of the ellipse of the spray for both the central and peripheral orifices. However the peak-to-peak differences between the numerical and experimental values for the spray of the central and peripheral orifices are not more than 20%, which indicates the capability of FDS in predicting the distribution of flux densities of sprays. Furthermore, the patterns of the distributions are generally well matched.

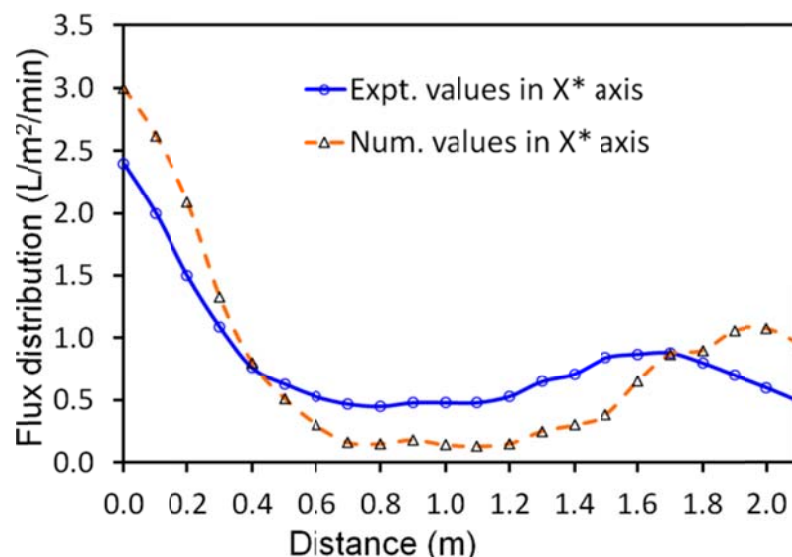


Figure 4.16: The distribution of the flux density of spray for the multi-orifice nozzle along the orifice axis for case B.

## 4.5 Conclusions

Water mists have the ability to suppress fires and their efficacy can be explored using computer software packages such as FDS. However it is essential that the software accurately predict the behaviour of the mists produced by spray nozzles. In this work we have validated FDS in terms of the distribution of flux densities of sprays that govern the prediction of the behaviour of spray nozzles. It has been found that the distribution of the sprays produced in the experiment and the numerical model for both the single- and multi-orifice nozzles are elliptical in shape. However the eccentricity of the ellipses for the distribution is less pronounced in the numerical model for both the single- and multi-orifice nozzle.

In this work it appears that the presence of a solid wall in the vicinity of the spray has influenced the distribution. The experimental and numerical results obtained in this study indicate that the distribution of flux is closer to the wall than would otherwise be the case. However the effect of the boundary wall on the distribution of the spray in the numerical model is less pronounced compared to that of the experimental results. Overall, the results obtained using FDS are in close agreement with the experimentally determined distribution of flux densities produced by the sprays.

In this chapter, a simple technique has also been suggested for determining the median diameter of a droplet produced by a nozzle. The numerical flux density distribution with the hypothetical median droplet size is found to agree well with the experimental measurements. This technique can be used to determine the median size of the droplets of a spray when a direct measurement is not available.

# Chapter 5

Validation of FDS for the burning of PMMA and the suppression of fires by water mists

# Chapter 5

## Validation of FDS for the burning of PMMA and the suppression of fires by water mists

---

### 5.1 Introduction

In the previous chapters the capability of FDS in modelling the behaviour of an individual water-mist droplet and predicting the distribution of sprays on a horizontal surface is presented. However it is also essential to understand the capabilities of FDS in modelling the pyrolysis of fuel, the ignition of fuel and the growth of fire, etc. Predicting these phenomena is challenging as, on the continuum scale, it involves complex dynamics and mechanisms that develop in length scales ranging from millimetres to meters and time scales from milliseconds to minutes [Jahn et al. 2008]. Moreover, the suppression mechanisms of fires are also complex in the case of water-mist systems compared with conventional sprinkler systems, as they involve dilution of fuel vapours/air ratio by the evaporation of water droplets [Liu and Kim 2000; Shu et al. 2005; Yang et al. 2010] and radiation attenuation from flames and hot surfaces [Mawhinney et al. 1994; Wighus 1995; Grant et al. 2000; Liu and Kim 2000]. Furthermore, experimental data with appropriate material properties are required to validate the accuracy of the model.

Therefore the objective of the work presented in this chapter is to validate the accuracy of FDS in predicting the growth and spread of fires and, finally, the capability of FDS in the suppression of fires using water mist. A better understanding

of FDS capabilities in modelling fire growth and extinction would help in designing fire suppression systems. It will also serve as a benchmark in identifying the ability of FDS to model fires resulting from the combustion of solids.

In this study, polymethyl methacrylate (PMMA) is used as a solid fuel in the simulation to observe the burning prediction capabilities of FDS and in simulating the behaviour of fire. PMMA is chosen as a burning material as it is one of the plastic materials widely used in buildings. The experimental data is taken from the study by [Magee and Reitz \[1974\]](#) for the purpose of validation. In the numerical study, similar to the experiment, the sample orientation (horizontal and vertical) and radiant flux rate ( $\text{kW/m}^2$ ) are varied.

## 5.2 The experiments of [Magee and Reitz \[1974\]](#)

[Magee and Reitz \[1974\]](#) conducted an investigation of the burning and extinction characteristics of PMMA fires by water spray. The configurations of the burning samples aligned both horizontally and vertically. The water was applied as a uniform spray from a single nozzle. The steady state burning rates of the PMMA slabs were measured as a function of an externally applied radiant flux, both with and without water spray. The authors investigated the response of the samples to the external radiant heat flux and the effectiveness of water in suppressing the fires.

The experimental apparatus used in the study by [Magee and Reitz \[1974\]](#) is shown in Figure 5.1. In their experiments they investigated the radiation augmented burning of PMMA slabs and water spray extinguishment characteristics in both the vertical and upward facing (horizontal) orientations. Figure 5.1 shows the burning of the PMMA slab for the vertical configuration. To investigate the burning of the horizontal sample, the radiant heaters and specimen were rotated 90 degrees to a horizontal position and the specimen holder changed. The specimens consisted of single slabs

of PMMA measuring 17.8 cm wide  $\times$  35.6 cm high  $\times$  5 cm thick when burned vertically and 17.8 cm wide  $\times$  17.8 cm high  $\times$  5 cm thick when burned horizontally. Two Armstrong speed foil radiant heaters were used as a heat source. The heaters were mounted 17.8 cm apart to allow passage of the water spray. These were positioned 25 cm in front of the specimen and inclined 45° to the plane normal to the centreline of the specimen (Figure 5.1).

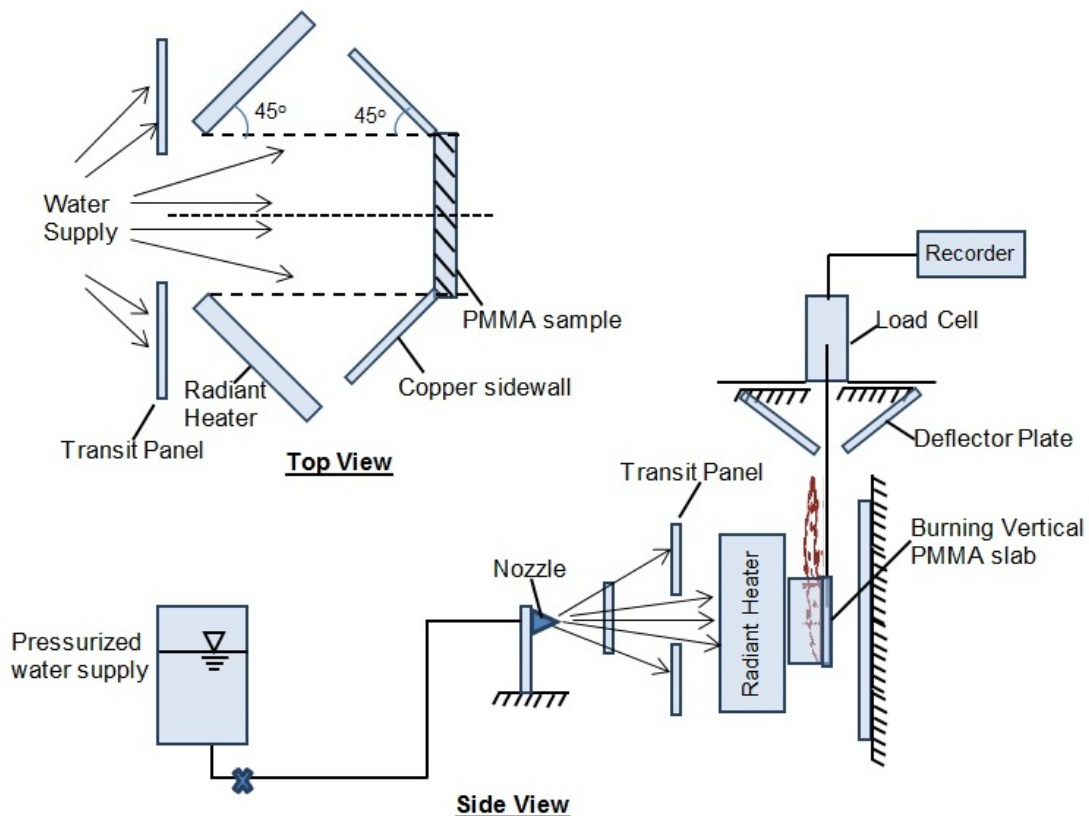


Figure 5.1: Experimental set-up for the burning of vertical specimens after the studies by [Magee and Reitz \[1974\]](#).

A HyCal calorimeter was employed to measure the radiant flux distribution over the specimen surface. The radiant flux was measured at the centre of the specimen, which represented the average radiant flux to the surface. The flux was varied from 8.4 kW/m<sup>2</sup> to 15.89 kW/m<sup>2</sup>. The maximum radiant flux incident on the specimen was 15.89 kW/m<sup>2</sup>. The water was applied to the specimen by means of a single nozzle fed

from a pressurised water tank. The nozzle employed in the majority of tests was a full cone centre jet nozzle.

### **5.3 Numerical simulation**

In this study the simulation of the burning of the PMMA slabs is conducted using FDS, version 6, and the burning rates of the samples are calculated in the simulation. For PMMA combustion, the MMA monomer ( $C_5 H_8 O_2$ ) is assumed to be liberated from the sample surface when pyrolysis occurs [Linteris et al. 2005]. In FDS, pyrolysis is assumed to occur as per the Arrhenius equation. The details of the computational domain, grid resolution, and operating and boundary conditions are discussed in the following sections.

#### **5.3.1 Computational domain**

Computational domains with dimensions of  $1\text{ m} \times 1\text{ m} \times 2\text{ m}$  and  $1\text{ m} \times 2\text{ m} \times 2\text{ m}$  are created for the simulation of burning and the suppression of horizontally and vertically oriented PMMA slabs, respectively. The set-up for the computational domain in the numerical simulation for the burning of horizontally and vertically oriented PMMA is illustrated in Figures 5.2 and 5.3. For samples with an imposed flux, the cone is located 2.54 cm away from the top of the PMMA surface. All sides of the domain are kept open to be consistent with the conditions associated with the experiment.

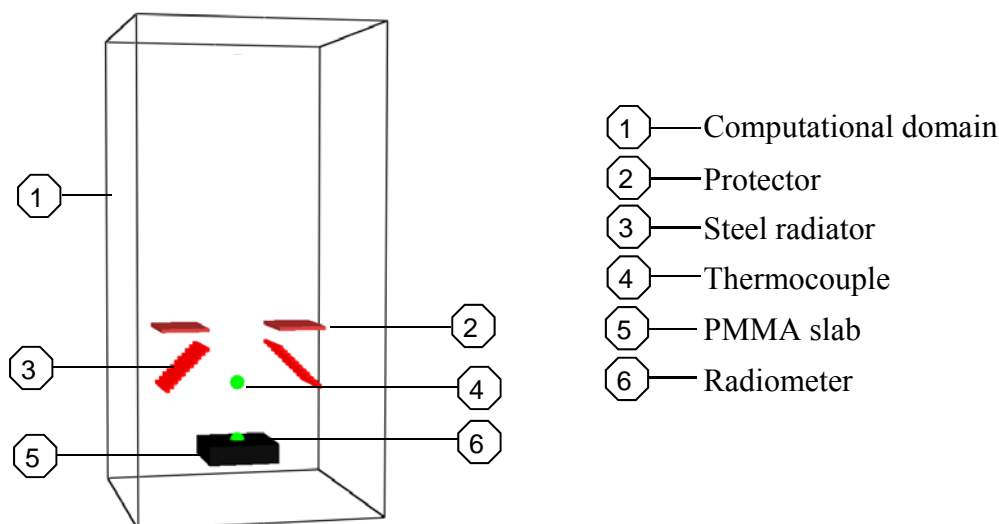


Figure 5.2: Three-dimensional view of the computational domain for the simulation of fires produced by the horizontally placed PMMA slabs.

In the case of the burning of the horizontal PMMA slab, the specimen of dimension 17.8 cm wide  $\times$  17.8 cm high  $\times$  5 cm thick is placed horizontally at a height of 0.5 cm from the floor. A set of two inclined steel plates is used as a heating source (radiant heaters) to the specimens and they are mounted 17.8 cm apart to allow passage of the water spray. They are positioned 25 cm above the specimen and inclined  $45^\circ$  to the plane normal to the centreline of the specimen. The green dots above and on the specimen surface are the locations where the temperature and radiation rate are calculated. The nozzle is located on top of the domain. The set-up of the specimen, steel plate, copper protector and water-mist nozzle in the domain for the simulation of the horizontally oriented PMMA slab are illustrated in Figure 5.2. In the case of the burning of the vertical PMMA slab, the orientation of the set-up is rotated  $90^\circ$  along the vertical centreline axis. The size of the PMMA slab is 17.8 cm wide  $\times$  35.6 cm high  $\times$  5 cm thick and placed horizontally at a height of 20 cm from the floor and 10 cm away from the rear side of the domain boundary. A nozzle is located at a distance of 1 meter from the specimen. The set-up for the burning of the vertically oriented PMMA slab is illustrated in Figure 5.3.

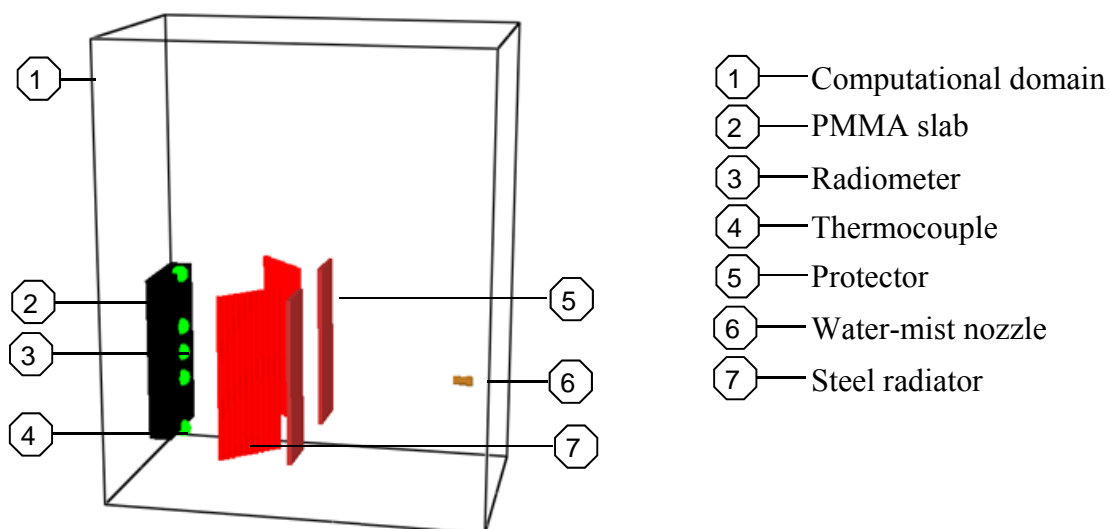


Figure 5.3: Three-dimensional view of the computational domain for the simulation of fires produced by the vertically placed PMMA slabs.

### 5.3.2 Operating and boundary conditions

The operating and boundary conditions for the simulation were as follows:

- The initial air temperature inside the computational domain is 20°C.
- The compartment floors are modelled as concrete and the side walls of the domain are kept open to be consistent with the experimental set-up.
- The domain is surrounded by free, neutral pressure boundaries.
- There are no external wind conditions.

### 5.3.3 Sensitivity analysis

The sensitivity of the numerical results for the three parameters is examined in this study. This included (i) the appropriate grid size for the computational domain; (ii) the effect of insulation of the rear surface of the sample on the burning rates of the PMMA slab; and (iii) the effect of the use of the absorption coefficient as one of the input parameters in the numerical simulations. The details of these analyses and the results are described below.

### 5.3.3.1 Grid spacing

The numerical results of any CFD model should be grid convergent. Therefore, in conducting a CFD analysis, it is essential to undertake a grid refinement process by gradually reducing the grid spacing (cell size) used in the analysis to examine the effect on the predicted results. It is usual to find that as the grid is refined, the results converge to a solution. Further reducing the cell size has virtually no effect on the results produced, and this result is known as a grid converged result. However convergence may only be obtained at an inordinate cost of computing resources and hence for this study a supercomputer has been required.

A grid sensitivity analysis was performed in a study by [Abu-Bakar and Moinuddin \[2015\]](#) using grid spacing of 10 mm, 5 mm and 2.5 mm (in the x, y and z directions). In the simulations, the specimen is subjected to 50 kW/m<sup>2</sup> of radiation. In all simulations the input parameters and boundary conditions are unchanged. The only change is the grid size. The heat release rates (HRR) of PMMA burning for these three cell sizes are calculated and compared. From the initial coarse grid sizes, the grid sizes are reduced by a factor of two. The results of HRR of these calculations, as illustrated in Figure 5.4, show that in the case of the 10 mm grid, the HRR is very high compared to that of the two other cell sizes. However the HRR for the 5 mm and 2.5 mm cell sizes are found to be almost identical. Therefore a mesh size of 5 mm is used to discretise the computational domain.

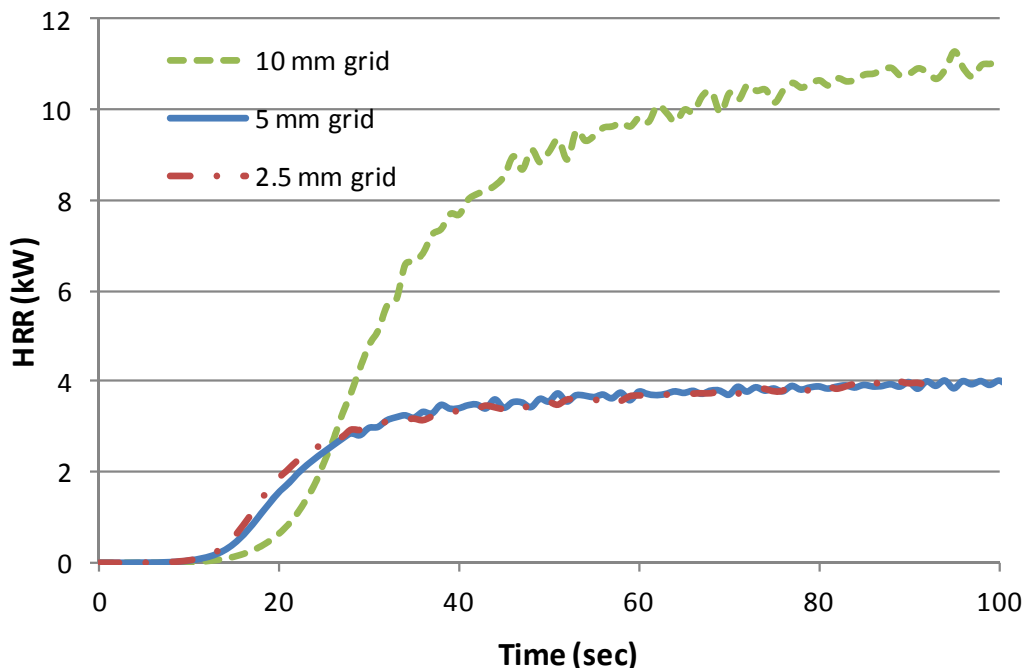


Figure 5.4: Grid convergence test for PMMA fire [Abu-Bakar and Moinuddin 2015].

### 5.3.3.2 Insulation of rear surface

The effect of insulation on the rear surface on the burning of the PMMA slab is also investigated in the simulation. If the rear surface of the specimen is kept insulated then there will not be heat loss from the rear surface of the sample [McGrattan et al. 2014]. Simulations are run with and without insulating the rear surface of the PMMA slab, and all other parameters are kept identical. The calculated burning rate, with and without insulation, is shown in Figure 5.5. The differences between the two cases are found to be not more than 8%. However in this study the rear of the sample is kept uninsulated to match the experiment by Magee and Reitz [1974].

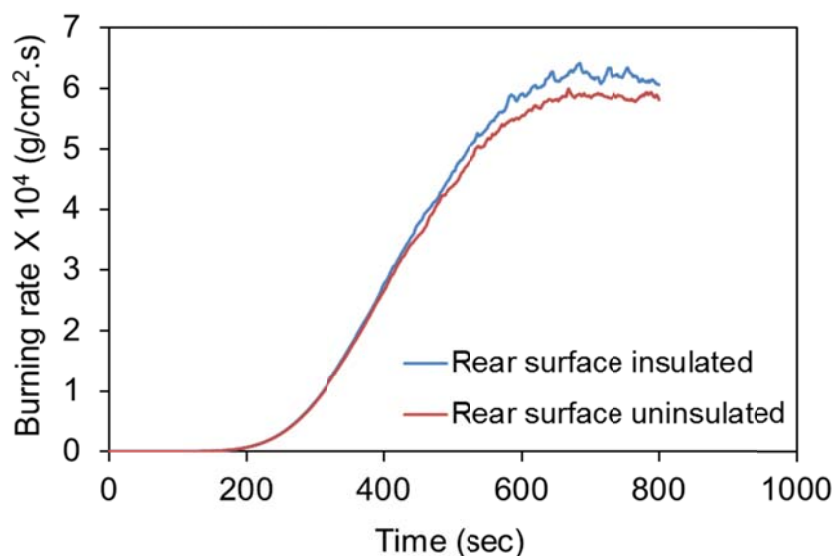


Figure 5.5: The effect of insulation on the rear surface of the PMMA slab.

### 5.3.3.3 Absorption coefficient

The effect of the absorption coefficient on the burning of the PMMA slab is calculated with and without using an absorption coefficient in the numerical simulation. The absorption coefficient signifies the attenuation of radiation as it penetrates the outer surface. Similarly the emission of radiation is based on the internal temperatures, not just the surface temperature [McGrattan et al. 2014]. However if the absorption coefficient is not defined then the radiation is only absorbed at the surface of the sample and the emission of radiation is a function of the surface temperature of the solid body.

In this study the magnitude of the difference of the burning rate of the PMMA slab with and without using the absorption coefficient is quantified. The burning rate of the sample is higher when the sample burning is calculated with the use of an absorption coefficient of PMMA. The highest difference of the burning rate of the sample with and without use of the absorption coefficient is about 12%. However, as there is penetration of thermal radiation through the surface of the PMMA slab in the experiment, the absorption coefficient is used as one of the input parameters in the numerical simulation to mimic the experiment by Mazze and Reitz [1974].

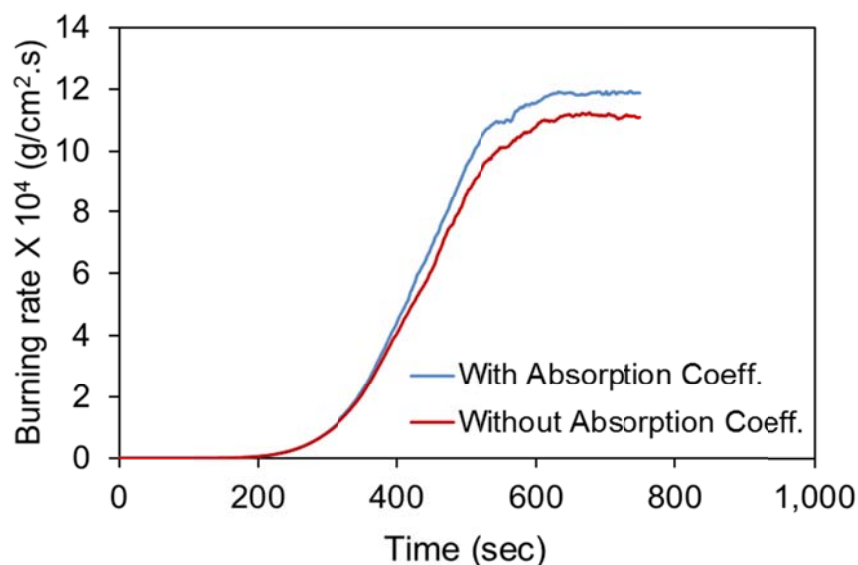


Figure 5.6: The effect of the use of the absorption coefficient of PMMA in the simulation.

#### 5.3.4 External radiation flux

The external radiation flux on the PMMA sample is varied in the simulation as it was in the experiment. In the simulation, the specimen is located underneath two hot steel plates. The radiant flux distribution over the PMMA surface is calculated by invoking a ‘device’ on the PMMA surface in the simulation. The heat flux over the PMMA surface resulted from the high temperature of the steel plates. To obtain the desired radiation flux rate on the PMMA slab surface, the steel plate temperature is varied and the radiation on the PMMA surface is calculated in the simulation. When the temperature of the steel plates gives the desired radiation flux rate, that temperature is used as the reference temperature of the steel plate. Radiation heat absorbed by the slab surface is calculated using an emissivity of 0.85 [Hallman et al. 1974] and an absorption coefficient of  $2700 \text{ (m}^{-1}\text{)}$  [Tsilingiris 2003]. The radiation flux rates used in the simulations are 15.89, 14.65 and 12.55  $\text{kW/m}^2$  for the burning of both horizontally and vertically oriented PMMA slabs.

### 5.3.5 Flammability parameters and chemical kinetics

The amount of energy consumed per unit mass of reactant in a solid phase reaction is specified by the heat of the reaction/pyrolysis (HoR). The amount of energy released per unit mass of fuel (kJ/kg) from a gas phase chemical reaction is specified as the heat of combustion (HoC) [McGrattan et al. 2014]. If the heat of combustion is specified, FDS calculates the enthalpy of the formation of the fuel such that the user-specified heat of combustion is maintained. The HoC and HoR of PMMA were determined in the Fire Dynamics Lab, CESARE, Victoria University using the cone calorimeter test, thermal gravimetric analysis (TGA) and DSC by Abu-Bakar and Moinuddin [2015]. The value of the HoR used in the simulation was 1627 kJ/kg for the heating rate of 5 K/min. The HoC data used in this analysis was 19490 kJ/kg for the irradiance of 50 kW/m<sup>2</sup>.

To define the solid phase chemistry (Arrhenius reaction), the kinetic parameters of the reaction rate are specified in the simulation. The kinetic parameters of the reaction rate are also sometimes defined as the Arrhenius parameters that include the activation energy ( $E$ ), the pre-exponential factor ( $A$ ) and the reaction order ( $N_s$ ). The value of the Arrhenius parameters varies with the variation of the heating rate to the specimen. Here, the values for a heating rate of 5 K/min is used for the simulation as the value for this heating rate gives a better prediction of HRR for PMMA fire [Abu-Bakar and Moinuddin 2015]. The value of the Arrhenius parameters was determined using TGA in the Fire Dynamic Lab, CESARE by Abu-Bakar and Moinuddin [2015]. These are specified in Table 5.1.

Table 5.1: Arrhenius parameters

Arrhenius parameters	Values
Activation energy ( $E$ ), J/mol	24234
Pre-exponential factor ( $A$ )	$1.47 \times 10^{18}$
Concentration exponents ( $N_s$ )	1.64

The input variables are the properties of PMMA, the radiative steel plate and the copper shield. The material properties and combustion parameters of the materials used for the simulations are listed in Table 5.2.

Table 5.2: Materials properties for the FDS input file

Material	Property	Value	Unit	Sources	
PMMA	Emissivity	0.85		[Abu-Bakar and Moinuddin 2015]	
	Density	1210	kg/m <sup>3</sup>		
	Heat of reaction	1625	kJ/kg		
	Heat of combustion	19490	kJ/kg		
	Absorption coefficient	2700	1/m		
	Activation energy	242.34	kJ/mol		
	Pre-exponential factor	$1.47 \times 10^{18}$			
	Reaction order	1.64			
	Soot yield	0.011	kg/kg		
	CO yield	0.006	kg/kg		
	Conductivity		1.9 at T = 20°C		W/m/K
			1.13 at T = 100°C		
Specific heat		1.55 at T = 20°C	kJ/kg/K	James [2014]	
		1.96 at T = 100°C			
		2.36 at T = 280°C			
Steel	Emissivity	0.9		Incropera and DeWitt [1990]	
	Density	7850	kg/m <sup>3</sup>		
	Conductivity		48 at T = 20°C		W/m/K
			30 at T = 677°C		
	Specific heat		0.45 at T = 20°C		kJ/kg/K
		0.60 at T = 377°C			
		0.85 at T = 677°C			

Copper	Emissivity	0.78		
	Density	8940	kg/m <sup>3</sup>	
	Conductivity	400 at T = 25°C	W/m/K	
		380 at T = 325°C		
	Specific heat	0.385 at T = 25°C	kJ/kg/K	
0.417 at T = 327°C				
0.432 at T = 527°C				
Gypsum board	Conductivity	0.158	W/m/K	
	Emissivity	0.6		
	Specific heat	1.09	kJ/kg/K	
	Density	800	kg/m <sup>3</sup>	
	Thickness	0.039	m	

Incropera  
and DeWitt  
[1990]

Incropera  
and DeWitt  
[1990]

## 5.4 Results and discussion

The burning of the vertical PMMA slab is simulated as coupled pyrolysis and combustion reaction using FDS and the burning rate of the specimen are calculated in the simulation. Figure 5.7 illustrates a three-dimensional view of the burning of the vertically placed specimen. The radiation flux rates on the specimen surfaces for the three different simulations are 15.89, 14.65 and 12.55 kW/m<sup>2</sup>, respectively. The samples are simulated to burn undisturbed until full burning is developed. When the burning rates are observed to be in a steady state, the nozzle activation is simulated in the simulation for the suppression of fires.

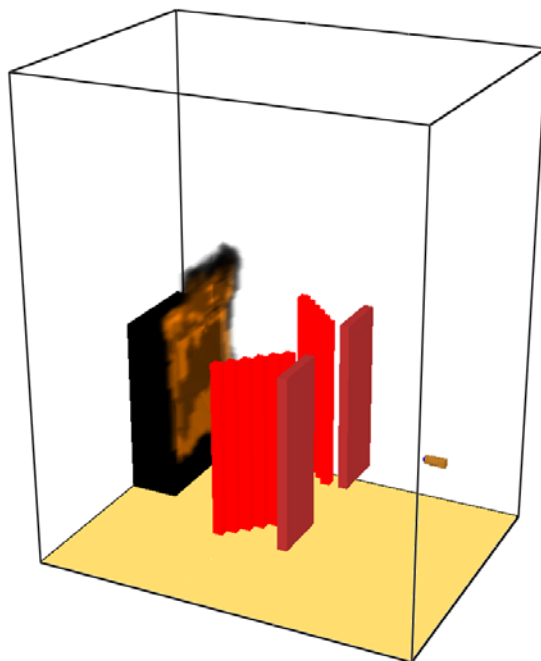


Figure 5.7: Three-dimensional view of the burning of the vertically oriented PMMA slab.

The burning rates of the specimens for the three different rates of radiation flux are presented in Figure 5.8. In the case of the radiation flux of  $15.89 \text{ kW/m}^2$ , the specimen is allowed to burn for up to 680 seconds until a steady state burning rate is observed. The water spray nozzle is then activated and, as a result, the burning rate of the sample begins to drop and becomes steady at 1100 seconds. The burning rates of the sample before and after activation of the nozzle in the numerical simulation are  $13.6$  and  $8.0 \text{ g/cm}^2\cdot\text{s}$ , respectively. These corresponding values in the experimental study by [Magee and Reitz \[1974\]](#) are  $16.5$  and  $9.2 \text{ g/cm}^2\cdot\text{s}$ , respectively, before and after activation of the nozzle. In the analysis it is found that the numerical value is about 18% and 15% lower than the experimental observation.

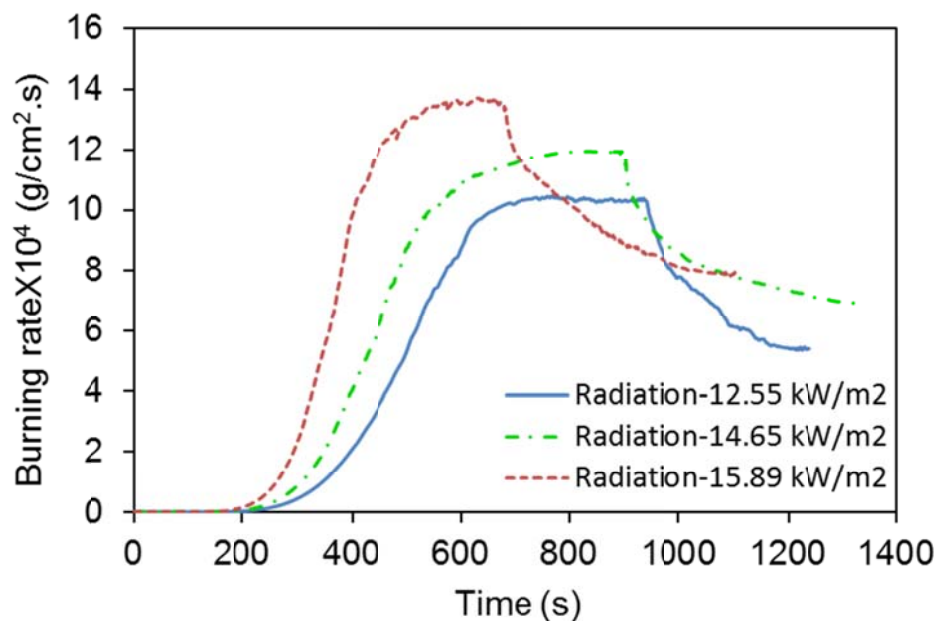


Figure 5.8: Burning rates of the vertically oriented PMMA slabs for the different flux of radiation ( $\text{kW/m}^2$ ) before and after activation of the spray.

The burning rates for the radiation flux of  $14.65$  and  $12.55$   $\text{kW/m}^2$  are also calculated in the numerical simulations and the results are presented in the same Figure 6.8. It is observed that the numerical results underpredict the burning rate in these two cases as has been found for the irradiance of  $15.89$   $\text{kW/m}^2$ . The difference between the numerical and experimental measurements of the burning rates for the irradiance of  $14.65$   $\text{kW/m}^2$  is 21% and 13% before and after the activation of the water-mist nozzle, respectively. This difference for the radiation flux of  $12.55$   $\text{kW/m}^2$  is 23% and 14% before and after the activation of the water-mist nozzle, respectively.

The ignition of the sample, development of the fire, burning of the specimen in steady state condition, activation of the water spray and burning of the sample with the water spray in the simulation at a different level of time for the radiation flux rate of  $15.89$   $\text{kW/m}^2$ , are also demonstrated sequentially in Figure 5.9.

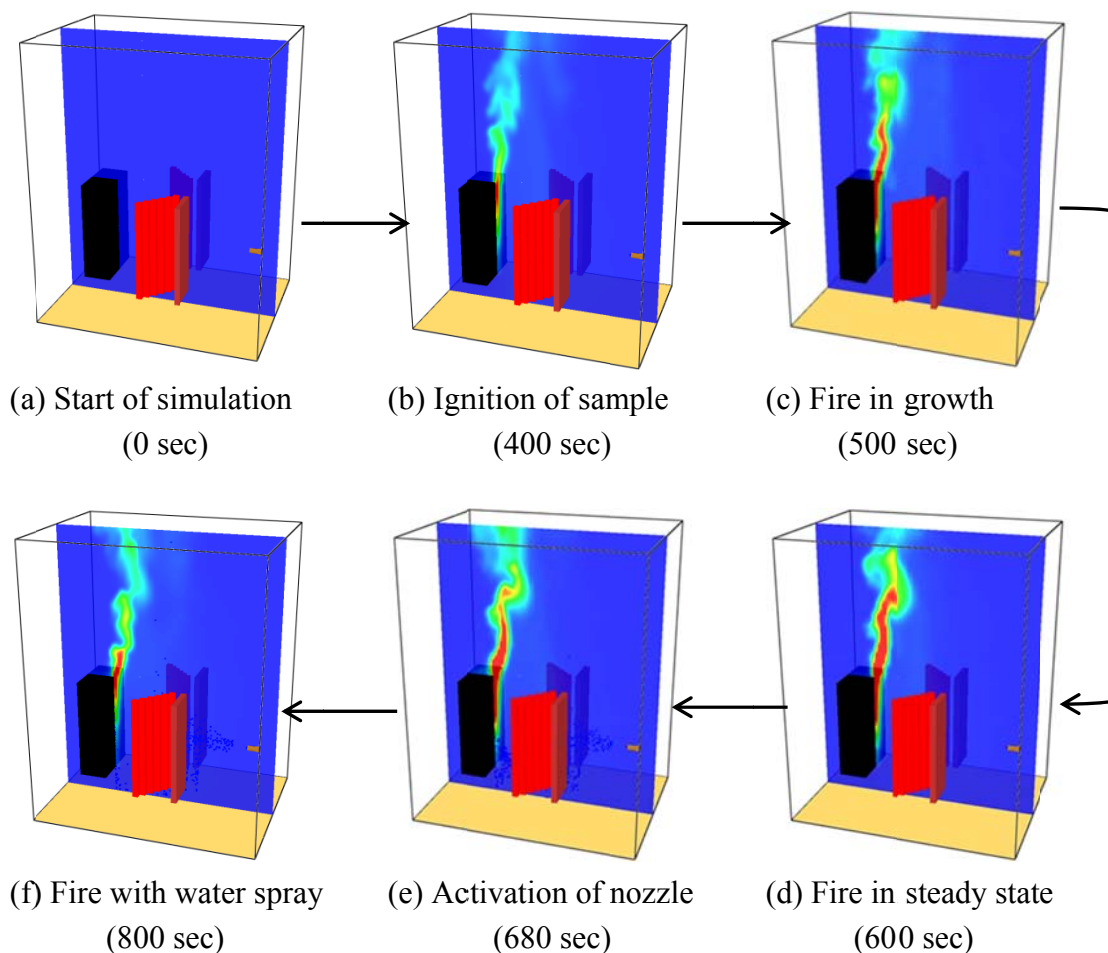


Figure 5.9: Burning and suppression of fire produced by the vertically oriented PMMA slab for the radiation flux rate of  $15.89 \text{ kW/m}^2$ .

The experimental and numerical values of the steady state burning rates for the vertically oriented PMMA slab, and the difference between the steady state burning rates before and after activation of the water spray, are presented in Table 5.3 and also presented graphically in Figures 5.10, 5.11 and 5.12.

Table 5.3: The experimental and numerical values of the steady state burning rates for the vertically oriented PMMA slab

Radiation flux (kW/m <sup>2</sup> )	Burning rate before activation of nozzle spray (g/cm <sup>2</sup> .s)			Burning rate after activation of nozzle spray (g/cm <sup>2</sup> .s)			Difference in burning rate before and after activation of nozzle spray (g/cm <sup>2</sup> .s)		
	Experimental values	Numerical values	% difference	Experimental values	Numerical values	% difference	Experimental values	Numerical values	% difference
15.89	16.5	13.6	18%	9.2	7.8	15%	7.3	5.8	21%
14.65	15.2	12.0	21%	7.7	6.7	13%	7.5	5.3	29%
12.55	13.8	10.6	23%	6.0	5.2	14%	7.8	5.4	31%

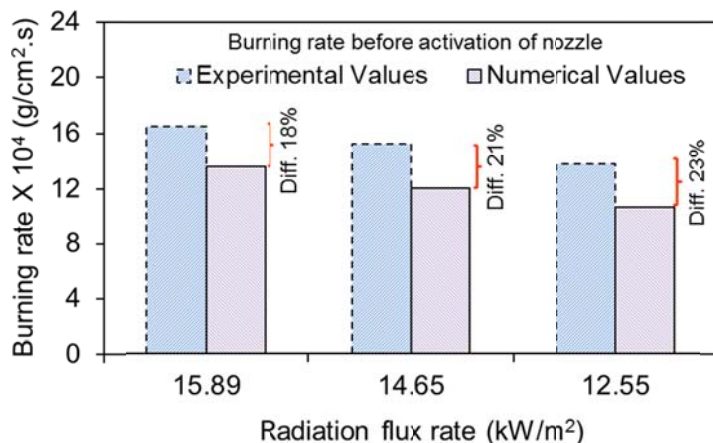


Figure 5.10: Comparison between the experimental and numerical steady state burning rates for the vertically oriented PMMA slab before activation of the spray.

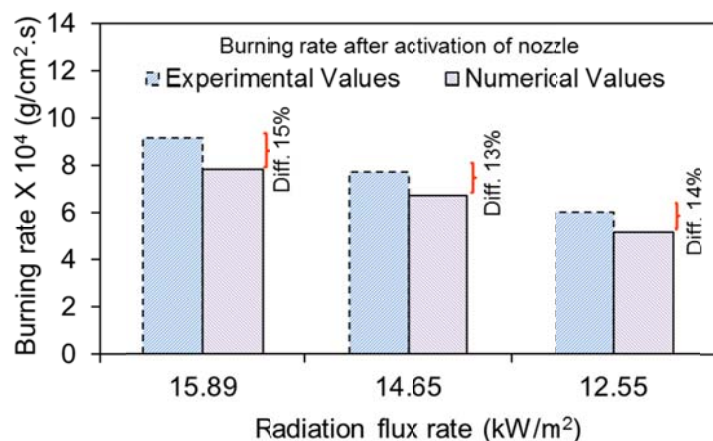


Figure 5.11: Comparison between the experimental and numerical steady state burning rates for the horizontally oriented PMMA slab before activation of the spray.

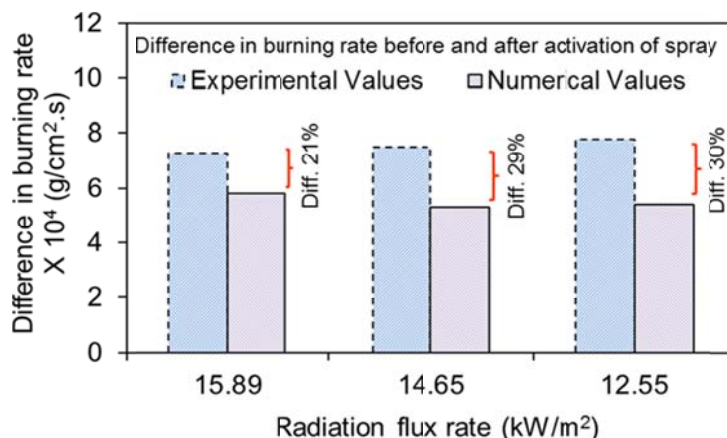


Figure 5.12: Comparison between the experimental and numerical values of difference in steady state burning rates before and after activation of spray for horizontally oriented PMMA slab.

The burning of the horizontally oriented PMMA slabs is also simulated using FDS and the burning rates of the specimens are determined. Three different radiation fluxes of 15.89, 14.65 and 12.55 kW/m<sup>2</sup> are used for the burning of specimens. The burning rates for the three different rates of radiation fluxes are presented in Figure 5.13.

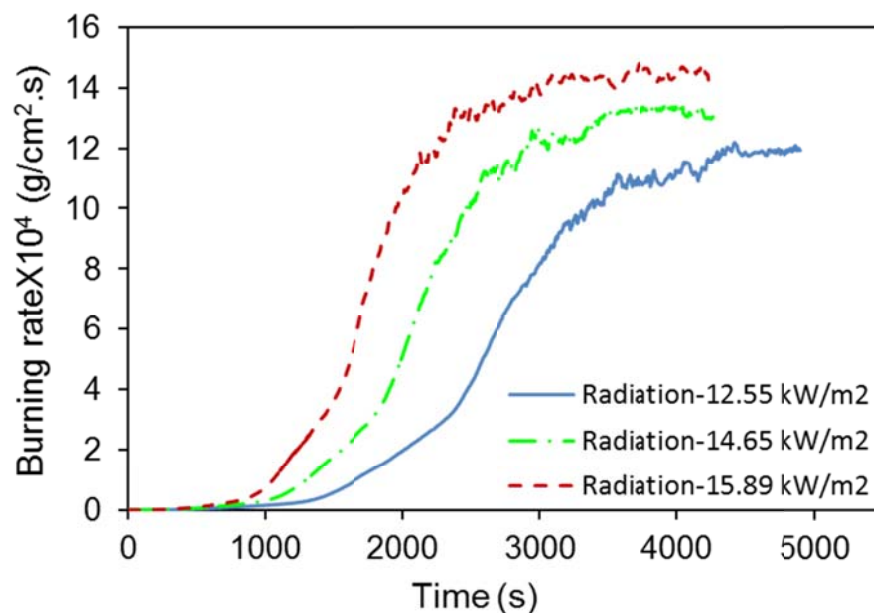


Figure 5.13: Burning rates of the horizontally oriented PMMA slabs at different levels of radiation fluxes (kW/m<sup>2</sup>).

In the numerical simulations, the samples are allowed to burn until full burning is developed. In the study by Magee and Reitz [1974], the burning rates of the horizontally oriented PMMA slabs are measured for different heating flux. However they did not have the measurement of the suppression of fires for the horizontally oriented PMMA slab. Therefore, in this case, the nozzle activation is not included in the numerical simulation. The predicted steady state burning rates of the horizontally placed PMMA slabs in the numerical simulation for the radiation flux of 15.85 kW/m<sup>2</sup> is 14.4 g/cm<sup>2</sup>.s, whereas this value in the experimental study is 17.2 g/cm<sup>2</sup>.s. The numerical result has underpredicted the burning rate by 17% compared to that of the experimental data. The ignition of the sample, development of the fire and the

burning of the specimen in a steady state condition in the simulation at different levels of time are also demonstrated sequentially in Figure 5.14.

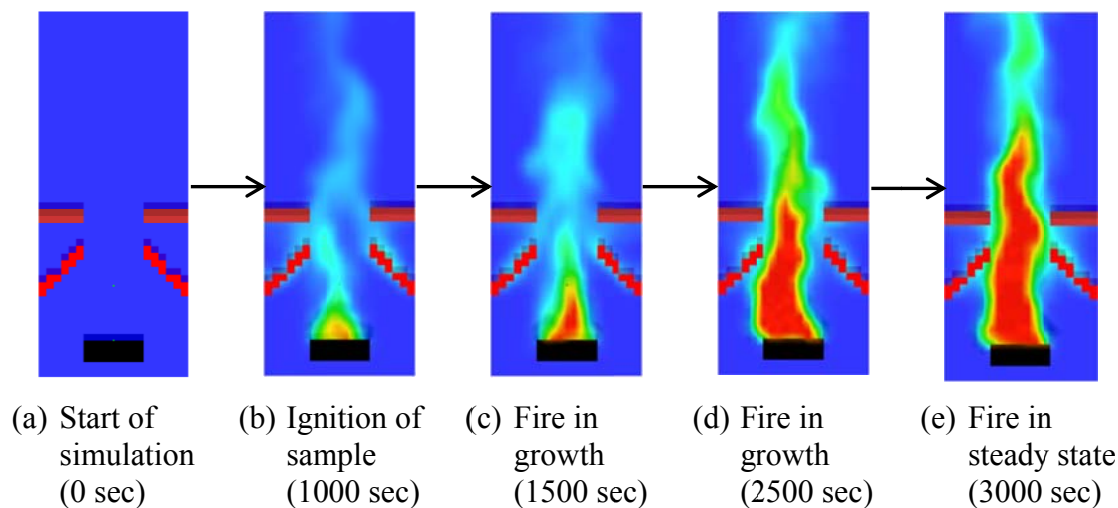


Figure 5.14: Burning of fire produced by the horizontally oriented PMMA slab for the radiation flux of 15.89 kW/m<sup>2</sup>.

The burning rates for the radiation levels of 14.65 and 12.55 kW/m<sup>2</sup> are also presented in the same Figure 5.13. It is observed that the numerical results have underpredicted the burning rates of the specimens. The differences between the numerical results and the experimental measurements for the radiation fluxes of 14.65 and 12.55 kW/m<sup>2</sup> are 19% and 20%, respectively. The experimental and numerical values of the steady state burning rates of the horizontally placed PMMA slab and the differences between them are presented in Table 5.4 and also presented graphically in Figure 5.15.

Table 5.4: The experimental and numerical values of steady state burning rates for the horizontally oriented PMMA slab

Radiation flux (kW/m <sup>2</sup> )	Experimental values (g/cm <sup>2</sup> .s)	Numerical values (g/cm <sup>2</sup> .s)	% difference
15.89	17.2	14.4	17%
14.65	16.2	13.2	19%
12.55	15.0	12.0	20%

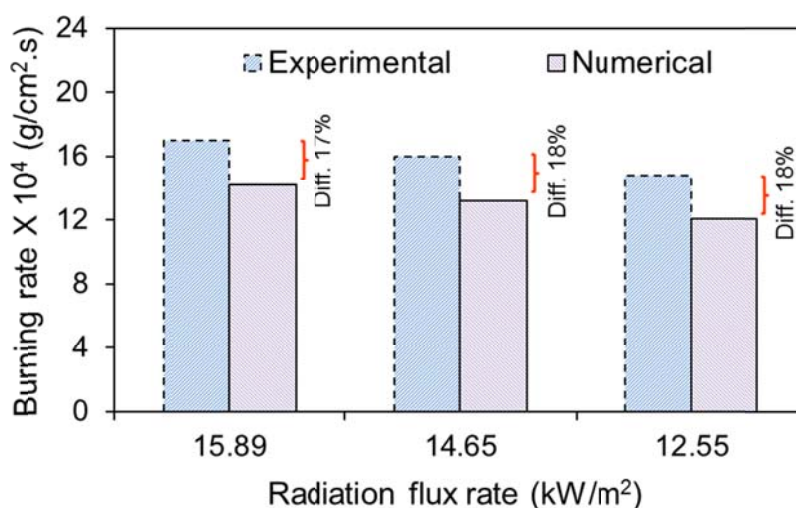


Figure 5.15: Comparison between the experimental and numerical steady state burning rates of the horizontally oriented PMMA slab.

In the numerical simulations an interesting phenomenon is observed that relates to the time required to reach the steady state burning of the PMMA slab for different orientations (i.e. vertical and horizontal orientation). The vertically oriented slab is found to ignite and attain a steady state burning rate earlier than the horizontally oriented slab. The vertically placed specimen is found to be ignited after 300 seconds and reached the steady state burning rate by 600 seconds, whereas these values are 1000 and 3000 seconds, respectively, for the horizontally placed specimen for the

radiation flux of  $15.89 \text{ kW/m}^2$ . The numerical result of the burning rate of the PMMA slab for the vertical orientation is also higher than for that of the horizontal orientation. From experimental evidence, it is also observed that the orientation does have a significant effect on the burning rate of a solid surface. The propagation of flame spread is also most rapid if it is directed upwards on a vertical surface [Drysdale 2011]. This phenomenon was also observed in the experimental work by Magee and Reitz [1974] and found in the numerical study by Yao and Chow [2005].

The reason for this behaviour is that the vertical specimen gets more convective and radiative heat feedback from the radiator and the fire itself due to its orientation, compared to the horizontal slab. The direction of the flame of any fire is in the upward direction due to the buoyancy driven flow. As a result, for the horizontal orientation of the burning surface, air entrainment into the flame leads to a 'counter current' of heat and flame spread. However, for the vertical orientation of the solid surface, the flame clings to the specimen surface and the natural buoyancy of the flame generates the 'concurrent' spread of heat and flame on the surface. This produces a greatly enhanced rate of the spread of the flame, and hot gases rise in the same direction, filling the layer and creating a high rate of heat transfer ahead of the burning zone [Drysdale 2011]. As a result, this phenomenon gives rise to more heat feedback to the specimen for the vertical orientation. The nature of this heat transfer into the burning surface is also presented graphically in Figure 5.16.

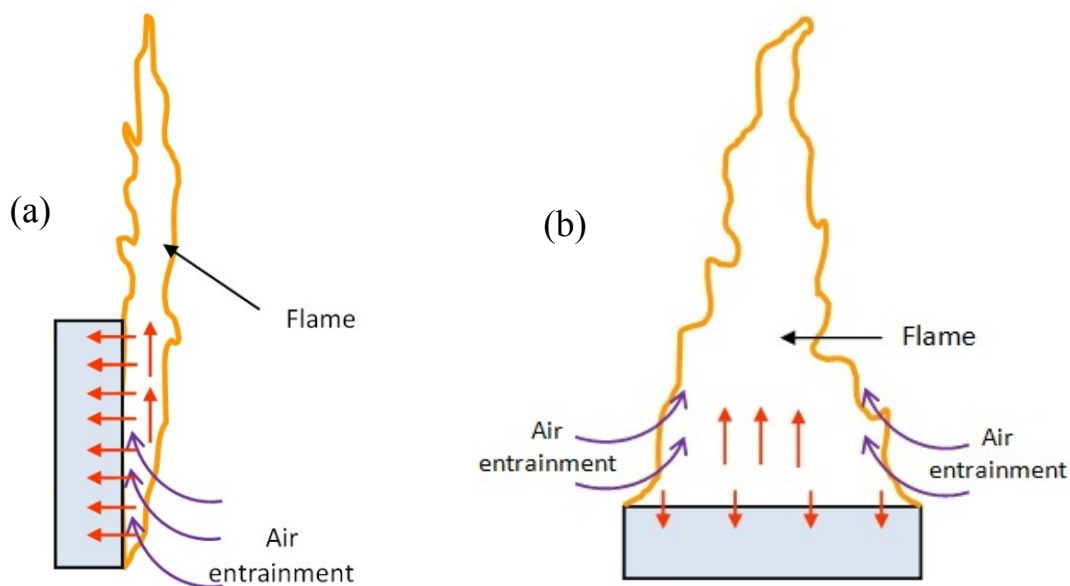


Figure 5.16: Convective and radiative heat transfer from the flame to the PMMA slab (a) vertical specimen; (b) horizontal specimen.

## 5.5 Conclusions

In this study, FDS is used to simulate the burning rates and suppression of radiation-augmented PMMA fires. Experimental data by [Magee and Reitz \[1974\]](#) are used to validate the numerical results. In the simulation, the heating rate on the PMMA specimens is varied and the burning rates before and after the activation of the water-mist nozzle are calculated. The outcomes of the study are summarised as below:

- i) The presence of insulation on the rear surface of a PMMA slab is found to have an effect on the burning rate compared to the absence of insulation. The burning rate was found to have increased by up to 8% in this study.
- ii) The use of an absorption coefficient in the simulation is found to have an effect on the burning rate of PMMA. The burning rate of the specimen has increased by up to 12%.

- iii) The calculated steady state burning rates of the specimen by FDS, before and after activation of the water-mist nozzle, are in reasonable agreement with the experimental measurements of [Magee and Reitz \[1974\]](#). The difference between the experimental and numerical values is not more than 23%, and in some cases, this difference is about 15%.
  
- iv) The orientation of the solid has a profound effect on the burning rate and time required to ignite and attain the steady state burning rate of the specimen. In this study, a vertically oriented specimen is found to ignite and reach the steady state burning rate in a shorter time than that of the horizontally oriented specimen of the PMMA slab.

## Chapter 6

Parametric study using FDS to assess  
the efficacy of water mist sprays

# Chapter 6

## Parametric study using FDS to assess the efficacy of water mist sprays

---

### 6.1 Introduction

In the previous chapters the capabilities of FDS in predicting the behaviour of evaporative droplets, flux density distribution of sprays, burning behaviour of solid fuels and suppression of fires produced by solid fuels have been validated against the experimental data. FDS has been found to be capable of predicting the experimental data with a difference of between 5 to 25%. This provides us with confidence in using FDS to simulate the behaviour of water mist and the suppression of fires. In this chapter, this model is used to investigate the ability of water mist in suppressing fires under a range of conditions. The factors considered include the number and location of the nozzles, the location of fires, obstruction on the fire and size of the droplets of a spray.

The extinguishment of obstructed fires cannot be achieved as readily as it can be achieved for unobstructed fires by directly interacting with a water-mist spray [Back et al. 2000]. The mechanisms that play a major role in the extinguishment of an obstructed fire by water mist are the dilution of oxygen by water vapour, the cooling of hot gases by water droplets, and the attenuation of thermal radiation feedback to the fire sources. In contrast, wetting burning surfaces and cooling the flame are additional mechanisms for the suppression of an unobstructed fire. The details of the mechanisms of the suppression of fires by water-mist sprays are described in section

1.2 of Chapter 1. The scenario of obstruction in between a fire and a spray can occur in residential or commercial buildings where the combustible materials such as papers, and electrical equipment such as computer CPUs may be located underneath tables, and flammable chemicals in industry may be potentially covered with an obstruction. Another potential obstruction around a fire can occur in the engine room of naval or commercial ships where flammable liquids, such as engine oil, diesel, etc., can be obstructed or hidden from water-mist spray by different machinery and equipment.

The location of a fire can also be an important issue in the case of suppression by water spray. The fire, which is located near ventilation, may be difficult to suppress by the spray as the fire can be supplied with oxygen by fresh air. This can also happen when the fire is located near an open door or window. On the other hand, fire that is located adjacent to boundary walls may receive a significant amount of radiation feedback to the fuel source. As a result, this can enhance combustion and increase the difficulty for a spray in suppressing the fire. However if a fire is located between an open door and the boundary walls of a room, then both of them may have an effect on the performance of the suppression of fires by the spray, depending on the distance from them.

The number and position of nozzles are a further issue that affects the suppression of fires by water-mist sprays. If a nozzle is located directly above a fire, the water droplets of the spray will have to travel the least distance to reach the fire. As a result, it may show better performance in suppressing the fire. In contrast, while installation of multiple nozzles will involve a higher cost for the system, multiple nozzles may show a better performance in suppressing the fire. However activation of two nozzles may render a drop in the valve pressure of the water supply and this can reduce the performance of the spray.

The size of the water droplets of a spray is another important issue that affects the performance of the spray. Droplets of a larger size have higher momentums and this may enable them to have a higher capacity in penetrating a fire plume and smoke layer. As a result, they may show better performance in suppressing the fire by the wetting and cooling of burning surfaces and hot gases. In contrast, droplets of smaller size have a higher rate of evaporation and time of suspension in the air. As a result, this may facilitate them to show a better performance in diluting oxygen and attenuating radiation feedback to the burning surfaces. Therefore a spray containing larger droplets may be superior to smaller droplets in suppressing an unobstructed fire, whereas the latter may be superior over the former size in suppressing an obstructed fire.

In the overall situation, if the above-mentioned factors act together, then the performance of the suppression of a spray might be severely compromised. For example, if a fire is horizontally obstructed and located near a source of ventilation and distant from a spray, then it might be difficult for the spray in suppressing the fire. Moreover, this situation might be more critical when the spray contains a larger size of droplets.

Therefore the considerations of these situations have prompted an investigation of the effects of a range of factors and their combination on the performance of the suppression of fires by water-mist sprays. In this chapter a qualitative parametric study is presented to evaluate the effect of these factors on the performance of water-mist sprays in suppressing fires. The factors that are evaluated are:

- (i) the type of obstruction around a fire
- (ii) the location of fire in an ISO room
- (iii) the number of nozzles above a fire
- (iv) the size of the droplets of a spray.

## 6.2 Numerical simulation

### 6.2.1 Computational domain

In this study the simulation of burning and the suppression of a wood fire is carried out in a domain similar to an ISO room. The reason for choosing an ISO room is that this is a standard size room that is normally used for the experimental and numerical study of fires [Yang et al. 2010; Moinuddin et al. 2011]. So, a computational domain similar to a standard ISO 9705 is created. The size of the room is 2.4 m × 2.4 m × 3.6 m. A hood of size 2.4 m × 2.4 m × 4 m is also attached to the room. The room is ventilated only by a doorway located at the centre of one of the 2.4 m wide walls. The size of the door is 2.0 m high and 0.8 m wide. The door is kept open during all of the tests. An illustration of the ISO room is presented in Figure 6.1.

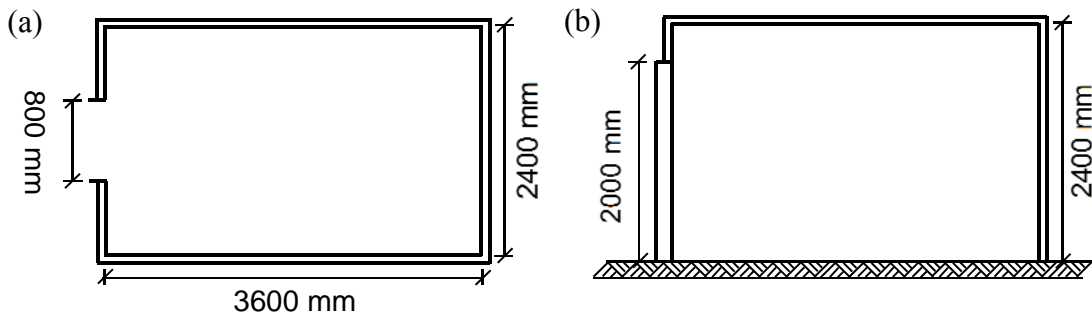


Figure 6.1: ISO room (a) plan view; (b) elevation [Moinuddin et al. 2011].

The size of the grid of the computational domain directly affects the computational results and time of the model. In any simulation an appropriate grid size should be selected so that the numerical results become independent of it (i.e. free from numerical error). Without such spatial resolution the numerical results become qualitative rather than quantitative. Quantitative solutions come at the cost of enormous computational resources. Therefore the selection of the size of a finer grid might be critical when it demands huge computational time and resources.

In the previous chapter (Ch. 5), a grid resolution of 5 mm has been found to give the grid independent results on the burning and suppression of PMMA fires in a domain of 2 m<sup>3</sup> in volume. A supercomputer consists of 16 processors with the specification of each of them of a 2000 MHz AMD Opteron 6100 series processor and 32 GB of RAM, and has taken about 750 hours to complete one simulation of 1200 seconds with that size of grid. However, in this part of the study, the computational domain is comprised of 43.78 m<sup>3</sup> in volume that is quite large, and in total, 24 simulations are required to run it. Therefore a quantitative analysis of fire behaviour using a grid resolution of 5 mm for this large size of domain is beyond the scope of the study of this part due to the constraints of computational resources and time. Therefore qualitative simulations are carried out in this part of the study to compare the results of the effect of different factors on the suppression of fires using a grid size of 50 mm to discretise the computational domain. In the studies by [Dac \[2014\]](#) and [Moinuddin et al. \[2011\]](#), 50 mm grid size has been found to give quantitative solutions for temperature and radiation flux when the HRR has been prescribed.

### **6.2.2 Type and location of fuel load**

Timber cribs are used as fuel load in all of the simulations. The cribs are formed of pine timber sticks 950 mm × 50 mm × 50 mm in dimension. Two sticks are placed on the floor parallel to each other along the longitudinal axis (parallel to the width of the ISO room) at a distance of 85 cm from the inside edge. These two sticks are used as a support for the stacks and for ventilation under the crib. Then the timber sticks are placed on the support in nine layers to form the crib. The gap in between the two sticks in the crib is 50 mm. The crib size is 950 mm long × 950 mm wide × 450 mm high.

The timber cribs are placed in three locations of the ISO room for three different cases, to investigate the effect on the location of the burning of fuel in the room. The

three locations are (i) adjacent to the open door (Case *a*); (ii) centre of the room (Case *b*); and (iii) distant from the open door (Case *c*). The locations of the timber cribs in the room are illustrated in Figure 6.2. In Case *a*, the timber crib is placed 50 cm from the door; in Case *b*, it is placed at the centre of the room; and in Case *c*, the timber crib is placed 50 cm away from the end of the room.

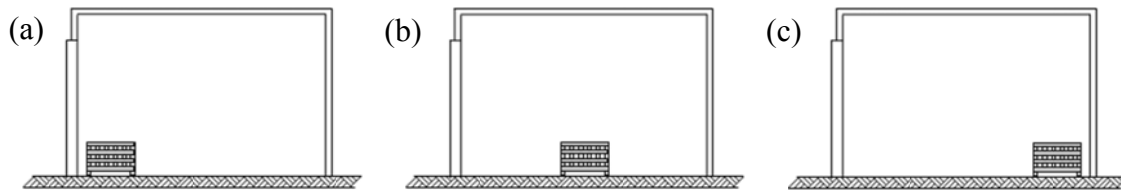


Figure 6.2: Location of timber crib in the ISO room (a) adjacent to the open door (Case *a*); (b) centre of the room (Case *b*); (c) distant from the open door (Case *c*).

### 6.2.3 Location of the nozzles

The nozzles are placed in two locations in the ISO room. In one case, a single nozzle is placed at the centre of the ceiling of the room, and in the second case, two nozzles are placed in the ceiling 1200 mm apart and 1200 mm from each side of the room. These two cases are designated as Case *A* and Case *B*, respectively. Details of the location of the nozzles in the ISO room are shown in Figures 6.3 and 6.4.

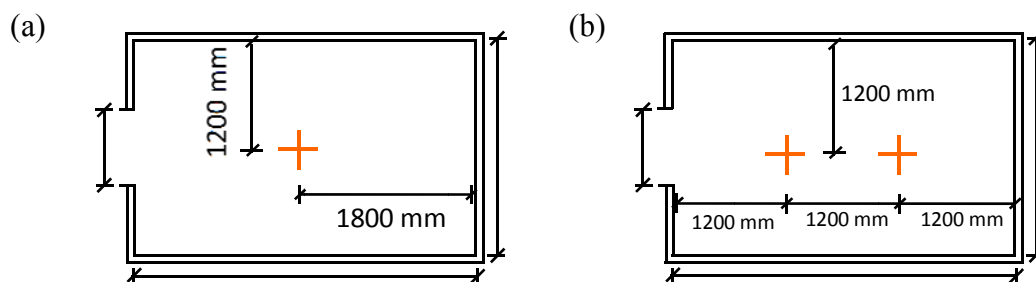


Figure 6.3: Plan view of the locations of the nozzles in the ISO room (a) a single nozzle (Case *A*); (b) a double nozzle (Case *B*).

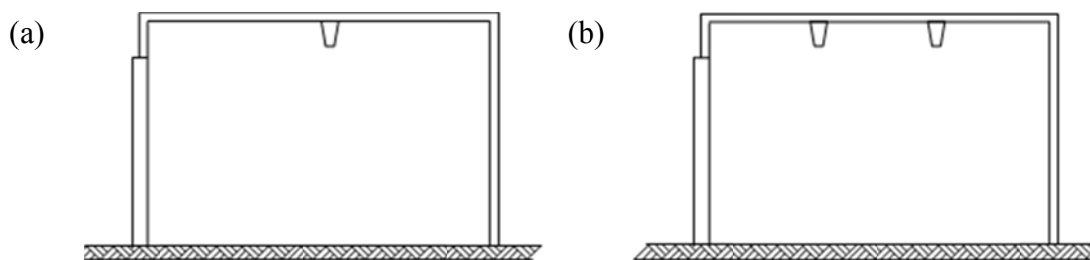


Figure 6.4: Side elevation of the location of the nozzles in the ISO room (a) a single nozzle (Case A); (b) a double nozzle (Case B).

### 6.2.4 Types of obstructions

Two types of obstruction of fires are selected to examine the effect of the obstruction on the burning and suppression of fires. Apart from this, the unobstructed condition of a fire is also considered. Therefore the condition of un-obstruction and two types of obstruction generated three cases – Case 1: no obstruction; Case 2: a horizontal obstruction; and Case 3: a vertical obstruction. In Case 1 a fire is allowed to grow and is suppressed without any obstruction. In Case 2 a fire is separated from the spray by a horizontal obstruction. And, finally, in Case 3 a vertical obstruction is placed next to a fire so that the spray nozzle may fall on any side of the obstruction. The dimensions of the horizontal and vertical obstructions are 100 cm × 100 cm × 10 cm and 120 cm × 100 cm × 10 cm, respectively. The condition of the obstructions used in the simulation is shown in Figure 6.5.

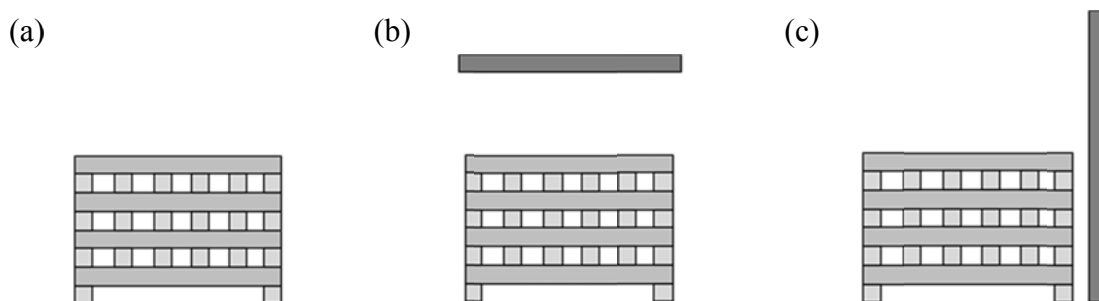


Figure 6.5: Condition of obstructions (a) no obstruction (Case 1); (b) horizontal obstruction (Case 2); (c) vertical obstruction (Case 3).

### 6.2.5 Orientation of nozzle, obstruction and fire load in the simulation

The combination of the location of the wood crib, condition of the obstruction and number of nozzles has generated 18 cases for simulation. These 18 cases of simulation are divided into three cases based on the condition of the obstruction. They are – Case 1: no obstruction; Case 2: a horizontal obstruction; Case 3: a vertical obstruction. These three cases are again divided into two sub-cases based on the number of nozzles. They are – Case A: single nozzle; Case B: double nozzles. Finally, these two sub-cases are divided into three cases based on the location of the fire load. They are – Case a: adjacent to the open door; Case b: centre of the room; Case c: distant from the open door. The combinations of the three parameters are tabulated in Table 6.1, and for clarity, they are presented graphically in Table 6.2. The FDS representations of these cases are also presented in Tables 6.3 to 6.6.

Table 6.1: Combination of the location of the fire, condition of obstruction and number of nozzles for different cases in the ISO room

Types of obstruction (Case 1/2/3)	Number of nozzles (Case A/B)	Location of fire (Case a/b/c)	Case number
No obst. (Case 1)	Single (Case A)	Adjacent to open door (Case a)	1-A-a
		Centre of the room (Case b)	1-A-b
		Distant from open door (Case c)	1-A-c
	Double (Case B)	Adjacent to open door (Case a)	1-B-a
		Centre of the room (Case b)	1-B-b
		Distant from open door (Case c)	1-B-c
Horizontal (Case 2)	Single (Case A)	Adjacent to open door (Case a)	2-A-a
		Centre of the room (Case b)	2-A-b
		Distant from open door (Case c)	2-A-c
	Double (Case B)	Adjacent to open door (Case a)	2-B-a
		Centre of the room (Case b)	2-B-b
		Distant from open door (Case c)	2-B-c

Vertical (Case 3)	Single (Case A)	Adjacent to open door (Case <i>a</i> )	<i>3-A-a</i>
		Centre of the room (Case <i>b</i> )	<i>3-A-b</i>
		Distant from open door (Case <i>c</i> )	<i>3-A-c</i>
	Double (Case B)	Adjacent to open door (Case <i>a</i> )	<i>3-B-a</i>
		Centre of the room (Case <i>b</i> )	<i>3-B-b</i>
		Distant from open door (Case <i>c</i> )	<i>3-B-c</i>

Chapter 6: Parametric study using FDS to assess the efficacy of water mist sprays

Table 6.2: Graphical presentation of the combination of the location of the fire, type of obstruction and number of nozzles for different cases

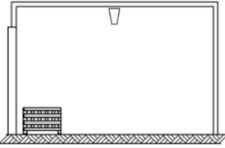
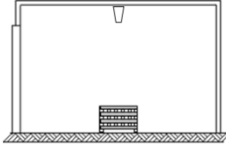
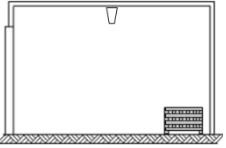
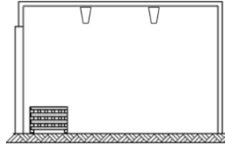
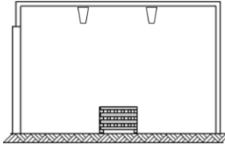
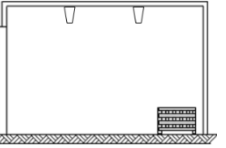
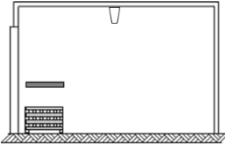
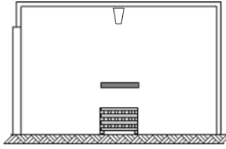
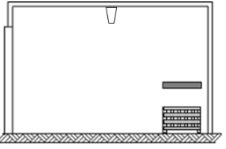
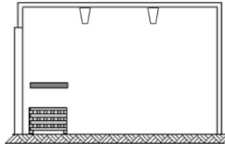
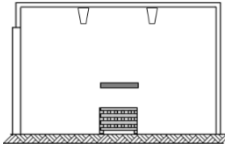
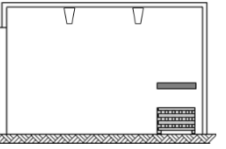
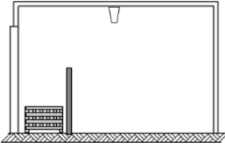
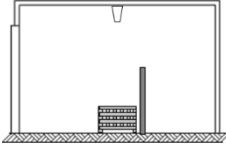
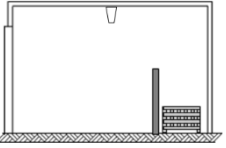
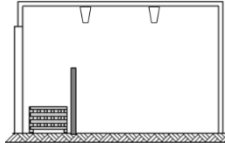
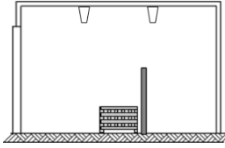
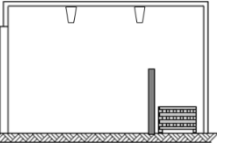
Type of obstruction	Single nozzle (Case A)			Double nozzle (Case B)		
	Adjacent to open door (Case a)	Centre of the room (Case b)	Distant from open door (Case c)	Adjacent to open door (Case a)	Centre of the room (Case b)	Distant from open door (Case c)
No obstruction (Case 1)						
Horizontal obstruction (Case 2)						
Vertical obstruction (Case 3)						

Table 6.3: Location of nozzle, obstruction and fuel load for Case 1(A)

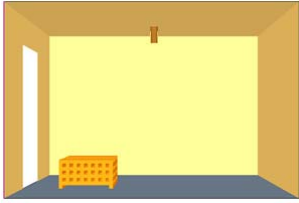
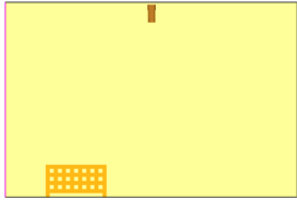
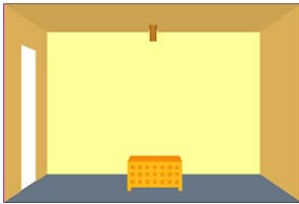
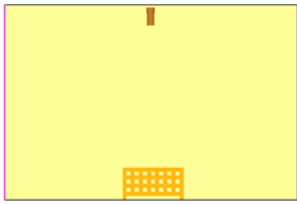
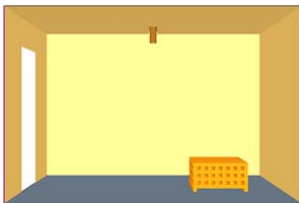
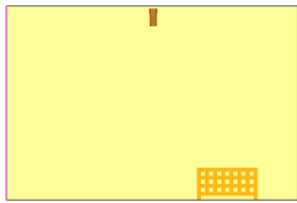
Case	3D-view	2D-view
Case 1(A-a)		
Case 1(A-b)		
Case 1(A-c)		

Table 6.4: Location of nozzle, obstruction and fuel load for Case 1(B)

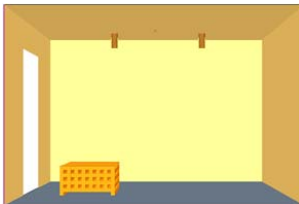
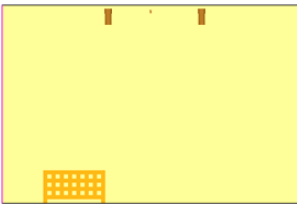
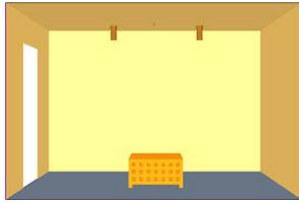
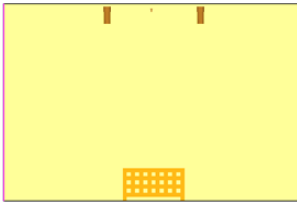
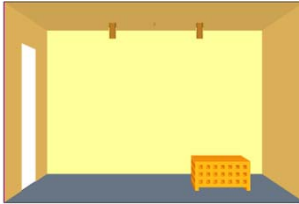
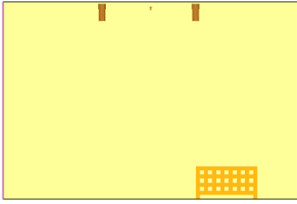
Case	3D-view	2D-view
Case 1(B-a)		
Case 1(B-b)		
Case 1(B-c)		

Table 6.5: Location of nozzle, obstruction and fuel load for Case 2(A)

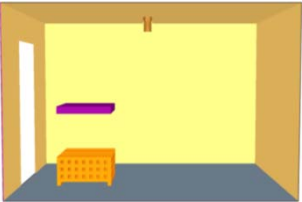
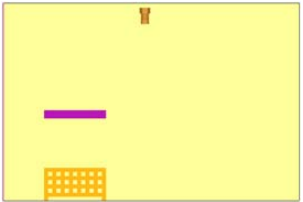
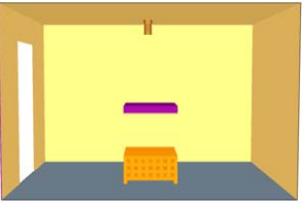
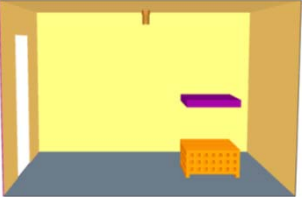
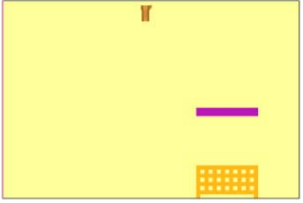
Case	3D-view	2D-view
Case 2(A-a)		
Case 2(A-b)		
Case 2(A-c)		

Table 6.6: Location of nozzle, obstruction and fuel load for Case 2(B)

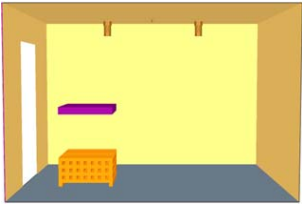
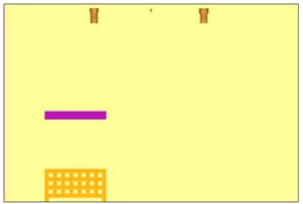
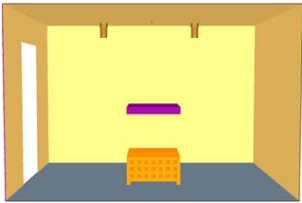
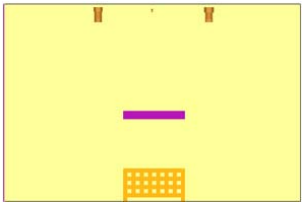
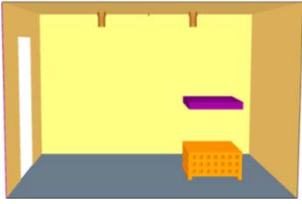
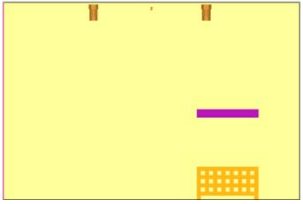
Case	3D-view	2D-view
Case 2(B-a)		
Case 2(B-b)		
Case 2(B-c)		

Table 6.7: Location of nozzle, obstruction and fuel load for Case 3(A)

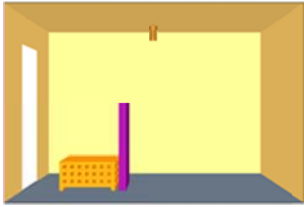
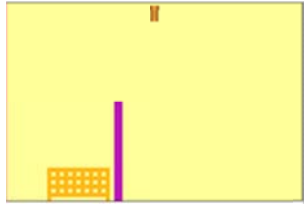
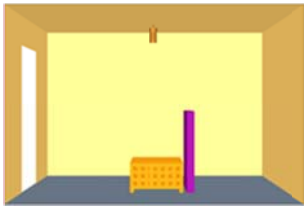
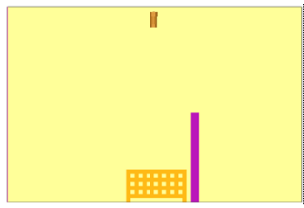
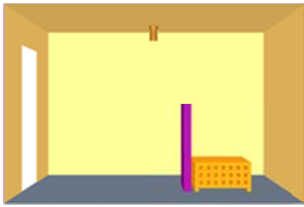
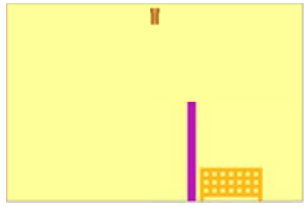
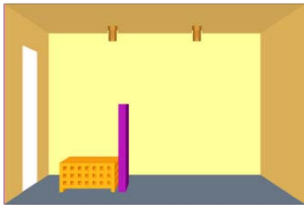
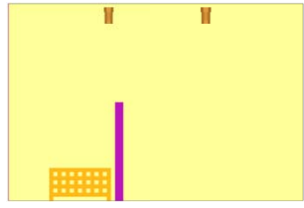
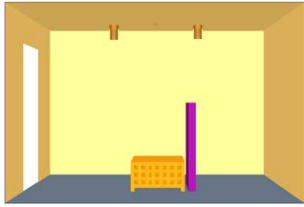
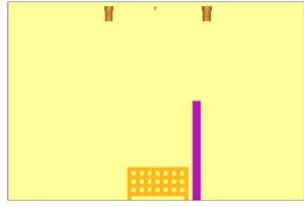
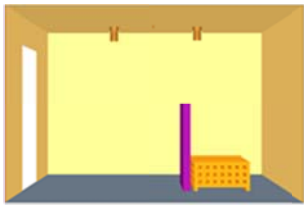
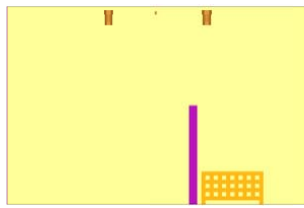
Case	3D-view	2D-view
Case 3(A-a)		
Case 3(A-b)		
Case 3(A-c)		

Table 6.8: Location of nozzle, obstruction and fuel load for Case 3(B)

Case	3D-view	2D-view
Case 3(B-a)		
Case 3(B-b)		
Case 3(B-c)		

### 6.2.6 Specification of the spray

A single-orifice nozzle is used for the spray of water mist in the numerical simulation. The spray from the nozzle is specified by the input parameters of the flow rate of water, angle of spray, height of spray, median diameter of the droplet size and the velocity of the droplet. The values of the parameters for the spray are tabulated in Table 6.9.

Table 6.9: Specification of the spray

Input variables	Values
Flow rate, L/min	1.7
Droplet diameter, $\mu\text{m}$	500*
Spray pattern	Solid
Spray angle	45°
Spray height, m	2.3
Droplet velocity, m/s	10

\* Note: Used for the simulation of 18 cases listed in Table 6.1.

### 6.2.7 Material properties of pinewood, ignition of the wood crib, and activation of the water-mist nozzle

The kinetic parameters and other material properties of virgin pine and char used for the numerical simulation are listed in Table 6.10. The kinetic parameters of pinewood and char, the heat of reaction (HoR) and the heat of combustion (HoC) of pine are taken from the experimental measurement conducted in the Fire Dynamics Lab, CESARE, Victoria University by [Abu-Bakar and Moinuddin \[2015\]](#).

To promote ignition of the fuel, a burner is placed underneath the timber crib with a heat release rate per unit area (HRRPUA) of 100 kW/m<sup>2</sup>. Fire spread takes place from the burner to the wood crib in the simulation. To facilitate this a temporary arrangement is made for promoting additional heat back to the wood crib by placing obstructions around three sides of the fire and this is removed after fire spread has

occurred. As stated earlier, this part of the study is a qualitative comparison. Therefore the simulation time is counted from when the fire reaches a quasi-steady-state level of HRR and is allowed to continue to burn for 100 seconds before activation of the water-mist spray. The water-mist nozzle is activated at 100 seconds and allowed to spray until the end of the simulation.

Table 6.10: Material properties for the FDS input file

Material	Properties	Value	Units	Sources
Pinewood	Emissivity	1		
	Density	423	kg/m <sup>3</sup>	
	Heat of reaction	429.35	kJ/kg	
	Heat of combustion	11210	kJ/kg	Abu-Bakar and Moinuddin [2015]
	Activation energy	78.41	kJ/mol	
	Pre-exponential factor	6.1 x 10 <sup>4</sup>		
	Reaction order	0.56		
	Soot yield	0.006	kg/kg	
	CO yield	0.007	kg/kg	
	Conductivity	0.17 at T = 20°C	W/m/K	James [2014]
	Specific heat	1.1 at T = 20°C	kJ/kg/K	
2.3 at T = 50°C				
	4.0 at T = 90°C			
Char	Emissivity	1		Abu-Bakar and Moinuddin [2015]
	Specific heat	0.43	kJ/kg/K	
	Density	140	kg/m <sup>3</sup>	
	Conductivity	0.08 at T = 20°C	W/m/K	
0.25 at T = 900°C				
Gypsum	Conductivity	0.158	W/m/K	Incropera and DeWitt [1990]
	Emissivity	0.6		
	Specific heat	1.09	kJ/kg/K	
	Density	800	kg/m <sup>3</sup>	
	Thickness	0.039	m	

### 6.3 Results and discussion

In this study, 18 cases are simulated as mentioned in Tables 6.1 and 6.2. According to the Fire Brigade Interaction Model (FBIM), if the HRR of fire is reduced to 30–35% after the activation of the spray, then the fire is considered to be suppressed by the spray [Zhao et al. 1998][AFAC 2004]. Wighus [1995] also conducted experiments to establish a connection between the size of a fire and the quantity of water required from a spray to suppress the fire and he found that if about one-third of heat produced by the fire was removed by the spray, the fire might be extinguished. Therefore, in this study, the suppression of fire is considered when it is lowered to a level of 65% of HRR of its quasi-steady-state by the water spray.

The predicting variables in the simulations are HRR, temperatures of the burning surfaces and hot gases, concentrations of oxygen and irradiance to the burning surface. The temperatures of the burning surface and radiation feedback to the wood crib are estimated at the middle of the top surface of the wood crib. The temperatures of hot gases and concentration of oxygen are computed at 5 cm above the wood crib and the location of the estimation is denoted by A as indicated in Figure 6.6.

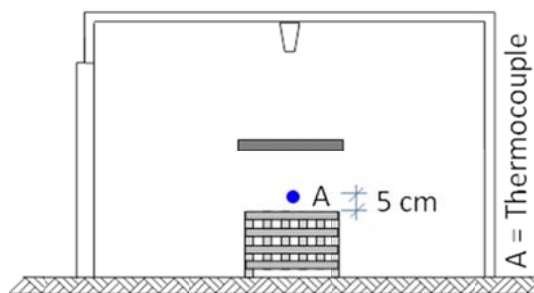


Figure 6.6: Location of the estimation of gas temperature and concentration of oxygen.

In this study, the results are analysed and compared for different combinations of parameters. The comparisons are with respect to (i) condition of obstructions; (ii) location of fires; and (iii) number of nozzles. Comparisons are made for the

prediction of HRR, burning rates, temperatures of the burning surface and hot gases. Other than the 18 cases, six cases are also run to see the effect of size of the droplets on the suppression of fires by sprays.

### **6.3.1 Effect of obstructions**

#### **6.3.1.1 Heat release rate**

The effect of obstructions on HRR and the suppression of fires have been analysed and compared. The results are presented in Figure 6.7, and the suppression times of the fires after activation of the water spray for different cases are tabulated in Table 6.11.

It is observed in Figures 6.7 (b) and (e) that the fires that are at the centre of the room and obstructed by a horizontal barrier take a longer time to be suppressed by the spray compared to the unobstructed and vertically obstructed fires. The fire that is located at the centre of the room and horizontally obstructed (Figure 6.7 (b)) is suppressed at 400 seconds by the water-mist spray; whereas unobstructed and vertically obstructed fires are suppressed at 175 and 150 seconds, respectively, by the water-mist spray. The reason is that as the fire is directly underneath the nozzle and the spray is completely separated from the fire by the obstruction, the water droplet cannot reach the fire. However the horizontally obstructed fires that are not directly underneath the water-mist nozzle (Figure 6.7 (a, c, d and e)) are suppressed in an earlier time compared to the fires that are directly underneath the nozzle (Figure 6.7 (b) and (e)) as a part of the spray can reach the fires. In the case of a vertical obstruction located adjacent to and distant from the open door (Figure 6.7 (a, c, d and f)), the fires take a little longer to be suppressed compared to that of the unobstructed fires. However, as might be expected, in all of the cases the unobstructed fires are quickly suppressed, and to a greater extent, compared to the horizontally and vertically obstructed fires.

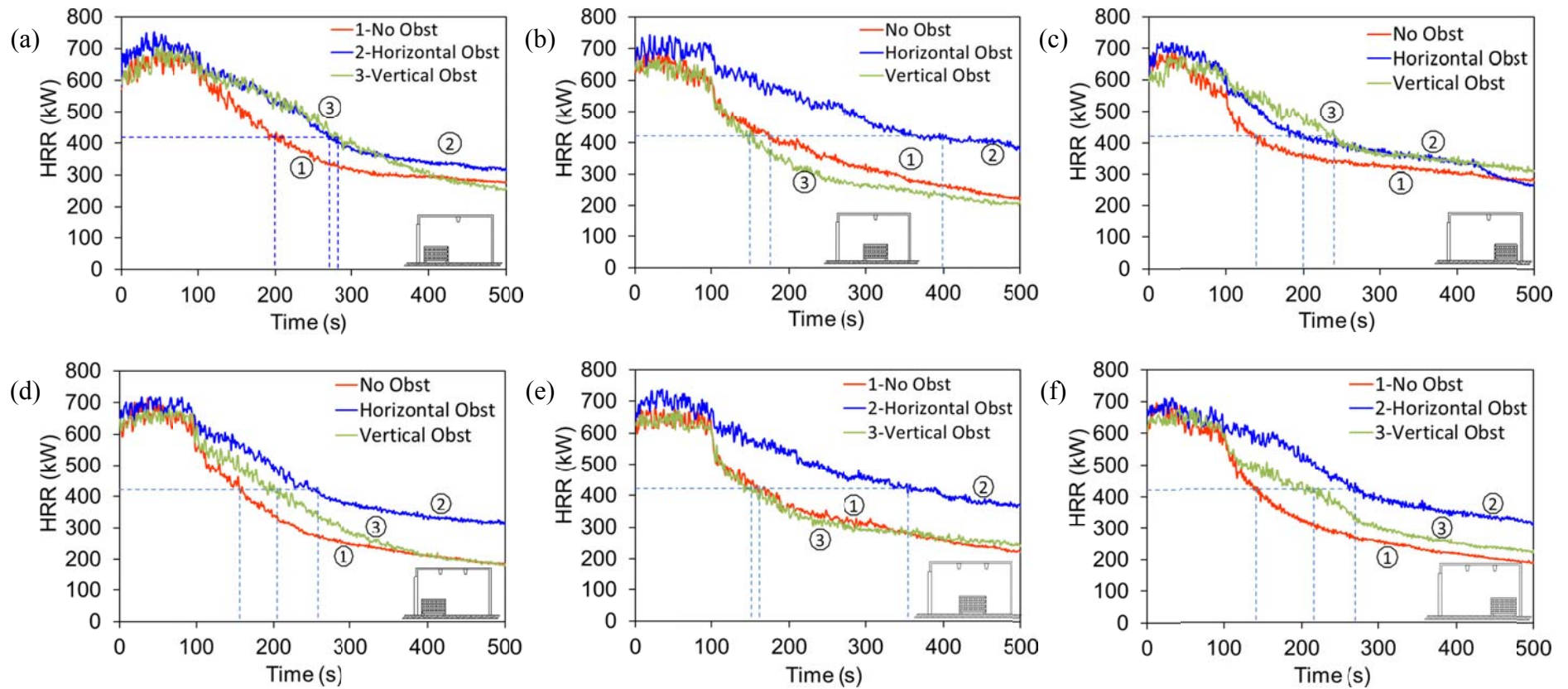


Figure 6.7: Comparison of the effect of the condition of the obstruction on the suppression of fires (HRR) by water spray (a) single nozzle – adjacent to the open door; (b) single nozzle – centre of the room; (c) single nozzle – distant from open door; (d) double nozzle – adjacent to the open door; (e) double nozzle – centre of the room; and (f) double nozzle – distant from the open door.

Table 6.11: Combination of parameters for the comparison of HRR with respect to the type of obstruction and time of suppression of fires with respect to 65% of HRR

Location of fire (Case a/b/c)	Number of nozzles (Case A/B)	Types of obstruction (Case 1/2/3)	Case number	Time of suppression (second)
Adjacent to door (Case a)	Single (Case A)	No obst. (Case 1)	a-A-1	200
		Horizontal (Case 2)	b-A-2	275
		Vertical (Case 3)	c-A-3	285
	Double (Case B)	No obst. (Case 1)	a-B-1	160
		Horizontal (Case 2)	b-B-2	260
		Vertical (Case 3)	c-B-3	210
Centre of room (Case b)	Single (Case A)	No obst. (Case 1)	a-A-1	175
		Horizontal (Case 2)	b-A-2	400
		Vertical (Case 3)	c-A-3	150
	Double (Case B)	No obst. (Case 1)	a-B-1	160
		Horizontal (Case 2)	b-B-2	360
		Vertical (Case 3)	c-B-2	150
Distant from door (Case c)	Single (Case A)	No obst. (Case 1)	a-A-1	140
		Horizontal (Case 2)	b-A-1	200
		Vertical (Case 3)	c-A-3	240
	Double (Case B)	No obst. (Case 1)	a-B-1	140
		Horizontal (Case 2)	b-B-2	275
		Vertical (Case 3)	c-B-3	220

### 6.3.1.2 Competing mechanisms for fire suppression

#### *Reduction of temperature of burning surface and hot gases*

Fires produced by solid fuels require pyrolysis for the ignition and combustion of fuel. Therefore reduction of the temperature of the burning surface by spray plays a major role in arresting the pyrolysis of the fuels and consequently suppresses the fires. Reduction of the temperature of hot gases is also important in suppressing fires. Water droplets, sprayed from a nozzle, absorb heat from hot gases and flames, and result in reduction of the temperature of the surrounding air and flames. Therefore it reduces the HRRs from the fires and consequently suppresses them.

In this section, the effect of obstruction on the reduction of temperature of the burning surface and hot gases by water spray is analysed and the results are presented in Figures 6.8 and 6.9. Here, the comparison is conducted for two positions of fire – at the centre of the room and at a distance from the open door – and the spray is from a single nozzle. These two positions of fire are related to Figures 6.7 (b) and (c), respectively. The location of the estimation of temperatures is shown in Figure 6.6. The results indicate that the spray is not able to reduce the temperatures of the burning surface and hot gases for two situations. They are, when the fire is (i) horizontally obstructed and located at the centre of the room as shown in Figure 6.8 (a) and (d); and (ii) vertically obstructed and located at a distance from the open door as shown in Figure 6.9 (a) and (d). In both cases, the fires are obscured from the spray by the obstructions. As a result, the water droplets cannot reach the fires and firebases. However, in other cases, the temperatures of the burning surface and hot gases are substantially reduced by the spray.

#### *Reduction of concentration of oxygen and rate of radiation*

The reduction of the concentration of oxygen and the attenuation of thermal radiation also play a significant role in suppressing a fire. As a minimum amount of oxygen is required to support the combustion of a fire, the reduction of concentration of oxygen below this limit will accelerate the suppression of a fire. According to [Drysdale \[2011\]](#), the critical oxygen limit for charring solid fuel is 7%. Similarly, the attenuation of thermal radiation also contributes to the suppression of a fire. The water droplets absorb radiant heat from the flame and block the radiation feedback to the fire from hot boundaries.

In this section, the effect of obstruction on the concentration of oxygen and irradiance to the wood surface are analysed and the results are presented in Figures 6.8 and 6.9. The concentration of oxygen is predicted at 5 cm above the wood surface and the irradiance is predicted on the top surface of the crib, as shown in

Figure 6.6. Here, comparison is made for the same cases as mentioned in the previous section. The concentrations of oxygen are quickly reduced before activation of the spray due to consumption by the growing fire. As presented in Figures 6.8 (b) and 6.9 (b), the level of concentration of oxygen is lowered to half the natural concentration before activation of the spray. However, after activation of the spray, this concentration is increased for unobstructed and vertically obstructed fires because at these conditions, the consumption of oxygen is reduced due to the suppression of fires.

In the case of the horizontally obstructed fire that is located at the centre of the room (Figure 6.8 (b) and (e)), rather than increasing, the concentration of oxygen remained unchanged. The same phenomenon is observed with little increase in the concentration for vertically obstructed fire located at a distance from the open door (6.9 (b) and (e)). This is because for horizontally obstructed conditions, as water droplets fall over the obstruction, they make vertical curtains around the fire, and for the vertically obstructed condition, as the obstruction is located in between the fire and the open door, it hinders the flow of oxygen to the fire source. In the case of radiation feedback to the fuel surface, it is also lowest for the horizontally obstructed condition of fire located at the centre of the room as can be seen in Figure 6.8 (c) and (f).

Therefore, from this analysis, it is concluded that the cooling of hot gases and burning surfaces by the water droplets of a spray play a major role in suppressing unobstructed fires. Whereas the blocking of air entrainment and attenuating radiation feedback to the fuel surface caused by the spray play a major role in suppressing horizontally obstructed fires with the condition that the fire is directly underneath the nozzle.

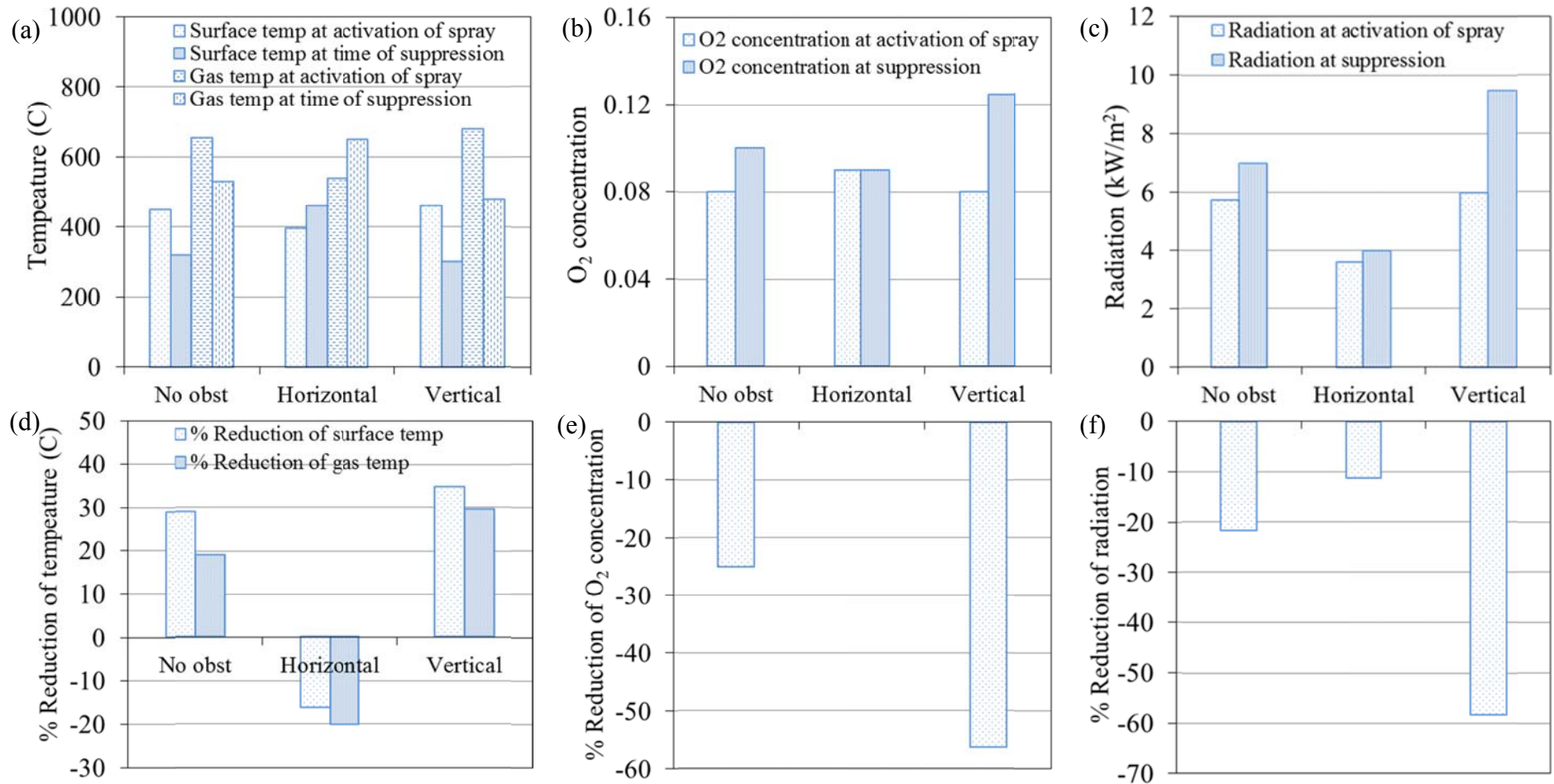


Figure 6.8: Comparison of the effect of obstructions on the reduction of temperatures of the burning surface and hot gases by water spray; the fire is related to Figure 6.7 (b) which is located at the centre of the room and the spray is from a single nozzle (a) temperature; (b) concentration of oxygen; (c) radiation; (d) % reduction of temperature; (e) % reduction of concentration of oxygen; and (f) % reduction of radiation.

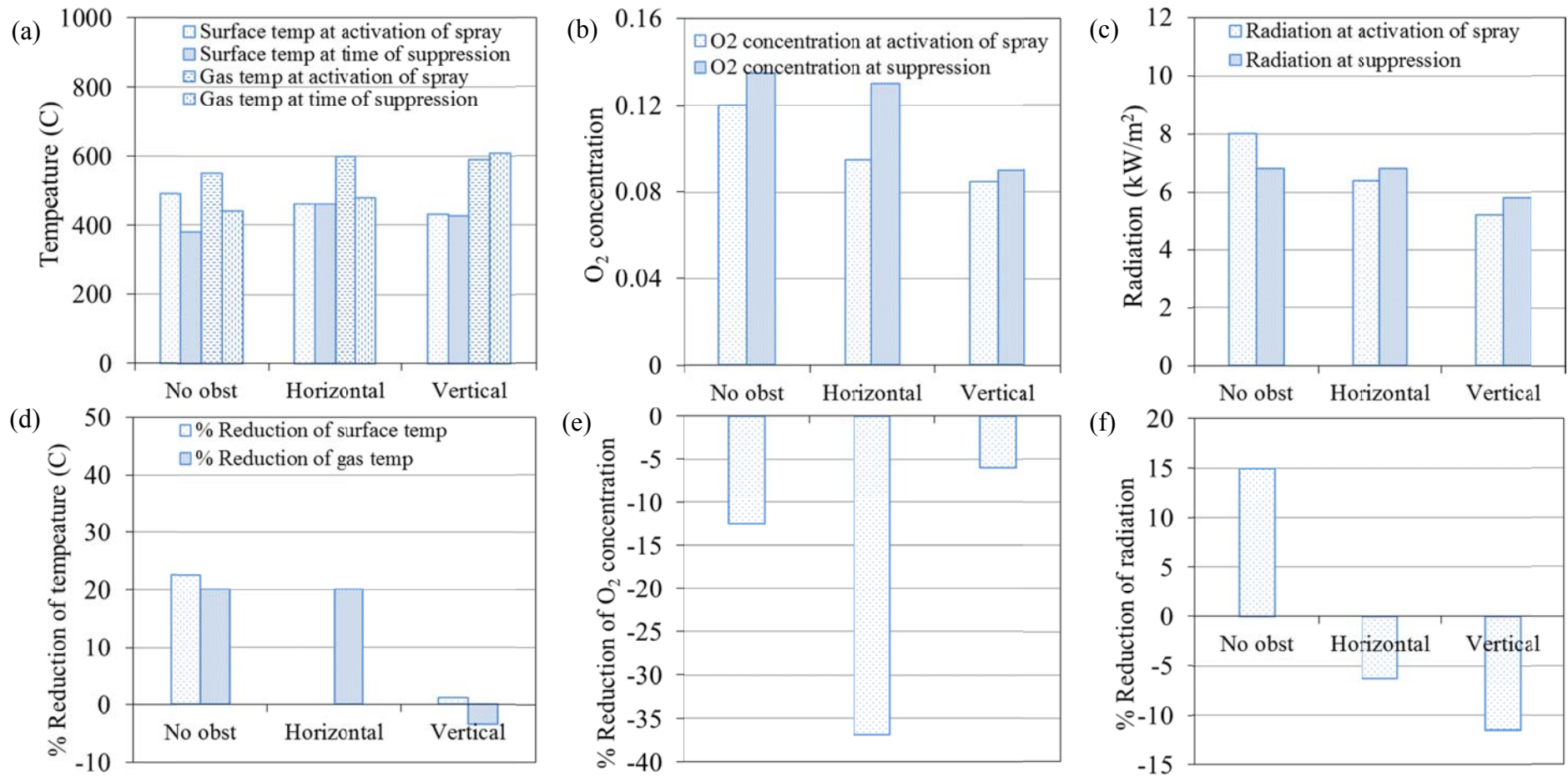


Figure 6.9: Comparison of the effect of obstructions on the reduction of temperature of the burning surface and hot gases by water spray; the fire is related to Figure 6.7 (c) which is located at a distance from open door and the spray is from a single nozzle (a) temperature; (b) concentration of oxygen; (c) radiation, (d) % reduction of temperature; (e) % reduction of concentration of oxygen; and (f) % reduction of radiation.

### **6.3.2 Effect of location of fires**

The location of a fire in a room has an effect on the burning rates of fires and, consequently, on the suppression of the fire by spray. When a fire is located closer to an opening or ventilation, it gets higher access to the air supply. As a result, it may cause a higher burning rate of the fuel, and subsequently, a spray might take a longer time to suppress the fire. On the other hand, if the fire is located in a position away from the open door, it may have less access to the air supply. As a result, it may cause a lower burning rate of the fuel, and subsequently, the spray might take a shorter time to suppress the fire. However, if the fire is obstructed, it is obscured from the spray and might take a longer time to be suppressed. Furthermore, the obstruction may enhance the radiation feedback to the fuel surface, which can increase the burning rate of the fuel. Therefore the combination of location of a fire and condition of obstruction might either enhance the burning rate of fuel and create a difficult situation for the spray in suppressing the fire, or it might reduce the burning rate of fuel and make it easier for the spray to suppress the fire.

The objective of this section is to investigate the effect of the location of fire in an ISO room on its suppression by a spray of water mist. HRRs, the temperatures of burning surfaces and hot gases are estimated in the simulations and compared with each other with respect to location of the fires. The combinations of 18 cases for the comparison of HRR with respect to the location of fires are presented in Table 6.12.

#### **6.3.2.1 Heat release rate**

The effect of the location of fire on HRR is analysed and compared in this section. The locations are: adjacent to the open door (ventilation); at the centre of the room; and at a distance from the open door (ventilation). The results and comparisons are presented in Figure 6.10.

The results indicate that, for unobstructed conditions and spray from the single nozzle (Figure 6.10 (a)), the spray is most effective when the fire is directly underneath the nozzle. The same phenomena are also observed for vertically obstructed fire and spray from the single nozzle as presented in Figure 6.10 (c). Notably, the opposite phenomenon is observed in Figure 6.10 (b) and (e) for horizontally obstructed fires. In these cases, the spray is least effective when the fire is directly underneath the nozzle. It is observed in Figure 6.10 (b) that the fire located at the centre of the room is suppressed at 400 seconds by the spray, whereas the fires located adjacent to and at a distance from the open door, are suppressed at 275 and 200 seconds, respectively, by the spray. In the case of fire that is horizontally obstructed and located directly underneath the nozzle, it is totally separated from the spray. In other cases, part of the spray can reach the burning surfaces of fires. It is observed in Figure 6.10 (c) and (f) that for the vertically obstructed condition, the spray is least effective, as the obstruction has obscured the spray from the fires. In this condition, as the fire is located adjacent to the boundary walls of the room, the solid fuel receives more radiation feedback. As a result, this enhances the burning of the fuel and consequently the spray takes a longer time to suppress the fire. The suppression times of fires after the activation of water spray for different cases are tabulated in Table 6.12.

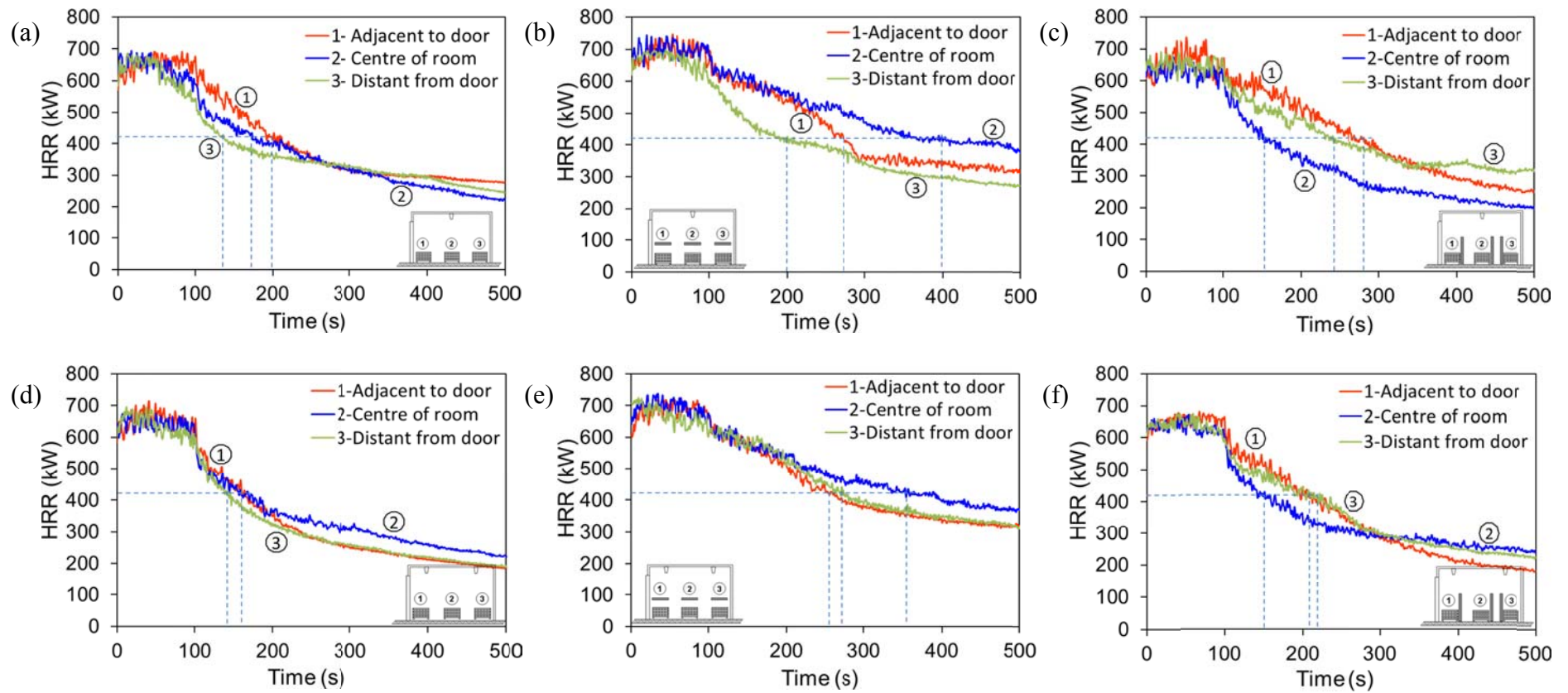


Figure 6.10: Comparison of the effect of location of fires on suppression of fires (HRR) by water spray (a) single nozzle – adjacent to the open door,; (b) single nozzle – centre of the room; (c) single nozzle – distant from the open door; (d) double nozzle – adjacent to the open door; (e) double nozzle – centre of the room; and (f) double nozzle – distant from the open door.

Table 6.12: Combination of parameters for the comparison of HRR with respect to the location of fires

Types of obstruction (Case 1/2/3)	Number of nozzles (Case A/B)	Location of fire (Case a/b/c)	Case number	Time of suppression after activation of spray (second)
No obst. (Case 1)	Single (Case A)	Adjacent to door (Case a)	1-A-a	200
		Centre of room (Case b)	1-A-b	175
		Distant from door (Case c)	1-A-c	140
	Double (Case B)	Adjacent to door (Case a)	1-B-a	160
		Centre of room (Case b)	1-B-b	160
		Distant from door (Case c)	1-B-c	140
Horizontal (Case 2)	Single (Case A)	Adjacent to door (Case a)	2-A-a	275
		Centre of room (Case b)	2-A-b	400
		Distant from door (Case c)	2-A-c	200
	Double (Case B)	Adjacent to door (Case a)	2-B-a	260
		Centre of room (Case b)	2-B-b	360
		Distant from door (Case c)	2-B-c	275
Vertical (Case 3)	Single (Case A)	Adjacent to door (Case a)	3-A-a	285
		Centre of room (Case b)	3-A-b	150
		Distant from door (Case c)	3-A-c	240
	Double (Case B)	Adjacent to door (Case a)	3-B-a	210
		Centre of room (Case b)	3-B-b	150
		Distant from door (Case c)	3-B-c	220

### 6.3.2.2 Competing mechanisms for fire suppression

#### *Reduction of temperatures of burning surface and hot gases*

In this section, the effect of location of a fire on the reduction of temperatures of burning surfaces and hot gases by a spray are analysed and the results are presented in Figures 6.11 (a) and (d), and 6.12 (a) and (d). Here, the comparison has been made for no obstructed and vertically obstructed condition of fires and the spray is from a single nozzle. These two cases are related to Figures 6.10 (a) and (c), respectively.

Figures 6.11 (d) and 6.12 (d) indicate that when the fire is located in proximity to the open door (ventilation) for both conditions of obstruction, the temperatures of the burning surfaces are not reduced; rather they increased. In this case, as the fire is distant from the water spray, only part of the spray can reach the burning surface. Moreover, as the fires are located near the ventilation, they get a supply of fresh air from the open door. As a result, although HRR is lowered by the spray, there is still burning on the surfaces of the wood crib. However, in other cases, except for the fire vertically obstructed and located at a distance from the open door (Figure 6.12 (d)), the temperatures of the burning surface and hot gases are substantially reduced by the spray.

#### *Reduction of the concentration of oxygen and rate of radiation*

The results of the concentration of oxygen are presented in Figures 6.11 (b) and (e), and 6.12 (b) and (e). The results show that the concentration of oxygen is increased at the time of suppression for all locations of fires except for the fire vertically obstructed and located adjacent to the open door. This is because before activation of the spray, the concentration of oxygen is reduced due to its consumption by the growing fire, and after activation of the spray the fire begins to be suppressed, resulting in less consumption of oxygen by the fire itself.

The results of irradiance to the burning surface are presented in Figures 6.11 (c) and (f), and 6.12 (c) and (f). The results show that irradiance is lowered after activation of the spray for the location of the fire at a distance from the open door and unobstructed; however, in the other two cases, it is increased after activation of the spray. In the case of the vertically obstructed condition, the spray is most effective for the fire that is located at a distance from the open door as shown in Figure 6.12 (f). In this case, the irradiance to the fuel surface increased little compared to the other two locations of fire.

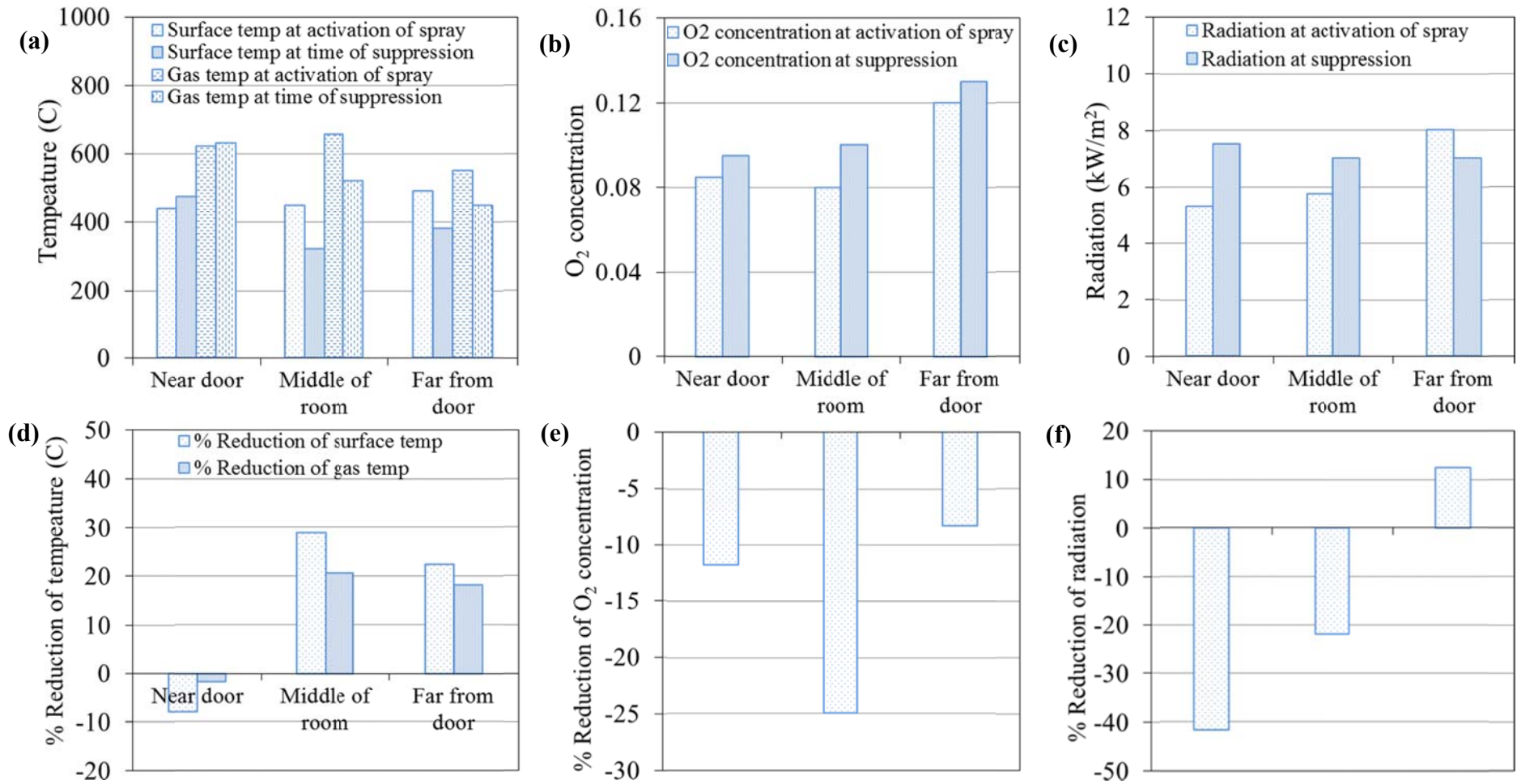


Figure 6.11: Comparison of the effect of the location of fire on the reduction of temperature of the burning surface and hot gases by water spray; the fire is related to Figure 6.10 (a) which is unobstructed and the spray is from a single nozzle (a) temperature; (b) concentration of oxygen; (c) radiation; (d) % reduction of temperature; (e) % reduction of concentration of oxygen; and (f) % reduction of radiation.

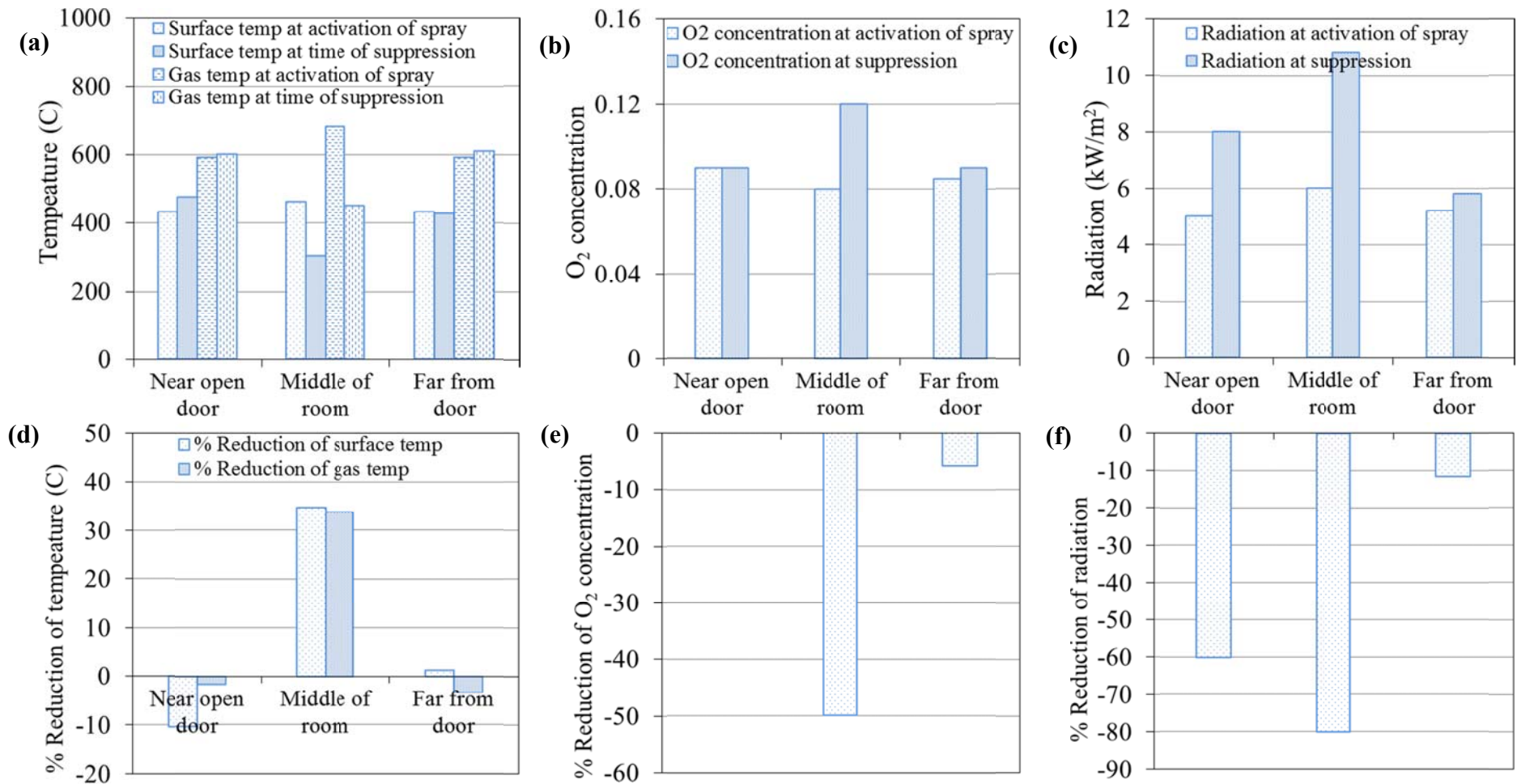


Figure 6.12: Comparison of the effect of the location of fire on the reduction of temperature of the burning surface and hot gases by water spray; the fire is related to Figure 6.10 (c) which is vertically obstructed and the spray is from a single nozzle (a) temperature; (b) concentration of oxygen; (c) radiation; (d) % reduction of temperature; (e) % reduction of concentration of oxygen; and (f) % reduction of radiation.

Therefore, from the above analysis, it can be concluded that reduction of temperatures of burning surfaces and hot gases plays a major role in the suppression of fires when they are located away from ventilation. Reduction of the concentration of oxygen and radiation feedback also has an effect on suppressing fires when they are away from ventilation, as the spray does not allow for an increase for this location of fire.

### **6.3.3 Effect of number of nozzles**

The effect of a number of nozzles on the reduction of HRR is analysed and compared in this section. Single and double nozzles are used for the suppression of fires. The positions of the single and double nozzles in the ISO room are shown in Figures 6.3 and 6.4. The influence of the nozzles are investigated for the three locations of fires and three conditions of obstruction; the three locations of fires are (i) adjacent to the open door; (ii) centre of the room; and (iii) distant from the open door; and three conditions of obstructions are (i) no obstruction; (ii) a horizontal obstruction; and (iii) a vertical obstruction. The combination of these parameters is tabulated in Table 6.13.

#### **6.3.3.1 Heat release rate**

In the simulations, the HRRs of fires are calculated and compared with respect to the number of nozzles. The results are presented in Figure 6.13. It is observed in Figure 6.13 (b) and (h) that the spray produced by the single nozzle shows a slightly better performance in reducing the HRR compared to that of the double nozzles for both unobstructed and vertically obstructed fires that are located at the centre of the room. In these cases, when the wood crib is at the centre of the room, the fire is located directly underneath the spray. As a result, the spray has direct access to the fire. In other cases, the sprays from the double nozzles are found to produce a better performance in suppressing fires. In these cases, the two nozzles are located at two

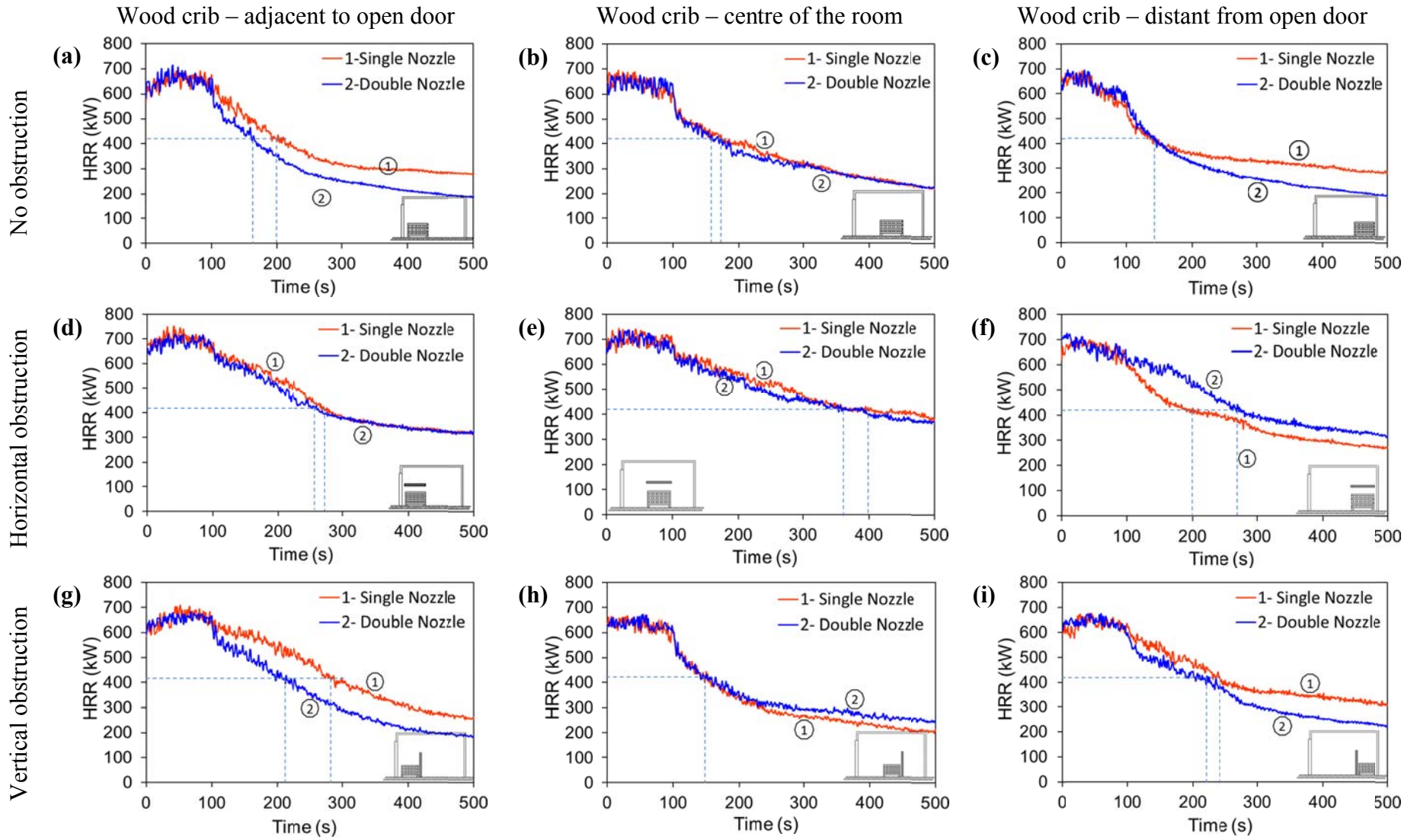


Figure 6.13: Comparison of reduction of HRR by the spray produced by the single and double nozzles.

sides of the room. As a result, when the wood crib is located adjacent to or distant from the open door of the room, one of the double nozzles is closer to the fire compared to the position of the single nozzle.

Table 6.13: Combination of parameters for the comparison of HRR with respect to location of fires

Types of obstruction (Case 1/2/3)	Location of fire (Case a/b/c)	Number of nozzles (Case A/B)	Case number	Time of suppression (second)
No obst. (Case 1)	Adjacent to door (Case a)	Single (Case A)	<i>1-a-A</i>	200
		Double (Case B)	<i>1-a-B</i>	160
	Centre of room (Case b)	Single (Case A)	<i>1-b-A</i>	175
		Double (Case B)	<i>1-b-B</i>	160
	Distant from door (Case c)	Single (Case A)	<i>1-c-A</i>	140
		Double (Case B)	<i>1-c-B</i>	140
Horizontal (Case 2)	Adjacent to door (Case a)	Single (Case A)	<i>2-a-A</i>	275
		Double (Case B)	<i>2-a-B</i>	260
	Centre of room (Case b)	Single (Case A)	<i>2-b-A</i>	400
		Double (Case B)	<i>2-b-B</i>	360
	Distant from door (Case c)	Single (Case A)	<i>2-c-A</i>	200
		Double (Case B)	<i>2-c-B</i>	275
Vertical (Case 3)	Adjacent to door (Case a)	Single (Case A)	<i>3-a-A</i>	285
		Double (Case B)	<i>3-a-B</i>	210
	Centre of room (Case b)	Single (Case A)	<i>3-b-A</i>	150
		Double (Case B)	<i>3-b-B</i>	150
	Distant from door (Case c)	Single (Case A)	<i>3-c-A</i>	240
		Double (Case B)	<i>3-c-B</i>	220

### 6.3.3.2 Competing mechanisms for the suppression of fires

The effect of the number of nozzles on the reduction of the temperature of hot surfaces and gases by water spray is analysed and the results are presented in Figures 6.14 and 6.15. Here, the comparison is for two situations of fires (i) unobstructed and

located at the centre of the room; and (ii) vertically obstructed and located in proximity to the open door. These two situations are related to Figure 6.13 (b) and (g), respectively. The results in Figure 6.14 (a) and (d) indicate that the spray produced by the single nozzle shows a better performance in the reduction of gas and surface temperatures and the blocking of radiation feedback to the burning surface for the first situation of fire. The surface and gas temperatures are reduced by about 28% and 22%, respectively, for the spray produced by the single nozzle, whereas this reduction is only 8% and 14%, respectively, for the sprays produced by the double nozzles. However as shown in Figure 6.14 (b) and (e), the sprays produced by the single and double nozzles do have an indifferent effect on the concentration of oxygen in this situation. In the case of the second situation of Figure 6.15 (a) and (d), the sprays produced by the double nozzles show a better performance in the reduction of gas and surface temperatures. The sprays produced by the double nozzles have reduced the surface and gas temperatures about 25% and 20%, respectively; whereas, the spray produced by the single nozzle could not reduce these temperatures, rather they are increased by about 13% and 2%, respectively. However the sprays from the single and double nozzles cannot reduce the concentration of oxygen and irradiance to the burning surfaces.

Therefore, for the above analysis, it can be concluded that when a fire is located directly underneath a nozzle, then the spray shows a better performance in reducing the temperatures of hot gases and burning surfaces. The spray for a single nozzle also shows a better performance in restricting radiation feedback to the fuel surface for the fire located directly underneath the spray.

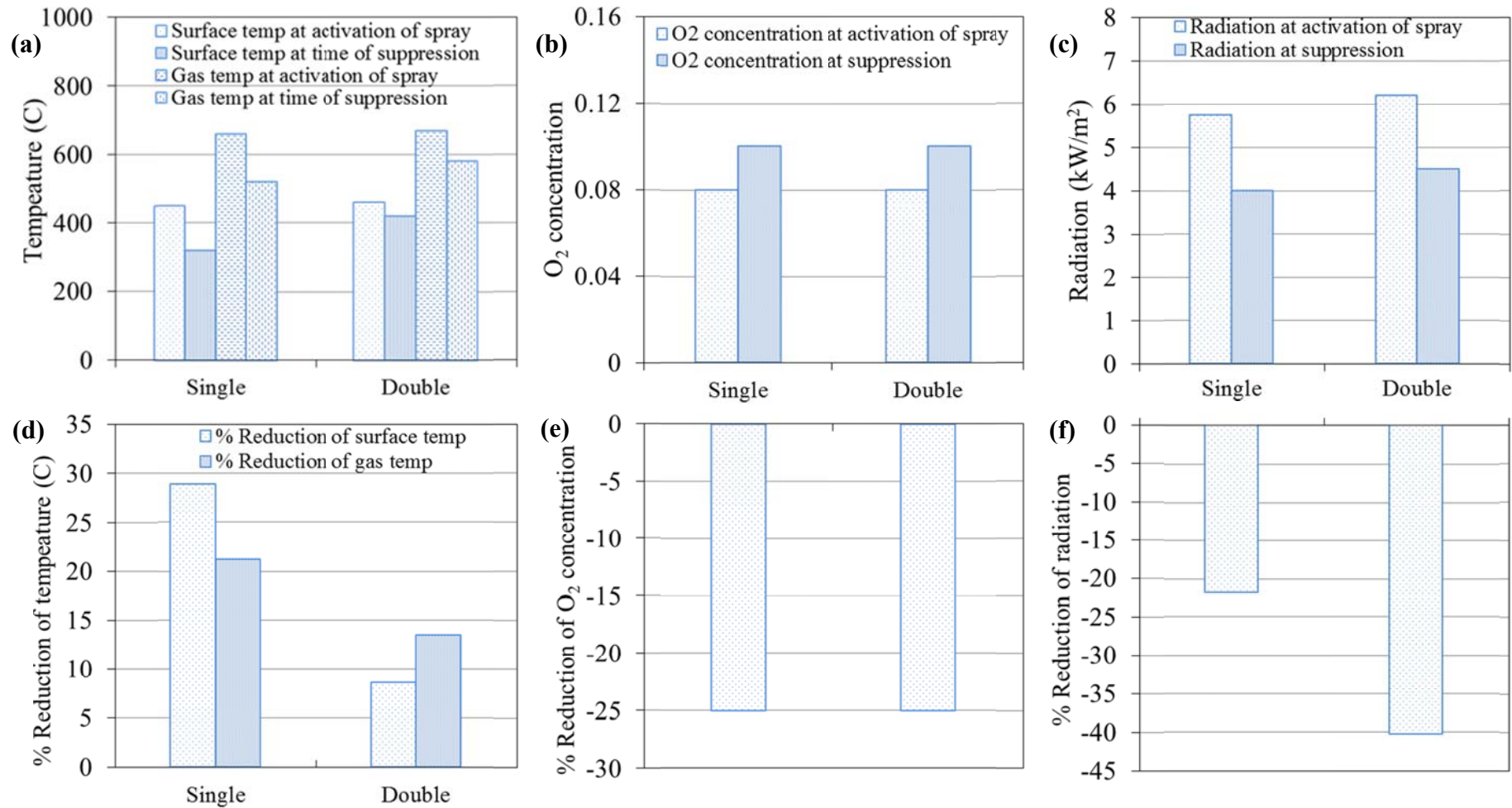


Figure 6.14: Comparison of the effect of the number of nozzles on the reduction of temperature of the burning surface and hot gases by water spray; the fire is related to Figure 6.13 (b) which is unobstructed and located at the centre of the room (a) temperature; (b) concentration of oxygen; (c) radiation; (d) % reduction of temperature; (e) % reduction of concentration of oxygen; and (f) % reduction of radiation.

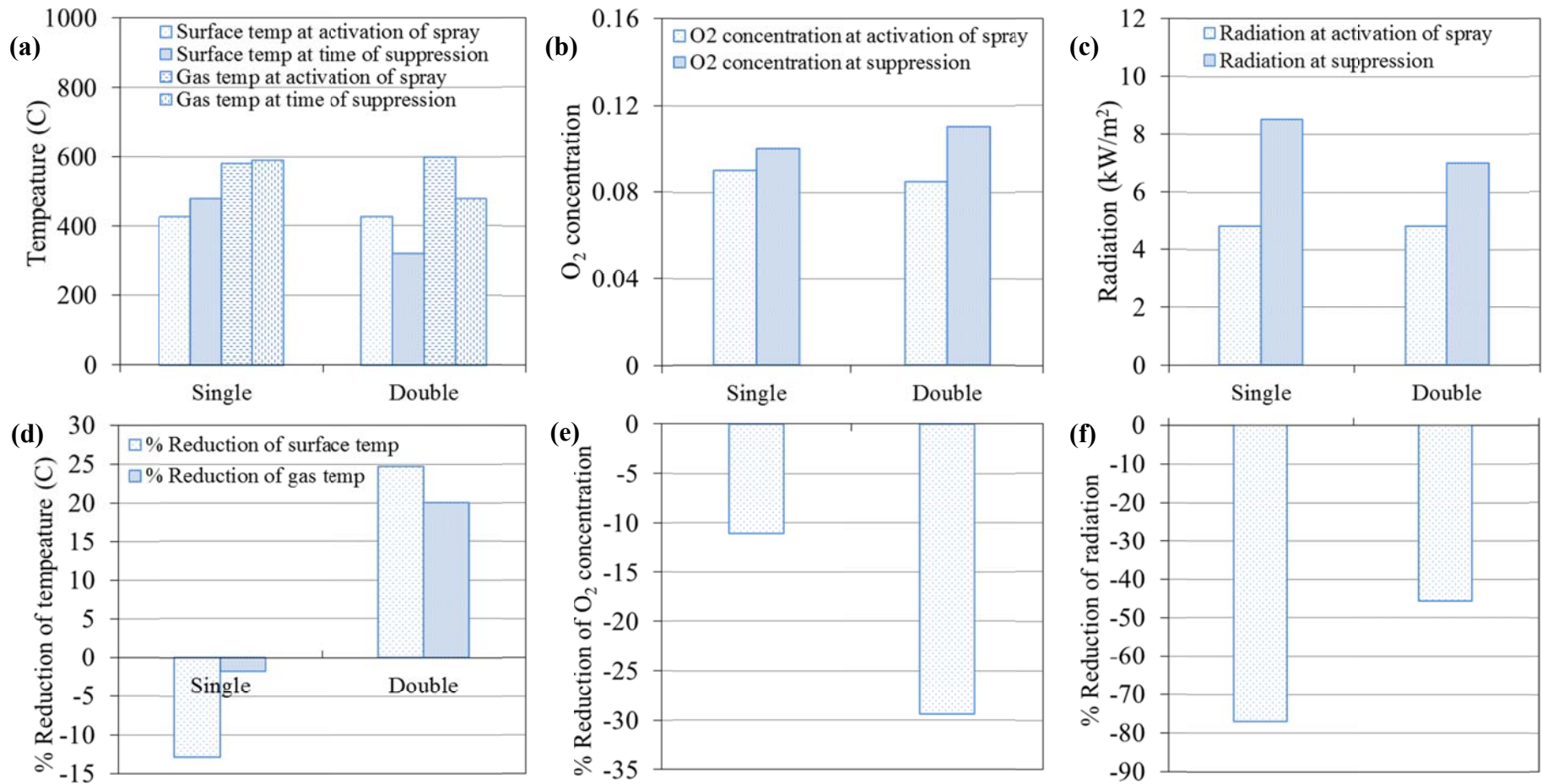


Figure 6.15: Comparison of the effect of the number of nozzles on the reduction of temperature of the burning surface and hot gases by water spray; the fire is related to Figure 6.13 (g) which is vertically obstructed and located adjacent to the open door (a) temperature; (b) concentration of oxygen; (c) radiation; (d) % reduction of temperature; (e) % reduction of concentration of oxygen; and (f) % reduction of radiation.

### 6.3.4 Effect of size of droplets

The size of the water droplets has an effect on the suppression of a fire. Droplets with a larger diameter have a higher capability of penetrating the fire plume and reaching the burning surface and consequently suppressing fires by wetting and cooling the hot surface of the solid fuel. In contrast, droplets with a smaller diameter have a higher surface area to volume ratio and this can enhance the evaporation rate via convection and radiation of heat from the flame, hot air and boundaries. The finer the water droplet the greater the surface area to volume ratio and the higher the evaporation rate of water. This results in the rapid cooling of hot gases and dilution of oxygen. The surface areas to volume ratios for the three sizes are presented in Table 6.14. However droplets with a smaller diameter are lower in weight and as a result they are less capable of penetrating the fire plume and reaching the fuel base that might be crucial in suppressing fires.

Table 6.14: The surface area to volume ratio for different sizes of droplets

Droplet size ( $\mu\text{m}$ )	Surface area of each droplet ( $\text{mm}^2$ )	Volume of one droplet ( $\text{mm}^3$ )	Surface area to volume ratio	Total surface area for $1 \text{ m}^3$ of water spray ( $\text{m}^2$ )
2500	19.63	8.18	2.4	2400
500	0.7855	0.0655	12	12000
100	0.03142	0.000524	60	60000

One of the aims of this study is to investigate the effect of the size of the droplets in reducing the HRRs from fires, cooling of the burning surface, concentration of water vapour and oxygen near the fire plume. Three sizes of droplets over a wide range are selected for the study, namely  $100 \mu\text{m}$ ,  $500 \mu\text{m}$  and  $2500 \mu\text{m}$ . One hundred  $\mu\text{m}$  represents a very fine mist,  $500 \mu\text{m}$  represents a fine mist and  $2500 \mu\text{m}$  represents a coarse water spray. The effect of droplet size is also investigated for two conditions of obstructions: no obstruction and horizontal obstruction. The location of the fires in

all cases is at the centre of the room. The temperatures of the hot gases are measured at 5 cm above the wood crib that is denoted by point A, as shown in Figure 6.6. The combination of obstruction and size of the droplets are presented in Table 6.15.

Table 6.15: Combination of parameters for the analysis of the effect of the size of droplets

Condition of obstruction (Case 1/2)	Number of nozzles (Case A)	Location of fire	Size of droplet ( $\mu\text{m}$ )
No obstruction (Case 1)	Single (Case A)	Centre of room (Case b)	100
			500
			2500
Horizontal (Case 2)	Single (Case A)	Centre of room (Case b)	100
			500
			2500

#### 6.3.4.1 Heat release rate

The effect of the size of droplets on HRR of a fire are investigated and presented in Figure 6.16. In Figure 6.16 (a) it is observed that when the fire is unobstructed, the suppression of fire is more affected by the larger droplets. Droplets with larger diameters suppress the fires at an earlier time compared to droplets with smaller diameters. In this case, the droplets with a diameter of 2500  $\mu\text{m}$  suppress the fire at 130 seconds, whereas droplets with a diameter of 100 and 500  $\mu\text{m}$  suppress the fire at 300 and 185 seconds. However, as shown in Figure 6.16 (b), the droplet sizes have less effect on the suppression of fires when they are horizontally obstructed. In this case, fires are suppressed between 400 to 500 seconds for all size of droplets.

As discussed in section 6.3.1.2, the fundamental of this behaviour remains in the burning process and the suppression mechanism of fires produced by solid fuels. Solid fuels require pyrolysis for the ignition and combustion of the fuels; as a result, the wetting and cooling of burning surfaces by a water spray play a major role in

arresting the pyrolysis. According to this mechanism, the water droplets need to reach the burning surface in restraining the pyrolysis of wood and eventually in suppressing the fire. Droplets with larger sizes have a higher capacity of reaching the burning surface as they have a higher momentum, which enables them to penetrate the fire plume and the fire-driven upward gas and smoke. Moreover they have a sufficiently high volume to reach the burning surface of fuel before they are completely evaporated by the high temperatures of fire and hot gases.

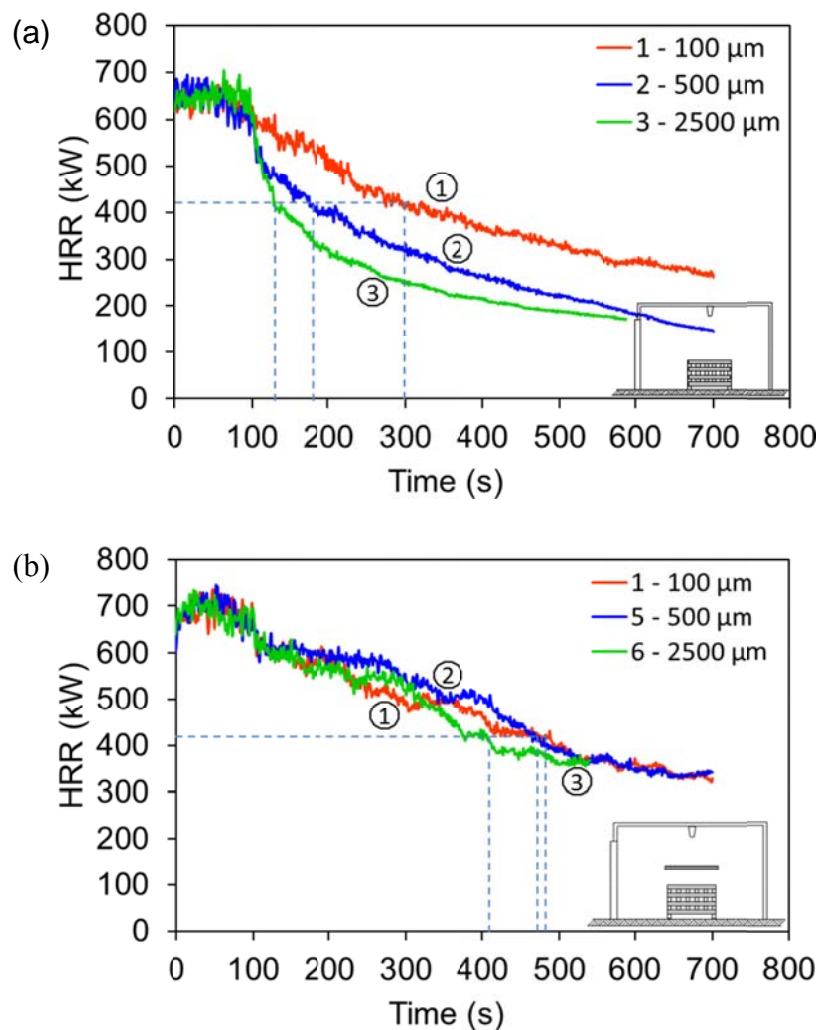


Figure 6.16: The effect of the size of droplets on HRR of fires (a) no obstruction; and (b) horizontal obstruction.

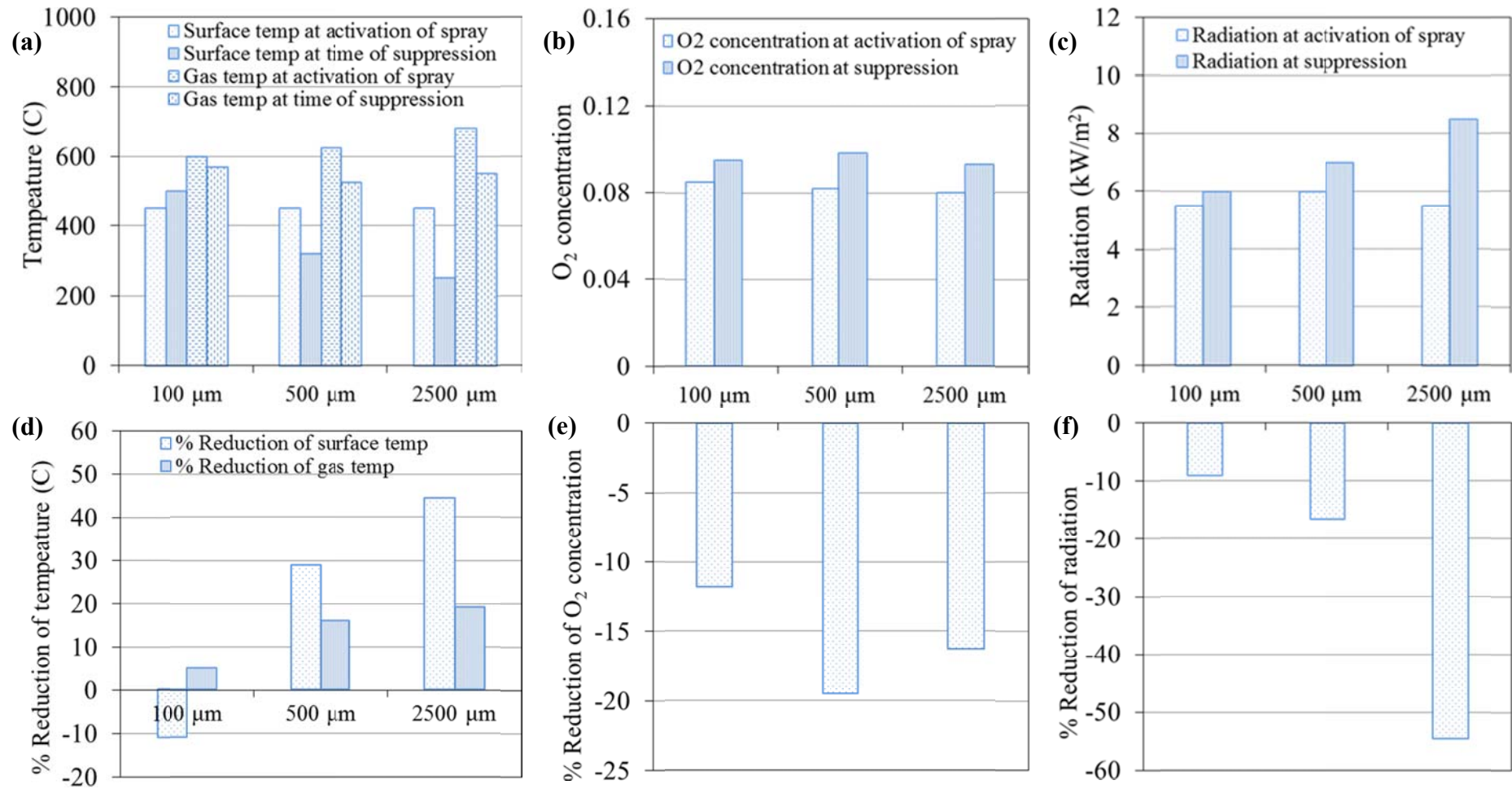


Figure 6.17: Comparison of the effect of the size of the droplets on the reduction of temperatures of the burning surface and hot gases by the spray at the time of suppression of fire; the fire is related to Figure 6.16 (a), which is unobstructed and located centre of the room (a) temperature; (b) oxygen concentration; (c) radiation; (d) % reduction of temperature; (e) % reduction of concentration of oxygen; and (f) % reduction of radiation.

#### **6.3.4.2 Competing mechanisms for the suppression of fires**

The performance of larger droplets is also observed when the temperatures of the burning surface and hot gases are estimated before and after activation of the water spray for the unobstructed condition of the fire. The results are presented in Figure 6.17. In Figure 6.17 (a) and (d) it is observed that the temperature of the burning surface and hot gases is reduced to a greater extent at the time of the suppression by droplets of 2500  $\mu\text{m}$  in diameter.

The reason for this phenomenon underlies the same mechanism described in the previous section. The larger the droplet sizes, the higher the momentum, and this results in a higher capacity to penetrate the fire plume. Moreover a larger volume of droplets enables them to reach the depth of the fire before they are completely evaporated by the high temperature of the fire plume and hot gases. However in the case of the reduction in concentration of oxygen and irradiance to the burning surfaces, as shown in Figures 6.17 (b and e) and 6.17 (c and f), respectively, 100  $\mu\text{m}$  shows a better performance compared to the other two sizes of droplets.

### **6.4 Conclusions**

The results of the parametric study are presented where the effect of different factors on the suppression of fires by water-mist sprays are discussed. The factors are the condition of obstruction, location of fire, number of nozzles, and size of droplets. The performance of the water-mist spray on the reduction of HRR of fires, temperature of the burning surfaces and hot gases, concentration of oxygen, and irradiance to the burning surface for different parametric conditions of fires are investigated. The results are summarised here.

Effect of obstruction:

- (i) The fires that are directly obscured by a horizontal obstruction take a longer time to be suppressed by the water spray. The reason is that the water droplets cannot reach the burning surface and fire due to the obstruction. However, as expected, in all of the cases the unobstructed fires are suppressed quickly and more completely compared to the horizontally and vertically obstructed fires.
- (ii) In the case of the reduction of the temperature of hot gases and a burning surface, the spray is effective for unobstructed and vertically obstructed fires; whereas the spray is found not to be effective for horizontally obstructed fires. This is because as the fire is obscured from the spray by the horizontal obstruction, the water droplets cannot reach the fire and firebase and result in the spray not being able to reduce the temperature of the burning surface and hot gases.
- (iii) In the case of a reduction in the concentration of oxygen and radiation feedback to the fuel surface, the spray is effective for horizontally obstructed fires, as the droplets have generated vertical curtains around the fire when they fall over the obstruction.

Effect of location of fire:

- (i) The spray is most effective when the fire is directly beneath the nozzle (location of the fire is at the centre of the room) for unobstructed fires. Interestingly, the opposite phenomenon is observed for this location if the fire is horizontally obstructed. However, for the location distant from the open door, the spray is least effective for vertically obstructed fires. In this case, the solid fuel receives more radiation feedback from the surrounding

boundary walls. As a result, it enhances the burning of the crib and delays the suppression of fire by the water-mist spray.

- (ii) The spray cannot reduce the temperatures of burning surfaces and hot gases for the fire located in proximity to the open door (ventilation); rather they are increased. However, for the other two locations of fires, the temperatures of the burning surface and hot gases are substantially reduced by the spray at the time of suppression of the fires.
- (iii) In the case of irradiance to the burning surface, it is reduced after activation of the spray for the fire located distant from the open door; however, in the other two cases it is increased after activation of the spray.

Effect of the number of nozzles:

- (i) The spray produced by the single nozzle shows a slightly better performance in suppressing fires that are located at the centre of the room, and for both unobstructed and vertically obstructed conditions. In other cases, the sprays from the double nozzles are more effective in suppressing fires. However, when the fire is obscured from the spray by horizontal obstruction, the performance of sprays produced by the single and double nozzles does not differ much in the reduction of HRR for all locations of fires in the room.
- (ii) In the case of the reduction of gas and surface temperature and obnubilating the radiation feedback to the burning surface, the spray produced by the single nozzle also shows a better performance for the unobstructed condition of fire.

Effect of size of droplets:

- (i) The droplets that are larger in size show better performance in the suppression of unobstructed fires; however, little effect of the variation of sizes is found on the suppression of horizontally obstructed fires.
  
- (ii) The spray with larger droplets reduced the temperatures of the burning surface and hot gases to a greater extent at the time of suppression. However, smaller droplets show better performance in reducing the concentration of oxygen and irradiance to burning surfaces.

# Chapter 7

## Summary and conclusions

# Chapter 7

## Summary and conclusions

---

An integrated research program comprising the development of a semi-empirical model of the evaporation of water droplets, an experimental study to validate FDS, a state-of-the-art CFD based model, validation of FDS in predicting the growth of fire and suppressing it by water-mist spray and, finally, a parametric study of the effect of different factors on the suppression of fires has been carried out. The overarching objective is to determine the efficacy of water mists in suppressing fires.

The semi-empirical model development is aimed at developing a detailed understanding of the science of droplet evaporation. Against this semi-empirical model, FDS is validated in terms of single droplet evaporation. Experiments have been conducted to obtain a set of benchmarked results for validation of the numerical modelling of the distribution of flux densities of water-mist sprays. Validation of FDS in relation to the evaporation of a single droplet and the behaviour of water-mist sprays has been carried out in four stages:

- The rates of evaporation of a single droplet predicted by FDS are compared with those produced by this semi-empirical model.
- Distributions of flux densities of water-mist sprays predicted by FDS have been compared with benchmark experiments conducted in this study.
- The predicted rates of pyrolysis and the combustion of a solid fuel (PMMA) have been compared with a set of literature data.

- The pyrolysis and combustion of PMMA fire combined with water-mist suppression have been validated against a set of literature data.

The semi-empirical model developed in this study can also be used to evaluate the performance of the different size of droplets at different air condition and to find an appropriate median size of droplets in a particular scenario. The experimental data on distribution of flux densities can be used to validate any other CFD based model in simulating sprays. As the overarching objective is to investigate the capability of a CFD based model in simulating the suppression of fires using water mists, this study has identified the ability of FDS in simulating this.

The validation study has led to a parametric study using FDS. However, due to the enormous computational requirement, this part is qualitative rather than quantitative. The results of this research are discussed below.

## **7.1 Development of a semi-empirical model for evaporation of water droplets**

### **7.1.1 Model development and validation**

The behaviour of individual water droplets in the hot air induced by a fire is examined using the ‘semi-empirical water droplet evaporation model’ developed in this study. The proposed model is validated against experimental and analytical data and the performance of FDS is evaluated and validated against the proposed model developed in this study. The analysis and FDS are found to be in close agreement when predicting the behaviour of droplets in hot air. The terminal velocities of droplets of different sizes are calculated using the proposed model and FDS. It is observed that estimated values by FDS are very close to the calculated results of the proposed model within a variation less than 8%. The proposed model and FDS are also used to calculate the saturation temperature of droplets at a different temperature

to the surrounding air. The FDS prediction does not differ by more than 10% of the calculated values of the proposed model.

### **7.1.2 Evaluation of the characteristics of the different sizes of droplets**

The proposed ‘water droplet evaporation model’ is also used to evaluate the characteristics of the different sizes of droplets in a layer of hot air i.e. whether a particular size of droplet is suitable for the cooling of hot gas by heat extraction or whether it is suitable for the wetting and cooling of the fuel surface by reaching there before complete evaporation. The results show:

- (i) The smaller droplets have a higher rate of evaporation and longer suspension time in the air, which enables them to extract heat more effectively from the hot gases; whereas the larger droplets have a higher terminal velocity, which results in a higher penetration capability through the hot air and enables them to reach the burning surfaces.
- (ii) The effect of the high mass transfer rate on the evaporation of a droplet is insignificant for droplets when the temperature of the air is in the range 0–100°C.

## **7.2 Spray distribution – a benchmark experiment and validation of FDS**

A set of experiments is conducted using a single and multi-orifice water-mist nozzle and when the distribution of flux densities on a horizontal surface is measured. A set of numerical simulations is also conducted to mimic the experiment. The distributions of flux densities are also estimated in the simulation and compared with the experimental measurements. It is observed that the numerical results are in good agreement with the experimental data. The distribution of the sprays in both cases of the single and the multi-orifice nozzle are elliptical in shape. However the

eccentricities of the ellipses are less pronounced in the numerical model in both of the cases of the sprays.

The distribution of the sprays is found to be influenced by the presence of a solid wall in the vicinity of the spray. The experimental and numerical results indicate that the flux distribution is closer to the wall than would otherwise be the case. However the effect of the boundary wall on the distribution of the spray in the numerical model is less pronounced compared to that of the experimental results. The overall results from FDS are in close agreement with a variation of less than 20% with the experimentally determined distribution produced by the spray nozzles.

### **7.3 Validation of FDS for the burning of PMMA and the suppression of fires by water-mist spray**

#### **7.3.1 Simulation of PMMA fire without the presence of a water-mist system**

The burning rates of PMMA fire are numerically simulated using FDS and the numerical results are compared with the published experimental data by [Magee and Reitz \[1974\]](#). The FDS results of the steady state burning rates of the PMMA slab are in reasonable agreement with the experimental measurements, with a difference of not more than 23%. The orientation of the specimen (vertical or horizontal) has a profound effect on the burning rate and time required to be ignited and attain the steady state burning rate of the material. In this study, the vertically oriented slab exhibits higher burning rates and shorter times to reach the steady state burning rate compared to that of the horizontally oriented PMMA slab.

### **7.3.2 Simulation of PMMA fire with the presence of a water-mist system**

Validation of FDS in the scenarios involving the interaction of fire with a spray is conducted. The numerical results of the burning rate of the PMMA slab after activation of the water spray are in reasonable agreement with the experimental measurements of [Magee and Reitz \[1974\]](#). The results show that FDS has predicted the burning rates of PMMA with an error not exceeding 15% of the experimental data.

## **7.4 Parametric study using FDS to assess the efficacy of water-mist sprays**

FDS is used to qualitatively examine a range of parameters that affects the performance of the suppression of fires by water-mist spray. This study is based on a qualitative analysis as the quantitative analysis demands enormous computational resources and time. The parameters are the effect of the obstruction and location of the fire, number of nozzles and size of the droplets of a spray. Suppression of a fire is considered when it is lowered to the level of 65% of HRR of its quasi-steady-state by the spray [[Zhao et al. 1998](#); [AFAC 2004](#)]. The outcomes of this study are summarised below:

- i) *Obstruction*: The spray is less effective in suppressing a horizontally obstructed fire. However unobstructed fires are suppressed in shorter times and to a greater extent than obstructed fires in all cases except for fires that are vertically obstructed and located directly underneath the spray.
- ii) *Location*: The spray is found to be most effective for unobstructed fires that are located directly underneath the nozzle. Notably, the opposite phenomenon is observed for horizontally obstructed fires.

- iii) *Number of nozzles*: The spray produced by a single nozzle shows a marginally better performance in suppressing fires when it is unobstructed and directly underneath the nozzle. However the performance of a spray produced by the single and double nozzle does not differ much when the fire is obscured from the spray by a horizontal obstruction. In other cases, the sprays from double nozzles perform better. However in most cases the reduction of the suppression time by the sprays from double nozzles is negligible.
- iv) *Size of the droplet*: The larger size of droplets exhibited better performance in the suppression of fires with the condition that the fire is unobstructed. However, for the horizontally obstructed fire, the variation of the size of the droplets showed little effect on the time of suppression of the fires.

The governing mechanisms of suppression of fires at different conditions have also been explored. It is observed that the cooling of hot gases and burning surfaces by the water droplets of a spray play a major role in suppressing unobstructed fires. Whereas the blocking of air entrainment and attenuating radiation feedback to the fuel surface caused by the spray play a major role in suppressing horizontally obstructed fires with the condition that the fire is directly underneath the nozzle.

## **7.5 Recommendations for future study**

During the course of this project a number of areas have been identified that are worthy of further research. They are:

- the expansion of the droplet evaporation model
- the experimental measurement of the median size of droplets
- the further investigation on factors that affect the efficacy of water-mist sprays in suppressing fires.

### **7.5.1 Expanding the droplet evaporation model**

In the development of the model of evaporation of water droplets, a number of assumptions are applied to simplify the model. However a quantitative analysis of the effect of these assumptions may enhance performance of the model. One of the assumptions is that the interaction between droplets is considered negligible. However it is important to identify whether or not the sprays can be treated in terms of single droplet relationships; if not, it is required to quantify the effect of their interactions on the evaporation of droplets. Another assumption is that the temperature of the smoke layer is considered to be within a range of 0 to 100°C. However this model can be expanded by considering the temperature of hot gases beyond 100°C. Finally, direct experimental data on the evaporation of water droplets in a smoke layer can be useful in examining the accuracy of the model.

### **7.5.2 Experimental measurement of the median size of droplets**

A technique is proposed to determine the median size of droplets of a water spray. However no direct experimental data are presented to support the accuracy of the technique. Laser-based measuring techniques are available to measure the median size of droplets of a spray. Therefore direct measurement and comparison with the analytical data will increase the confidence of using this method for determining the median size of droplets.

### **7.5.3 Further investigation on factors that affect the efficacy of water-mist sprays in suppressing fires**

Experiments are required to examine the effect of a range of parameters, such as the obstruction and location of the fire, the number of nozzles, and size of droplets on the efficacy of the water-mist spray in the suppression of fires. Numerical simulations are required for the quantitative analysis of the effect of those parameters on the efficacy of the suppression of fires by water-mist spray.

## References

# References

---

- Australasian Fire Authorities Council. (2004). "Fire brigade intervention model", Version. 2.2. Melbourne.
- Abu-Bakar, A. S. and Moinuddin, K. A. M. (2015). "Investigation of effects of variation in heating rate on chemical kinetics and heat of reaction for pyrolysis and combustion." (Submitted as a technical paper in Fire and Materials).
- Adiga, K. C., Hatcher Jr, R. F., Sheinson, R. S., Williams, F. W. and Ayers, S. (2007). "A computational and experimental study of ultra fine water mist as a total flooding agent." *Fire Safety Journal* 42(2): 150-160. DOI: <http://dx.doi.org/10.1016/j.firesaf.2006.08.010>.
- Alexander, D. and Li, E. (2009). "Water-mist fire suppression modeling." Defence R&D Canada – Atlantic, DRDC Atlantic, Canada.
- Alpert, R. L. (1972). "Calculation of response time of ceiling-mounted fire detectors." *Fire Technology* 8(3): 181-195. DOI: <http://dx.doi.org/10.1007/bf02590543>.
- ASHRAE (1985). "ASHRAE handbook - Fundamentals." American Society of Heating, Refrigeration and Air Conditioning Engineers, New York, pp. 5.5.
- Back, G. G., Beyler, C. L. and Hansen, R. (2000). "A quasi-steady-state model for predicting fire suppression in spaces protected by water-mist systems." *Fire Safety Journal* 35(4): 327-362. DOI: [http://dx.doi.org/10.1016/S0379-7112\(00\)00038-2](http://dx.doi.org/10.1016/S0379-7112(00)00038-2).
- Back Iii, G. G., Beyler, C. L. and Hansen, R. (2000). "A quasi-steady-state model for predicting fire suppression in spaces protected by water-mist systems." *Fire Safety Journal* 35(4): 327-362. DOI: [http://dx.doi.org/10.1016/S0379-7112\(00\)00038-2](http://dx.doi.org/10.1016/S0379-7112(00)00038-2).
- Barrow, H. and Pope, C. W. (2007). "Droplet evaporation with reference to the effectiveness of water-mist cooling." *Applied Energy* 84(4): 404-412. DOI: <http://dx.doi.org/10.1016/j.apenergy.2006.09.007>.
- Beard, K. V. and Pruppacher, H. R. (1971). "A wind tunnel investigation of the rate of evaporation of small water drops falling at terminal velocity in air." *Journal of the Atmospheric Sciences* 28(8): 1455-1464. DOI: [http://dx.doi.org/10.1175/1520-0469\(1971\)028<1455:awtiot>2.0.co;2](http://dx.doi.org/10.1175/1520-0469(1971)028<1455:awtiot>2.0.co;2).

## References

- Beyler, C. L. (2002). "Flammability limits of premixed and diffusion flames (Section 2, Chapter 7)." SFPE Handbook of Fire Protection Engineering. DiNenno, P. J. (editors). National Fire Protection Association, Inc., Quincy, Massachusetts, pp. 2-172.
- Bill, R. G. and Ural, E. A. (1999). "Water-mist protection of combustion turbine enclosures." In Proceedings of the 6th International Symposium on Fire Safety Science, (eds.), International Association for Fire Safety Science, July 5-9, Poitiers, France, pp. 457-468.
- Bird, R. B., Stewart, W. E. and Lightfoot, E. N. (1960). "Transport phenomena." John Wiley and Sons, New York, pp. 59 and 505.
- Braidech, M. M., Neale, J. A., Matson, A. F. and Dufour, R. E. (1955). "The mechanism of extinguishment of fire by finely divided water." Underwriters Laboratories Inc., for the National Board of Fire Underwriters, New York, USA, pp. 73.
- Braidech, M. M., Neale, J. A., Matson, A. F. and Dufour, R. E. (1955). "The mechanisms of extinguishment of fire by finely divided water." Underwrites Laboratories Inc. for the National Board of Fire Underwriters, New York.
- Brown, P. P. and Lawler, D. F. (2003). "Sphere drag and settling velocity revisited." Journal of Environmental Engineering 129(3): 222-231. DOI: [http://dx.doi.org/10.1061/\(asce\)0733-9372\(2003\)129:3\(222\)](http://dx.doi.org/10.1061/(asce)0733-9372(2003)129:3(222)).
- Buck, A. L. (1981). "New equations for computing vapor pressure and enhancement factor." Journal of Applied Meteorology 20(12): 1527-1532. DOI: [http://dx.doi.org/10.1175/1520-0450\(1981\)020<1527:nefcvp>2.0.co;2](http://dx.doi.org/10.1175/1520-0450(1981)020<1527:nefcvp>2.0.co;2).
- Bullen, M. L. (1977). "The effect of a sprinkler on the stability of a smoke layer beneath a ceiling." Fire Technology 13(1): 21-34. DOI: <http://dx.doi.org/10.1007/bf02338883>.
- Burch, I. (2006). "Water mist for ship machinery spaces." Technical Report, Maritime Platforms Division, Defence Science and Technology Organisation (DSTO), Fishermans Bend, Victoria 3207, Australia.
- Byström, A., Cheng, X., Wickström, U. and Veljkovic, M. (2012). "Full-scale experimental and numerical studies on compartment fire under low ambient temperature." Building and Environment 51: 255-262. DOI: <http://dx.doi.org/10.1016/j.buildenv.2011.11.010>.
- Çengel, Y. A. and Turner, R. H. (2005). "Fundamentals of thermal-fluid sciences." 2nd Edition, McGraw-Hill Companies, New York, pp. 1088-1089.
- Chen, C.-J., Hsieh, W.-D., Hu, W.-C., Lai, C.-m. and Lin, T.-H. (2010). "Experimental investigation and numerical simulation of a furnished office fire." Building and Environment 45(12): 2735-2742. DOI: <http://dx.doi.org/10.1016/j.buildenv.2010.06.003>.

## References

- Chow, W. K. (1989). "On the evaporation effect of a sprinkler water spray." *Fire Technology* 25(4): 364-373. DOI: <http://dx.doi.org/10.1007/bf01040382>.
- Chow, W. K. and Cheung, Y. L. (1994). "Simulation of sprinkler—hot layer interaction using a field model." *Fire and Materials* 18(6): 359-379. DOI: <http://dx.doi.org/10.1002/fam.810180604>.
- Chow, W. K. and Tang, A. C. (1994). "Experimental studies on sprinkler water spray - smoke layer interaction." *Journal of Applied Fire Science* 4: 171-184. DOI: <http://dx.doi.org/10.2190/54B4-5AUL-MNCV-F825>
- Chow, W. K. and Yao, B. (2001). "Numerical modeling for interaction of a water spray with smoke layer." *Numerical Heat Transfer, Part A: Applications* 39(3): 267-283. DOI: <http://dx.doi.org/10.1080/104077801300006580>.
- Chow, W. K. and Yin, R. (1999). "Water spray pattern discharged from high headroom atrium sprinkler." *Journal of Architectural Engineering* 5(4): 133-140. DOI: [http://dx.doi.org/10.1061/\(ASCE\)1076-0431\(1999\)5:4\(133\)](http://dx.doi.org/10.1061/(ASCE)1076-0431(1999)5:4(133)).
- Cong, B. H., Liao, G. X., Yao, B., Qin, J. and Chow, W. K. (2008). "Numerical studies on extinguishing solid fires by water-mist." *Journal of Applied Fire Science* 18(3): 241-270. DOI: <http://dx.doi.org/10.2190/AF.18.3.c>.
- Cooper, L. Y. (1995). "The interaction of an isolated sprinkler spray and a two-layer compartment fire environment." *International Journal of Heat and Mass Transfer* 38(4): 679-690. DOI: [http://dx.doi.org/10.1016/0017-9310\(94\)00188-2](http://dx.doi.org/10.1016/0017-9310(94)00188-2).
- Dac, N. T. (2014). "Designing an experimental rig for a scaled fire enclosure model using numerical simulation." MS Thesis, Centre for Environmental Safety and Risk Engineering, Victoria University, Melbourne.
- Darwin, R. L. and Williams, F. W. (2000). "The development of water-mist fire protection systems for U.S. navy ships." *Naval Engineers Journal* 112(6): 49-57. DOI: <http://dx.doi.org/10.1111/j.1559-3584.2000.tb03380.x>.
- Debye, P. (1909). "Der lichtdruck auf kugeln von beliebigem material." *Annalen der Physik* 335(11): 57-136. DOI: <http://dx.doi.org/10.1002/andp.19093351103>.
- Dembele, S., Wen, J. X. and Sacadura, J. F. (2001). "Experimental study of water sprays for the attenuation of fire thermal radiation." *Journal of Heat Transfer* 123(3): 534-543. DOI: <http://dx.doi.org/10.1115/1.1371921>.
- Drysdale, D. (2011). "An introduction to fire dynamics." 3rd Edition, John Wiley and Sons, New York, pp. 158, 285.
- Fleming, R. P. (2008). "Automatic sprinkler system calculations (Chapter 4)." In: *The SFPE Handbook of Fire Protection Engineering*. DiNenno, P. J. (editors). Society of Fire Protection Engineers, Quincy, MA 02269, pp. 4-86.

## References

- Fujita, A., Kurose, R. and Komori, S. (2010). "Experimental study on effect of relative humidity on heat transfer of an evaporating water droplet in air flow." *International Journal of Multiphase Flow* 36(3): 244-247. DOI: <http://dx.doi.org/10.1016/j.ijmultiphaseflow.2009.10.004>.
- Fuss, S. P., Chen, E. F., Yang, W., Kee, R. J., Williams, B. A. and Fleming, J. W. (2002). "Inhibition of premixed methane/air flames by water mist." *Proceedings of the Combustion Institute* 29(1): 361-368. DOI: [http://dx.doi.org/10.1016/S1540-7489\(02\)80048-7](http://dx.doi.org/10.1016/S1540-7489(02)80048-7).
- Grant, G., Brenton, J. and Drysdale, D. (2000). "Fire suppression by water sprays." *Progress in Energy and Combustion Science* 26(2): 79-130. DOI: [http://dx.doi.org/10.1016/S0360-1285\(99\)00012-X](http://dx.doi.org/10.1016/S0360-1285(99)00012-X).
- Gunn, R. and Kinzer, G. D. (1949). "The terminal velocity of fall for water droplets in stagnant air." *Journal of Meteorology* 6(4): 243-248. DOI: [http://dx.doi.org/10.1175/1520-0469\(1949\)006<0243:ttvoff>2.0.co;2](http://dx.doi.org/10.1175/1520-0469(1949)006<0243:ttvoff>2.0.co;2).
- Hallman, J. R., Welker, J. R. and Sliepcevich, C. M. (1974). "Polymer surface reflectance-absorptance characteristics." *Polymer Engineering & Science* 14(10): 717-723. DOI: <http://dx.doi.org/10.1002/pen.760141010>.
- Hart, R. A. (2005). "Numerical modelling of tunnel fires and water mist suppression." School of Chemical, Environmental and Mining Engineering, University of Nottingham, UK.
- Hinds, W. C. (1999). "Aerosol technology: properties, behavior, and measurement of airborne particles." 2nd Edition, John Wiley & Sons, Inc, New York.
- Holman, J. P. (2002). "Heat transfer." 9th edition, McGraw-Hill Book Company, New York, pp. 133.
- Hostikka, S. and McGrattan, K. (2006). "Numerical modeling of radiative heat transfer in water sprays." *Fire Safety Journal* 41(1): 76-86. DOI: <http://dx.doi.org/10.1016/j.firesaf.2005.09.003>.
- Incropera, F. P. and DeWitt, D. P. (1990). "Fundamentals of heat and mass transfer." Wiley, New York.
- Jahn, W., Rein, G. and Torero, J. (2008). "The effect of model parameters on the simulation of fire dynamics." In *Proceedings of the 9th International Symposium on Fire Safety Science*, 21-26 September 2008, Karlsruhe, Germany, pp. 1341-1352. DOI: <http://dx.doi.org/10.3801/iafss.fss.9-1341>.
- James, H. (2014). "Measurement of thermal conductivity and specific heat of building construction materials as functions of temperature." Centre for Environmental Safety and Risk Engineering, Victoria University, Melbourne.

## References

- Jenft, A., Collin, A., Boulet, P., Pianet, G., Breton, A. and Muller, A. (2014). "Experimental and numerical study of pool fire suppression using water-mist." *Fire Safety Journal* 67: 1-12. DOI: <http://dx.doi.org/10.1016/j.firesaf.2014.05.003>.
- Kakatsios, X. K. and Krikkis, R. N. (2001). "Effect of surface tension and evaporation on phase change of fuel droplets." *Heat Transfer Engineering* 22(3): 33-40. DOI: <http://dx.doi.org/10.1080/01457630120403>.
- Kanury, A. M. (1994). "Introduction to combustion phenomena." Eighth ed., Gordon and Breach Science Publishers, USA.
- Kim, A. (2002). "Overview of recent progress in fire suppression technology." *Proceedings of 2nd Symposium of the National Research Institute of Fire and Disaster*, July 17-19, Tokyo, Japan, pp. pp.1-13.
- Kim, S. C. and Ryou, H. S. (2003). "An experimental and numerical study on fire suppression using a water-mist in an enclosure." *Building and Environment* 38(11): 1309-1316. DOI: [http://dx.doi.org/10.1016/s0360-1323\(03\)00134-3](http://dx.doi.org/10.1016/s0360-1323(03)00134-3).
- Kung, H.-C. (1977). "Cooling of room fires by sprinkler spray." *Journal of Heat Transfer* 99(3): 353-359. DOI: <http://dx.doi.org/10.1115/1.3450702>.
- Lage, P. L. C. and Rangel, R. H. (1993). "Single droplet vaporization including thermal radiation absorption." *Journal of Thermophysics and Heat Transfer* 7(3): 502-509. DOI: <http://dx.doi.org/10.2514/3.446>.
- Lee, S. H. (2006). "Material property estimation method using a thermoplastic pyrolysis model " MS Thesis, Fire Protection Engineering, Worcester Polytechnic Institute, pp. 4.
- Lefebvre, A. H. (1989). "Atomisation and sprays." Hemisphere Publishing Corporation, New York.
- Li, K. Y., Hu, L. H., Huo, R., Li, Y. Z., Chen, Z. B., Li, S. C. and Sun, X. Q. (2009). "A mathematical model on interaction of smoke layer with sprinkler spray." *Fire Safety Journal* 44(1): 96-105. DOI: <http://dx.doi.org/10.1016/j.firesaf.2008.04.003>.
- Li, Y. F. and Chow, W. K. (2004). "Modelling of water mist fire suppression systems by a one-zone model." *Combustion Theory and Modelling* 8(3): 567-592. DOI: <http://dx.doi.org/10.1088/1364-7830/8/3/008>.
- Li, Y. F. and Chow, W. K. (2006). "A zone model in simulating water mist suppression on obstructed fire." *Heat Transfer Engineering* 27(10): 99-115. DOI: 10.1080/01457630600908693.
- Li, Y. F. and Chow, W. K. (2008). "Study of water droplet behavior in hot air layer in fire extinguishment." *Fire Technology* 44(4): 351-381. DOI: <http://dx.doi.org/10.1007/s10694-007-0036-2>.

## References

- Liang, T. S., Liu, Z. L., Xiao, X. K., Luo, S. M., Liao, G. X. and Zhong, W. (2013). "Experimental and Numerical Study of Fire Suppression Performance of Ultral-Fine Water Mist in a Confined Space." *Procedia Engineering* 52(0): 208-213. DOI: <http://dx.doi.org/10.1016/j.proeng.2013.02.128>.
- Linteris, G., Gewuerz, L., Mcgrattan, K. and Forney, G. (2005). "Modeling solid sample bumng." In *Proceedings of the 8th International Symposium on Fire Safety Science*, (eds.), International Association for Fire Safety Science (IAFSS), 18-23 September 2005, Beijing, China, pp. 625-636. DOI: <http://dx.doi.org/10.3801/IAFSS.FSS.8-625>.
- Liu, J. (2003). "Progress in research and application of water-mist fire suppression technology." *Chinese Science Bulletin* 48(8): 718. DOI: <http://dx.doi.org/10.1360/02ww0180>.
- Liu, Y., Moser, A. and Sinai, Y. (2004). "Comparison of a CFD Fire Model against a Ventilated Fire Experiment in an Enclosure." *International Journal of Ventilation* 3(2): 169-181. DOI: doi:10.5555/ijov.2004.3.2.169.
- Liu, Z. and Kim, A. K. (2000). "A review of water-mist fire suppression systems - fundamental studies." *Journal of Fire Protection Engineering* 10(3): 32-50. DOI: <http://dx.doi.org/10.1177/104239159901000303>.
- Liu, Z. and Kim, A. K. (2001). "A review of water-mist fire suppression technology: Part II - Application studies." *Journal of Fire Protection Engineering* 11(1): 16-42. DOI: <http://dx.doi.org/10.1106/mmgh-xuag-hp5b-ytdg>.
- Liu, Z., Kim, A. K. and Carpenter, D. (2007). "A study of portable water-mist fire extinguishers used for extinguishment of multiple fire types." *Fire Safety Journal* 42(1): 25-42. DOI: <http://dx.doi.org/10.1016/j.firesaf.2006.06.008>.
- Magee, R. S. and Reitz, R. D. (1974). "Extinguishment of radiation augmented plastic fires by water sprays." In *Proceedings the 15th Symposium on Combustion*, (eds.), The Combustion Institute, 25-31 August 1974, Tokyo, Japan, pp. 337-347.
- Mätzler, C. (2002). "MATLAB functions for Mie scattering and absorption, Version 2." Report No. 2002-11, Institute of Applied Physics, Bern.
- Mawhinney, J. R. (1995). "Water mist fire suppression systems: principles and limitations." In *Proceedings of International Conference on Fire Protection in the HVDC Industry*, Vancouver, Canada.
- Mawhinney, J. R., Dlugogorski, B. Z. and Kim, A. K. (1994). "A closer look at the fire extinguishing properties of water mist." *Fire Safety Science—Proceedings 4th International Symposium on Fire Safety Science*, (eds.), International Association for Fire Safety Science, July 13-17, 1994, Ottawa, Ontario, Canada, pp. 47-60.

## References

- McGrattan, K., Hostikka, S., McDermott, R., Floyd, J., Weinschenk, C. and Overholt, K. (2014). "Fire dynamics simulator (Version 6) - Technical reference guide, Volume 1: Mathematical model." NIST Special Publication 1018, Sixth Edition. Technical Reference Guide, NIST Special Publication 1018, Sixth Edition.
- McGrattan, K., Hostikka, S., McDermott, R., Floyd, J., Weinschenk, C. and Overholt, K. (2014). "Fire dynamics simulator (Version 6) - User's guide." Sixth Edition. User's Guide, NIST Special Publication 1019, Sixth Edition.
- McGrattan, K. B. (2001). "Research and Practice: Bridging the gap." Proceedings of Fire Suppression and Detection Research Application Symposium, (eds.), Fire Protection Research Foundation, February 7-9, Orlando, FL, pp. 596-603.
- Mell, W., McNamara, D., Maranghides, A., McDermott, R., Forney, G., Hoffman, C. and Ginder, M. (2011). "Computer modeling of wildland-urban interface fires." Proceedings of the 12th international conference on Fire and Materials, 31 Jan - 2 Feb, San Francisco, California, USA.
- Mell, W. E., McDermott, R. J. and Forney, G. P. (2010). "Wildland fire behaviour modeling: perspectives, new approaches and applications." Proceedings of the 3rd Fire Behavior and Fuels Conference, (eds.), International Association of Wildland Fire, 25-29 October, Spokane, Washington, pp. 1-16.
- Mie, G. (1908). "Beiträge zur optik trüber medien, speziell kolloidaler metallösungen." *Annalen der Physik* 330(3): 377-445. DOI: <http://dx.doi.org/10.1002/andp.19083300302>.
- Mizukami, W., Mu, C. and Tanaka, F. (2013). "Fire suppression with water sprays." Proceedings of International Symposium on Advanced Mechanical and Power Engineering (ISAMPE), 14-23 November, 2013, University of Fukui, Japan.
- Moinuddin, K. A. M., Al-Menhali, J. S., Prasannan, K. and Thomas, I. R. (2011). "Rise in structural steel temperatures during ISO 9705 room fires." *Fire Safety Journal* 46(8): 480-496. DOI: <http://dx.doi.org/10.1016/j.firesaf.2011.08.001>.
- Moinuddin, K. A. M. and Li, J.-D. (2010). "A new convective heat transfer model for fire dynamics simulator." Proceedings of the 13th Asian Congress of Fluid Mechanics (ACFM), 17-21 December 2010, Dhaka, Bangladesh, pp. 819 - 822.
- Moinuddin, K. A. M., Prasannan, K., Lalunio, R. and Thorpe, G. R. (2010). "Numerical modelling of fire spread in landscapes." Proceedings of the 8th Asia-Oceania Symposium for Fire Science and Technology, Dlugogorski, B. Z., Thomas, I. R. and Kennedy, E. M. (eds.), Asia-Oceania Association for Fire Science and Technology, 7-9 Dec, Melbourne, pp. 1-11.
- Morgan, H. P. (1979). "Heat transfer from a buoyant smoke layer beneath a ceiling to a sprinkler spray. 1—a tentative theory." *Fire and Materials* 3(1): 27-33. DOI: <http://dx.doi.org/10.1002/fam.810030106>.

## References

- Morgan, H. P. and Baines, K. (1979). "Heat transfer from a buoyant smoke layer beneath a ceiling to a sprinkler spray. 2—an experiment." *Fire and Materials* 3(1): 34-38. DOI: <http://dx.doi.org/10.1002/fam.810030107>.
- NFPA (2010). "Standard on water mist fire protection systems." NFPA 750, National Fire Protection Association, Batterymarch Park, Quincy, MA.
- Novozhilov, V. (2001). "Flashover control under fire suppression conditions." *Fire Safety Journal* 36(7): 641-660. DOI: [http://dx.doi.org/10.1016/S0379-7112\(01\)00019-4](http://dx.doi.org/10.1016/S0379-7112(01)00019-4).
- Pope, N. D. and Bailey, C. G. (2006). "Quantitative comparison of FDS and parametric fire curves with post-flashover compartment fire test data." *Fire Safety Journal* 41(2): 99-110. DOI: <http://dx.doi.org/10.1016/j.firesaf.2005.11.002>.
- Prasad, K., Patnaik, G. and Kailasanath, K. (2002). "A numerical study of water-mist suppression of large scale compartment fires." *Fire Safety Journal* 37(6): 569-589. DOI: [http://dx.doi.org/10.1016/S0379-7112\(02\)00004-8](http://dx.doi.org/10.1016/S0379-7112(02)00004-8).
- Pruppacher, H. R. and Rasmussen, R. (1979). "A wind tunnel investigation of the rate of evaporation of large water drops falling at terminal velocity in air." *Journal of the Atmospheric Sciences* 36(7): 1255-1260. DOI: [http://dx.doi.org/10.1175/1520-0469\(1979\)036<1255:awtiot>2.0.co;2](http://dx.doi.org/10.1175/1520-0469(1979)036<1255:awtiot>2.0.co;2).
- Putorti, A. D., Belsinger, T. D. and Twilley, W. H. (1995). "Determination of water spray drop size and velocity from a low pressure, high momentum, water-mist nozzle." Test report FR 4000, Building and Fire Research Laboratory, National Institute of Standards and Technology (NIST), Gaithersburg, MD 20899.
- Radford, M. W. (1996). "An investigation of the effect of sprinklers on compartment fires." *Fire Engineering Research Report 96/6*, New Zealand.
- Ranz, W. E. and Marshall, W. R. J. (1952). "Evaporation from droplets, Part I." *Chemical Engineering Progress* 48(3): 141-146.
- Rasbash, D. J., Rogowski, Z. W. and Stark, G. W. V. (1960). "Mechanisms of extinction of liquid fires with water sprays." *Combustion and Flame* 4(0): 223-234. DOI: [http://dx.doi.org/10.1016/S0010-2180\(60\)80026-0](http://dx.doi.org/10.1016/S0010-2180(60)80026-0).
- Ravigururajan, T. S. and Beltran, M. R. (1989). "A model for attenuation of fire radiation through water droplets." *Fire Safety Journal* 15(2): 171-181. DOI: [http://dx.doi.org/10.1016/0379-7112\(89\)90002-7](http://dx.doi.org/10.1016/0379-7112(89)90002-7).
- Ren, N., Baum, H. R. and Marshall, A. W. (2011). "A comprehensive methodology for characterizing sprinkler sprays." *Proceedings of the Combustion Institute* 33(2): 2547-2554. DOI: <http://dx.doi.org/10.1016/j.proci.2010.06.107>.

## References

- Renksizbulut, M. and Yuen, M. C. (1983). "Experimental study of droplet evaporation in a high-temperature air stream." *Journal of Heat Transfer* 105(2): 384-388. DOI: <http://dx.doi.org/10.1115/1.3245590>.
- Rosander, M. and Giselsson, K. (1984). "Making the best use of water for fire extinguishing purposes." *Fire*: 43-46.
- Segelstein, D. J. (1981). "The complex refractive index of water." MS Thesis, Department of Physics, University of Missouri, Kansas City, Missouri.
- Shen, T.-S., Huang, Y.-H. and Chien, S.-W. (2008). "Using fire dynamic simulation (FDS) to reconstruct an arson fire scene." *Building and Environment* 43(6): 1036-1045. DOI: <http://dx.doi.org/10.1016/j.buildenv.2006.11.001>.
- Shu, Y. L., Jeng, W. J., Chiu, C. W. and Chen, C. H. (2005). "Assessment of fire protection performance of water mist applied in exhaust ducts for semiconductor fabrication process." *Fire and Materials* 29(5): 295-302. DOI: <http://dx.doi.org/10.1002/fam.890>.
- Siegel, R. and Howell, J. R. (1992). "Thermal radiation heat transfer." 3rd Edition, Taylor & Francis, Washington DC.
- Sifner, O. and Klomfar, J. (1996). "International standards of thermo-physical properties of water and water vapour." Academia, Prague.
- Slattery, J. C. and Bird, R. B. (1958). "Calculation of the diffusion coefficient of dilute gases and of the self-diffusion coefficient of dense gases." *AIChE Journal* 4(2): 137-142. DOI: <http://dx.doi.org/10.1002/aic.690040205>.
- Smolík, J., Džumbová, L., Schwarz, J. and Kulmala, M. (2001). "Evaporation of ventilated water droplet: connection between heat and mass transfer." *Journal of Aerosol Science* 32(6): 739-748. DOI: [http://dx.doi.org/10.1016/S0021-8502\(00\)00118-X](http://dx.doi.org/10.1016/S0021-8502(00)00118-X).
- Swamy, K. S. K. (2010). "Physics of comets - Chapter 8: Light scattering theory." 3rd Edition. World Scientific Series in Astronomy and Astrophysics – Vol. 12, World Scientific Publishing Co. Pte. Ltd, 5 Toh Tuck Link, Singapore 596224.
- Tang, Z., Fang, Z. and Merci, B. (2014). "Development of an analytical model to quantify downward smoke displacement caused by a water spray for zone model simulations." *Fire Safety Journal* 63(0): 89-100. DOI: <http://dx.doi.org/10.1016/j.firesaf.2013.12.002>.
- Tang, Z., Vierendeels, J., Fang, Z. and Merci, B. (2013). "Description and application of an analytical model to quantify downward smoke displacement caused by a water spray." *Fire Safety Journal* 55(0): 50-60. DOI: <http://dx.doi.org/10.1016/j.firesaf.2012.10.012>.

## References

- Tanner, G. and Knasiak, K. F. (2003). "Spray characterization of typical fire suppression nozzles." In the Proceedings of 3rd International Water Mist Conference, September 22-24, 2003, Madrid, Spain.
- Tewarson, A. (2002). "Generation of Heat and Chemical Compounds in Fires, Section 3/Chapter 4." The SFPE Handbook of Fire Protection Engineering. DiNunno, P. J. (editors). NFPA, Quincy, MA, pp. 3-83–83-161.
- Thomas, G. O. (2002). "The quenching of laminar methane-air flames by water-mists." *Combustion and Flame* 130(1–2): 147-160. DOI: [http://dx.doi.org/10.1016/S0010-2180\(02\)00351-6](http://dx.doi.org/10.1016/S0010-2180(02)00351-6).
- Thorpe, G. R. (2001). "Ambient air properties in aeration (Chapter 3)." In *The Mechanics and Physics of Modern Grain Aeration Management*. Navarro, S. and Noyes, R. (editors). CRC Press, Boca Raton, Florida, pp. 111.
- Thorpe, G. R. (2001). "Chapter 3: Ambient air properties in aeration." *The Mechanics and Physics of Modern Grain Aeration Management*. Navarro, S. and Noyes, R. (editors). CRC Press, Boca Raton, pp. 111.
- Touloukian, Y. S., Liley, P. E. and Saxena, S. C. (1970). "Thermo-physical properties of matter. The TRPC data series, Volume 3: Thermal conductivity, non-metallic liquids and gases." IFI / Plenum, New York pp. 120, 125, 512.
- Touloukian, Y. S. and Makita, T. (1970). "Thermo-physical properties of matter. The TRPC data series, Volume 6: Specific heat, non-metallic liquids and gases." IFI / Plenum, New York, pp. 293.
- Touloukian, Y. S., Saxena, S. C. and Hestermans, P. (1975). "Thermo-physical properties of matter - the TRPC data series, Volume 11: Viscosity." IFI / Plenum, New York.
- Trelles, J. and Mawhinney, J. R. (2010). "CFD investigation of large scale pallet stack fires in tunnels protected by water mist systems." *Journal of Fire Protection Engineering* 20(3): 149-198. DOI: <http://dx.doi.org/10.1177/1042391510367359>.
- Tsilingiris, P. T. (2003). "Comparative evaluation of the infrared transmission of polymer films." *Energy Conversion and Management* 44(18): 2839-2856. DOI: [http://dx.doi.org/10.1016/S0196-8904\(03\)00066-9](http://dx.doi.org/10.1016/S0196-8904(03)00066-9).
- Vaari, J. (2002). "A transient one-zone computer model for total flooding water-mist fire suppression in ventilated enclosures." *Fire Safety Journal* 37(3): 229-257. DOI: [http://dx.doi.org/10.1016/S0379-7112\(01\)00046-7](http://dx.doi.org/10.1016/S0379-7112(01)00046-7).
- Veltre, J. V. (1997). "A full-scale experimental study of water-mist spray convection." *Proceedings of 2nd International Conference on Fire Research and Engineering*, (eds.), Society of Fire Protection Engineering, August 3–8, 1997, Gaithersburg, Maryland, USA, pp. 282–292.

## References

- Wedding, J. B., Kim, Y. J. and Dennison, R. S. (1986). "Mass transfer from water droplets under simulated free-fall conditions." *Atmospheric Environment* (1967) 20(5): 1039-1045. DOI: [http://dx.doi.org/10.1016/0004-6981\(86\)90289-1](http://dx.doi.org/10.1016/0004-6981(86)90289-1).
- Widmann, J. F. (2001). "Phase Doppler interferometry measurements in water sprays produced by residential fire sprinklers." *Fire Safety Journal* 36(6): 545-567. DOI: [http://dx.doi.org/10.1016/S0379-7112\(01\)00009-1](http://dx.doi.org/10.1016/S0379-7112(01)00009-1).
- Wighus, R. (1991). "Extinguishment of enclosed gas fires with water spray." In *Proceedings of the Third International Symposium on Fire Safety Science*, Edinburgh, Scotland, pp. pp. 997-1006. DOI: 10.3801/IAFSS.FSS.3-997.
- Wighus, R. (1995). "Engineering relations for water-mist fire suppression systems." *Proceedings: Halon Alternatives Technical Working Conference*, Albuquerque, New Mexico, pp. pp. 397.
- Wighus, R. and Brandt, A. W. (2001). "WATMIST—a one zone model for water mist fire suppression." *Proceedings: Halon Options Technical Working Conference*, 24-26 April, Albuquerque, New Mexico, USA, pp. 111–121.
- Woo, S. E. and Hamielec, A. E. (1971). "A numerical method of determining the rate of evaporation of small water drops falling at terminal velocity in air." *Journal of the Atmospheric Sciences* 28(8): 1448-1454. DOI: 10.1175/1520-0469(1971)028<1448:anmodt>2.0.co;2.
- Yang, P., Liu, T. and Qin, X. (2010). "Experimental and numerical study on water-mist suppression system on room fire." *Building and Environment* 45(10): 2309-2316. DOI: 10.1016/j.buildenv.2010.04.017.
- Yao, B. and Chow, W. K. (2005). "Extinguishment of a PMMA fire by water spray with high droplet speeds." *International Journal of Thermal Sciences* 44(4): 410-419. DOI: <http://dx.doi.org/10.1016/j.ijthermalsci.2004.06.006>.
- Yu-chuan, Y., Chung-hwei, S. and Kee-chiang, C. (2004-2005). "The effect of water droplet size of water spray on liquid pool fire suppression." *Journal of Applied Fire Science* 13(4): 315-327.
- Yuen, M. C. and Chen, L. W. (1978). "Heat-transfer measurements of evaporating liquid droplets." *International Journal of Heat and Mass Transfer* 21(5): 537-542. DOI: [http://dx.doi.org/10.1016/0017-9310\(78\)90049-2](http://dx.doi.org/10.1016/0017-9310(78)90049-2).
- Zhang, C. and Chow, W. (2013). "Numerical studies on the interaction of sprinkler and smoke layer." *Procedia Engineering* 62(0): 453-462. DOI: <http://dx.doi.org/10.1016/j.proeng.2013.08.087>.
- Zhao, J. H., Gao, Y. and Wu, H. M. (2010). "Numerical simulation and research of pool fire suppressed by water mist in the engineroom of a ship." *Applied Mechanics and Materials* 29-32: 651-657. DOI: 10.4028/[www.scientific.net/AMM.29-32.651](http://www.scientific.net/AMM.29-32.651)

## References

- Zhao, L., Beck, V. R. and Kurban, N. (1998). "Fire brigade intervention model for residential buildings." Proceedings of the Third Asia-Oceanian Symposium on Fire Sciences and Technology, (eds.), International Association for Fire Safety, 10-12 June, Singapore, pp. pp. 604-615.

# Appendix A

Calculation of theoretical adiabatic  
saturation temperature

# Appendix A

## Calculation of the theoretical adiabatic saturation temperature

---

The adiabatic saturation temperature is the temperature attained if the air were saturated by an adiabatic process, and the adiabatic process is the process in which air, having a relative humidity (RH) less than 100%, flows over water contained in a well-insulated duct. Since the air has  $RH < 100\%$ , some of the water will evaporate and the temperature of the air-vapour mixture will decrease. If the channel is long enough, the airstream will exit as saturated air (100 per cent relative humidity) at the exit temperature. The temperature of the air leaving the system is known as the adiabatic saturation temperature. Figure A.1 represents the adiabatic process of the air-water system.

The basic principle involved in the saturation temperature of an evaporating droplet is the same as the adiabatic saturation temperature of the air-water system. Due to the temperature difference between air and droplet, there is a form of heat transfer in between them. When a droplet travels through a hot air layer, it absorbs heat from the surrounding air and raises its temperature and reach to a level where the temperature of the droplet does not increase. The absorbed heat by the droplet is used for the evaporation of water particles from the droplet. The temperature of the droplet at this level is known as saturation temperature or steady state temperature. From the equation of enthalpy balance in the adiabatic process, the saturation temperature can be calculated. The expressions for the calculation of this temperature are given below [\[Thorpe 2001\]](#):

Appendix A: Calculation of the theoretical adiabatic saturation temperature

$$f(T_s) = 1.003 (T - T_s) + w (2501.33 + 1.814 * T - 4.177 * T_s) - w_s (2501.33 - 2.363 * T_s) \quad (A.1)$$

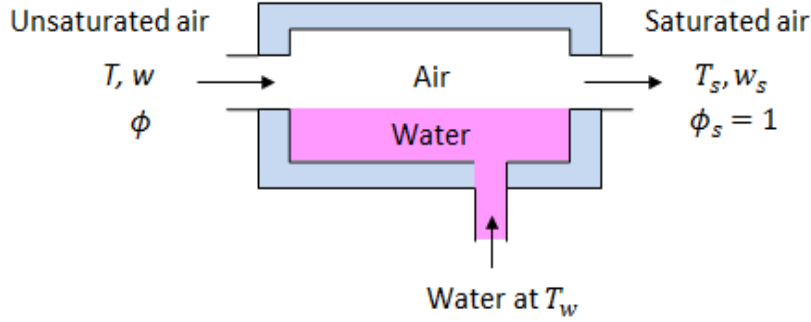


Figure A.1: A schematic diagram of the adiabatic saturation process (after Çengel and Turner [2005]).

The task is to find the value of  $T_s$  which makes  $f(T_s) = 0$ . This can be solved by using the Newton-Raphson method. The details of this procedure are given by Thorpe [2001]. The solution algorithm is expressed as:

$$T_s^{p+1} = T_s^p - \frac{f(T_s^p)}{\frac{df(T_s^p)}{dT_s^p}} \quad (A.2)$$

$$\frac{df(T_s)}{dT_w} = -1.003 - 4.177 * w - 2.363 * w_s - \frac{dw_s}{dT_w} (2501.33 - 2.363 * T_s) \quad (A.3)$$

$\frac{dw_s}{dT_s}$  can be determined for the following equations:

$$\frac{dw_s}{dT_s} = \frac{dw_s}{dP_s} \frac{dP_s}{dT_s} \quad (A.4)$$

$$\frac{dw_s}{dP_s} = \frac{0.622 * P_{atm}}{(P_{atm} - P_s)^2} \quad (A.5)$$

Appendix A: Calculation of the theoretical adiabatic saturation temperature

$$\frac{dP_s}{dT_s} = \frac{4098.17 * P_s}{(T_s + 237.3)^2} \quad (A.6)$$

where,  $w_s = 0.622 \frac{P_s}{P_{atm} - P_s}$  (A.7)

# Appendix B

Scattering, absorption and extinction  
of radiation by water mists

# Appendix B

## Scattering, absorption and extinction of radiation by water mists

---

### B.1 Introduction

Thermal radiation plays a significant role in propagating heat due to the high temperatures encountered in building or industrial fires. It is perhaps more important in naval ships, as ordnance in ships' magazines must be shielded from radiation. According to experiments, about 30 per cent of the heat released by a fire is in the form of thermal radiation [Tewarson 2002; Liu et al. 2004]. The problem may be mitigated by wetting the surface of combustible material and ordnance. However blocking or attenuating the radiation also plays an important role in reducing the transmission of heat developed by a fire. Water-based fire suppression systems i.e. sprinklers and water mist, can reduce the propagation of heat from fire to unburnt fuel by blocking the thermal radiation. Water droplets attenuate radiation by absorbing and scattering radiation that is intercepted by the droplets. A schematic of the attenuation of the thermal radiation by a spray is presented in Figure B.1.

However the attenuation of radiation by water droplets depends on the wavelength of the radiation, size of the water droplets and concentration of the water loading of the spray. Therefore a good understanding on the effect of those factors in attenuating thermal radiation is required to design an effective WMFSS.

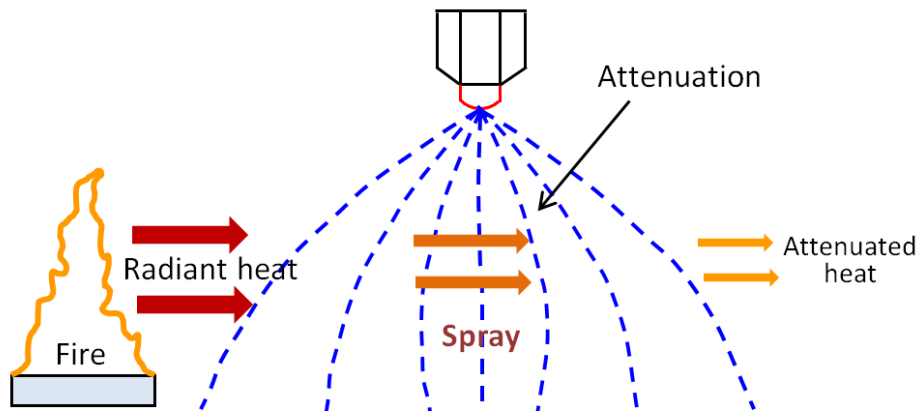


Figure B.1. Conceptual diagram of the attenuation of thermal radiation by a water spray.

Hence one of the object of this research is to investigate the characteristics of water mists in scattering and absorbing radiation and their performance in attenuating the thermal radiation. The effect of the concentration of water loading for the different sizes of droplets is also investigated. In this chapter, the scattering and absorption properties of water mists are analysed using the theory of Mie [1908]. Details of the theory of Mie [1908] and results of the analysis are presented. It is shown that the attenuation of radiation by water mists increases as the diameter of the droplets decrease, and as one might expect, attenuation increases with the loading of water.

## B.2 Theory of scattering

The theory of scattering by spherical water particles of homogeneous composition involves the solution of Maxwell's equations with appropriate boundary conditions on the sphere. Mie [1908] and Debye [1909] independently obtained an analytical solution of Maxwell's equation for the scattering of light by spherical particles [Swamy 2010]. The relevant formulae, particularly the reference to the scattering and absorption by water droplets, are described below.

The scattering properties of a particles depend on the following quantities [Swamy 2010]:

1. The complex refractive index,  $m = n + ik$ , where  $n$  is the real part and  $k$  is the imaginary part
2. The wavelength of the incident radiation ( $\lambda$ )
3. The diameter of the particle ( $d$ ).

When thermal radiation interacts with a particle, a fraction of the radiation is absorbed and a fraction of it is refracted or scattered, as illustrated in Figure B.2. Hence the total amount of radiation lost (extinction) from the incident beam is the summation of the absorbed and the scattered components. These are generally expressed in terms of the dimensionless efficiency factors  $q_{sca}$  and  $q_{abs}$  for the scattering and absorption components, respectively. The efficiency factor for the total extinction is given by:

$$q_{ext} = q_{sca} + q_{abs} \quad (\text{B.1})$$

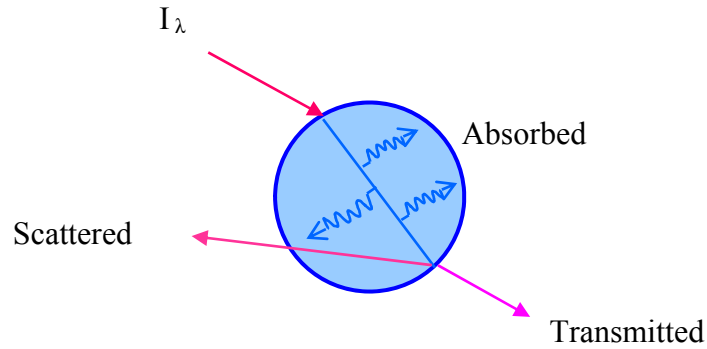


Figure B.2: The scattering of incident radiation of wavelength,  $\lambda$ , by a water droplet.

The extinction efficiency factor ( $q_{ext}$ ) and the scattering efficiency factor ( $q_{sca}$ ) can be computed using the theory of Mie [1908] i.e.

$$q_{sca} = \frac{2}{x^2} \sum_{n=1}^{\infty} (2n + 1) [|a_n|^2 + |b_n|^2] \quad (\text{B.2})$$

$$q_{ext} = \frac{2}{x^2} \sum_{n=1}^{\infty} (2n + 1) [Re(a_n + b_n)] \quad (B.3)$$

where  $a_n$  and  $b_n$  are the coefficients of Mie and they are calculated using the following relations:

$$a_n = \frac{\left[ \frac{A_n(z)}{m} + \frac{n}{x} \right] \psi_n(x) - \psi_{n-1}(x)}{\left[ \frac{A_n(z)}{m} + \frac{n}{x} \right] \zeta_n(x) - \zeta_{n-1}(x)} \quad (B.4)$$

Here,  $\psi_n$  and  $\zeta_n$  are the modified Bessel functions that are known as the Riccati-Bessel functions and  $A_n$  is the logarithmic derivative of  $\psi_n$ . The other two variables  $x$  and  $z$  are independent dimensionless variables and defined as:

$$x = \frac{\pi d}{\lambda} \quad (B.5)$$

$$z = m x \quad (B.6)$$

where  $d$  = diameter of the scattering water droplets,  $\lambda$  = wavelength of incident radiation and  $m$  is the complex refractive index of the water droplets relative to the medium.

$$m = n + ik \quad (B.7)$$

where  $n$  and  $k$  are, respectively, the real and imaginary parts of the refractive index relative to the medium. The real part accounts for the refractive component of the index and the imaginary part accounts for the absorptive component of the index.

The extinction efficiency factor ( $q_{ext}$ ) is used to determine a monochromatic transmissivity ( $\tau_\lambda$ ) of water droplets. The correlation of transmissivity is expressed as:

$$\tau_{\lambda} = \text{Exp} \left[ \frac{6 q_{ext} W L}{4 d \rho} \right] \quad (\text{B. 8})$$

in which  $W$  is the concentration of droplets,  $\text{kg/m}^3$ ,  $d$  is the diameter of the droplet and  $L$  is the travel path of the radiative wavelength. The monochromatic radiation intensity of a wavelength ( $I_{\lambda}$ ) can be calculated using Planck's spectral distribution of emissive power [Siegel and Howell 1992].

$$I_{\lambda} = \frac{C_1 \lambda^{-5}}{e^{C_2/\lambda T} - 1} \quad (\text{B. 9})$$

where  $\lambda$  is the wavelength of the incident radiation in  $\mu\text{m}$ ,  $T$  is the temperature of the radiative body in  $K$ , and  $C_1$  and  $C_2$  is the constant in Planck's distribution of spectral intensity. The total intensity of radiation can be calculated by integrating the radiation for all wavelengths.

$$I_{0-\infty} = \int_0^{\infty} I_{\lambda} d\lambda \quad (\text{B. 10})$$

The integration of  $I_{\lambda}$  for all wavelengths yields the radiation equation:

$$Q_R = \int_0^{\infty} I_{\lambda} d\lambda = \sigma T^4 \quad (\text{B. 11})$$

However the intensity in an interval of wavelengths can be calculated by integrating across the corresponding interval of wavelengths:

$$Q_{\lambda_1-\lambda_2} = I_{\lambda_1-\lambda_2} = \int_{\lambda_1}^{\lambda_2} I_{\lambda} d\lambda \quad (\text{B. 12})$$

The amount of radiation transmitted through the medium due to water loading can be calculated by the following equation:

$$Q_{T(\lambda_1 - \lambda_2)} = I_{T(\lambda_1 - \lambda_2)} = \int_{\lambda_1}^{\lambda_2} \tau_\lambda I_\lambda d\lambda \quad (\text{B.13})$$

A set of MATLAB functions developed by Mätzler [2002] is used to solve those equations. The details of these programs are available in the relevant reference.

### B.3 Characteristics of water mist in scattering

The data of Segelstein [1981] are used for the complex index of the refraction of water. Figure B.3 illustrates the variation of  $n$  and  $k$  with the wavelength of the incident radiation. The wavelength range available in the Segelstein [1981] data is much larger than that required for the study of thermal radiation.

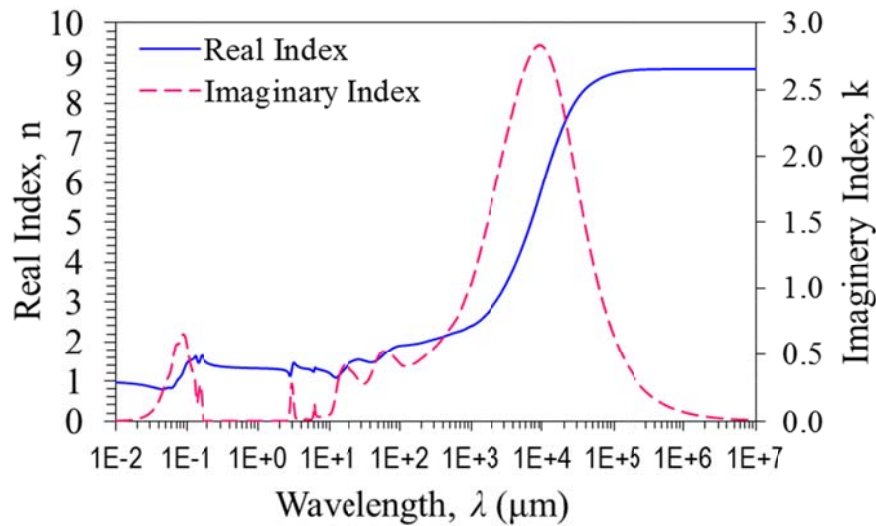


Figure B.3: Complex refractive index of water.

The scattering properties of water mist are examined with five different diameters of droplets: namely 100, 200, 300, 400 and 500  $\mu\text{m}$ . Primarily, five concentrations of water loading are considered for the study i.e. 0.1, 0.25, 0.5, 0.75 and 1.0  $\text{kg}/\text{m}^3$ . The scattering efficiency factors of the five diameters of water-mist droplets are calculated using the theory of Mie [1908] and are illustrated in Figure B.4.

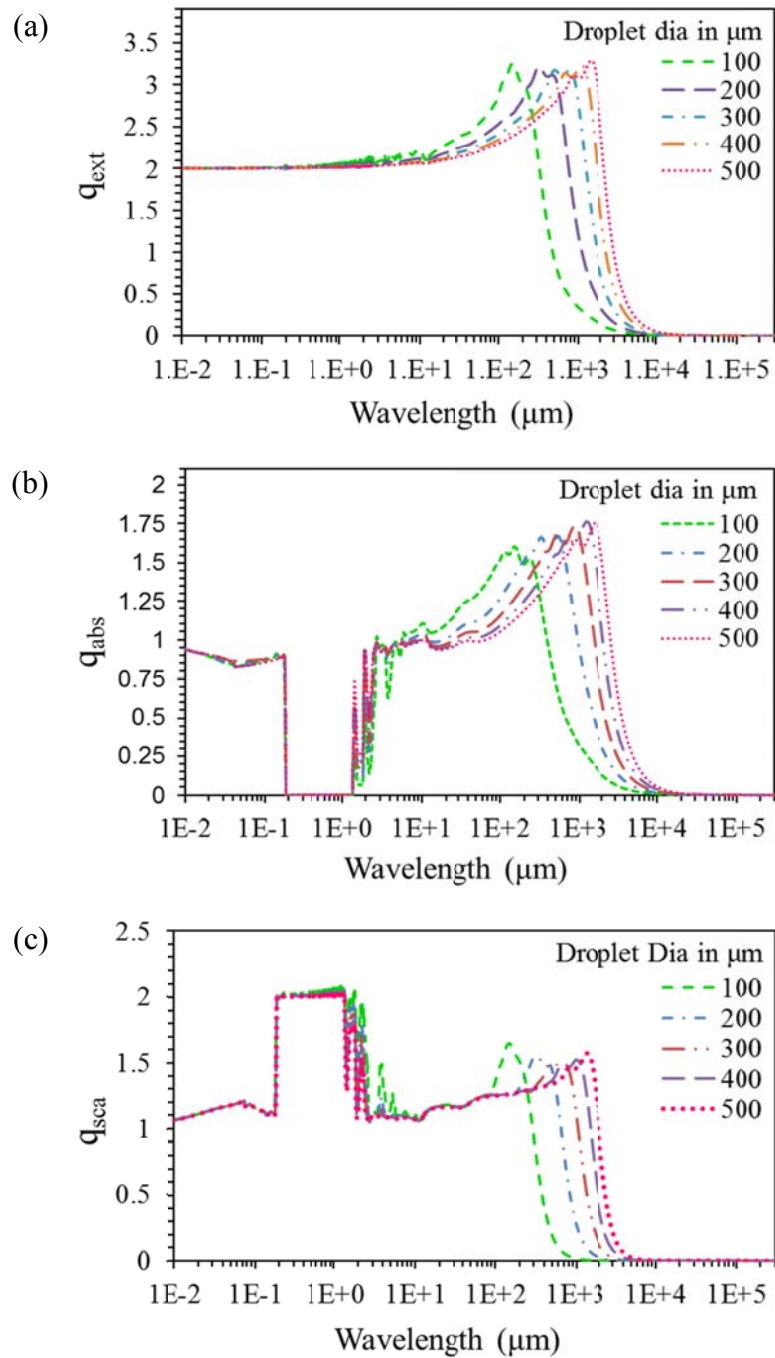


Figure B.4: Efficiency factors for water-mist droplets (a) extinction efficiency factor,  $q_{ext}$ ; (b) absorption efficiency factor,  $q_{abs}$ ; and (c) scattering efficiency factor,  $q_{ext}$ .

The figure shows that the extinction efficiency factor in the spectrum between wavelengths of 0.01–40 μm is about 2.06, fluctuating with a range of 1.99 to 2.42. The maximum value of  $q_{ext}$  is 3.28, which is independent of the size of the droplets.

However this value occurs at lower wavelengths in the case of droplets that have smaller diameters. For example, the maximum value of  $q_{ext}$  occurs at a wavelength of 150  $\mu\text{m}$  when the droplets have a diameter of 100  $\mu\text{m}$ , whereas the maximum value occurs when the diameter is 500  $\mu\text{m}$  and the wavelength is 1400  $\mu\text{m}$ . The scattering and absorption efficiency factors show that absorption and scattering have an almost equal contribution in the extinction of radiation within the spectrum of .01–0.18  $\mu\text{m}$ . Absorption dominates over scattering within the spectrum of 1.4–10000  $\mu\text{m}$ . It is important to note that the droplets absorb negligible radiation in the spectrum of 0.18–1.4  $\mu\text{m}$ .

In Figure B.4 the efficiency factors are presented for a wide range of wavelengths. However, the interest of this study is within the spectrum of 0.01–100  $\mu\text{m}$ , as this corresponds to the radiation emitted in fires. The plot of monochromatic intensity of radiation with the spectrum of 0.1–100  $\mu\text{m}$  is illustrated in Figure B.5. As presented in this figure, a calculation of radiation emission for 1500 K shows that the 99.5% of the radiation occurs with the spectrum of 0.5–20  $\mu\text{m}$  and 96.7% falls within the spectrum of 0.7–10  $\mu\text{m}$ . Therefore the wavelength spectrum of 0.7–10  $\mu\text{m}$  is considered for the analysis of attenuation of radiation by water-mist droplets.

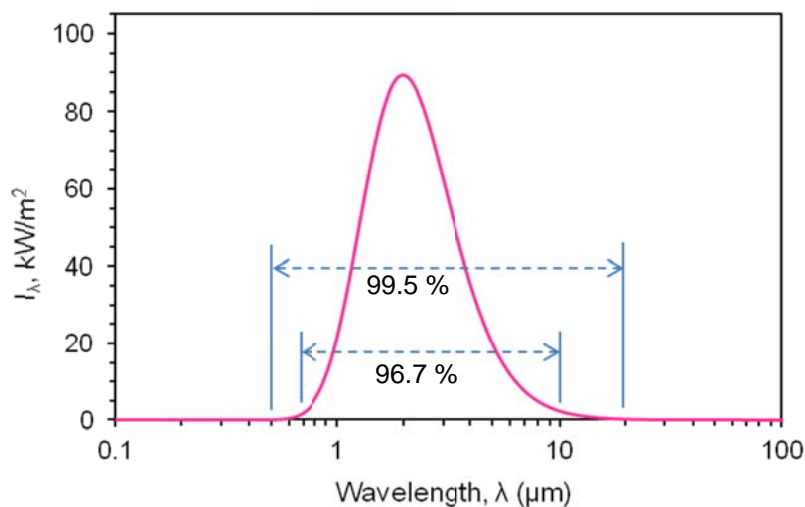


Figure B.5: Monochromatic radiation intensity for a spectrum of wavelength at 1500K.

## Appendix B: Scattering, absorption and extinction of radiation by water mists

Transmissivity of water mist for different loading concentrations with different sizes of droplets are calculated for a wavelength of 3  $\mu\text{m}$  and the results are illustrated in Figure B.6. The minimum concentration of water loading for each size of droplet is also determined. Here, the minimum concentration of water loading is considered when the transmissivity for the size of droplet approaches zero ( $\tau_\lambda \leq 0.001$ ).

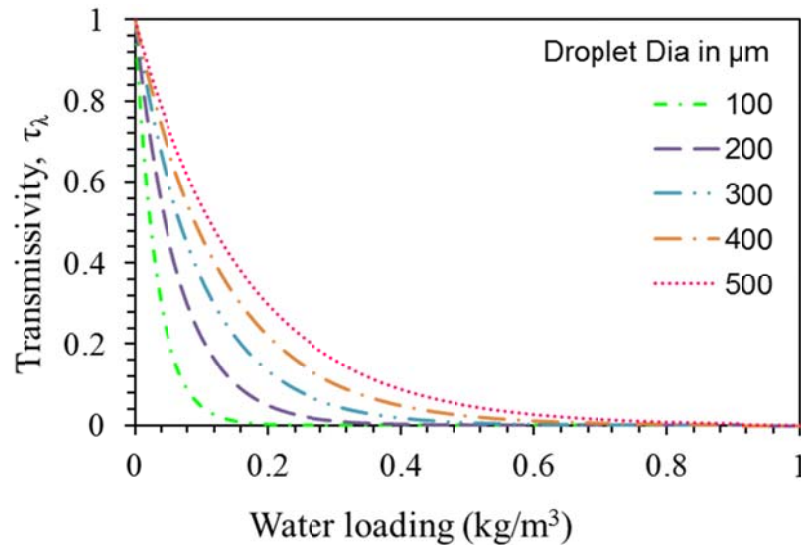


Figure B.6: Transmissivity of water droplets for different sizes at a wavelength of 3  $\mu\text{m}$ .

The figure shows that this concentration increases with the increase in size of the droplets. The maximum concentration of loading of water for droplets with a diameter of 100  $\mu\text{m}$  is 0.3  $\text{kg/m}^3$ , whereas this amount is more than 1  $\text{kg/m}^3$  for droplets with a diameter of 500  $\mu\text{m}$ . However, as shown in Figure B.7, a linear relationship is found between the optimum concentration of water loading and size of the droplets.

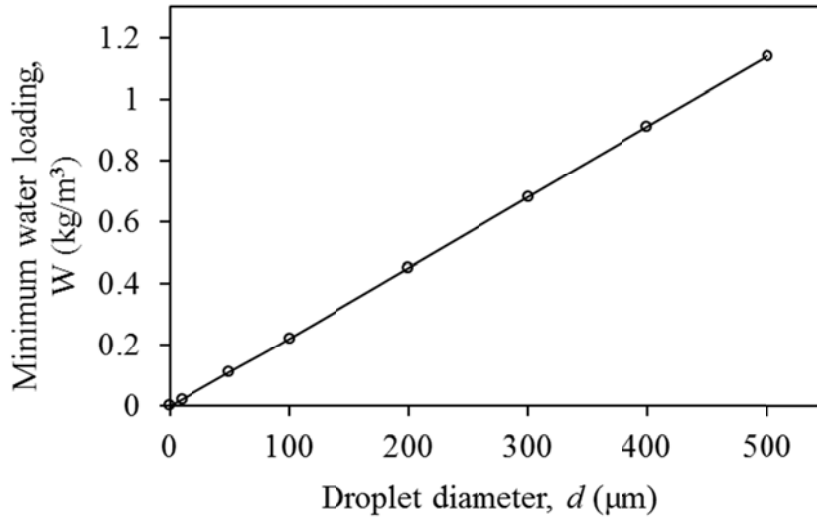


Figure B.7: The minimum concentration of water loading for different size of droplets.

The attenuation of thermal radiation is calculated based on the transmissivity of radiation through the droplets. An incident radiation ( $Q_R$ ) is passing through a medium width of  $L$  filled with water droplets, as illustrated in Figure B.8. While passing through the medium, a part of the radiation is extinguished ( $Q_{ext}$ ) and a part is transmitted ( $Q_T$ ). The values of  $Q_{ext}$  can be calculated for both monochromatic and a spectrum of wavelength.

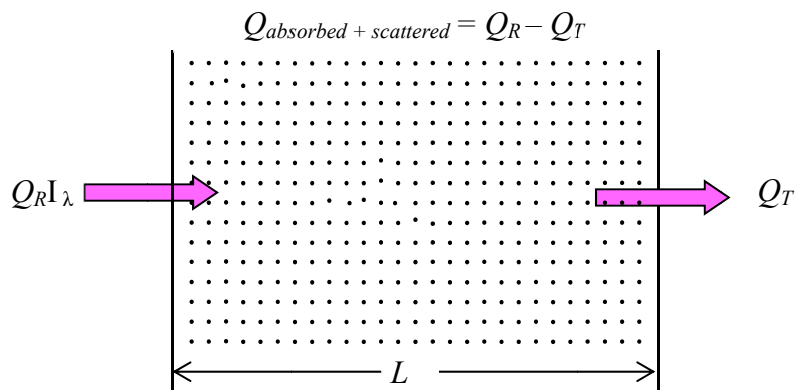


Figure B.8: A spectrum of radiation passing through a medium filled with droplets.

Here, a case is considered where a medium of 1 meter of width is filled with droplets. The temperature of the radiative plate is considered to be 1500 K. The attenuation for the spectrum of 0.5–20  $\mu\text{m}$  wavelengths is considered for the

calculation. The attenuation of radiation for five sizes of droplets is calculated and the results are presented in Figure B.9. The comparison is conducted for five different concentrations of water loading. The results show that the droplets with smaller sizes have a higher capacity in the attenuation of thermal radiation and the attenuation for a particular size of droplet increases with the increase of concentration of water loading. However the radiation is attenuated completely at the optimum level of water loading for a certain size of droplet.

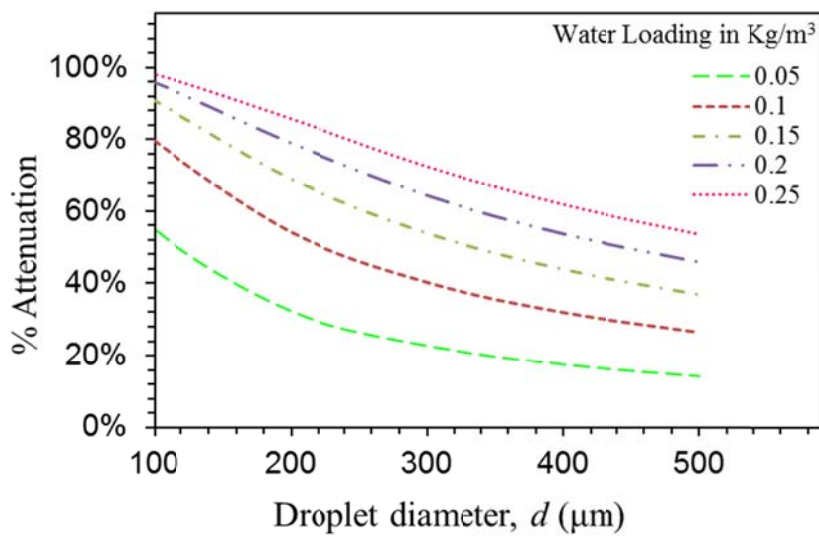


Figure B.9: The attenuation of thermal radiation by water-mist droplets.

## B.4 Conclusions

In this study, the extinction efficiency factors of water mist on thermal radiation are calculated based on the theory of Mie [1908]. The attenuation of thermal radiation is calculated for the different sizes of droplets. The analysis shows that smaller droplets have a better capability in attenuating thermal radiation compared to that of large droplets due to their ability to scatter thermal radiation more efficiently. The effect of the concentration of water loading is evaluated. The results show that the higher concentration of loading increase the attenuation up to a minimum level of concentration. However the amount of minimum concentration of water loading is lower for the smaller size of droplets.

# Appendix C

## Journal papers

# Appendix C

## Journal papers

---

Included in this appendix is the following journal paper:

Mahmud, H.M.I., Moinuddin, K.A.M., Thorpe, G.R. Study of water-mist behaviour in hot air induced by a room fire: Model development, validation and verification, *Fire and Materials*, 2014, Published online in Wiley Online Library, doi: 10.1002/fam.2279.

## Study of water-mist behaviour in hot air induced by a room fire: Model development, validation and verification

H. M. Iqbal Mahmud<sup>\*,†</sup>, Khalid A.M. Moinuddin and Graham R. Thorpe

*Centre for Environmental Safety and Risk Engineering, Victoria University P.O. Box 14428, Melbourne, Victoria 8001, Australia*

### SUMMARY

Water-mists are emerging as an effective agent for the suppression of fires. However, the mechanisms of suppression are complex and the behaviour of individual water droplets in a smoke layer generated by fires must be quantified. This study investigates the behaviour of individual droplets injected from a nozzle into a hot air environment induced by a room fire. A semi-empirical model has been developed based on the conservation of mass, momentum and energy to evaluate the heat and mass transfer phenomena in an air-water droplet system. The model has considered the effect of change of momentum of an evaporating droplet. A forward finite difference approach is applied to solve the governing time dependent ordinary differential equations. The droplets are considered to be 'lumped mass' and variable thermo-physical properties of water and air and the change of Reynolds number of the droplets, due to the change of their diameter and velocity are considered. The effect of high evaporation rate on the mass and heat transfer coefficient and the contribution of radiation emanating by a flame and the surrounding boundary walls are also considered in the model which were not taken into account in the previous studies. Experimental data on terminal velocity and adiabatic saturation temperature are used to validate and verify the model. The validation and verification indicate that the proposed model predicted the terminal velocity within 4% of the experimental data and predicted the saturation temperature within 5% of the adiabatic saturation temperature. This semi-empirical model is also used as a tool to validate a more comprehensive computational fluid dynamics (CFD) based tool, Fire Dynamics Simulator (FDS). It is found that FDS results agree well with the results of the proposed model. Furthermore, the proposed model can be used to evaluate the temperature, velocity, diameter and other physical properties of a droplet travelling through a layer of hot air. Copyright © 2014 John Wiley & Sons, Ltd.

Received 16 September 2013; Revised 19 September 2014; Accepted 30 September 2014

**KEY WORDS:** water-mist; fire suppression; heat and mass transfer; droplet evaporation; fire dynamic simulator (FDS)

### 1. INTRODUCTION

Water-mist fire suppression systems (WMFSS) are being installed in a wide range of situations. If we are to design and deploy WMFSS effectively, we must have a deep understanding of the physics of their operation. The performance of WMFSS depends on many interacting factors, such as the mass flow rate of water, and the diameters, velocities and spatial distributions of the droplets. The droplets have the potential to cool the surrounding air, attenuate thermal radiation and the water vapour produced by evaporation reduce the fuel vapour/air ratio by displacing oxygen [1-8]. Not all droplets evaporate before striking burning surfaces, and this provides a direct method of suppressing fires [2-3, 6-7, 9-10].

A distinguishing feature of water-mist nozzles is that they produce fine mists consisting of droplets with diameters of less than 1000  $\mu\text{m}$ . The fine mists display fog-like behaviour that renders their fire

\*Correspondence to: H. M. Iqbal Mahmud, Centre for Environmental Safety and Risk Engineering, Victoria University, P.O. Box 14428, Melbourne, Vic. 8001, Australia.

†E-mail: hm.mahmud@live.vu.edu.au

suppression characteristics quite different from conventional water sprays. Studies of the interaction of conventional sprinkler sprays with hot air or smoke layers [11-16] have focused primarily on the convective heat transfer phenomena between large water droplets and hot air layer. It is found that the evaporation of larger droplets discharged by conventional sprinklers is not affected significantly by the fire plume [8, 15]. In contrast, the small droplets of water that comprise fine mists have a higher surface area/volume ratio and this result in their rapid evaporation.

A number of studies [17-27] reported in the published literature account for the rate of evaporation of droplets in the analysis. The rate of evaporation of falling droplets defers from that of stationary droplets due to different heat and mass transfer coefficient resulted from change of momentum. *Ceteris paribus*, the drag coefficients of droplets depends on their diameters and velocities. In case of water droplets, emanating from a nozzle these two variables change, and this affects the drag coefficient. However, this phenomenon was neglected by Novozhilov [21] in the analysis of the transport of water droplets. When sprinkler systems are activated at a temperature of 60 °C, say, the relative humidity (RH) of the surrounding air is very low, typically 5%. This is in sharp contrast with the data generated by Li and Chow [22] who assumed that the RH of the air was 53%, yet the dry bulb temperature was 60 °C. Vaari [23] assumed the droplet temperature to be identical to the surrounding air temperature in his transient one-zone model that described the total flooding water mist fire suppression. The Reynolds number (Re) does have an effect on the heat and mass transfer coefficient in between water and air. However, Barrow and Pope [24] had neglected this effect by assuming the Re of droplets to be zero and this has limited the use of their model. The use of a one-zone model and its limitations in studying water-mist fire suppression systems is reported by Li and Chow [25]. However, none of these reported studies considered the effects of thermal radiation on the behaviour of water droplets, though the radiative heat transfer is important in case of fire. In addition, the effect of high mass transfer rate and low humidity should be considered in case of room fires.

If we are to accurately model the behaviour of water-mists we must be able to quantify the rate of evaporation of water considering all of the issues as discussed above. The principal objective of this work is to develop a detailed model of evaporation water droplets by considering:

- (i) The contribution of radiation emanating by the flame and the surrounding boundary walls to the rate of evaporation of water droplets.
- (ii) The effect of high mass transfer rates on the mechanism of evaporation.
- (iii) The change of the momentum of the droplets.
- (iv) The variable thermo-physical properties of water and air.

In this study, the proposed model is compared against experimental and theoretical data available in the published literature for validation and verification purposes. Once validated and verified, the proposed semi-empirical model can be used as a validation tool for more comprehensive CFD based models. In this study, such validation of FDS, version 6, is carried out.

## 2. MATHEMATICAL FORMULATION

The rate of evaporation of a moving droplet is a manifestation of simultaneous heat, mass, and momentum transfer process as between the particle and surrounding air. Momentum transfer affects motion of the particle, mass transfer causes changes of the particle size, and heat transfer determines the temperature of the particle. In fact, these mechanisms are interdependent [21]. In the proposed model, the effect of high-mass-transfer rate, due to high temperature and low humidity, are taken into account by modifying the heat and mass transfer coefficients. The changes of diffusivity of water vapour through air, density and latent heat of vaporization of water with the change of temperature are also taken into account to improve the accuracy of the model. The droplet is considered as a 'lumped mass' on account the low Biot number [28]. The shape of droplet is assumed to be spherical as this is not expected to give any significant error in the computation [29]. The assumption of uniform temperature

distribution in the droplet considerably simplify the analysis of the overall computational process, since it avoids the need for a conjugate heat-conduction analysis for the internal transient temperature-distribution inside the droplet [24]. The hot air or smoke layer is assumed to be in quasi-steady-state and this refers to a stable smoke layer which is formed finally when the ceiling jet reach to the boundary wall and rebounded several times [22]. This assumption is more appropriate for the nozzles and smoke layers, which are located away from the fire source or burning object. This distance can be quantified using Alpert's [30] equation taking into account of the size of the fire and the height of the ceiling [30, 31]. This is also supported by the experimental observations in [32-33]. Moreover, this assumption is also used in few analytical and numerical studies [15, 21, 34-36].

### 2.1. Mass Transfer Model

The mass flow rate equation can be expressed as [37];

$$\dot{m} = h_m A (\rho_s - \rho_\infty) \quad (1)$$

where,  $\rho_s$  and  $\rho_\infty$  are the density of water vapour on the droplet surface and in the air, respectively.

The rate of change of droplet diameter can be determined from the following equation;

$$\frac{dD}{dt} = 2 h_m \frac{(\rho_s - \rho_\infty)}{\rho_w} \quad (2)$$

where,  $\rho_w$  is the density of water. The density of water particle at the surface of droplet depends on the partial vapour pressure at the droplet surface. In thermodynamic equilibrium condition, the partial vapour pressure at the droplet surface depends on the surface temperature. Under this condition, evaporation keeps the droplet surface in saturated condition until the droplet is totally vaporized due to heat transfer [38]. The vapour concentration at the surface is the saturated mass fraction of air at temperature of droplet. As the density of water particle depends on vapour pressure of water, this can be found out from the ideal gas equation of state.

### 2.2. Heat Transfer Model

When a droplet is exposed to a higher temperature, it receives heat from the surrounding and temperature rises to a threshold limit, at a given pressure, which is known as steady state or saturation temperature. At this temperature, the water droplet changes its phase from liquid to vapour, keeping the droplet surface in saturated condition until the droplet is completely vaporized [39]. Under this condition, the heat of vaporization is supplied to the droplet surface from surrounding air, flame and hot objects. The transient equation of conservation of heat can be expressed as;

$$c_{pw} m \frac{dT}{dt} = h_c A (T_\infty - T) + \{ \sigma \epsilon F A (T_f^4 - T^4) + \sigma \epsilon A (1 - F) (T_{bw}^4 - T^4) \} - \frac{dm}{dt} L \quad (3)$$

Here, the first part on the right side of the equation is due to convective heat transfer from air to droplet, the second part is due to radiative heat transfer from fire flame and boundary walls to the droplet and the third part contributes to the evaporation of water droplets.

### 2.3. Momentum Model

The velocity of the droplet can be obtained by solving the momentum equation for the droplet. The momentum equation can be written as:

$$\frac{dv}{dt} = g \frac{(\rho_w - \rho_a)}{\rho_w} - \frac{3 C_d \rho_a v^2}{4 \rho_w D} - \frac{3v}{D} \frac{dD}{dt} \quad (4)$$

In the above equation,  $\rho_a$  is the density of air,  $C_d$  is the coefficient of drag and  $v$  is the velocity (or relative velocity) of the droplet. In case of droplet travelling through a stationary hot layer,  $v$  becomes the absolute velocity. It is to be noted that  $C_d$  for a droplet depends on the  $Re$ , which is based on the air droplet relative velocity. Brown and Lawler [40] proposed a correlation between drag coefficient and  $Re$  and compared it with 178 experimental data points. The proposed correlation was found to be quite satisfactory in relation to the experimental data in the range of  $Re < 2 \times 10^5$ . Therefore, the correlation by Brown and Lawler [40] is used here which is;

$$C_d = \frac{24}{Re} (1 + 0.15 Re^{0.681}) + \frac{0.407}{1 + \frac{8710}{Re}} \quad (5)$$

The position of droplet in the air can be found from the velocity equation;

$$\frac{dy}{dt} = v \quad (6)$$

Where,  $y$  is a position vector. It is along the downward direction of movement of the droplet with upward positive.

#### 2.4. Calculation of Rate Constants

The mass transfer coefficient,  $h_m$ , can be calculated using the correlation for the Sherwood number,  $Sh$  [41], where  $Sh$  is  $h_m D / \mathcal{D}_{AB}$ . The Sherwood number can be calculated using the following correlation [42];

$$Sh = a + b \left( Re^{\frac{1}{2}} Sc^{\frac{1}{3}} \right)^c \quad (7)$$

Here,  $a=2$ ,  $b=0.216$  and  $c = 2$  for  $Re^{\frac{1}{2}} Sc^{\frac{1}{3}} < 1.4$ ; and  $a = 1.56$ ,  $b = 0.616$  and  $c = 1$  for  $Re^{\frac{1}{2}} Sc^{\frac{1}{3}} \geq 1.4$ .

The heat transfer coefficient,  $h_c$ , can be calculated by using the correlation for Nusselt number,  $Nu$  [41], where  $Nu$  is  $h_c D / k_a$ . The Nusselt number can be calculated using the following correlation [42];

$$Nu = a + b \left( Re^{\frac{1}{2}} Pr^{\frac{1}{3}} \right)^c \quad (8)$$

Here,  $a=2$ ,  $b=0.216$  and  $c = 2$  for  $Re^{\frac{1}{2}} Pr^{\frac{1}{3}} < 1.4$ ; and  $a = 1.56$ ,  $b = 0.616$  and  $c = 1$  for  $Re^{\frac{1}{2}} Pr^{\frac{1}{3}} \geq 1.4$ .

In the above equations,  $Re$  is the Reynolds number, which is the ratio of inertia force to viscous force, i.e.  $Re = \rho v D / \mu$ ,  $Sc$  is the Schmidt number, which is defined as the ratio of momentum diffusivity (viscosity), i.e.  $Sc = \mu_a / \rho_a \mathcal{D}_{AB}$  and  $Pr$  is the Prandtl number which is the ratio of viscous diffusion rate to thermal diffusion rate of air, i.e.  $Pr = c_p \mu / k$ . The above two equations was found to agree most closely with the experimental results by [43].

The mass diffusivity coefficient,  $\mathcal{D}_{AB}$ , can be calculated using the following expression [44];

$$\frac{P \mathcal{D}_{AB}}{(P_{crA} P_{crB})^{1/3} (T_{crA} T_{crB})^{5/12} \left( \frac{1}{M_A} + \frac{1}{M_B} \right)^{1/2}} = a \left( \frac{T}{\sqrt{T_{crA} T_{crB}}} \right)^b \quad (9)$$

where,  $a$  and  $b$  are constant of the empirical relationship. For air-water system,  $a = 3.64 \times 10^{-4}$  and  $b = 2.334$ . The advantage of this correlation is that it is convenient to use as the critical temperature and molar volume of different species are available.

2.5. Correction to the Rate Constants for High Mass Transfer Rate

The use of the coefficients,  $h_m$  and  $h_c$ , are limited to the case of low-mass-transfer-rate. In case of high temperature and low humidity, the evaporation rate is high and this invokes the high mass transfer rate and affects the heat transfer rate, as well. Hence, correction factors,  $\theta_m$  and  $\theta_c$ , are applied to get the coefficient of mass and heat transfer, respectively, for high mass transfer rates [41]. The correction factors,  $\theta_m$ , can be expressed as [41];

$$\theta_m = \frac{h_m^*}{h_m} \quad (10)$$

where,  $h_m^*$  is the coefficient of mass transfer for high-mass-transfer rate. Therefore,  $h_m$  in Equations (1) and (2) is replaced by  $h_m^*$ .  $\theta_m$  can be calculated from the following equations;

$$\theta_m = \frac{\ln(\tilde{R}_m + 1)}{\tilde{R}_m} \quad (11)$$

$$\tilde{R}_m = \frac{x_{w0} - x_{w\infty}}{1 - x_{w0}} \quad (12)$$

where,  $x_{w0}$  is the mole fraction of water at surface of droplet and  $x_{w\infty}$  is the mole fraction of water in the air. The value of  $x_{w0}$  can be determined by using the following expression [41];

$$x_{w0} = \frac{P_{water}}{P_{air}} \quad (13)$$

where,  $P_{water}$  and  $P_{air}$  are the water vapour and air pressure, respectively, in air-water system. The correction factors,  $\theta_c$ , can be expressed as [41];

$$\theta_c = \frac{h_c^*}{h_c} \quad (14)$$

where,  $h_c^*$  is the coefficient of heat transfer for high-mass-transfer rate. Therefore,  $h_c$  in Equation (17) is replaced by  $h_c^*$ .  $\theta_c$  can be calculated from the following equations;

$$\theta_c = \frac{\ln(\tilde{R}_c + 1)}{\tilde{R}_c} \quad (15)$$

$$\tilde{R}_c = e^\phi - 1 \quad (16)$$

$$\phi = \frac{N_{w0} c_{pw}}{h_c} \quad (17)$$

$$N_{w0} = h_m \ln(1 + \tilde{R}_m) \quad (18)$$

where,  $\phi$  is the dimensionless rate factor and  $N_{w0}$  is the molar flux of water particle at the droplet surface.

2.6. Thermo-Physical Properties of Air and Water

The density of humid air can be calculated, using the ideal gas law, as the sum of the densities of the two gases, dry air and water vapour in proportion with their partial pressures; i.e.

$$\rho_{humid\ air} = \frac{P_{dryair} M_a}{RT} + \frac{P_{vapor} M_w}{RT} \quad (19)$$

Saturation vapour pressure can be obtained from the equation suggested by Buck [45]:

$$P_{sat} = [1.0007 + (3.46 \times 10^{-6} P_{air})] \times 6.1121 \times \exp\left[\frac{17.502 T}{240.97 + T}\right] \quad (20)$$

In this equation,  $P_{sat}$  and  $P_{air}$  are in mbar, and  $T$  is in °C.

It is to be noted that latent heat of evaporation of water,  $L$ , is not constant, rather it varies with temperature; the higher the initial temperature of the liquid water the lesser will be the heat required to evaporate it. A fourth order temperature dependent equation derived from the steam chart [39] is used to determine  $L$  within the range of 0 to 100 °C. The relationship between  $L$  and  $T$  is as follow;

$$L = 7 \times 10^{-8} T^4 - 2 \times 10^{-5} T^3 + 4 \times 10^{-4} T^2 - 2.3657 T + 2500.9 \quad (21)$$

The other temperature depended physical properties of air such as viscosity [46], thermal conductivity [47] and specific heat capacity [48] were determined by using the following correlations;

$$\mu_a = (0.1005 + 0.07848 * T - 0.6696 E - 4 * T^2 + 0.3376 E - 7 * T^3) \times 10^{-6} \quad (22)$$

$$k_a = (-6.4224 + 0.1571 * T - 0.2101 E - 3 * T^2 + 0.16 E - 6 * T^3) \times 10^{-3} \quad (23)$$

$$c_{pa} = (1023.2 - 0.176021 * T + 4.02405 E - 4 * T^2 - 4.87272 E - 8 * T^3) \quad (24)$$

here,  $T$  is in K. The density of water is calculated by using the following correlation [49];

$$\rho_w = (0.322 + 0.64166 * Z^{(1/3)} + 0.35409 * Z^{(2/3)} - 0.16449 * Z^{(5/3)} - 0.56509 * Z^{(16/3)} - 14.65649 * Z^{(43/3)} - 2.17251 * Z^{(110/3)}) * 10^3 \quad (25)$$

where,  $Z = 1 - \frac{T}{T_{cr}}$ ;  $T_{cr}$  is the critical temperature of water in K.

### 3. COMPUTATIONAL PROCEDURE

A computational model has been developed using the equations of conservation of mass, momentum and energy as defined in the previous section. The governing differential equations are discretised and solved explicitly using a finite difference approach. The initial droplet conditions of  $D$ ,  $T$ ,  $v$  and  $y$ , together with the relevant thermo-physical properties of water and air are specified. The sequence of calculation is –

- i) Initialise  $D$ ,  $T$ ,  $v$  and  $y$  of droplet, and  $T$  and  $RH$  of air.
- ii) The mass transfer and heat transfer coefficients are calculated using Equations (7) and (8), respectively, incorporating a correction factor for high mass and heat transfer rate, using Equations (10) and (14), respectively.
- iii) The discretised differential Equations (2), (3), (4) and (6) are solved sequentially using the Euler method, to obtain the time trajectories of  $D$ ,  $T$ ,  $v$  and  $y$  of the droplet.

A general form of the discretised equations can be expressed as –

$$\Phi_{t+\Delta t} = \Phi_t + \left. \frac{d\Phi}{dt} \right|_t \Delta t \quad (26)$$

where, the variable  $\Phi$  can represent the diameter, temperature and velocity; i.e.  $D$ ,  $T$  and  $v$ . The position vector of the droplets in air is discretised as follow

$$y = \sum_{i=1}^N v \times \Delta t \quad (27)$$

where,  $N = \text{time}/\Delta t$ .

It is essential that the histories of  $D$ ,  $T$ ,  $v$  and  $y$  are independent of the time step,  $\Delta t$ . In our analysis, it has been found that if the ratio of diameter of droplets to the time step is less than or equal to 0.01, the solution is independent of time step. Here, as an example, a time-step independency test has been conducted for droplets with diameter 200  $\mu\text{m}$ . Figure 1 represents the graphical presentation of the results of analysis and Table 1 represents the numeric values of the analysis. Temperature ( $T$ ) and terminal velocity ( $v$ ) of droplets are compared with three different time steps of 0.1, 0.01 and 0.001 seconds. In the analysis, numerical instabilities are observed when the time step is 0.1 seconds. However, it is found that results of temperature and velocity, for the time steps of 0.01 and 0.001 seconds, are identical up to six and four significant digits of numeric, respectively. Hence, a time step of 0.01 seconds can be used as a time step.

#### 4. MODEL VALIDATION AND VERIFICATION

For the validation of the proposed model, computed results of this model are compared against the experimental data (terminal velocity) of Gunn and Kinzer [50]. For the verification of the proposed model, the predicted results of saturation temperature of this model are compared with the adiabatic saturation temperature. The details of the theory of adiabatic saturation temperature used in this study are described in reference [51].

##### 4.1. Comparison with Experimental Data

Gunn and Kinzer [50] carried out an experimental study to determine the terminal velocities of free falling water droplets in stagnant air. The experiments were conducted at 20 °C of air temperature, 1 atm pressure, 50% relative humidity and an initial temperature of the droplet was 20 °C. The terminal velocities of droplets are calculated using the proposed model and compared with the experimental data. The comparison is presented in Figure 2. It is observed that the predicted values from the proposed model almost collapsed on the experimental data. The deviation between the predicted and experimental values are not greater than 4%.

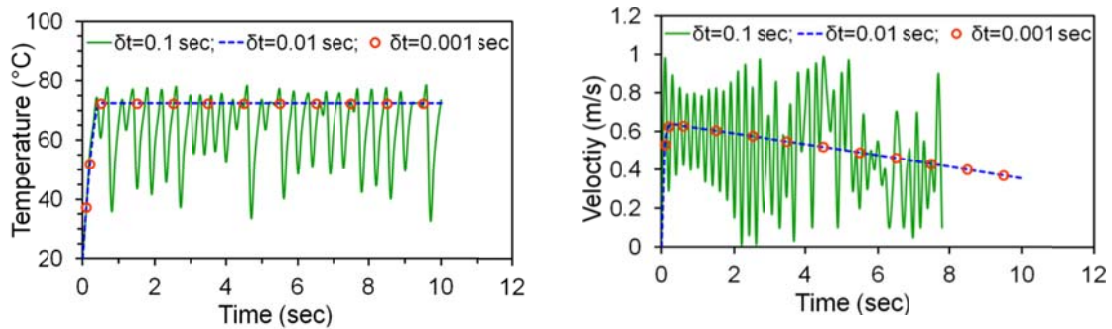


Figure 1. Time step dependency test of a droplet (a) temperature ( $T$ ) and (b) velocity ( $v$ ).

Table I. The dependence of the calculated saturation temperature ( $T$ ) and terminal velocity ( $v$ ) of droplet on the time step.

Time step, $\Delta t$ (s)	0.1	0.01	0.001
Saturation temperature, $T$ (°C)	72.8018	72.4004	72.4004
Terminal velocity, $v$ (m/s)	0.6251	0.4308	0.4308

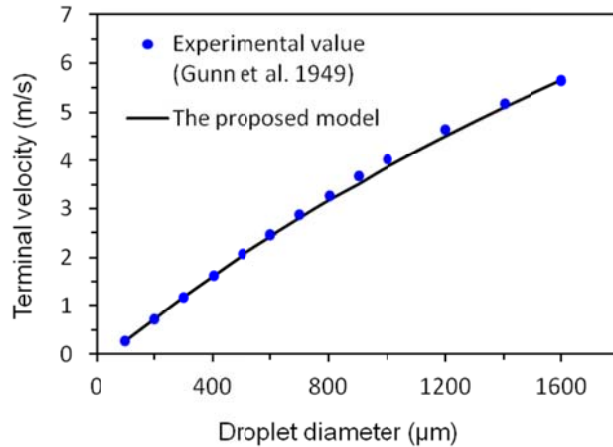


Figure 2. Terminal velocity of the droplets.

#### 4.2. Comparison of Saturation Temperature with Adiabatic Saturation Temperature

The saturation temperatures of droplets are calculated using the proposed model and compared with the theoretical adiabatic saturation temperatures for different temperatures of surrounding air. Temperatures of surrounding air are varied from 5 to 95 °C with relative humidity 40%. Initial temperature of water is taken as 20 °C. The comparison is presented in Figure 3. It is found that the predicted values by the proposed model agree well with the values of adiabatic saturation temperature.

The comparison of the predicted values of terminal velocity with the experimental data and the saturation temperatures of droplets with the adiabatic saturation temperature reveal that the proposed model is capable of predicting these two parameters reasonably well. This provides confidence to use the model as a tool to study the behaviour of individual water droplets and to validate CFD based models.

### 5. USE OF THE MODEL AS A VALIDATION TOOL

In the previous section, the proposed model has been validated and verified against experimental and analytical data. In this section, this model is used to verify a more comprehensive CFD based model. We have considered FDS, CFD based model developed by the Building and Fire Research Laboratory of the National Institute of Standards and Technology (NIST), as an example for validation. The proposed model is also compared with two other models by Li and Chow [22], and Barrow and Pope [24]. The details of the theory of droplet model in FDS [52] and the details of the model by Li and Chow [22], and Barrow and Pope [24] are reported in the relevant references.

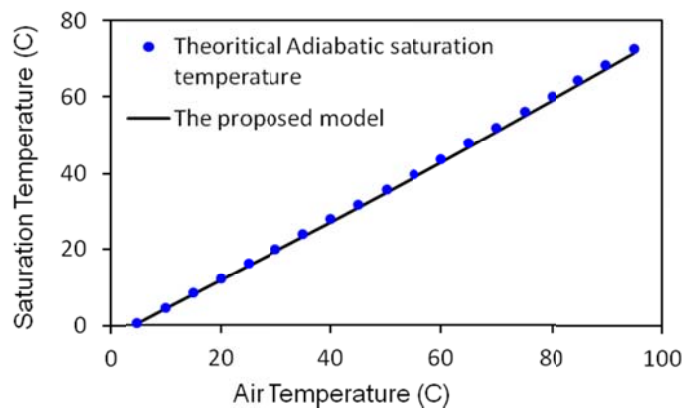


Figure 3. Saturation temperature of the droplets.

### 5.1. Comparison with FDS

In FDS, droplets are represented as discrete spheres travelled through air and transport of droplet is modelled by Lagrangian approach. A semi-empirical heat and mass transfer model is used to simulate the droplet evaporation. The velocity and position of droplet is obtained from theory of conservation of momentum. Details of those models are given in the FDS Technical Reference Guide [52].

A computational domain with dimensions of  $0.5\text{m}\times 0.5\text{m}\times 10\text{m}$  is created to calculate the terminal velocity and saturation temperatures of droplets. The set-up for the computational domain in the FDS model is presented in Figure 4. The nozzle is located at the top of the domain and a single droplet of certain diameter is allowed to fall from the top of the domain. All sides of the domain are kept open to be consistent with the conditions associated with the proposed model. Once the computational domain is set-up, the input parameters of the computational measurements are incorporated in the model. The input variables are the diameter of droplets, the initial temperature of air and droplets, and the relative humidity of air. Then the simulation is allowed to run to calculate the terminal velocities and saturation temperatures of droplets. The input parameters for the numerical model are tabulated in Table 2.

The terminal velocities of droplets of different sizes are calculated using the proposed model and FDS. The simulation of falling of water droplets in air is modelled using FDS with the initial condition as tabulated in Table 2. The calculated values of the terminal velocity of the proposed model are compared with the prediction of FDS and presented in Figure 5. It is observed that FDS predicted values are very close to the calculated values of the proposed model. The differences in the prediction by the two models are less than 8%.

The proposed model and FDS are again used to calculate the saturation temperatures of the same size of droplet ( $1000\ \mu\text{m}$ ) at different temperatures of surrounding air. The surrounding air temperatures are varied between 5 and  $95\ ^\circ\text{C}$ . The comparison of the results is presented graphically in Figure 6. Like Figure 5, a very close result is observed. FDS prediction does not differ more than 10% of the calculated values by the proposed model. Hence, it enforces our confidence in the FDS's capability in predicting the parameters (i.e. temperature, velocity, etc.) associated with the behaviour of an evaporative droplet in hot air.

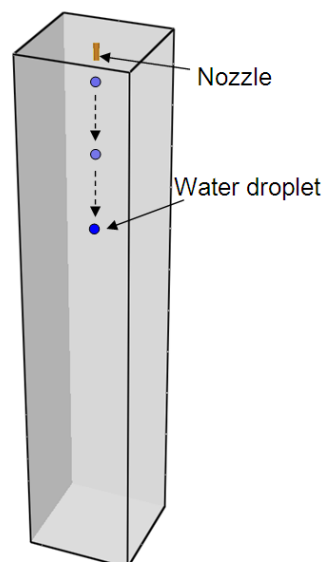


Figure 4. Computational domain set-up of the FDS model.

Table II. The input parameters in the FDS model

Input parameters	Model for Terminal vel.	Model for Saturation Temp.
Droplet diameters, $\mu\text{m}$	100 – 1600	1000
Initial droplet temperature, $^{\circ}\text{C}$	20	20
Surrounding air temperature, $^{\circ}\text{C}$	20	5 – 95
Relative humidity of air, %	50	40

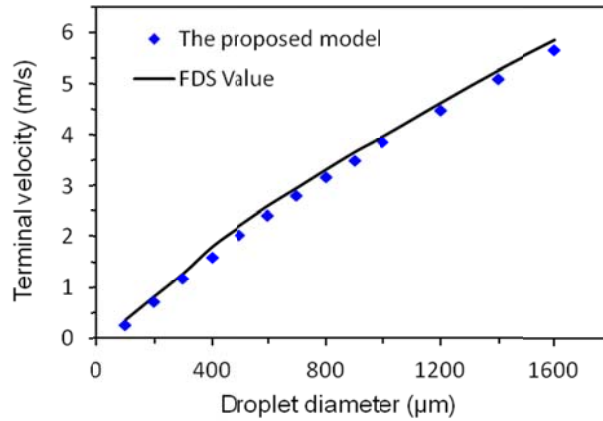


Figure 5. Terminal velocity of the droplets.

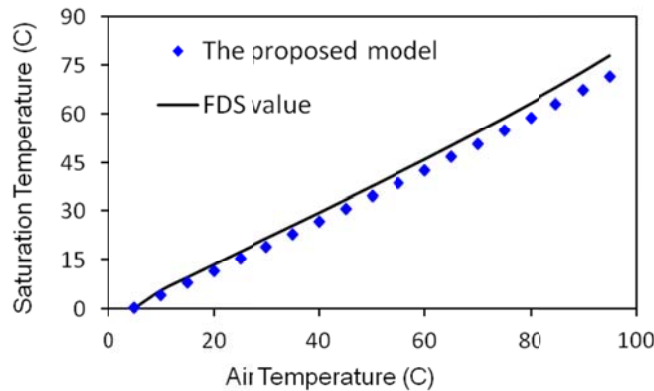


Figure 6. Saturation temperature of the droplets.

5.2. Comparison with the Study by Li and Chow [22]

Li and Chow [22] conducted a study on the evaporation of water-mist droplets. They determined the diameter history of individual droplets travelling through hot air. The same analysis is replicated, in two cases, using the proposed model with the same initial condition as used in [22] (initial droplet diameter 100  $\mu\text{m}$ , air temperature 60  $^{\circ}\text{C}$ , droplet temperature 10  $^{\circ}\text{C}$  and relative humidity 76%). In the first case, the contribution of radiation is ignored and in the second case, the contribution of radiation is considered in the proposed model. The results of the analysis using the proposed model are compared with their results and presented in Figure 7. The results of the proposed model, in first case, are almost identical with the results by Li and Chow [22]. However, the analysis by Li and Chow [22] predicted slower evaporate rate, in second case, compared to the prediction of that by the proposed model. It may be primarily due to the fact that Li and Chow [22] did not consider the contribution of radiation emanating by a flame and the surrounding boundary walls on the evaporation of droplet. However, flame and the boundary walls

WATER-MIST BEHAVIOUR

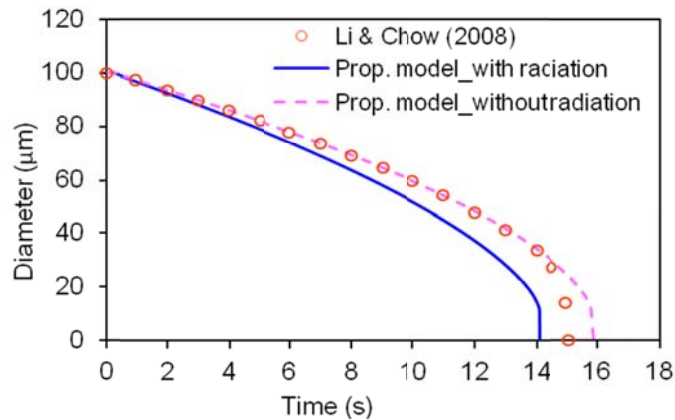


Figure 7. The history of diameter of the droplets in air.

emanate a substantial amount of energy through radiation. As a result, the subject droplets in the analysis by Li and Chow [22] received lesser amount of energy. Hence, their analysis showed a slower rate of evaporation compared to the analysis of that of the proposed model.

5.3. Comparison with the Study by Barrow and Pope [24]

Barrow and Pope [24] conducted a theoretical analysis of evaporating water droplets moving in moist air. They determined the time of evaporation and distance travelled by a range of droplets of different sizes. The same study is replicated using the proposed model with the same initial condition as used in [24] (initial ambient temperature 28 °C, droplet temperature 15.5 °C and relative humidity 40%). A comparison of the results is presented in Figure 8. It is found that the model by Barrow and Pope [24] predicts the droplets with a diameter exceeding 50 µm evaporate more slowly than predicted by the proposed model. This is likely because Barrow and Pope [24] assumed  $Re$  to be zero, which results in the rate of heat and mass transfer to be controlled by diffusive processes; these are slower than those that involve advection.

This assumption may be applicable when the diameter of droplet is less than about 50 µm or reduced to this size in the downstream due to evaporation. However, this assumption breaks down for droplets larger than 50 µm and this result in higher Nusselt numbers and consequently, higher values of the heat transfer coefficient. The history of the Nusselt numbers of droplets with a diameter of 200 µm is presented in Figure 9. It can be seen that at the start of the evaporation process when the droplets are large, the Nusselt numbers predicted by Barrow and Pope [24] are about 2/3 that predicted by the proposed model. Hence, the rate of heat and mass transfer are predicted by Barrow and Pope [24] to be lower than those predicted by the proposed model. Therefore, the proposed model may provide more

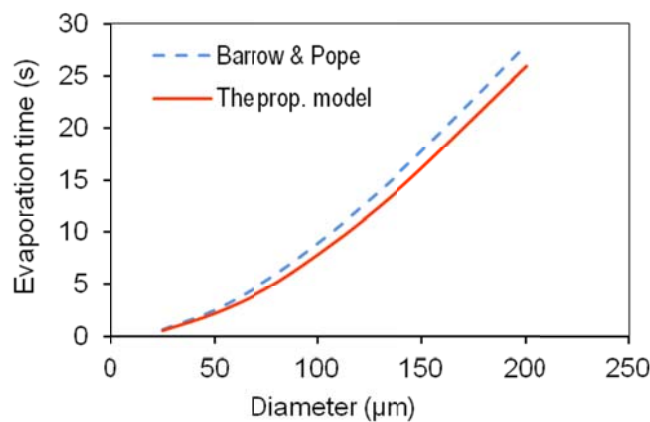


Figure 8. Time of evaporation of the droplets.

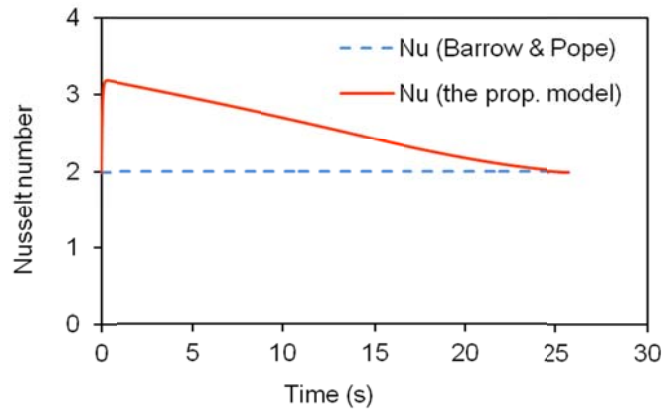


Figure 9. The history of Nusselt number of the droplets for the diameter of 200  $\mu\text{m}$ .

accurate predictions of the rate at which oxygen is displaced from the fire surroundings. The cooling rate of the surrounding air may also be more accurately calculated by the proposed model.

In the conservation of momentum equations of droplets, Barrow and Pope [24] used Stokes' law to calculate the drag force,  $F_d$ . However, Stokes' law is restricted to  $Re$  of less than about 0.1 [39], hence, this law under-predicts the drag force when  $Re$  exceed this value. Barrow and Pope's [24] model is therefore expected to under-predict the drag force for droplets larger than 50  $\mu\text{m}$  in diameter. The drag force history of droplets with diameters of 200  $\mu\text{m}$  is presented in Figure 10.

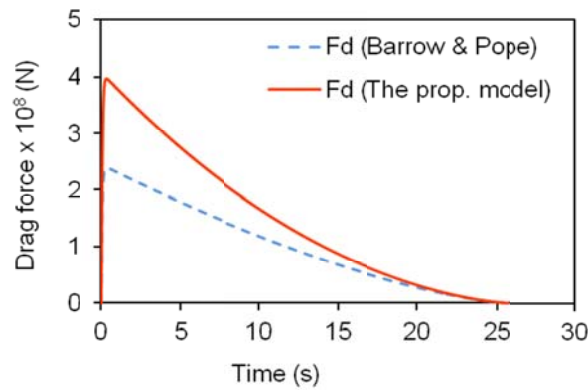


Figure 10. Drag force on the droplets for the diameter of 200  $\mu\text{m}$ .

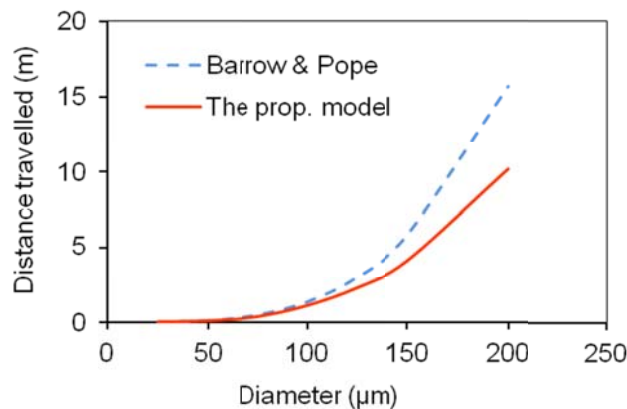


Figure 11. Distance travelled by droplets.

## WATER-MIST BEHAVIOUR

It can be seen that the drag force estimated by Barrow and Pope's [24] model is lower by up to 40% compared to that value of the proposed model. As a result, it predicts that the distance travelled by the droplets is larger. A comparison of the results of distance travelled by the droplets is presented in Figure 11. The droplets of diameter 200  $\mu\text{m}$  have travelled about 15 meters from the point of insertion in the air by the model of Barrow and Pope [24], whereas the droplets have travelled only 10 meters as estimated by the proposed model. As a result, one might expect that the proposed model would predict that the droplets penetrate the hot air or smoke layer induced by a fire to a greater extent than predicted by Barrow and Pope [24]. This may be a crucial consideration when one needs to know that if droplets will contact any hot surface in a fire environment.

## 6. CONCLUSION

In this study, a semi-empirical model of the interaction of water droplets with hot air has been developed based on the principles of conservation of mass, momentum and energy, and some empirical correlations. The contribution of radiation emanating by a flame is considered on the evaporation of droplet. The effect of high evaporation rate and the change of  $Re$  to the mass and heat transfer coefficient is also considered in the proposed model. A forward finite difference technique is used to solve the resulting ordinary differential equations. A time step convergence analysis is conducted and an appropriate time step is selected leading to time step convergent results.

This proposed model has been validated and verified against experimental data and adiabatic saturation temperature. The validation indicates that the proposed model has predicted the terminal velocities within 4% of the experimental data. The saturation temperatures of droplets predicted by the proposed model agree well with the calculated adiabatic saturation temperatures. In this study, the proposed model is also used to validate FDS. The prediction of FDS for saturation temperatures and terminal velocities of droplets agrees well with the calculated values by the proposed model. Therefore, it has given us confidence to use FDS in simulating the behaviour of water-mist droplet in hot air environment. In comparison, Li and Chow [22], and Barrow and Pope's [24] models should be treated with caution as it predicts the longevity of the droplets, and the distance into which they penetrate through a smoke layer or hot air environment induced by a fire. This work provides a further tool with which to predict the behaviour of water droplets evaporating in a hot environment.

## ACKNOWLEDGEMENT

The authors wish to acknowledge the technical and financial assistance provided by Defence Science Technology Organisation (DSTO), Australia.

## NOMENCLATURE

$A$	surface area, $\text{m}^2$
$Bi$	biot number
$C_d$	drag coefficient
$c_{pa}$	specific heat capacity of air, $\text{J/kg}^\circ\text{C}$
$c_{pw}$	specific heat capacity of water, $\text{J/kg}^\circ\text{C}$
$D$	diameter, $\text{m}$
$F$	force, $\text{kg}\cdot\text{m/s}^2$
$G$	gravitational acceleration, $\text{m/s}^2$
$h_c$	convective heat transfer coefficient, $\text{W/m}^2\text{C}$
$h_m$	mass transfer coefficient, $\text{m/s}$
$L$	latent heat of vaporization of water, $\text{J/kg}$
$M$	molecular weight, $\text{kg/mol}$
$m$	mass, $\text{kg}$
$\dot{m}$	mass flow rate of water particle from droplet surface, $\text{kg/s}$
$N$	molar flux, $\text{moles/m}^2\text{s}$
$Nu$	Nusselt number

$P$	vapour pressure, Pa
$Pr$	Prandtl number
$R$	universal gas constant, 8314 J/(Kg.mol.K)
$\tilde{R}$	dimensionless flux ratio
$Re$	Reynolds number
RH	relative humidity, %
$Sc$	Schmidt number
$Sh$	Sherwood number
$T$	temperature, °C
$V$	volume, m <sup>3</sup>
$v$	air droplet relative velocity, m/s
$x$	mole fraction
$Y$	vapour mass fraction

#### GREEK SYMBOLS

$\theta$	dimensionless correction factor
$\Phi$	generalised form of variables
$\mu$	viscosity, Pa.s
$\rho$	density, kg/m <sup>3</sup>
$\phi$	dimensionless rate factor
$\mathcal{D}$	mass diffusivity coefficient
$\sigma$	Stefan-Boltzmann constant
$\varepsilon$	emissivity factor

#### SUBSCRIPTS

$A$	gas/liquid A
$a$	air
$atm$	atmosphere
$AB$	binary system of A and B
$B$	gas/liquid B
$b$	buoyancy
$bw$	boundary wall
$c$	convective heat
$cr$	critical value
$d$	drag
$e$	evaporation
$f$	flame
$g$	gravitation
$m$	mass transfer
$p$	water particle/droplet
$s$	droplet surface
$sat$	saturation
$w$	water
$\infty$	refers to the far field value

#### SUPERSCRIPTS

- transfer coefficient for high mass transfer rate

#### REFERENCES

1. Liu Z, Kim AK. A review of water mist fire suppression systems- fundamental studies. *Journal of Fire Protection Engineering* 2000; 10(3):32-50, DOI: 10.1177/104239159901000303.
2. Grant GJ, Brenton J, Drysdale D. Fire suppression by water sprays. *Progress in Energy and Combustion Science* 2000; 26(2):79-130, DOI: 10.1016/S0360-1285(99)00012-X.

## WATER-MIST BEHAVIOUR

3. Liu Z, Kim AK. A review of water mist fire suppression systems- fundamental studies. *Journal of Fire Protection Engineering* 2000; 10(3):32-50, DOI: 10.1106/MMGH-XUAG-HP5B-YTDG.
4. Yang P, Liu T, Qin X. Experimental and numerical study on water mist suppression system on room fire. *Building and Environment* 2010; 45:2309-2316, DOI: 10.1016/j.buildenv.2010.04.017.
5. Shu YL, Jeng WJ, Chiu CW, Chen CH. Assessment of fire protection performance of water mist applied in exhaust ducts for semiconductor fabrication process. *Fire and Materials* 2005; 29:295–302, DOI: 10.1002/fam.890.
6. Braidech NM, Neale JA, Matson AF, Dufour RE. The Mechanism of Extinguishments of Fire by Finely Divided Water. Underwriters Laboratory, Inc., National Board of Fire Underwriters, New York, 1955, pp. 73.
7. Rashbash DJ, Rogowski ZW, Stark GWV. Mechanism of Extinction of Liquid Fires with Water Sprays. *Combustion and Flame* 1960; 4:223-234, DOI: 10.1016/S0010-2180(60)80026-0.
8. Yao B, Chow WK. Extinguishment of a PMMA fire by water spray with high droplet speeds. *International Journal of Thermal Sciences* 2005; 44(4):410-419, DOI: 10.1016/j.ijthermalsci.2004.06.006.
9. Mawhinney JR, Dlugogorski BZ, Kim AK. A closer look at the fire extinguishing properties of water mist. *Fire Safety Science—Proceedings 4th International Symposium on Fire Safety Science*. Ottawa, Ontario, Canada, July 13-17, 1994, pp. 47-60.
10. Wighus R. Engineering relations for water mist fire suppression systems. *Proceedings: Halon Alternatives Technical Working Conference*, Albuquerque, New Mexico, 1995, pp. 397.
11. Chow W K, Yao B. Numerical modeling for interaction of a water spray with smoke layer. *Numerical Heat Transfer* 2001; 39(3):267-283, DOI: 10.1080/104077801300006580.
12. Cooper LY. The interaction of an isolated sprinkler spray and a two-layer compartment fire environment. *International Journal of Heat and Mass Transfer* 1995; 38(4):679–690, DOI: 10.1016/0017-9310(94)00188-2.
13. Chow WK, Tong AC. Experimental studies on sprinkler water spray-smoke layer interaction. *Journal of Applied Fire Science* 1995; 4(3):171-184, DOI: 10.2190/54B4-5AUL-MNCV-F825.
14. Chow WK, Cheung YL. Simulation of Sprinkler-Hot Layer Interaction Using a Field Model. *Fire and Materials* 1994; 18:359-379, DOI: 10.1002/fam.810180604.
15. Morgan HP. Heat transfer from a buoyant smoke layer beneath a ceiling to a sprinkler spray: 1-A tentative theory. *Fire and Materials* 1979; 3(1):27–33, DOI: 10.1002/fam.810030106.
16. Morgan H P, Baines K. Heat Transfer from a Buoyant Smoke Layer Beneath a Ceiling to a Sprinkler Spray: 2-An Experiment. *Fire and Materials* 1979; 3(1):34-38, DOI: 10.1002/fam.810030107.
17. Yuen MC, Chen LW. Heat and mass transfer measurements of evaporating liquid droplets. *International Journal Heat and Mass Transfer* 1978; 21:537–542, DOI: 10.1016/0017-9310(78)90049-2.
18. Ranz WE, Marshall WR Jr. Evaporation from droplets, Part II. *Chemical Engineering Progress* 1952; 48(3):141–146.
19. Renksizbulut M, Yuen MC. Experimental study of droplet evaporation in a high-temperature air steam. *Journal of Heat Transfer* 1983; 105(2):384–388, DOI:10.1115/1.3245590.
20. Fujita A, Kurose R, Komori S. Experimental study on effect of relative humidity on heat transfer of an evaporating water droplet in air flow. *International Journal of Multiphase Flow* 2010; 36(3):244–247, DOI: 10.1016/j.ijmultiphaseflow.2009.10.004.
21. Novozhilov V. Flashover control under fire suppression conditions. *Fire Safety Journal* 2001; 36:641–660, DOI: 10.1016/S0379-7112(01)00019-4.
22. Li YF, Chow WK. Study of water droplet behaviour in hot air layer in fire extinguishment. *Fire Technology* 2008; 44(4):351–381, DOI: 10.1007/s10694-007-0036-2.
23. Vaari J. A transient one-zone computer model for total flooding water mist fire suppression in ventilated enclosures. *Fire Safety Journal* 2002; 37:229–257, DOI: 10.1016/S0379-7112(01)00046-7.
24. Barrow H, Pope CW. Droplet evaporation with reference to the effectiveness of water-mist cooling. *Applied Energy* 2007; 84:404–412, DOI: 10.1016/j.apenergy.2006.09.007.
25. Li YF, Chow WK. Modelling of water mist fire suppression system by a one-zone model. *Combustion Theory and Modelling* 2004; 8(3):567-592, DOI: 10.1088/1364-7830/8/3/008.
26. Liu Z, Kim AK, Carpenter D. A study of portable water-mist fire extinguishers used for extinguishment of multiple fire types. *Fire Safety Journal* 2007; 42:25-42, DOI: 10.1016/j.firesaf.2006.06.008.
27. Thomas GO. The quenching of laminar methane-air flames by water mists. *Combustion and Flame* 2002; 130(1-2):147–160, DOI: 10.1016/S0010-2180(02)00351-6.
28. Holman JP. Heat transfer. *McGraw-Hill Book Company, 9th ed*, New York, 2002; p.133.
29. Katsios XKKa, Krikkis RN. Effect of surface tension and evaporation on phase change of fuel droplets. *Heat Transfer Engineering* 2001; 22:33–40, DOI: 10.1080/01457630120403.
30. Alpert RL. Calculation of Response Time of Ceiling - Mounted Fire Detectors. *Fire Technology* 1972; 8(3):181–195, DOI: 10.1007/BF02590543.
31. Drysdale D. An Introduction to Fire Dynamics. *3rd ed.*, John Wiley and Sons, New York, 2011; pp.158.
32. John VV. A full-scale experiment study of water mist spray convection. *Proceedings of 2nd International Conference on Fire Research and Engineering*, Maryland, USA, Aug 3–8, 1997; pp. 282–289.

33. Bullen ML. The effect of a sprinkler on the stability of a smoke layer beneath a ceiling. *Fire Technology* 1977; 13(1):21-34, DOI: 10.1007/BF02338883.
34. Tang Z, Fang Z, Merci B. Development of an analytical model to quantify downward smoke displacement caused by a water spray for zone model simulations. *Fire Safety Journal* 2014; 63:89–100, DOI: 10.1016/j.firesaf.2013.12.002.
35. Tang Z, Vierendeels J, Fang Z, Merci B., Description and application of an analytical model to quantify downward smoke displacement caused by a water spray. *Fire Safety Journal* 2013; 55:50–60, DOI: 10.1016/j.firesaf.2012.10.012.
36. Li KY, Hu LH, Huo R, Li YZ, Chen ZB, Li SC, Sun XQ. A mathematical model on interaction of smoke layer with sprinkler spray. *Fire Safety Journal* 2009; 44(1):96–105, DOI: 10.1016/j.firesaf.2008.04.003.
37. ASHRAE Handbook. Fundamentals. *American Soc. of Heating, Refrigeration and Air Conditioning Engineers, Inc.*, New York, 1985; pp. 5.5.
38. William CH. Aerosol technology. *John Wiley & Sons, Inc.*, New York, 1999.
39. Cengel YA, Turner RH. Fundamental of thermal fluid sciences. 2nd ed., *McGraw - Hill Book Company*, New York, 2005; pp.1088–1089.
40. Brown PP, Lawler DF. Sphere drag and settling velocity revisited. *Journal of Environmental Engineering (ASCE)* 2003; 129(3):222–231, DOI: 10.1061/(ASCE)0733-9372(2003)129:3(222).
41. Bird RB, Stewart WE, Lightfoot EN. Transport phenomena. *John Willy and Sons, Inc.*, New York, 1960; pp. 59 and 505.
42. Beard KV, Pruppacher HR. A wind tunnel investigation of the rate of evaporation of small water drops falling at terminal velocity in air. *Journal of Atmospheric Science* 1971; 28:1455–1464, DOI: 10.1175/1520-0469(1971)028<1455:AWTIOT>2.0.CO;2.
43. Smolik J, Dzumbova L, Schwarz J, Kulmala M. Evaporation of ventilated water droplet: connection between heat and mass transfer. *Aerosol Science* 2001; 32:739–748, DOI: 10.1016/S0021-8502(00)00118-X.
44. Slattery J.C, Bird RB. *A.I.Ch.E.J.* 1958; 4(2):pp.137.
45. Buck AL. New equations for computing vapour pressure and enhancement factor. *Journal of Applied Meteorology* 1981; 20:1527-1532, DOI: 10.1175/1520-0450(1981)020<1527:NEFCVP>2.0.CO;2.
46. Touloukian YS, Saxena SC, Hestermans P. Thermophysical properties of matter. *The TRPC Data Series, volume 11: Viscosity, IFI/Plenum*, New York 1975; pp. 96 and 611.
47. Touloukian YS, Makita T. Thermo-physical properties of matter. *The TRPC Data Series, Volume 6: Specific heat, non-metallic liquids and gases, IFI/Plenum*, New York 1970; pp. 293.
48. Touloukian YS, Liley PE, Saxena SC. Thermo-physical properties of matter. *The TRPC Data Series, Volume 3: Thermal conductivity, non-metallic liquids and gases, IFI/Plenum*, New York 1970; pp. 120, 125, 512.
49. Sifner O, Klomfar J. International standards of thermo-physical properties of water and water vapour. *Academia, Prague* 1996.
50. Gunn R, Kinzer GD. The terminal velocity of fall for water droplets in stagnant air. *Journal of Meteorology* 1949; 6:243-248, DOI: 10.1175/1520-0469(1949)006<0243:TTVOFF>2.0.CO;2.
51. Thorpe GR. Ambient air properties in aeration (Chap - 3). In: Navarro S, Noyes R T (Eds.). *The Mechanics and Physics of Modern Grain Aeration Management, CRC Press* 2001, pp. 111.
52. McGrattan K, Hostikka S, Floyd J, Baum H, Rehm R, Mell W, Macdermott R. Fire Dynamics Simulator (Version 5) Technical Reference Guide, Volume 1: Mathematical Model. *NIST Special Publication 1018-5, National Institute of Standards and Technology*, U.S. Department of Commerce, Gaithersburg, Maryland, USA, 2010 (June).

Filename: 1. Thesis\_s3873326\_For single side printing\_Final Printing.docx  
Directory: C:\Users\Iqbal Mahmud\Documents  
Template: C:\Users\Iqbal Mahmud\AppData\Roaming\Microsoft\Templates\Normal.dotm  
Title: Simulation of the Suppression of Fires Using Water Mists  
Subject: PhD Thesis  
Author: Iqbal Mahmud  
Keywords:  
Comments:  
Creation Date: 4/03/2016 9:04:00 AM  
Change Number: 11  
Last Saved On: 4/03/2016 3:53:00 PM  
Last Saved By: Iqbal Mahmud  
Total Editing Time: 121 Minutes  
Last Printed On: 4/03/2016 4:27:00 PM  
As of Last Complete Printing  
Number of Pages: 249  
Number of Words: 97,375 (approx.)  
Number of Characters: 496,617 (approx.)